



UNIVERSIDADE DE ÉVORA

# *Biochemical Mechanisms and Target Drugs in Neurodegenerative Diseases*

*Patrícia Alexandra Anico Gazimba Bacalhau*

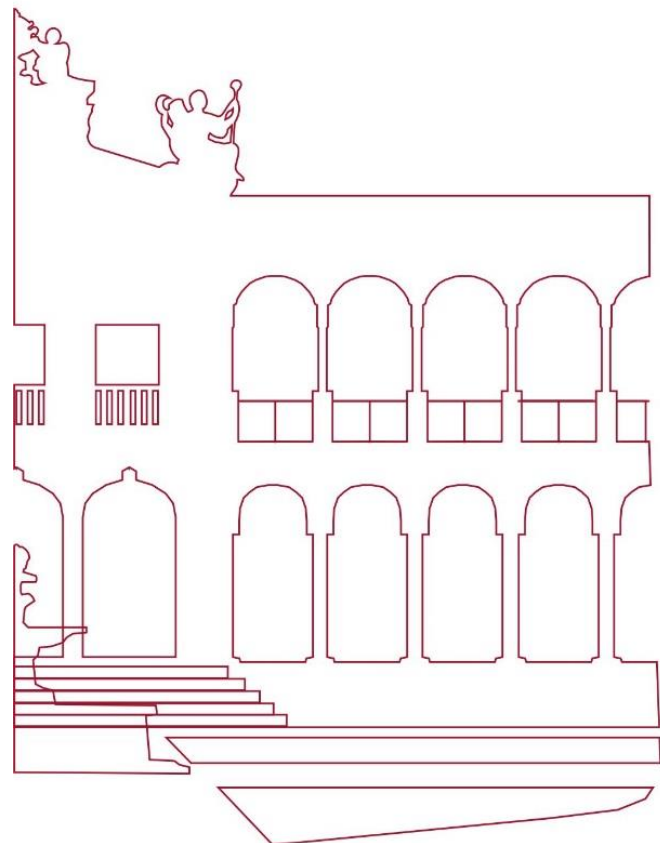
SUPERVISORS: *Prof. Doutora Maria do Rosário Martins*

*Prof. Doutora Ana Teresa Caldeira*

*Prof. Doutor Anthony Joseph Burke*

Thesis presented to University of Évora  
to obtain the PhD degree in Biochemistry

Évora, 2017



INSTITUTO DE INVESTIGAÇÃO E FORMAÇÃO  
AVANÇADA



UNIVERSIDADE DE ÉVORA

# *Biochemical Mechanisms and Target Drugs in Neurodegenerative Diseases*

*Patrícia Alexandra Anico Gazimba Bacalhau*

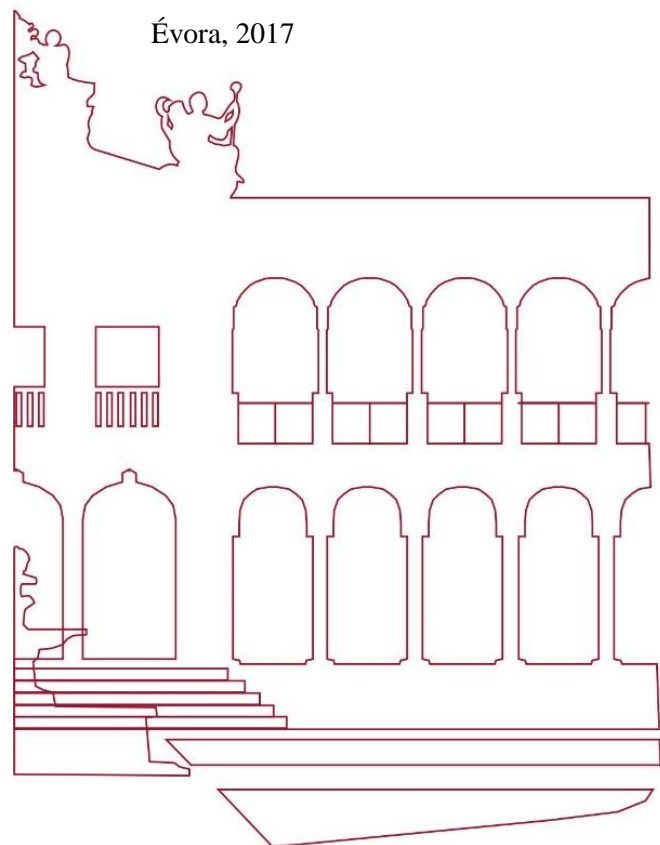
SUPERVISORS: *Prof. Doutora Maria do Rosário Martins*

*Prof. Doutora Ana Teresa Caldeira*

*Prof. Doutor Anthony Joseph Burke*

Thesis presented to University of Évora  
to obtain the PhD degree in Biochemistry

Évora, 2017



INSTITUTO DE INVESTIGAÇÃO E FORMAÇÃO  
AVANÇADA

*To Sara*



## Acknowledgements

Working in the area of neurodegenerative diseases was a premiere in Évora University, and like all new projects needs an enormous commitment and dedication, so I would like to thank Prof. Maria do Rosário Martins, Prof. Ana Teresa Caldeira and Prof. Anthony Joseph Burke, from the University of Évora, for accepting this challenge. This work wouldn't be possible without them.

To Dr. Fátima Candeias, from the Chemistry Department of the University of Évora, I thank the help on the toxicological and pharmacological experiments.

To the lab technician, Anabela Cabeça, I thank for all the assistance in the lab work and for her friendship.

To the Group of Medicinal Chemistry/Organic Synthesis of Prof. Anthony Burke from the University of Évora and to the Group of Organic Synthesis of Prof. Maurizio Benaglia from the University of Milan, I'd like to thank for the compounds synthesized for my research.

I also would like to thank my colleagues in the chemistry department, for making me feel welcome and hearing me out in these last years.

To Dr. Albertino Goth for assisting me in the STD-NMR experiments.

My thanks to the project – INMOLFARM - funded by FEDER under the INALENTEJO program ALENT-07-0224-FEDER-001743, for the 8 months grant to my research.

For the unconditional support of my family, specially Sara, that had to share me with my research, I have no words to thank you all enough.



## Abstract

Neurodegenerative diseases, namely Alzheimer's and Parkinson's diseases are a major challenge for medicine and public health due to their prevalence in developed countries. Thus, the research for therapies for neurodegenerative diseases, such as Parkinson's and Alzheimer's diseases, should be based on understanding their molecular and biochemical pathogenesis.

The research conducted in this thesis involves *screening* of different families of compounds (isoquinolinones, azepanones, indolinones, diether-esters, chromanones, chromanols and rivastigmine derivatives) based on their ability to inhibit the activity of the therapeutic targets acetylcholinesterase, butyrylcholinesterase and monoamine oxidase B. These targets were chosen for their importance in the neuropathology of Alzheimer's and Parkinson's diseases. The most promising compounds were then selected, and the determination of their action at the molecular level was studied via STD-NMR. These studies allow us to understand the importance of different functionalities within the inhibitor molecule on the inhibition of the selected targets, and thus direct the investigation in the sense of developing compounds that can be better inhibitors. Toxicological and pharmacological evaluation of the most promising synthesized compounds was performed using two different biological models, *A. salina* and *Swiss* mouse model. Compound 4-[(3-hydroxy-2-oxo-3-phenylindolin-1-yl)methyl]piperidin-1-ium chloride was tested *ex vivo* against hepatic AChE and BuChE, showing  $IC_{50}$  values of 594.64  $\mu$ M and 434.51  $\mu$ M, respectively. This compound was also assayed *in vivo* after intraperitoneal administration of 3 mg kg<sup>-1</sup> and 6 mg kg<sup>-1</sup> in *Swiss* mice, using donepezil (3 mg kg<sup>-1</sup>) as a benchmark. This synthetic compound gave better brain AChE inhibition than donepezil, indicating that this compound might have a similar brain uptake mechanism to that of donepezil.

**Key words:** Alzheimer, Parkinson, acetylcholinesterase, butyrylcholinesterase, monoamine oxidase B, spectrometry, fluorometry, STD-NMR, inhibitors.





## Resumo

### Mecanismos bioquímicos e alvos terapêuticos em patologias neurodegenerativas

As doenças neurodegenerativas, nomeadamente as doenças de Alzheimer e Parkinson são um enorme desafio quer para a medicina quer em termos de saúde pública devido à sua prevalência nos países desenvolvidos. Assim, a pesquisa de terapias para doenças neurodegenerativas, como o Parkinson e o Alzheimer, deve ser baseada na compreensão da sua patogénese molecular e bioquímica.

Este trabalho envolve *screening* de diferentes famílias de compostos; derivados de isoquinolinonas, azepanonas, indolinonas, dieter-ester, cromanonas, cromanois e de rivastigmina, baseado na sua capacidade de inibir a atividade de alvos terapêuticos de algumas doenças neurodegenerativas como Alzheimer e Parkinson, nomeadamente: acetilcolinesterase, butirilcolinesterase e monoamino oxidase B. Os compostos promissores foram selecionados para determinação da sua ação a nível molecular por STD-NMR. Este estudo permite compreender a importância dos diferentes grupos funcionais na inibição dos alvos selecionados, e desta forma, direcionar a investigação no sentido de desenvolver compostos com maior atividade inibitória. A avaliação toxicológica e farmacológica dos compostos sintetizados mais promissores foi efetuada utilizando dois modelos biológicos diferentes, *A. salina* e ratinho *Swiss*. O composto cloreto de 4-[(3-hidroxi-2-oxo-3-fenilindolin-1-il) metil] piperidin-1-ium foi testado *ex vivo* em homogenatos de hepatócito de murganho *Swiss*, tendo apresentado valores de IC<sub>50</sub> de 594.64 µM e de 434.51 µM para as atividades de AChE e BuChE, respetivamente. A capacidade inibitória deste composto foi também avaliada *in vivo* após administração interperitoneal de 3 mg kg<sup>-1</sup> e 6 mg kg<sup>-1</sup> em ratinhos *Swiss*, utilizando donepezilo (3 mg kg<sup>-1</sup>) como padrão. Os resultados mostraram que o composto sintetizado apresentou valores de inibição de atividade de AChE no cérebro superiores aos observados para o donepezilo, podendo indicar que a sua captação pelos tecidos cerebrais poderá ser efetuada de modo semelhante à do donepezilo.

**Palavras chave:** Alzheimer, Parkinson, acetilcolinesterase, butirilcolinesterase, monoamino oxidase B, espetrometria, fluorimetria, STD-NMR, inibidores.



---

**Abbreviations**

A $\beta$	Amyloid $\beta$
ACh	Acetylcholine
AChE	Acetylcholinesterase
AcetylCoA	Acetyl coenzyme A
AD	Alzheimer's Disease
ALS	Amyotrophic Lateral Sclerosis
ApoE	Apolipoprotein E
APP	Amyloid precursor protein
ATCI	Acetylthiocholine iodide
ATP	Adenosine triphosphate
BBB	Blood brain barrier
BTCI	Butyrylthiocholine iodide
BuChE	Butyrylcholinesterase
CNS	Central nervous system
CSF	Cerebrospinal fluid
COMT	Catechol-O-methyltransferase
DAQ	Dopamine quinone
DMSO	Dimethyl sulfoxide
DOPA	Dihydroxyphenylalanine
DTNB	5,5-dithio-bis-(2-nitrobenzoic acid)
DS	Down's Syndrome
FAD	Flavin Adenine Dinucleotide
FIAD	Familial Alzheimer's Disease
FTD	Frontemporal Dementia
HD	Huntington's Disease
HRP	Horseradish peroxidase
IC <sub>50</sub>	Half maximal inhibitory concentration
LB	Lewy bodies
LBD	Lewy Body Dementia
LC <sub>50</sub>	Half maximal lethal concentration
LDLR	Low density lipoprotein receptor

MAO	Monoamine Oxidase
MTDL	Multitarget directed ligand
NAD	Nicotinamide adenine dinucleotide
NFT	Neurofibrillary tangles
NMDA	N-methyl-D-aspartate
NMR	Nuclear magnetic resonance
NOAEL	No Observed Adverse Effect Levels
PAS	Peripheral anionic site
PD	Parkinson's Disease
PNS	Peripheral nervous system
PSEN1	Presenilin-1
PSEN2	Presenilin-2
OCDE	Organisation for Economic Co-operation and Development
ROS	Reactive oxygen species
SN	Substantia nigra
STD-NMR	Saturation transfer difference - nuclear magnetic resonance

---

**Units**

°C	Celcius degree
U	Enzyme unit
μL	Microliter
μM	Micromolar
mg	Milligram
mL	Milliliter
mM	Millimolar
min	Minute
nm	Nanometer
nM	Nanomolar
%	Percentage
s	Second



---

**Table of Contents**

Acknowledgements .....	V
Abstract.....	VII
Resumo .....	IX
Abbreviations.....	XI
Units.....	XIII
Table of Contents.....	XV
List of Tables .....	XXIV
Chapter 1: An Overview on Neurodegenerative Diseases .....	1
1.1. Objectives.....	3
1.2. Nervous System and Brain.....	3
1.3. Neurodegenerative diseases.....	10
1.3.1. Alzheimer’s Disease .....	11
1.3.1.1. Cholinergic Neurotransmission.....	12
1.3.1.2. Catalytic reaction mechanism of AChE and BuChE .....	15
1.3.1.3. Cholinergic hypothesis .....	18
1.3.1.4. Amyloid- $\beta$ hypothesis and the Amyloid Precursor Protein.....	19
1.3.1.5. Hyperphosphorylation of Tau ( $\tau$ ) protein .....	22
1.3.1.6. Oxidative stress.....	23
1.3.2. Parkinson’s Disease .....	23
1.3.2.1. Adrenergic neurotransmission .....	25
1.3.2.2. Catalytic reaction mechanism of MAO-B .....	29
1.3.2.3. $\alpha$ -Synuclein .....	33
1.3.2.4. Oxidative Stress .....	35
1.3.3. Therapeutic approaches .....	36

---

Chapter 2: Methodology optimization for selecting therapeutic targets.....	43
2.1. Introduction.....	45
2.2. Materials and Methods .....	46
2.2.1. Enzymatic activity quantification for AChE and BuChE by spectrophotometry .....	46
2.2.1.1. Chemicals.....	46
2.2.1.2. Influence of substrate concentration in enzymatic activity.....	46
2.2.1.3. Determination of the kinetic parameters for AChE and BuChE.....	47
2.2.1.4. Evaluation of enzymatic selectivity for the substrate .....	47
2.2.1.5. Evaluation of <i>ee</i> AChE and <i>eq</i> BuChE inhibitory activity of rivastigmine, donepezil and galantamine .....	47
2.2.2. Enzymatic activity quantification for MAO-B by spectrophotometry .....	48
2.2.2.1. Chemicals.....	48
2.2.2.2. Influence of MAO-B concentration .....	48
2.2.2.3. Influence of substrate concentration in enzymatic activity.....	48
2.2.2.4. Determination of kinetic parameters for MAO-B.....	49
2.2.2.5. Evaluation of MAO-B inhibitory activity of pargyline and rasagiline .....	49
2.2.3. Enzymatic activity determination for MAO-B by fluorometry .....	50
2.2.3.1. Influence of MAO-B concentration .....	50
2.2.3.2. Evaluation of MAO-B inhibitory activity of pargyline and rasagiline .....	50
2.2.4. Statistical analysis .....	51
2.3. Results and Discussion.....	52
2.3.1 Enzymatic activity of AChE and BuChE by UV-Vis spectrometry .....	52
2.3.1.1. Evaluation of enzymatic selectivity for the substrate .....	55
2.3.1.2. <i>ee</i> AChE and <i>eq</i> BuChE inhibitory activity evaluation for rivastigmine, donepezil and galantamine .....	56



---

2.3.2. Enzymatic activity for MAO-B .....	63
2.3. Conclusions .....	69
Chapter 3: Screening therapeutic target molecules for neurodegenerative diseases .....	71
3.1. Introduction .....	73
3.2.1. Chemicals .....	74
3.2.2. <i>ee</i> AChE and <i>eq</i> BuChE IC <sub>50</sub> evaluation of isoquinolinone, azepanone, indolinone, diether ester, chromanone, chromanol and rivastigmine derivatives .....	85
3.2.3. MAO-B IC <sub>50</sub> evaluation of isoquinolinone, azepanone, indolinone, diether ester, chromanone, chromanol and rivastigmine derivatives .....	85
3.2.4. Statistical analysis.....	85
3.3. Results and discussion .....	86
3.3.1. <i>ee</i> AChE and <i>eq</i> BuChE IC <sub>50</sub> evaluation .....	86
3.3.1.1. Isoquinolinone and Azepanone derivatives .....	86
3.3.1.2. Indolinone derivatives .....	93
3.3.1.3. Diether-ester derivatives.....	103
3.3.1.4. Chromanone and chromanol derivatives .....	108
3.3.1.5. Rivastigmine analogues .....	111
3.3.2. MAO-B IC <sub>50</sub> evaluation.....	115
3.4. Conclusions .....	116
4.1. Introduction .....	121
4.2.1. Chemicals.....	122
4.2.2. Conducting the STD experimente .....	122
4.2.3. Calculation of the STD Amplification factor.....	123
4.2.4. Mapping of the binding moieties .....	123
4.3. Results and discussion .....	123

---

4.3.1. Protein-ligand interaction studies by STD-NMR.....	123
4.3.1.1. STD-NMR of AChE-Donepezil hydrochloride.....	125
4.3.1.2. STD-NMR of AChE-Galantamine bromide.....	127
4.3.1.3. STD-NMR of BuChE-Rivastigmine tartrate.....	129
4.3.1.4. STD-NMR MAO-B-Rasagiline mesylate .....	131
4.3.1.5. STD - NMR study of the interaction of AChE with 4-methoxy-3,4-dihydroisoquinolin-1(2H)-one (6) and 4-methoxy-3,4-dihydroisoquinolin-1(2H)-one (6) with BuChE.....	134
4.3.1.6. STD-NMR study of the BuChE-1-benzyl-3-hydroxy-3-phenylindolin-2-one (17) interaction.....	139
4.3.1.7. STD-NMR study of the AChE-4-((3-hydroxy-2-oxo-3-phenylindolin-1-yl)methyl)piperidin-1-ium chloride (48a) interaction and of 4-((3-hydroxy-2-oxo-3-phenylindolin-1-yl)methyl)piperidin-1-ium chloride (48a) with BuChE.....	144
4.4. Conclusions.....	147
Chapter 5: Pharmacological and toxicological evaluation of selected target molecules for neurodegenerative diseases .....	149
5.1 Introduction.....	151
5.2 Materials and Methods.....	152
5.2.1 Samples .....	152
5.2.2 Citotoxicity in <i>Artemia salina</i> L.....	153
5.2.3 Acute toxicity in animal model.....	153
5.2.3.1 Animals .....	153
5.2.3.2 Acute intraperitoneal toxicity evaluation .....	154
5.2.4 <i>Ex vivo</i> pharmacological evaluation .....	154
5.2.4.1 Animals .....	154
5.2.4.2 Spectrophotometric measurement of cholinesterase and monoamine oxidase activity ...	154

---

5.2.5 <i>In vivo</i> pharmacological evaluation .....	155
5.2.5.1 Animals.....	155
5.2.5.2 Spectrophotometric measurement of cholinesterase activity .....	155
5.2.6 Statistic analysis .....	156
5.3 Results and Discussion .....	156
5.3.1 Citotoxicity in <i>Artemia salina</i> L. of cholinesterase and monoamine oxidase inhibitors ....	156
5.3.2 Acute intraperitoneal toxicity evaluation of cholinesterase inhibitors .....	158
5.3.3 <i>Ex vivo</i> pharmacological evaluation .....	159
5.3.4 <i>In vivo</i> pharmacological evaluation .....	163
5.4. Conclusions .....	164
Chapter 6: Final Considerations and Future Perspectives .....	167
References .....	173
Appendix .....	199
Appendix 1. Enzymatic Monitorization .....	201
Appendix 2. STD-NMR sobreposition spectra.....	203
Appendix 3. Statistical Analysis.....	207
Appendix 4. Publications.....	209

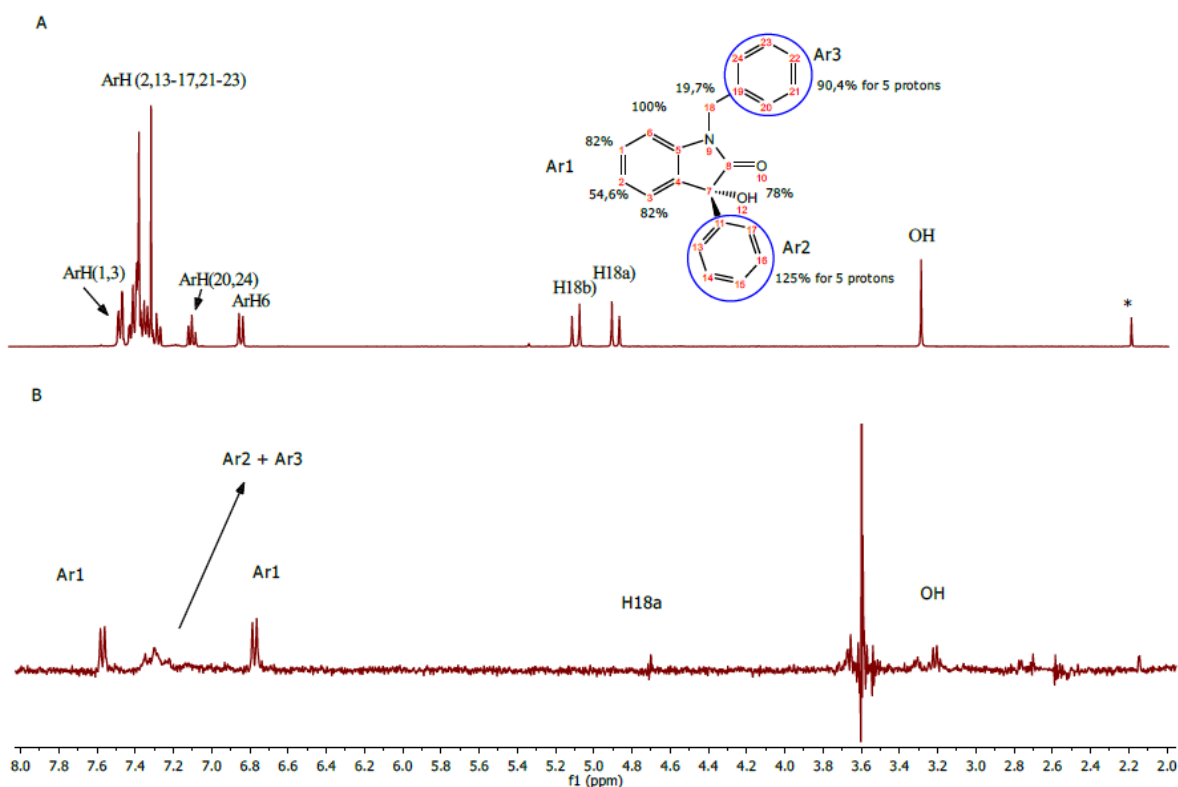
## List of Figures

Figure 1 - Nervous system organization. Adapted from [2].....	4
Figure 2 - Cells of the nervous system. Adapted from [3].....	4
Figure 3 - Neuron structure. (A) Constitution of a neuron. (B) Components of the neuron: the cell membrane, nucleus, nuclear membrane, nucleolus, and the organelles. Adapted from [4].....	5
Figure 4 – A chemical synapse: 1- Action potentials arriving at the presynaptic terminal cause voltage-gated $\text{Ca}^{2+}$ channels to open; 2- $\text{Ca}^{2+}$ diffuses into the cell and causes synaptic vesicles to release neurotransmitter molecules; 3- Neurotransmitter molecules diffuse from the presynaptic terminal across the synaptic cleft; 4- Neurotransmitter molecules combine with their receptor sites and cause ligand-gated $\text{Na}^+$ channels to open. $\text{Na}^+$ diffuses into the cell (shown in illustration) or out of the cell (not shown) and causes a change in membrane potential. Adapted from [10].....	7
Figure 5 - Regions of the brain. Medial view of a mid-sagittal section of the right half of the brain. Adapted from [10].....	8
Figure 6 – Lateral view of the left cerebral hemisphere, showing the lobes, as well as the motor and sensory regions of the cerebral cortex. Adapted from [12]. ....	9
Figure 7 - Overview of the anatomical location, macroscopic and microscopic changes characteristic of neurodegenerative disorders. Note that the full neuropathological spectrum of these disorders is much more complex than depicted here. When there is more than one characteristic histopathological feature, these are depicted from left to right, as indicated in the labels listing microscopic changes (e.g., the 2 panels for AD depict an $\text{A}\beta$ plaque [left] and neurofibrillary tangles [right]). AD-Alzheimer disease; PD-Parkinson disease; ALS–Amyotrophic lateral sclerosis; HD-Huntington disease; LBD-Lewy body dementia; FTD-Frontotemporal dementia. Adapted from [14]. ....	10
Figure 8 – Cholinergic neurotransmission: 1. Facilitated diffusion of glucose; 2. Glycolysis; 3. Acetyl group derived from pyruvic acid combines with coenzyme-A; 4. Active transport of choline; 5. Acetylcholine is synthesized; 6. Acetylcholine is then transported into vesicles and stored there; 7. Exocytosis of Acetylcholine; 8. Acetylcholinesterase hydrolyze acetylcholine to choline and acetate. Adapted from [6, 32].....	14
Figure 9 – Ribbon diagram based on the X-ray crystallography structures of (A) human AChE (Protein Data Bank ID: 4PQE) and (B) human BuChE (Protein Data Bank ID: 4P0I).....	15
Figure 10 - Stick representation of the active site gorge with homologous residues shown for hAChE (Protein Data Bank ID: 1B41) and hBuChE (Protein Data Bank ID: 1POI). Adapted from [46].....	16
Figure 11 - Cholinergic pathway. Adapted from [57].....	18
Figure 12 - Schematic diagram illustrating proteolytic cleavage of the amyloid precursor protein (APP). Adapted from [62].....	19
Figure 13 – Histological cut formation of amyloid plaques and neurofibrillary tangles (NFTs). Adapted from [64]. ....	20
Figure 14 - The normal processing of B-amyloid precursor protein as well as the effect on processing of alterations in the protein resulting from missense mutations associated with early-onset familial Alzheimer’s disease. Adapted from [71]. ....	21
Figure 15 – (A) Tau protein in healthy neurons; (B) Formation of neurofibrillary tangles (NFTs) in AD neurons. Adapted from [68]. ....	22
Figure 16 – Molecular pathways linking idiopathic and genetic forms of PD. Adapted from [80]. ....	24
Figure 17 - Adrenergic neurotransmission: 1. Tyrosine enters the neuron by active transport; 2. Tyrosine is converted into DOPA by tyrosine hydroxylase; 3. DOPA is converted to dopamine in the cytoplasm by the enzyme DOPA-decarboxylase; 4. Dopamine is then stored in vesicles by the vesicular transport mechanism; 5. Dopamine is ready for release by exocytosis; 6. Dopamine released into the synaptic cleft is actively transported back into the neuronal terminal; 7. Part of the dopamine that enters the neuronal terminal is destroyed by monoamine oxidase (MAO); 8. Some of the dopamine that is released into the synaptic cleft is actively transported into the effector cells and is inactivated primarily by an enzyme, catechol-O-methyltransferase (COMT) [6]. ....	28
Figure 18 - Dopaminergic pathway. Adapted from [57]. ....	29
Figure 19 – Ribbon diagram based on the X-ray crystallography structures of (A) MAO-A (Protein Data Bank ID: 2Z5Y) and (B) MAO-B (Protein Data Bank ID: 1GOS). ....	29
Figure 20 - Ribbon diagram of (A) human MAO-A structure and (B) human MAO-B structure. The covalent flavin moiety is shown in a ball and stick model in yellow. The flavin binding domain is in blue, the substrate domain in red and the membrane binding domain in green. Adapted from [90]. ....	30
Figure 21 - Illustration of FAD binding site in MAO-B. Dashed lines indicate H-bonds. Carbons are in black,	

nitrogens in blue, oxygens in red, and sulfurs are shown as cyan spheres. Adapted from [96].	31
Figure 22 – Schematic representation of micelle-bound $\alpha$ -synuclein (Protein Data Bank ID: 1XQ8).	33
Figure 23 - Mechanisms of $\alpha$ -synuclein aggregation and propagation. Adapted from [103].	34
Figure 24 - Drugs currently approved by INFARMED against Alzheimer's disease.	36
Figure 25 - The amyloid hypothesis. Adapted from [63].	37
Figure 26 – The multitarget directed ligand Ladostigil. Adapted from [158]. The carbamate group of Rivastigmine is highlighted in blue and the propargyl group of Rasagiline is highlighted in purple.	38
Figure 27 - Anticholinergic drugs for treating Parkinson's disease.	38
Figure 28 - Dopamine mimetic drugs used in Parkinson's disease.	39
Figure 29 – Michaelis–Menten curve for (A) eeAChE in the presence of ATCI; (B) eqBuChE in the presence of BTCl.	53
Figure 30 - Michaelis–Menten curve kinetic representation of eeAChE and eqBuChE using: (A) ATCI as substrate; (B) BTCl as substrate.	55
Figure 31 – eeAChE dose-response curves for donepezil, rivastigmine and galantamine in Tris-HCl buffer and 405 nm, at 25 °C (A, C, E) and 37 °C (B, D, F).	57
Figure 32 - eeAChE dose-response curves for donepezil, rivastigmine and galantamine in Tris-HCl buffer and 412 nm, at 25 °C (A, C, E) and 37 °C (B, D, F).	58
Figure 33 – eeAChE dose-response curves for donepezil, rivastigmine and galantamine in phosphate buffer and 405 nm, at 25 °C (A, C, E) and 37 °C (B, D, F).	60
Figure 34 - eqBuChE dose-response curves for donepezil, rivastigmine and galantamine in phosphate buffer and 405 nm, at 25 °C (A, B, C).	62
Figure 35 - Determination of kinetic parameters for MAO-B.	65
Figure 36 - Dose-response graph of MAO-B activity against rasagiline and pargyline.	66
Figure 37 - Dose-response curves and IC <sub>50</sub> values for pargyline and rasagiline by fluorometry.	68
Figure 38 – Isoquinolinone and azepanone derivatives.	86
Figure 39 - Dose-response curves for compounds 1, 6, 7, 8 and rivastigmine for eeAChE inhibition; and of compounds 4, 6, 7, 8, galantamine and rivastigmine for eqBuChE inhibition.	87
Figure 40 - Dose-response curves for compounds 5, 9, 10, 11, 12, 13, 14, 15 and 16 for eeAChE inhibition; and of compounds 2, 10, 12, 15 and 16 for eqBuChE inhibition (continues next page).	88
Figure 41 – In vitro eeAChE activity, in the presence of rivastigmine, galantamine and compounds 1, 5-13 and 15-16. Different letters represent values significantly different (p<0.05).	92
Figure 42 – In vitro eqBuChE activity, in the presence of rivastigmine, galantamine and compounds 1, 2, 4, 6-10 and 16. Different letters represent values significantly different (p<0.05).	93
Figure 43 - Indolinone derivatives (continued in next page).	94
Figure 44 – Dose-response curves for compounds (17)-(56) for eeAChE and eqBuChE (continued in next page).	96
Figure 45 - In vitro eeAChE activity, in the presence of donepezil and compounds 17-17b, 19-33 and 36-56. Different letters represent values significantly different (p<0.05).	102
Figure 46 - In vitro eqBuChE activity, in the presence of donepezil and compounds 17-27, 29-45, 47-49 and 51-56. Different letters represent values significantly different (p<0.05).	103
Figure 47 – Diether-ester derivatives.	104
Figure 48 - Dose-response curves with and without incubation, for eeAChE and eqBuChE with diether-ester derivatives.	105
Figure 49 - In vitro eeAChE activity, in the presence of rivastigmine and compounds 57 to 60. Different letters represent values significantly different (p<0.05).	106
Figure 50 - In vitro eqBuChE activity, in the presence of rivastigmine and compounds 57 to 60. Different letters represent values significantly different (p<0.05).	107
Figure 51 - Chromanone and chromanol derivatives.	108
Figure 52 - Dose-response curve for eeAChE and eqBuChE with chromanone and chromanol derivatives.	109
Figure 53 - In vitro eeAChE and eqBuChE activity, in the presence of donepezil and compounds 61 to 66. Different letters represent values significantly different for each enzyme experiment (p<0.05).	110
Figure 54 - Rivastigmine analogues.	112
Figure 55 – Dose-response curves of compounds 73 and 74 for eeAChE, and of compounds 67, 68, 69, 70, 71, 73 and 74 for eqBuChE activities.	113
Figure 56 - In vitro AChE and BuChE activity, in the presence of rivastigmine, compounds 67 to 71 and 73-74. Different letters represent values significantly different for each enzyme experiment (p<0.05).	114
Figure 57 - Binding mode of compound (21) obtained by docking with hMAO-B (1OJA, resolution 1.7 Å). Water molecules in the active site are represented as red and grey spheres. (A) Scheme and (B) Catalytic	

---

site view.....	116
Figure 58 -Key binding regions of donepezil. Adapted from [243].....	125
Figure 59 - STD-AF values of selected protons of donepezil as a function of saturation time for a 200-fold ligand excess.....	125
Figure 60 - STD-NMR of donepezil with eeAChE, performed at 400 MHz, 15 °C, and 3 s saturation time. (A) STD of donepezil (0.8 mM) with eeAChE enzyme (4 μM) and binding epitope of donepezil from STD NMR experiment. The numerical values designate the fraction of saturation as percentage, between the ligand protons and the protein active site, based on the maximum ligand STD signal (H3; 100%). Percentage saturation (75–100%) signifies strong interatomic contacts to the eqBuChE active site.; (B) Reference of donepezil (0.8 mM) with eeAChE enzyme (4 μM).....	126
Figure 61 - STD-AF values of selected protons of galantamine as a function of saturation time. The sample contained 0.8 mM of ligand and 4 μM of eeAChE. ....	128
Figure 62 - STD-NMR of galantamine with eeAChE: (A) reference <sup>1</sup> H spectrum of galantamine with eeAChE and (B) STD spectrum of the solution of galantamine (0.8 mM) with eeAChE (4 μM) (3s of saturation time). The relative degree of saturation of the individual hydrogens are mapped into the structure and normalized to that of hydrogen H6. Percentage saturation (75–100%) signifies strong interatomic contacts to the eeAChE active site. ....	129
Figure 63 - STD-AF values of selected protons of rivastigmine as a function of saturation time for a 200-fold ligand excess.....	130
Figure 64 - STD-NMR of rivastigmine with EqBuChE, performed at 400 MHz, 15 °C, and 3 s saturation time. (a) Reference (top) and STD (bottom) of the rivastigmine (0.8 mM) with EqBuChE enzyme (4 μM). (b) Binding epitope of rivastigmine from STD NMR experiment. The numerical values designate the fraction of saturation as percentage, between the ligand protons and the protein active site, based on the maximum ligand STD signal (H6; 100%). Percentage saturation (75–100%) signifies strong interatomic contacts to the EqBuChE active site. ....	131
Figure 65 – Chemical formula of the covalent adduct formed between rasagiline and FAD. The atomic numberings of the flavin and the covalently bound rasagiline are shown. Adapted from [258]. ....	132
Figure 66 - Ligplot schematic drawings showing the interactions of Rasagiline with MAO-B. Carbon atoms are in black, oxygen atoms are in red, nitrogen atoms are in blue, and sulfur atoms are in yellow. Water molecules are shown as cyan spheres. Dashed lines indicate all potential H bonds. “Radiating” spheres indicate hydrophobic contacts between carbon atoms of the inhibitor and the neighboring residues. Adapted from [94].....	132
Figure 67 - STD-AF values of selected protons of rasagiline as a function of saturation time.....	133
Figure 68 - STD-NMR of rasagiline with MAO-B, performed at 400 MHz, 15 °C, and 3 s saturation time. (A) reference <sup>1</sup> H spectrum of rasagiline with MAO-B and (B) STD spectrum of the solution of rasagiline (5 mM) with MAO-B (5 μM) (3s of saturation time). The relative degree of saturation of the individual hydrogens are mapped into the structure and normalized to that of hydrogens H1 and H2. (a) Reference (top) and STD (bottom) of the rivastigmine (0.8 mM) with EqBuChE enzyme (4 μM). (b) Binding epitope of rivastigmine from STD NMR experiment. The numerical values designate the fraction of saturation as percentage, between the ligand protons and the protein active site, based on the maximum ligand STD signal (H1,H2; 100%). Percentage saturation (75–100%) signifies strong interatomic contacts to the EqBuChE active site. ....	134
Figure 69 - STD amplification factor of compound 6 interaction with AChE as a function of saturation time.....	135
Figure 70 - STD amplification factor of compound 6 with BuChE as a function of saturation time.....	135
Figure 71 - STD-NMR of 4-methoxy-3,4-dihydroisoquinolin-1(2H)-one (6) with both AChE and BuChE, performed at 400 MHz, 15°C, and 3 s saturation time. (A) reference spectrum, (B) STD spectrum of compound (6) (0.8 mM) with AChE enzyme (4μM) and (C) STD spectrum of compound 6 (0.8 mM) with BuChE enzyme (4 μM). Binding epitope of 6 from the STD NMR experiment. The numerical values designate the fraction of saturation as a percentage, between the ligand protons and the protein active site, based on the maximum ligand STD signal (H1,3 of Ar; 100%). ....	137
Figure 72 - Binding mode of compound (6) obtained by docking with hAChE. Hydrogen bonds are shown as green dotted lines, formed between the ligand (6) (green color) with the residues in the active site (grey color). Water molecules in the active site are represented as red spheres. Adapted from [210]. ....	138
Figure 73 - Binding mode of compound 6 obtained by docking with hBuChE. Hydrogen bonds are shown as green dotted lines, formed between the ligand 6 (green color) with the residues in the active site (grey color). Water molecules in the active site are represented as red spheres. Adapted from [210] . ....	138
Figure 74 - STD amplification factor of selected protons of compound 17 as a function of saturation time. ....	139



- Figure 75 - STD-NMR of 1-benzyl-3-hydroxy-3-phenylindolin-2-one (17) with BuChE: (A) reference  $^1\text{H}$  spectrum of 17 with BuChE and (B) STD spectrum of the solution of 17 (5 mM) with BuChE (5  $\mu\text{M}$ ) (3s of saturation time). The relative degree of saturation of the individual hydrogens are mapped into the structure and normalized to that of hydrogen H6. ....140
- Figure 76 - Binding mode for compound 17 interaction with hBuChE. Hydrogen bonds are shown as green dotted lines, formed between compound 17 (green color) with the residues in the active site (grey color). Water molecules in the active site are represented as red spheres. Adapted from [211]. ....140
- Figure 77 - (A) Interaction diagram of compound 17a with hBuChE (PDB file 4TPK); (B) Binding mode for compound 17a with hBuChE (PDB file 4TPK). ....141
- Figure 78 - (A) Interaction diagram of compound 17b with hBuChE (PDB file 4TPK); (B) Binding mode for compound 17b with hBuChE (PDB file 4TPK). ....141
- Figure 79 - Binding mode for compound 17 interaction with hAChE. Hydrogen bonds are shown as green dotted lines, formed between compound 17 (green color) with the residues in the active site (grey color). Adapted from [211]. ....142
- Figure 80 - (A) Interaction diagram of compound 17a with hAChE (PDB file 4EY7); (B) Binding mode for compound 17a interaction with hAChE (PDB file 4EY7). ....143
- Figure 81 - (A) Interaction diagram of compound 17b with hAChE (PDB file 4EY7); (B) Binding mode for compound 17b interaction with hAChE (PDB file 4EY7). ....143
- Figure 82 - STD-NMR of 48a with eeAChE, performed at 400 MHz, 15°C, and 3 s saturation time. (A) reference spectrum, (B) STD spectrum of compound 48a (0.8 mM) with AChE enzyme (4 $\mu\text{M}$ ). Binding epitope of 48a from STD NMR experiment. The numerical values designate the fraction of saturation as a percentage, between the ligand protons and the protein active site, normalized to the maximum ligand STD signal (H19; 100%). ....144
- Figure 83 - (A) Interaction diagram of compound 48a with hAChE; (B) Binding mode for compound 48a interaction with hAChE. ....145
- Figure 84 - STD-NMR of 48a with BuChE, performed at 400 MHz, 15°C, and 3 s saturation time. (A) reference spectrum, (B) STD spectrum of compound 48a (0.8 mM) with BuChE enzyme (4 $\mu\text{M}$ ). Binding epitope of 48a from STD NMR experiment. The numerical values designate the fraction of saturation as a percentage, between the ligand protons and the protein active site, normalized to the maximum ligand STD signal (H2, H14, H16; 100%). ....146
- Figure 85 - (A) Interaction diagram of compound 48a with hBuChE; (B) Binding mode for compound 48a

interaction with hBuChE. ....	146
Figure 86 - Compounds tested for their toxicity with <i>A. salina</i> . ....	157
Figure 87 - Dose-response relation in <i>A. salina</i> , in the presence of potassium dichromate. ....	157
Figure 88 - Dose-response relation in <i>A. salina</i> , in the presence of (A) rasagiline mesylate, (B) pargiline hydrochloride and (C) compound 21. ....	158
Figure 89 - Dose-response relation of AChE in the brain of Swiss mice in the presence of (A) donepezil, (B) galantamine and (C) rivastigmine. ....	159
Figure 90 - Dose-response relation of AChE and BuChE in the liver of swiss mice, in the presence of (A-B) donepezil, ....	160
Figure 91 - Dose-response relation of AChE and BuChE in the liver of swiss mice, in the presence of (A-B) compound 48a, ....	161
Figure 92 - Dose-response relation of MAO –B in the liver of swiss mice, in the presence of (A) compound 48a, ....	162
Figure 93 - In vivo AChE activity in the brain of swiss mice, in the presence of donepezil and compound 48a. Different letters represent values significantly different ( $p < 0.05$ ). ....	163
Figure 94 - In vivo AChE and BuChE activity in the liver of swiss mice, in the presence of donepezil and compound 48a. Different letters represent values significantly different ( $p < 0.05$ ) to each enzymatic activity. ....	164

## List of Schemes

Scheme 1 - Formation of ACh involving choline acetyltransferase, choline and acetic acid. The source of the acetic acid moiety is acetyl coenzyme A. Adapted from [28]. ....	12
Scheme 2 - Reaction mechanism of ACh hydrolysis catalyzed by AChE. Adapted from [44]. ....	17
Scheme 3 - The biosynthetic pathway of norepinephrine and epinephrine. Adapted from [31]. ....	26
Scheme 4 - Proposed reaction mechanisms for amine deamination by MAO-B in the literature. Adapted from [92]. ....	32
Scheme 5 – FAD catalyzed deamination of a primary amine to its corresponding aldehyde. Adapted from [92]. ....	32
Scheme 6 - ATCI hydrolysis by AChE. Adapted from [178]. ....	52
Scheme 7 - Reaction pathway of monoamine metabolism by oxidative deamination by mitochondrial MAO. Adapted from [195]. ....	64
Scheme 8 - Peroxidase assay for MAO-B activity determination. Adapted from [179]. ....	64
Scheme 9 – Horseradish peroxidase assay (showing the catalytic cycle of peroxidase) for MAO-B activity determination by tracing hydrogen peroxide. Adapted from [202]. ....	67
Scheme 10 – Mechanism of action of Rivastigmine on AChE. Adapted from [36]. ....	111

## List of Tables

Table 1 - Drugs approved by INFARMED for PD treatment (used individually or as a combination therapy). ....	40
Table 2 - Kinetic parameters for eeAChE using ATCI as substrate. ....	53
Table 3 - Kinetic parameters for eqBuChE using BTCl as substrate. ....	53
Table 4 – Kinetic parameters for eeAChE (using ATCI as substrate) and eqBuChE (using both ATCI and BTCl as substrates) ....	56
Table 5 - eeAChE IC <sub>50</sub> values of the active ingredients of the commercial drugs used in AD treatment with Tris-HCl 0.05 M, pH 8, measured at 25 °C and 37 °C (with/without pre-incubation at 405 nm). ....	59
Table 6 - eeAChE IC <sub>50</sub> values of the active ingredients of the commercial drugs used in AD treatment with Tris-HCl 0.05 M, pH 8, measured at 25 °C and 37 °C (with/without pre-incubation at 412 nm). ....	59
Table 7 – eeAChE IC <sub>50</sub> values of the active ingredients of the commercial drugs used in AD treatment with phosphate buffer 0.1 M, pH 8 measured at 25 °C and 37 °C (with/without pre-incubation at 405 nm). ....	61
Table 8 - eqBuChE IC <sub>50</sub> values of the active ingredients of the commercial drugs used in AD treatment with Tris-HCl 0.05 M, pH 8, measured at 25 °C (with/without pre-incubation at 405 nm). ....	62



---

<b>Table 9 - Kinetic parameters for MAO-B using benzylamine as substrate. ....</b>	<b>65</b>
<b>Table 11 – Inhibition studies for eeAChE and eqBuChE activities. ....</b>	<b>90</b>
<b>Table 12 - Inhibition studies for eeAChE and eqBuChE activities with oxindole derivatives (continued next page). ....</b>	<b>99</b>
<b>Table 12 - (continued). ....</b>	<b>100</b>
<b>Table 13 - Inhibition studies for eeAChE and eqBuChE with diether-ester derivatives. ....</b>	<b>104</b>
<b>Table 14 – Selectivity index for cholinesterase studies with diether-ester derivatives. ....</b>	<b>107</b>
<b>Table 15 – Inhibition studies for eeAChE and eqBuChE activities with chromanone and chromanol derivatives. ....</b>	<b>110</b>
<b>Table 16 - Inhibition studies of eeAChE and eqBuChE activities with rivastigmine analogues. ....</b>	<b>114</b>
<b>Table A 1 - Analysis of variance (ANOVA) of enzymatic activity of isoquinolinone, azepanone, indolinone, and diether ester derivatives. ....</b>	<b>207</b>
<b>Table A 2 - Analysis of variance (ANOVA) of enzymatic activity of chromanone and chromanol derivatives and rivastigmine analogues. ....</b>	<b>208</b>
<b>Table A 3 - Analysis of variance (ANOVA) of enzymatic activity for the brain and liver of Swiss mice in the presence of compound 48a and donepezil. ....</b>	<b>208</b>







## *Chapter 1*

# *An Overview on Neurodegenerative Diseases*

---

*“Everyone is a genius at least once a year.  
The real geniuses simply have their bright ideas closer together.”*

George Christoph Lichtenberg (1742-1799)



For purposes of better understanding neurodegenerative diseases, this chapter is divided into two main sections. The first section describes general aspects of the brain's anatomy, in order that the reader can easily identify the areas affected by these illnesses, and a brief description of the nervous system function, as well as metabolic pathways of two different neurotransmitters involved in AD and PD. The importance of understanding how these neurotransmitters work and how they are degraded by specific enzymes is crucial for the development of new strategies for treatment of neurodegenerative diseases. The second one is devoted to neurodegenerative diseases, particularly Alzheimer's disease (AD) and Parkinson's disease (PD); including epidemiology, etiology and neuropathological aspects of these disorders. This chapter also comprises a review of the existing therapeutic approaches for AD and PD diseases.

## **1.1. Objectives**

The present thesis has its main focus on the study of biochemical mechanisms in neurodegenerative diseases, involving the relation with the chemical structure of commercial drugs used in AD and PD treatment and different families of synthesized compounds with biological activity, their protein-ligand and molecular interactions and toxicological and pharmacological studies.

## **1.2. Nervous System and Brain**

The Nervous System is responsible for the coordination of many of the activities of the human body. It is divided into the central nervous system (CNS) and the peripheral nervous system (PNS). The CNS is constituted by the brain and the spinal cord, and is surrounded and protected by three connective tissue coverings called meninges. Within the CNS are fluid-filled spaces called ventricles. The bone of the skull and vertebral column surround the brain and spinal cord, respectively. The PNS is constituted by neurons, that divide into sensory neurons (receive information) and motor neurons (transmit information). The autonomic nervous system innervates smooth muscle and glands, whereas the somatic nervous system innervates mainly musculoskeletal structures and the sense organs of skin (Fig. 1) [1].

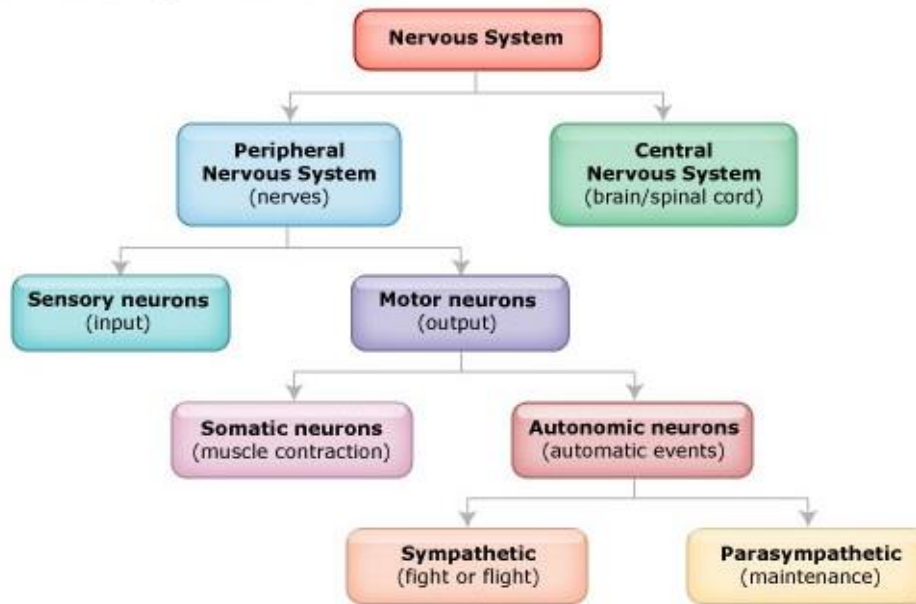


Figure 1 - Nervous system organization. Adapted from [2].

The CNS is composed entirely of two kinds of specialized cells: neurons and glia; while the PNS is only composed by neurons (Fig. 2). Neurons are the anatomical and functional unit of the nervous system, which consists of a nerve cell body, dendrites (which receive signals from other neurons), and an axon (which transmits the signal to another neuron) [1].

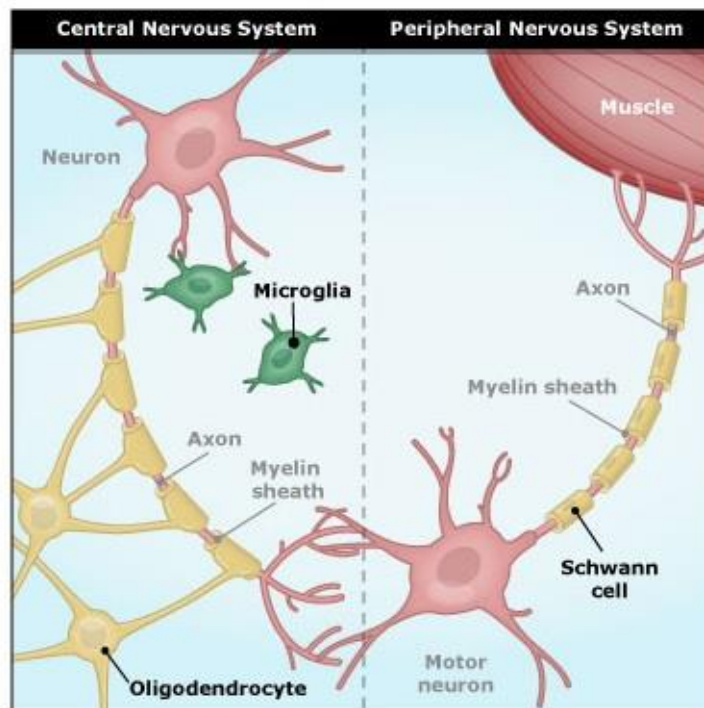


Figure 2 - Cells of the nervous system. Adapted from [3].



Glia (or glial cells) are the cells that provide support to the neurons. These non-neural cells form the interstitial tissue of the nervous system. There are different types of glial cells, which include astrocytes, oligodendrocytes, microglia, ependymal and Schwann cells [1].

The neuron is constituted by four different parts (Fig. 3A): the cell body (or soma), where neuronal proteins are synthesized (Fig. 3B); the dendrites, that receive incoming signals from other neurons; the axon, that allows the flow of the outgoing signal to the axon terminals to another neuron [4].

The cytoskeleton of a neuron consists of fibrillar elements (e.g., neurofilaments and microfilaments) and their associated proteins (Fig. 3B) [4]. In Alzheimer's disease (AD), neurofilaments become modified and form a neurofibrillary tangle [5].

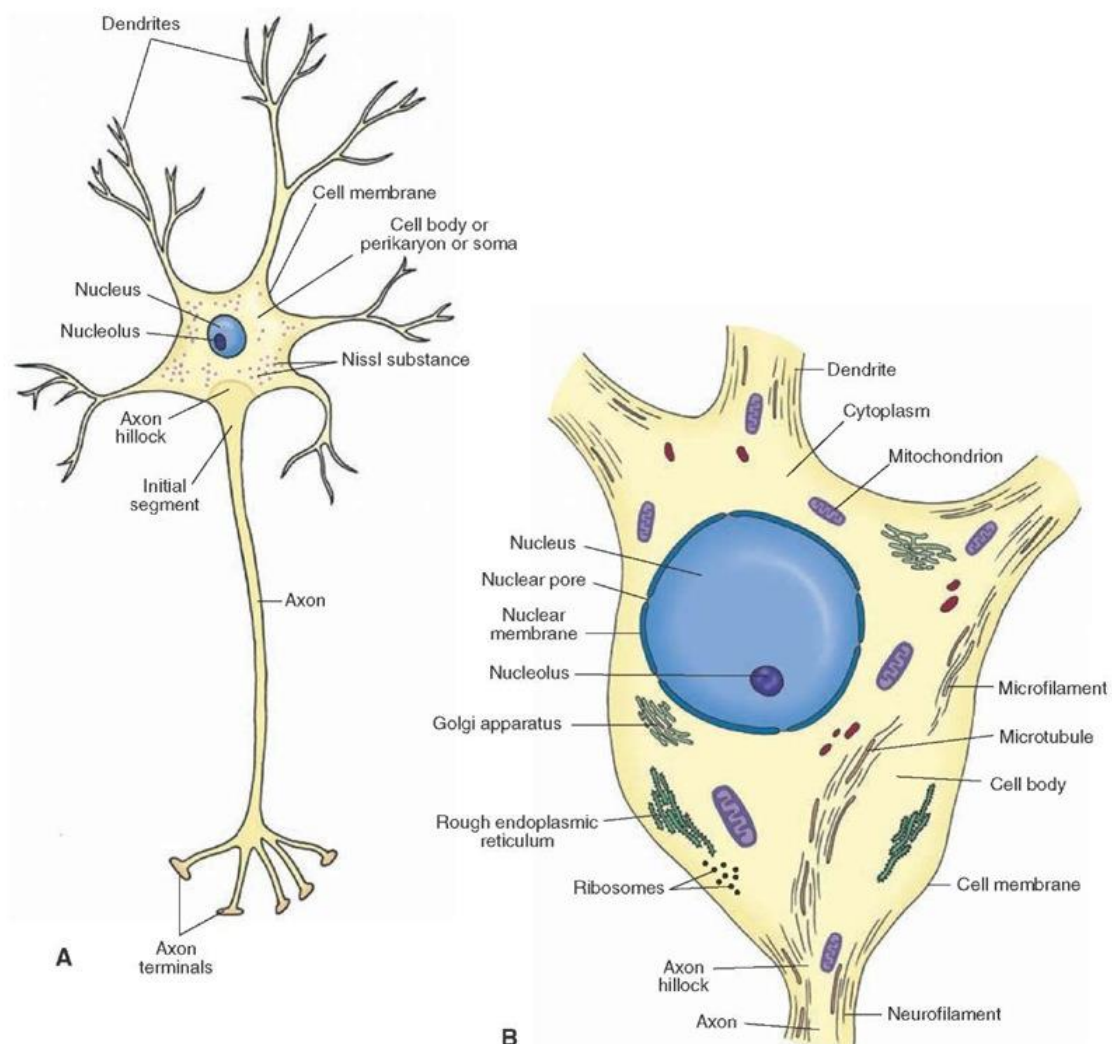


**Figure 3** - Neuron structure. (A) Constitution of a neuron. (B) Components of the neuron: the cell membrane, nucleus, nuclear membrane, nucleolus, and the organelles. Adapted from [4].

To support the general function of the nervous system, neurons have evolved unique capabilities for intracellular and intercellular signaling. To achieve long distance, rapid communication, neurons have evolved special abilities for sending electrical signals (action potentials) along axons. This mechanism, called conduction, is how the cell body of a neuron communicates with its own terminals via the axon. Communication between neurons is achieved at synapses by the process of neurotransmission [6].

Neurotransmission (or synaptic transmission) is communication between neurons as accomplished by the movement of chemicals or electrical signals across a synapse.

At electrical synapses, two neurons are physically connected to one another through gap junctions. Gap junctions permit changes in the electrical properties of one neuron to affect the other, and vice versa, so the two neurons essentially behave as one. Electrical synapses are not common in the nervous system, but they exist between adjacent cardiac muscle cells. These types of synapses are also important in many types of smooth muscle (i.e. stomach walls, blood vessels walls) [7].

Electrical neurotransmission is the communication between two neurons at electrical synapses [8]. Chemical neurotransmission occurs at chemical synapses (Fig. 4). In chemical neurotransmission, the presynaptic neuron and the postsynaptic neuron are separated by a small gap — the synaptic cleft. The synaptic cleft is filled with cerebrospinal fluid (CSF). The synaptic cleft creates a physical barrier for the electrical signal carried by one neuron to be transferred to another neuron. The neurotransmitter acts like a chemical messenger, thereby linking the action potential of one neuron with a synaptic potential in another [9]. In Figure 4 we can see that when an action potential reaches the presynaptic terminal, voltage-gated  $\text{Ca}^{2+}$  channels open, and  $\text{Ca}^{2+}$  moves into the cell. This influx of  $\text{Ca}^{2+}$  causes the release of neurotransmitters by exocytosis from the postsynaptic terminal. The neurotransmitters diffuse across the synaptic cleft and bind to specific receptor molecules on the postsynaptic membrane. The binding of neurotransmitters to these membrane receptors causes chemically gated channels for  $\text{Na}^+$ ,  $\text{K}^+$  or  $\text{Cl}^-$  to open or close in the postsynaptic membrane, depending on the type of neurotransmitter in the presynaptic terminal and the type of receptors on the postsynaptic membrane. The response maybe either stimulation or inhibition of an action potential in the postsynaptic cell. For example, if a  $\text{Na}^+$  channels opens, the postsynaptic cell becomes depolarized, and an action potential will result if a threshold is reached. If  $\text{K}^+$  or  $\text{Cl}^-$  channels open, the inside of the postsynaptic cell tends to become more negative, or hyperpolarized, and an action potential is inhibited from occurring [7].

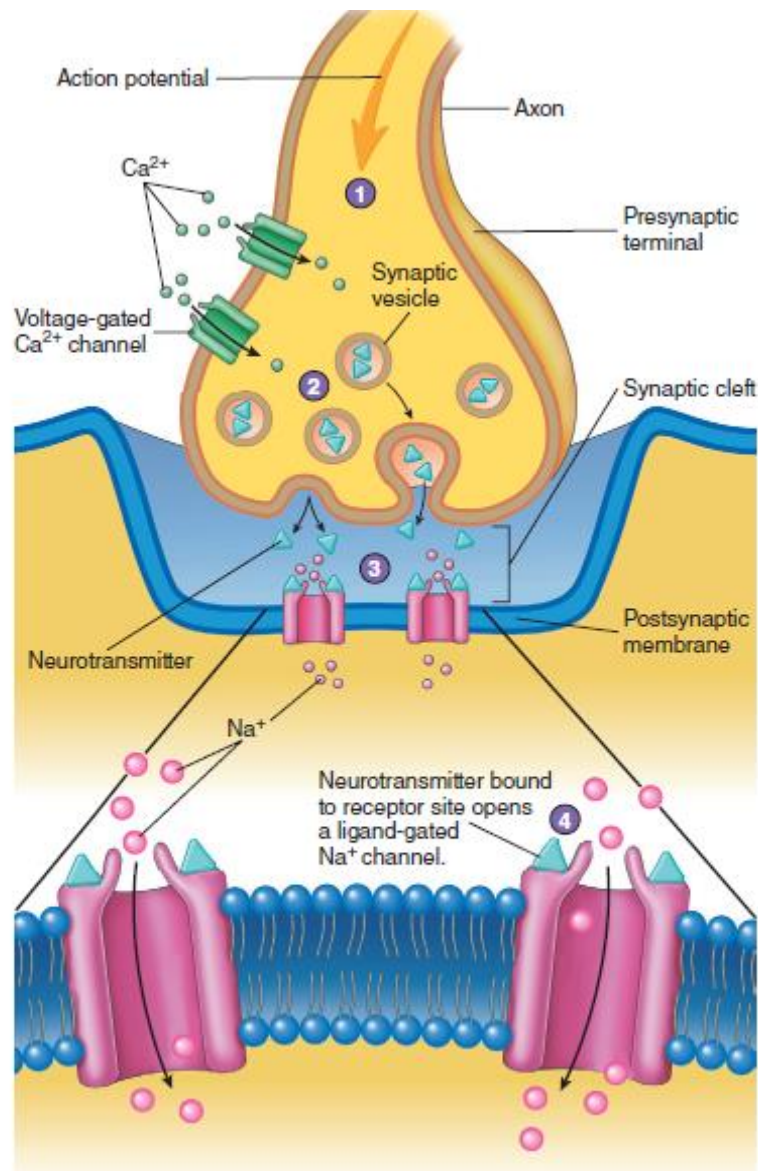


**Figure 4** – A chemical synapse: 1- Action potentials arriving at the presynaptic terminal cause voltage-gated  $\text{Ca}^{2+}$  channels to open; 2-  $\text{Ca}^{2+}$  diffuses into the cell and causes synaptic vesicles to release neurotransmitter molecules; 3- Neurotransmitter molecules diffuse from the presynaptic terminal across the synaptic cleft; 4- Neurotransmitter molecules combine with their receptor sites and cause ligand-gated  $\text{Na}^{+}$  channels to open.  $\text{Na}^{+}$  diffuses into the cell (shown in illustration) or out of the cell (not shown) and causes a change in membrane potential. Adapted from [10].

The decrease in the neurotransmitter acetylcholine which is involved in AD (see section 1.3.1.1.) and the decrease in the neurotransmitter dopamine that is involved in PD (see section 1.3.2.1.) cause a decrease in chemical synapses.

The brain is the part of the central nervous system (CNS) that is contained within the cranial cavity.

It's major regions are the cerebrum, the cerebellum, the brainstem and the diencephalon (Fig. 5) [7].

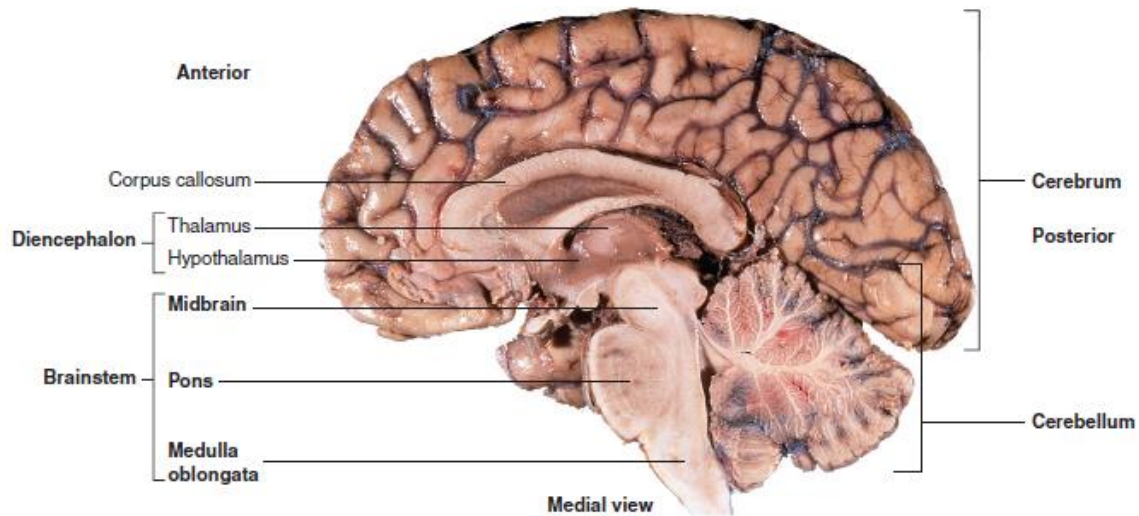


**Figure 5** - Regions of the brain. Medial view of a mid-sagittal section of the right half of the brain. Adapted from [10].

The cerebellum controls muscle movement, governs balance and is involved in learning motor skills [10].

The diencephalon connects the brainstem to the cerebrum and is divided into two parts: the thalamus and the hypothalamus. The thalamus is responsible for relaying and integrating information to different regions of the cerebral cortex from a variety of structures associated with sensory, motor, autonomic, and emotional processes. The hypothalamus roles include the regulation of a host of visceral functions, such as temperature, endocrine functions, feeding, drinking, emotional and sexual behaviors [11].

The brainstem connects the spinal cord to the cerebrum and consists of the *medulla oblongata*, pons and midbrain. The medulla oblongata functions as center for vital reflexes, such as those involved in regulating heart rate, blood vessel diameter, breathing, coughing, sneezing, swallowing, vomiting, balance and coordination [10]. The pons relay information between the cerebrum and the cerebellum and is also involved, along with medulla oblongata, in controlling balance, breathing and swallowing. The midbrain is involved in visual reflexes and receive touch and auditory input. The *substantia nigra* is part of the *basal nuclei*, which comprises the midbrain, the diencephalon and the cerebrum, and is involved in general body movement [7]. Damage to this region results in motor dysfunctions such as dyskinesias (i.e., disorders of movement at rest). Other prominent structures of the *basal nuclei* are the *caudate nucleus*, *putamen*, and *globus pallidus* [11].

The cerebrum is the largest part of the brain. It is divided into left and right hemispheres by a longitudinal fissure. On the surface of each hemisphere are numerous folds called *gyri* (sing. *gyrus*) which increase the surface area of the cortex, and intervening grooves called *sulci* (sing. *sulcus*) [7]. Each cerebral hemisphere is divided into four lobes: frontal lobe, parietal lobe, occipital lobe and temporal lobe. Analysis of Figure 6 shows the major structures that include the central sulcus, the precentral *gyrus* (primary motor) and postcentral *gyrus* (primary somatosensory). The cortex consists of both cells and nerve fibers. The cellular components constitute the gray matter<sup>1</sup> of cortex and the nerve fibers constitute the white matter<sup>2</sup> of the cortex [11].

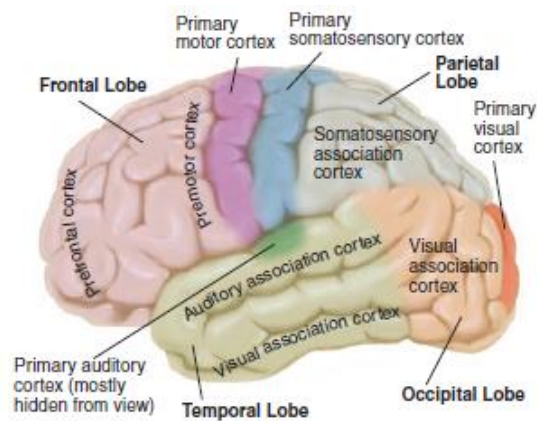


**Figure 6** – Lateral view of the left cerebral hemisphere, showing the lobes, as well as the motor and sensory regions of the cerebral cortex. Adapted from [12].

The lobes of the cerebral cortex integrate motor, sensory, autonomic, and intellectual processes. The frontal lobe is important in the control of voluntary motor functions, motivation, aggression, mood and olfactory reception. The parietal lobe is the principal center for receiving and consciously perceiving most sensory information, such as pain, touch, balance and temperature. The frontal and parietal lobes are separated by the central sulcus. The occipital lobe functions in receiving and perceiving visual input and is not distinctly separate from the other lobes. The temporal lobe is involved in olfactory (smell) and auditory (hearing) functions and plays an important role in memory [10].

<sup>1</sup>The gray matter consists mainly of neuronal cell bodies (nuclei) and lacks myelinated axons.

<sup>2</sup>The white matter consists of a large number of myelinated axons (largely lipid membranes that wrap around the axons).

Although the two cerebral hemispheres perform somewhat different functions, the human being perceptions and memories are unified. This unity is accomplished by the corpus callosum, a large band of axons that connects corresponding parts of the cerebral cortex of the left and right hemispheres: The left and right temporal lobes are connected, the left and right parietal lobes are connected, and so on. Because of the *corpus callosum*, each region of the association cortex knows what is happening in the corresponding region of the opposite side of the brain [12].

### 1.3. Neurodegenerative diseases

More than 600 disorders are related to the brain and the nervous system. Neurodegenerative diseases are defined as hereditary and sporadic conditions which are characterized by progressive nervous system dysfunction. These disorders are often associated with atrophy of the affected central or peripheral structures of the nervous system (Fig. 7). They include diseases such as Alzheimer's Disease and other dementias, Brain Cancer, Degenerative Nerve Diseases, Encephalitis, Epilepsy, Genetic Brain Disorders, Head and Brain Malformations, Hydrocephalus, Stroke, Parkinson's Disease, Multiple Sclerosis, Amyotrophic Lateral Sclerosis (ALS or Lou Gehrig's Disease), Huntington's Disease, Prion Diseases, among others [13, 14].

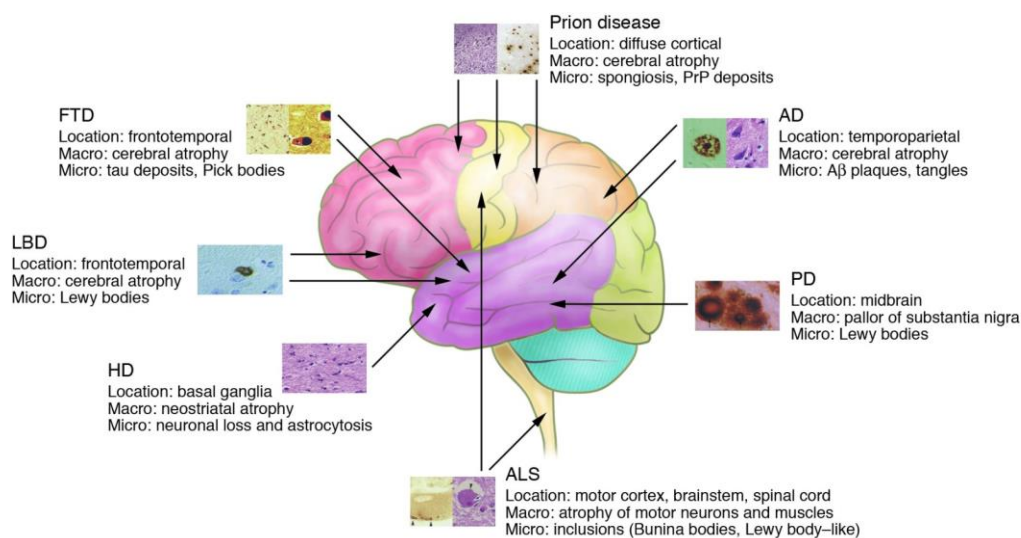


**Figure 7** - Overview of the anatomical location, macroscopic and microscopic changes characteristic of neurodegenerative disorders. Note that the full neuropathological spectrum of these disorders is much more complex than depicted here. When there is more than one characteristic histopathological feature, these are depicted from left to right, as indicated in the labels listing microscopic changes (e.g., the 2 panels for AD depict an Aβ plaque [left] and neurofibrillary tangles [right]). AD-Alzheimer disease; PD-Parkinson disease; ALS-Amyotrophic lateral sclerosis; HD-Huntington disease; LBD-Lewy body dementia; FTD-Frontotemporal dementia. Adapted from [14].

---

Neurodegenerative disorders will become a major challenge for medicine and public health in future years because of demographic changes worldwide. AD, PD, and ALS share two main characteristics: (1) the incidence and prevalence increase with age; (2) most cases are sporadic, although are familial, including monogenetic forms with early age of onset under 50 years old [15]. The number of people living with neurodegenerative disorders has increased worldwide, mainly because of population ageing. The associated increase in demand for care raises two main types of economic questions. First, the increasing societal costs due to neurodegenerative disorders are becoming a major health policy issue. Costs-of-illness studies investigate the level of care expenditures and the main drivers for these expenditures. Second, studies of the organization of care giving point out the importance of informal caregivers who are the main care providers for most community-dwelling patients: it has been estimated that informal care time represents 80% of total care in AD [16].

### **1.3.1. Alzheimer's Disease**

Alzheimer's disease (AD) was discovered by Alois Alzheimer in 1907 [17]. AD, the most common cause of dementia [18], is a neurodegenerative disorder characterized by progressive decline of memory and cognition [19]. Biochemical changes affecting multiple pathways contribute to AD pathology. Neuropathologically, it is characterized by the presence of amyloid- $\beta$  plaques ( $A\beta$ ) between nerve cells in the brain and neurofibrillary tangles (NFT) [5].

Familial Alzheimer's disease is a very rare autosomal dominant disease with early onset, caused by mutations in the amyloid precursor protein and presenilin genes, both linked to  $A\beta$  metabolism [20]. By contrast with familial disease, sporadic Alzheimer's disease is very common with more than 15 million people affected worldwide. The cause of the sporadic form of the disease is unknown, probably because the disease is heterogeneous [21], caused by ageing in concert with a complex interaction of both genetic and environmental risk factors [5].

As Alzheimer's disease progresses, brain tissue shrinks. However, the ventricles, chambers within the brain that contain cerebrospinal fluid, are noticeably enlarged. In the early stages of Alzheimer's disease, short-term memory begins to decline when the cells in the hippocampus degenerate. Those with the disease lose the ability to perform routine tasks. As Alzheimer's disease spreads through the cerebral cortex (the outer layer of the brain), judgment worsens, emotional outbursts may occur and language is impaired. Advancement of the disease leads to the death of more nerve cells and subsequent changes in behavior, such as wandering and agitation [22, 23]. In the final stages, people

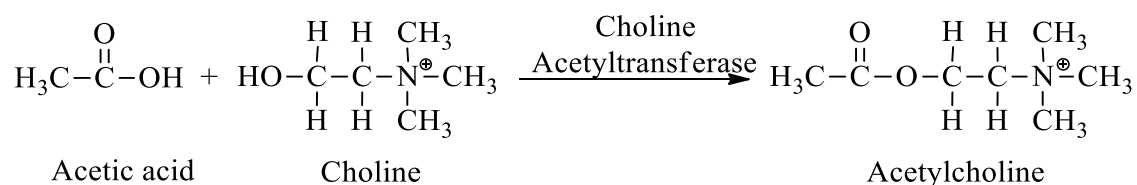
may lose the ability to feed themselves, speak, recognize people and control bodily functions. Memory worsens and may become almost non-existent, and eventually death [24]. Constant care is typically necessary. About 20% of individuals over 80 years are affected by the disease. The annual incidence of AD increases with age, ranging from 1% to 8% for people with 65 to 85 years old [25]. The incidence in women is slightly higher than in men [26]. On average, those with Alzheimer's live for 8 to 10 years after diagnosis, but this terminal disease can last for as long as 20 years [25].

In this section several hypotheses are reviewed that try to explain this multifactorial disorder, as well as a summary of therapeutic strategies related with the pathophysiological mechanisms of AD.

### 1.3.1.1. Cholinergic Neurotransmission

Acetylcholine (ACh) is the neurotransmitter substance at most parasympathetic neuroeffector junctions, autonomic ganglia, the adrenal medulla, somatic myoneural junctions, and certain CNS regions [27-29].

ACh is synthesized within cholinergic nerves by the enzymatic transfer of an acetyl group from acetyl coenzyme A to choline. This reaction is catalyzed by the enzyme choline acetylase (also referred to as choline acetyltransferase) (Scheme 1). The acetyl coenzyme A (AcetylCoA) is formed by the action of an enzyme, acetyl kinase, which mediates the transfer of an acetyl group from adenylylacetate (formed from acetate and ATP) to the coenzyme A molecule. Choline is transported from the extracellular fluid into the cholinergic nerve by an energy-requiring axoplasmic uptake process. ACh is stored within the axonal vesicular structures in a concentrated solution or bound to the membrane or both.



**Scheme 1** - Formation of ACh involving choline acetyltransferase, choline and acetic acid. The source of the acetic acid moiety is acetyl coenzyme A. Adapted from [28].

ACh is released from the nerve terminal upon arrival of an axonal action potential. ACh within the junctional spaces is rapidly inactivated by hydrolysis by a specific enzyme, acetylcholinesterase



(AChE, EC 3.1.1.7). AChE is present in cholinergic nerves, autonomic ganglia, and neuromuscular and neuroeffector junctions [30]. A somewhat similar enzyme, pseudocholinesterase or butyrylcholinesterase (BuChE, EC 3.1.1.8), is present in serum and other body tissues [31].

The mechanism of cholinergic neurotransmission is summarized in Figure 8. Briefly, glucose arrives through the nerve terminal by facilitated diffusion, glycolysis occurs in the neuronal cytoplasm, and pyruvate molecules are generated. Pyruvate is transported into the mitochondria, and an acetyl group derived from pyruvic acid combines with coenzyme-A present in the mitochondria to form acetylcoenzyme-A, which is transported back into the cytoplasm [32]. Choline, the precursor for ACh, is actively transported into the neuronal terminal from the synaptic cleft via Na<sup>+</sup> (sodium) and choline transporters. ACh is synthesized in the cytoplasm of the nerve terminal from choline and acetylcoenzyme-A in the presence of an enzyme, choline acetyltransferase. ACh is then transported into vesicles and stored there. It is then released into the synaptic cleft by exocytosis and hydrolyzed by acetylcholinesterase. High concentrations of an enzyme, acetylcholinesterase, are present on the outer surfaces of the nerve terminal (prejunctional site) and the effector cell (postjunctional site). Acetylcholinesterase is synthesized in the endoplasmic reticulum of neuronal cell bodies and major dendrites and is transported to the presynaptic terminal membrane by microtubules. This enzyme hydrolyses ACh in the junctional extracellular space; choline liberated in this reaction re-enters the nerve terminal and is again used for the synthesis of ACh.

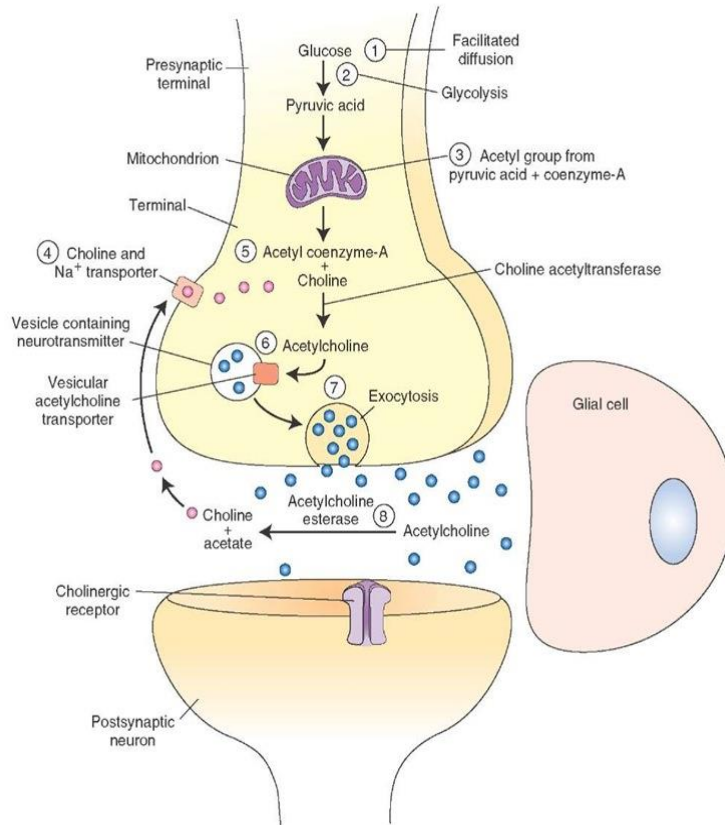


**Figure 8 – Cholinergic neurotransmission:** 1. Facilitated diffusion of glucose; 2. Glycolysis; 3. Acetyl group derived from pyruvic acid combines with coenzyme-A; 4. Active transport of choline; 5. Acetylcholine is synthesized; 6. Acetylcholine is then transported into vesicles and stored there; 7. Exocytosis of Acetylcholine; 8. Acetylcholinesterase hydrolyze acetylcholine to choline and acetate. Adapted from [6, 32].

There are two basic types of cholinergic receptors with the peripheral efferent autonomic nerve tracts: nicotinic and muscarinic. Early studies demonstrated that small doses of nicotine mimicked certain actions of ACh, and large doses inhibited the same ACh responses. The nicotinic responsive sites were found to be present in autonomic ganglia, adrenal medullary chromaffin cells, and also the neuromuscular junctions of the somatic nervous system. Accordingly, these sites have been referred to as nicotinic cholinergic receptors.

However, nicotine does not simulate or block the action of ACh at the parasympathetic neuroeffector junctions in heart muscle, smooth muscle, or secretory glands. The plant alkaloid muscarine was found to simulate the activity of ACh at these sites but not at the previously described

nicotinic receptors. Muscarinic receptors therefore designate the type of receptor present at cholinergic neuroeffector junctions in muscle and glands [33].

A nicotinic response usually denotes an excitatory response, whereas muscarinic receptor activation may elicit an excitatory or inhibitory response, depending on the tissue. This seems to be related to either a general increase in permeability to all ions (depolarization-excitatory) or a selective increase in permeability to small ions like  $K^+$  (hyperpolarization-inhibitory) respectively [33, 34].

### 1.3.1.2. Catalytic reaction mechanism of AChE and BuChE

Cholinesterases are serine hydrolases. AChE is located at neuromuscular junctions and the CNS on the outside of post-synaptic cell membrane, mainly in a tetrameric form [35], although it also exists as a monomer in lower amounts [36]. BuChE is found mostly in plasma as a soluble monomer secreted by glial cells [37], but is also present in intestine, liver and lung [38]. These two cholinesterases share 65% homology and a similar hydrophobic active site structure. Their main difference lies on two aromatic residues (Phe295 and Phe297) present in AChE, that constrict its gorge, giving AChE and BuChE different specificities [37, 39]. Figure 9 shows the three-dimension structures of human acetylcholinesterase (A) and butyrylcholinesterase (B).

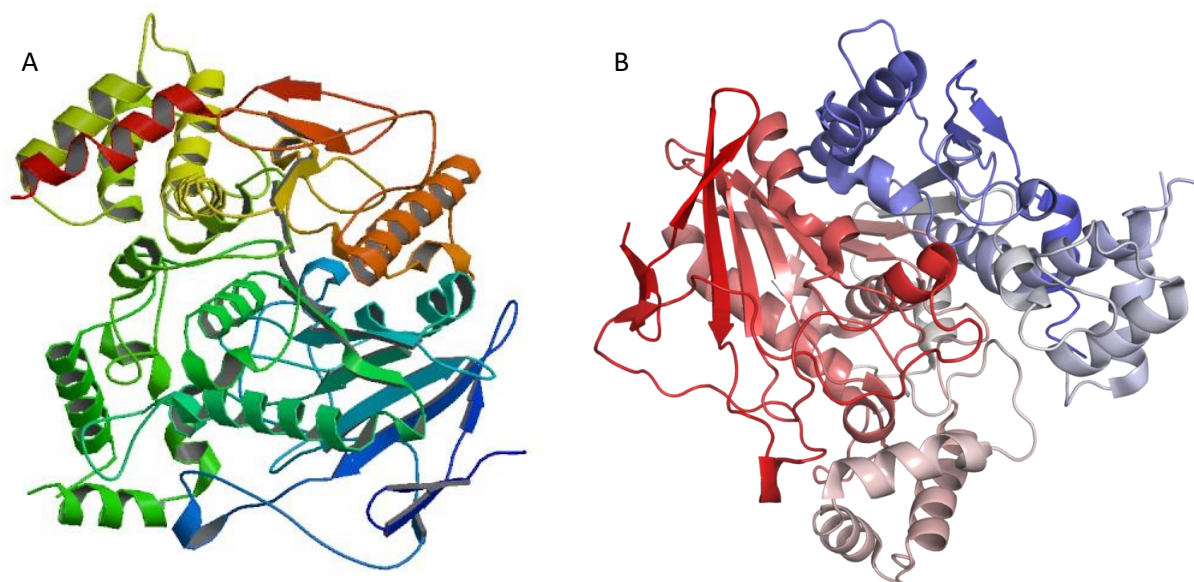


**Figure 9** – Ribbon diagram based on the X-ray crystallography structures of (A) human AChE (Protein Data Bank ID: 4PQE) and (B) human BuChE (Protein Data Bank ID: 4POI).

Figure 10 illustrates both AChE and BuChE active site with homologous residues. The active site of human AChE (*hAChE*) is located at the base of a long gorge of 20 Å and consists of two subsites [40-42]. An “esteratic” subsite includes the catalytic triad (side chains of Ser203, His447, and Glu334) and the oxyanion hole (peptidic NH groups of Gly121, Gly122, and Ala204) and is the essential catalytic functional unit of AChE [40-43]. The “anionic” subsite is formed by side chains of Glu202, Trp86, and Tyr337 and is mainly responsible for binding the quaternary trimethylammonium tail group of ACh [44, 45].

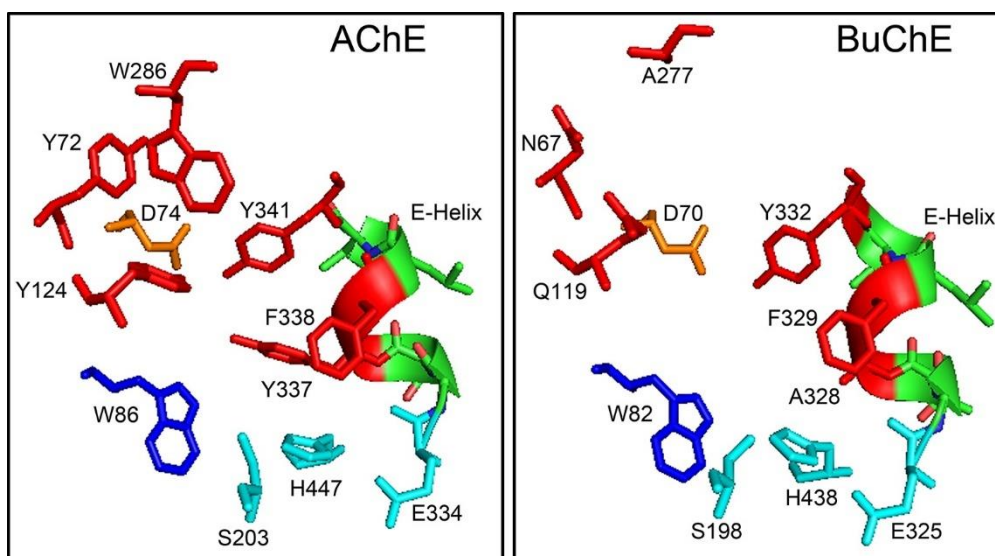
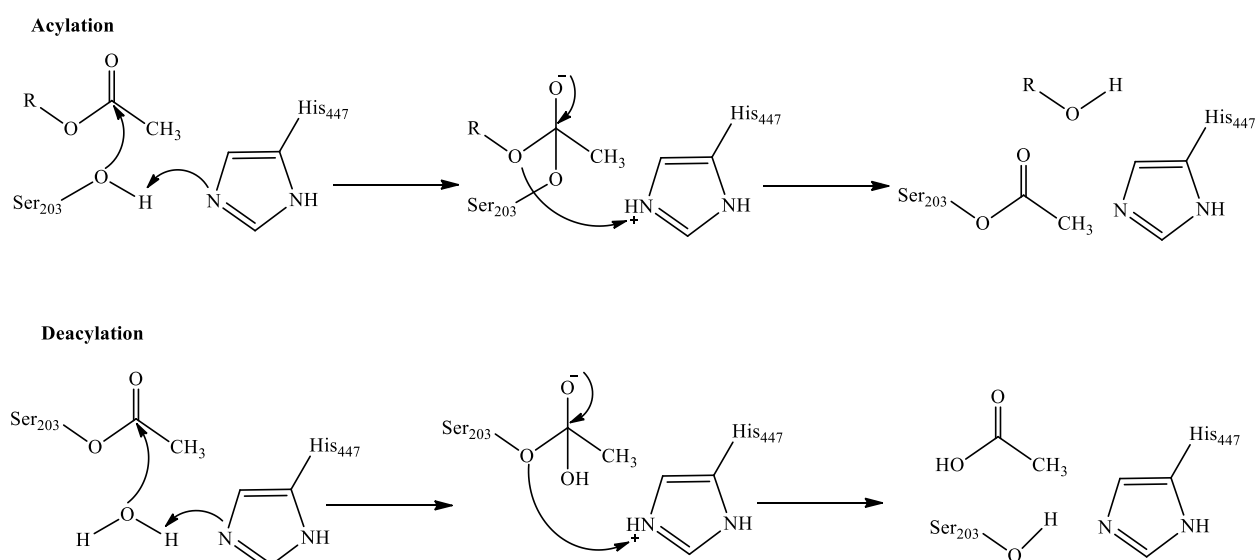


**Figure 10** - Stick representation of the active site gorge with homologous residues shown for *hAChE* (Protein Data Bank ID: 1B41) and *hBuChE* (Protein Data Bank ID: 1POI). Adapted from [46].

The active site of human BuChE (*hBuChE*) is located at the base of a long gorge of 20 Å, whose catalytic triad is composed by Ser198, His438, and Glu325. The oxyanion hole comprises Gly116, Gly117, and Ala199. The acyl pocket, which accommodates the acyl group of substrates, is comprised of residues Leu286 and Val288. The central residue of the choline binding site at the bottom of the gorge is Trp82. Substrates are bound between these two subsites [39].

AChE is one of the most efficient enzymes in nature and catalyzes the hydrolysis of the neurotransmitter acetylcholine (ACh) with a reaction rate close to the diffusion-controlled limit [43]. Like many other members of the serine hydrolase and serine protease families [47, 48], the catalytic process of AChE [43] has been suggested to proceed in two successive stages, acylation and deacylation, as shown in Scheme 2. AChE employs the catalytic triad (Ser203, His447, and Glu334)

as the essential catalytic functional unit. Ser203 serves as a nucleophilic attacking group to initiate the whole ACh hydrolysis process, and His447 is generally assumed to act like a general acid-base element in both acylation and deacylation stages. The main catalytic role of Glu334 is to stabilize the positive charge on the imidazole ring of His447 at transition states and intermediates through electrostatic interactions [30].



**Scheme 2** - Reaction mechanism of ACh hydrolysis catalyzed by AChE. Adapted from [44].

The physiological role of BuChE remains unclear [49, 50]. Although it is capable of hydrolyzing ACh, so far, no endogenous natural substrate has been described for this enzyme. BuChE is relatively abundant in plasma (3 mg/L) and can degrade a large number of ester-containing compounds [51]. Due to its characteristics, this enzyme plays an important pharmacological and toxicological role that can be used as a prophylactic scavenger against neurotoxic organophosphates such as the nerve gas soman [52-55].

### 1.3.1.3. Cholinergic hypothesis

The nature of the cholinergic system makes it important in determining the clinical manifestations of AD, as well as its response to treatment. The cholinergic system is the most affected in AD because it is the location of the neurons responsible for cognitive functions, like memory and learning (Fig. 11) [56].

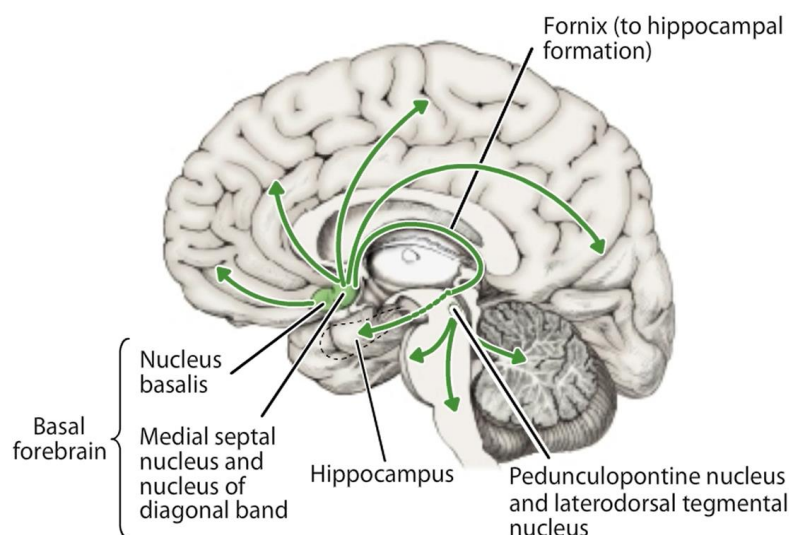


**Figure 11** - Cholinergic pathway. Adapted from [57].

The basal forebrain includes major groups of cholinergic cells in the medial septal nucleus, the nucleus of the diagonal band and the *nucleus basalis*. These cholinergic cells project to the hippocampus and amygdala as well as throughout the cerebral cortex. A smaller group of cholinergic cells in the pedunclopontine and laterodorsal tegmental nuclei project to the reticular formation and thalamus, and are believed to be involved in arousal and the sleep/wake cycle [57]. Cholinergic systems in the cortex are crucial for learning and memory, and wide spread loss of these cells is a characteristic of AD, so it is believed that there is a direct connection between basic cerebral functions and the decrease of ACh [58]. These discoveries lead to the cholinergic hypothesis, that postulates that the cognitive decline associated to AD and aging is the result of loss of cholinergic function in the CNS [58, 59]. According to the cholinergic hypothesis there is an irreversible deficiency in cholinergic functions in the brain that leads to memory impairment of patients with AD [56]. However, one of the major therapeutic strategies adopted for primarily symptomatic AD is based on the cholinergic hypothesis targeting cholinesterase enzymes [60, 61].

### 1.3.1.4. Amyloid- $\beta$ hypothesis and the Amyloid Precursor Protein

One of the hallmarks of Alzheimer's disease is the accumulation of amyloid plaques between neurons. The amyloid hypothesis states that a 42-amino-acid form of  $A\beta$  ( $A\beta_{42}$ ) becomes harmful when, owing to its overproduction or reduced clearance from the brain, individual  $A\beta_{42}$  monomers come together in various numbers and conformations to form soluble oligomers and insoluble fibrils. Amyloid- $\beta$  is a fragment of a protein snipped from another protein called amyloid precursor protein (APP) (Fig. 12).

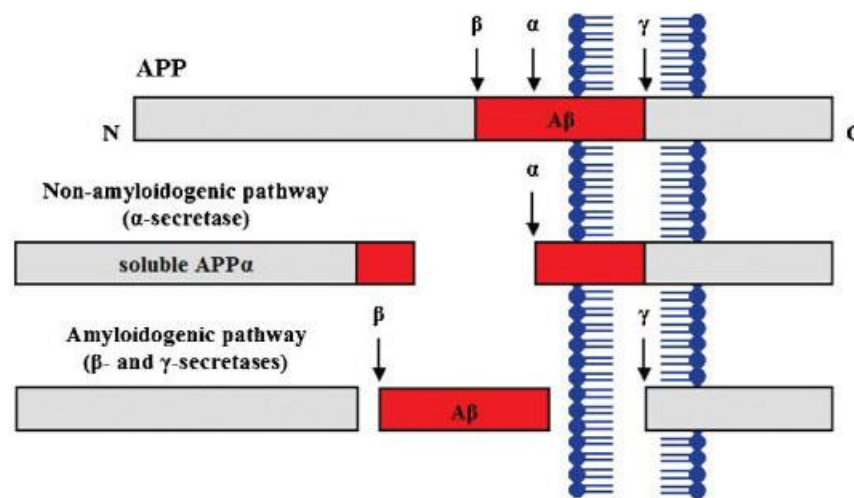


**Figure 12** - Schematic diagram illustrating proteolytic cleavage of the amyloid precursor protein (APP). Adapted from [62].

In the non-amyloidogenic pathway,  $\alpha$ -secretase cleaves APP within the  $A\beta$  domain to liberate two peptides, including the neuroprotective soluble  $APP\alpha$ , whereas in the amyloidogenic pathway,  $\beta$ - and  $\gamma$ -secretases cleave APP sequentially in the N- and C-terminal portions of the  $A\beta$  region, producing  $A\beta_{42}$  peptide and initiating neurodegenerative activity [62]. In a healthy brain, the APP protein fragments would break down and be eliminated. In AD the  $A\beta_{42}$  fragments aggregate to trigger a cascade of neurobiological events, including: certain inflammatory responses; aggregation, phosphorylation and propagation of protein tau ( $\tau$ ) that is associated with microtubules. These events contribute to the formation of  $A\beta$  plaques and  $\tau$ -containing tangles (Fig. 13). Affected neurons and synapses become dysfunctional and can die, leading to additional inflammatory responses. Loss of neurons and the synaptic connections between them is associated with cognitive decline and disability, and other features of AD [63].

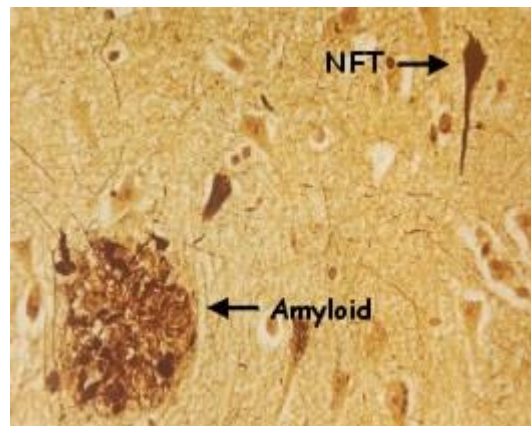


**Figure 13** – Histological cut formation of amyloid plaques and neurofibrillary tangles (NFTs). Adapted from [64].

A common feature of most Familial Alzheimer's Disease (FIAD) mutations is an increase in the generation of A $\beta$  peptides, particularly A $\beta_{42}$ . Mutations associated with early-onset FIAD are found in the APP gene itself on chromosome 21, in presenilin-1 (PSEN1) gene on chromosome 14 and in presenilin-2 (PSEN2) gene on chromosome 1 [65]. Ubiquilin, a ubiquitin-like protein, interacts with PSEN2 and is believed to promote presenilin protein accumulation. FAD genetics and mouse models have shed light on early-onset AD pathogenesis, but the vast majority of AD cases occur late in life. The 4 allele of the apolipoprotein E (ApoE) gene (ApoE  $\epsilon$ 4 variant) is a major risk for late-onset AD (LOAD) compared to the ApoE  $\epsilon$ 2 and ApoE  $\epsilon$ 3 variants [66]. ApoE mediates binding, internalization and catabolism of lipoprotein particles via interaction with members of the low density lipoprotein receptor (LDLR) family. The basic functions of ApoE in normal brain and the role of ApoE in neurodegenerative disease remain unknown. It is thought the full length and soluble forms of the ApoE receptors alter APP processing and A $\beta$  clearance, thus contributing to AD pathogenesis.

Down's syndrome (DS) patients, who have an extra copy of the APP gene on chromosome 21, and FIAD families with a duplicated APP gene locus, exhibit total A $\beta$  overproduction and all develop early-onset AD. In FIAD, the A $\beta_{42}$  increase is present years before AD symptoms arise, suggesting that A $\beta_{42}$  is likely to initiate AD pathophysiology [67, 68]. Figure 14 represents the normal processing of APP as well as missense mutations associated to FIAD. These mutations (indicated by the yellow burst symbols) either interfere with  $\alpha$ -secretase or enhance  $\beta$ - or  $\gamma$ -secretase cleavage, resulting in an increase in the production of the toxic A $\beta_{42}$  peptide rather than the wild-type A $\beta_{40}$  peptide. The thickness of the arrows represents the amount of each peptide being made relative to the other peptides. The mutation of Ala692 to Gly692 favors the cleavage of the APP gene by  $\beta$ - and  $\gamma$ -secretase, increasing the production of A $\beta_{40}$  and A $\beta_{42}$  instead of the normal APP $\alpha$ . The mutation of Val717 to Gly, Ile, or Phe increases the production of A $\beta_{42}$  neurotoxic form.



Importantly, in specific transgenic mouse models of AD the lack of  $A\beta_{42}$  correlates with the absence of neuronal loss and improved cognitive function [69]. Such data provides direct evidence for the amyloid hypothesis in vivo, and also indicates that  $A\beta_{42}$  is directly responsible for neuronal death [70].

Drugs with selectivity for certain secretases might reduce or eliminate the processing of  $\beta$ -amyloid precursor protein to the toxic  $A\beta_{42}$  and therefore can contribute to prevent Alzheimer's disease or to avoid its progression.[71]

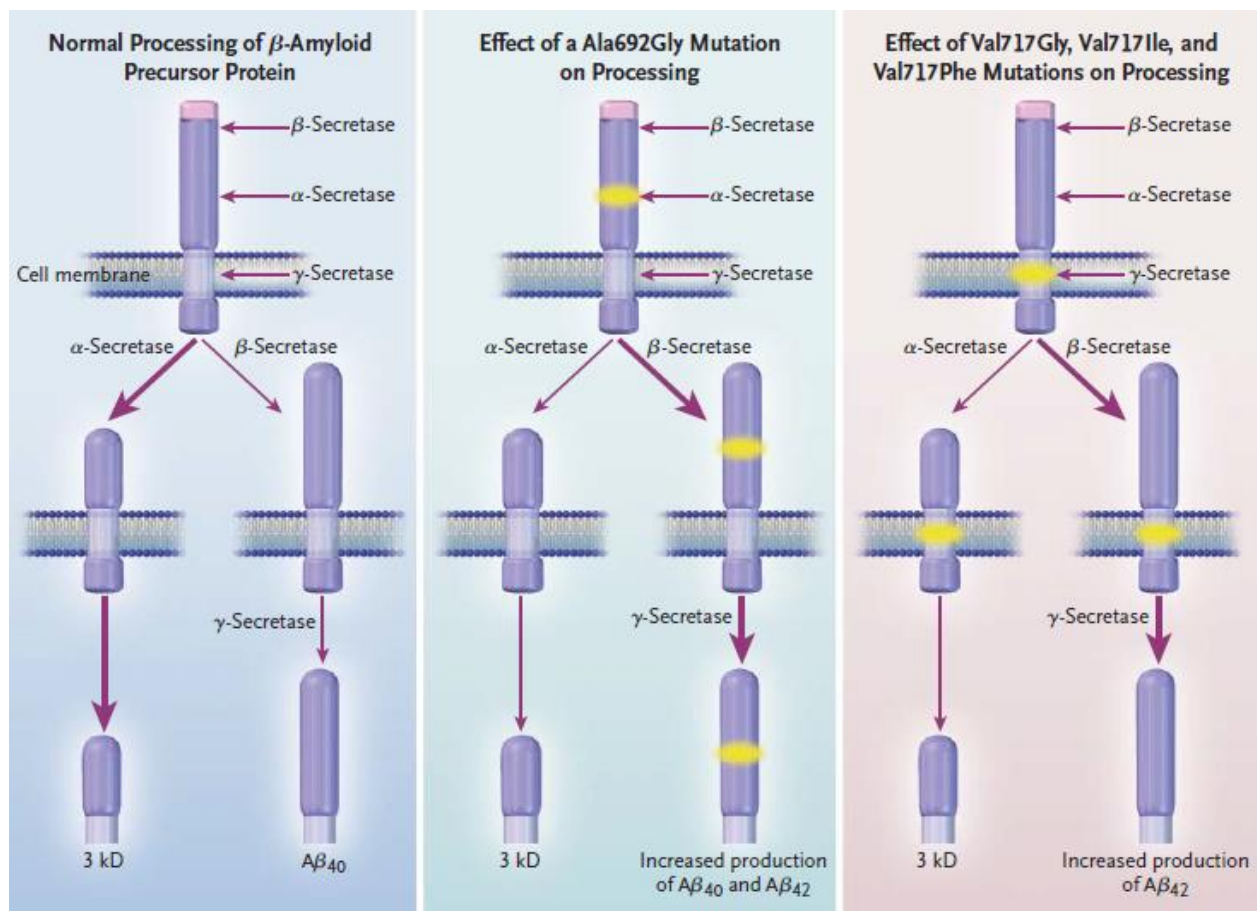


**Figure 14** - The normal processing of  $\beta$ -amyloid precursor protein as well as the effect on processing of alterations in the protein resulting from missense mutations associated with early-onset familial Alzheimer's disease. Adapted from [71].

### 1.3.1.5. Hyperphosphorylation of Tau ( $\tau$ ) protein

Another focus in AD research centers on inflammation caused by neurofibrillary tangles (NFT), which are insoluble twisted fibers found inside the brain's nerve cells. They primarily consist of a protein called Tau ( $\tau$ ), which forms part of a microtubule. The microtubule helps transport nutrients and other important substances from one part of the nerve cell to another [72]. In Alzheimer's disease the  $\tau$  protein is abnormal and the microtubule structures collapse. Hyperphosphorylation of *tau* reduces its binding affinity to microtubules, thus disrupting the structural organization and maintenance. Excess levels of unbound  $\tau$  protein leads to the formation of *tau* aggregates, insoluble fibrils, and intracellular neurofibrillary tangles observed in AD and other tauopathies (Fig. 15) [73].

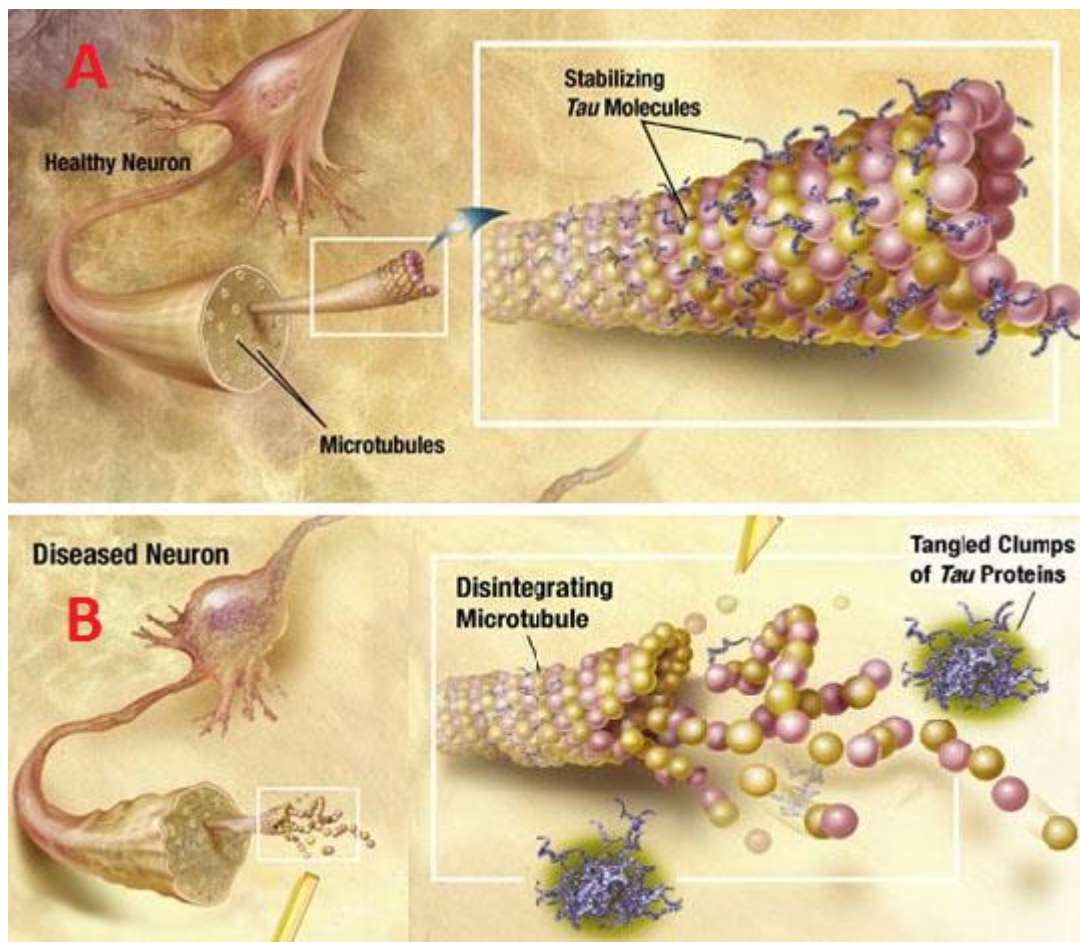


**Figure 15** – (A) *Tau* protein in healthy neurons; (B) Formation of neurofibrillary tangles (NFTs) in AD neurons. Adapted from [68].

---

### 1.3.1.6. Oxidative stress

Oxidative stress and inflammatory processes in the CNS are involved in Alzheimer's progression [74]. Given the high oxygen consumption in the brain, the formation of reactive oxygen species (ROS) (e.g. superoxide anion, hydroxyl radical) may cause damage in neuron lipids or DNA. ROS may also be implied in A $\beta$  aggregation and in the process of *tau* hyperphosphorylation. Alteration in metals homeostasis is also responsible for the increase of ROS in the brain. Given the complexity of AD and ROS paper in its etiology, some therapeutic strategies include antioxidants administration [74, 75].

### 1.3.2. Parkinson's Disease

Parkinson's disease (PD) is the second most common degenerative disease after Alzheimer's disease. Although PD is most common in the over 60's, many people are diagnosed in their 40's and younger. The prevalence of the disease is of 360 per 100000 persons and the incidence of 18 per 100000 persons [2]. The prevalence increases in people over 60 years old. About 1% of the human population over 65 years suffers from PD [1]. With the progressive aging of the population, the incidence and prevalence of PD will increase in the future [1]. Geographically, the prevalence of the disease is higher in Europe and North America (100 to 300 per 10000 person) and smaller in Africa and Asia (10 to 60 per 100000 person). European studies presented an overall incidence rate 529 per 100000 person/year [28]. A recent study in North America reported an incidence rate of 224 per 100000 person/year in people with more than 65 years [34]. Asian studies showed an incidence or 17 per 100000 person/year [32]. This disease is two times more frequent in men than women [55].

The disease is characterized by the loss of dopaminergic cells in the *substantia nigra pars compacta*, resulting in the dopamine diminution in the basal ganglia [76], and by the presence of Lewy bodies (LB), proteinaceous inclusions mainly composed of filamentous  $\alpha$ -synuclein ( $\alpha$ -syn) aggregates [77]. Patients suffer a progressive degeneration in the motor system [78]. The core symptoms are tremor, rigidity (stiffness), bradykinesia (slowness of movement) and postural instability (balance difficulties). The high metabolic velocity of the *substantia nigra* associated to high levels of oxidized species and iron, high levels of free radicals (ROS) and low levels of antioxidants contribute to the apoptosis of dopaminergic neurons [78].

Mutations in the  $\alpha$ -synuclein gene are associated with hereditary cases of PD due to the ability of this protein to aggregate with sinaptosin and *tau*, forming the Lewy bodies. Mutations in LRRK2, PINK and Parkin genes are also associated with PD [79]. Figure 16 relates idiopathic and genetic forms of PD. In most of the cases, PD is a sporadic disorder caused by the loss of dopaminergic neurons in the *substantia nigra pars compacta* and associated with Lewy bodies. Actually, less than 10% of the cases are caused by mutations in genes with autosomal dominant or recessive inheritance. Most cases with autosomal recessive PD are due to mutations in genes with mitochondrial functions, like PINK or Parkin. At the neuropathological level, it most often presents as pure nigral dopaminergic cytopathy without Lewy bodies, although sometimes, autosomal recessive PD may be clinically indistinguishable from sporadic PD. Autosomal dominant PD, caused by mutations in the  $\alpha$ -syn gene SCNA and in LRRK2, is clinically similar to sporadic PD and most often presents with typical Lewy body pathology. It is still unclear whether sporadic PD and familial PD with distinct genetic causes are separate clinical and etiological entities. Nevertheless, mitochondrial dysfunction, impaired autophagy/lysosomal degradation of proteins/organelles, altered glutathione homeostasis, and abnormal  $\alpha$ -syn build-up are pathogenic mechanisms that may be shared between these diseases (Fig. 16) [80].

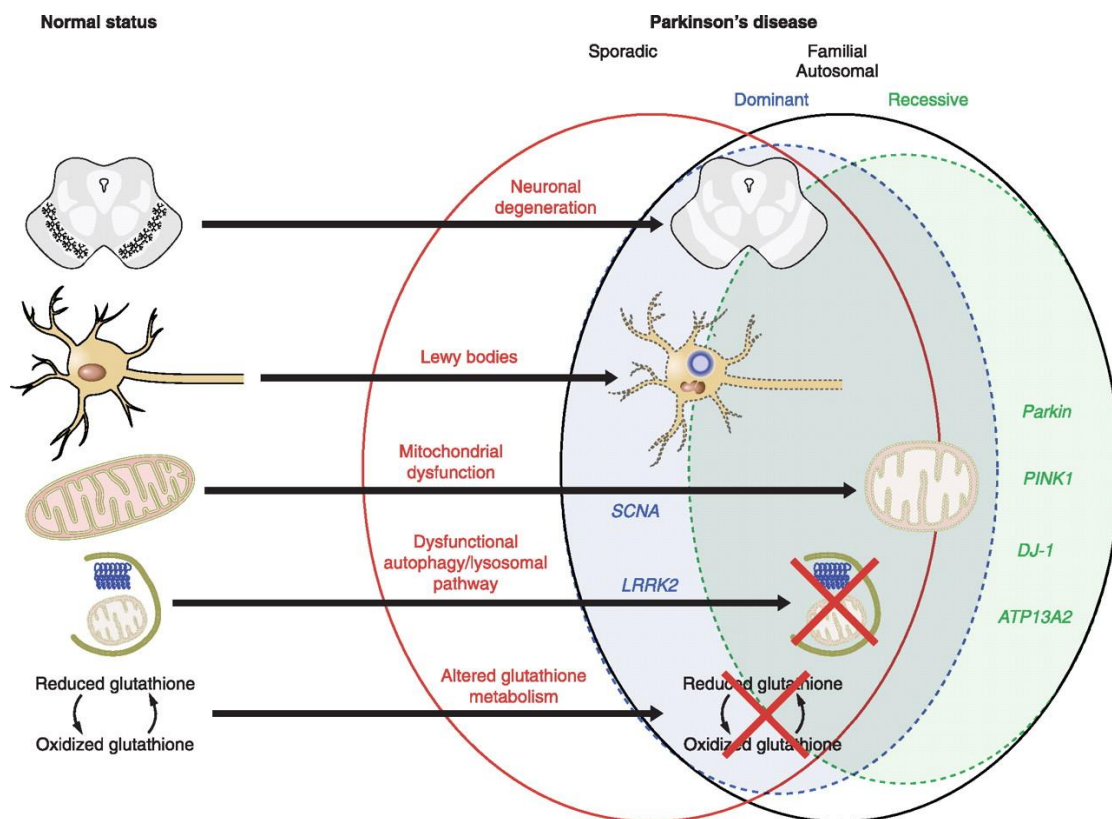


Figure 16 – Molecular pathways linking idiopathic and genetic forms of PD. Adapted from [80].

---

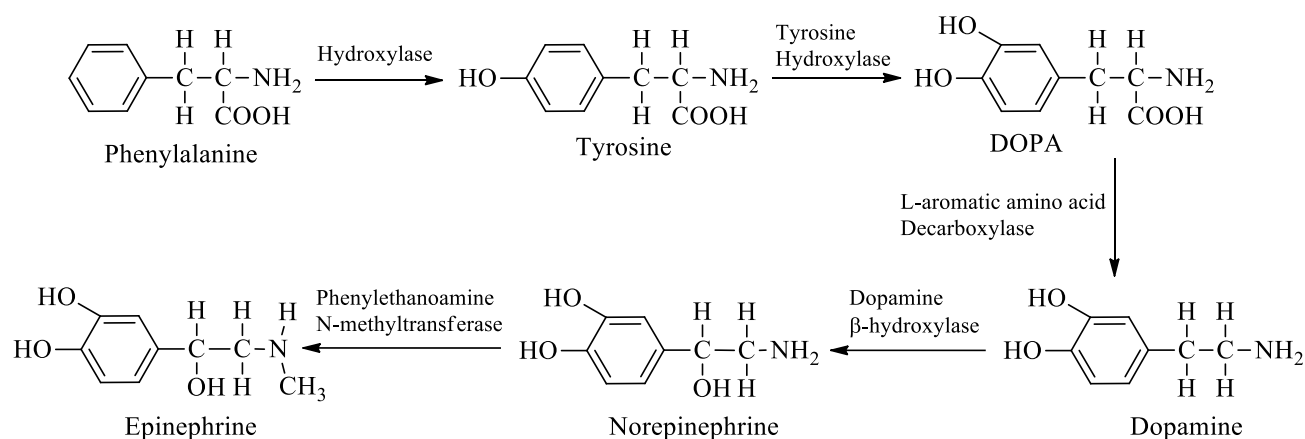
Standard care medical treatments for PD are limited to medications that focus on symptom management. Unfortunately, to date no medication has been shown to slow progression in PD. Some supportive therapies such as physical exercise have shown improved quality of life [81, 82], but there is a significant need to continue exploring therapies that might improve symptoms and positively impact the disease process.

### 1.3.2.1. Adrenergic neurotransmission

Norepinephrine, epinephrine and dopamine are endogenous catecholamines; they are sympathetic neural and humoral transmitter substances in most mammalian species. Norepinephrine and dopamine are believed to transmit impulse information in specific areas within the CNS; norepinephrine is also the neurotransmitter at most peripheral sympathetic neuroeffector junctions. Epinephrine is the major hormone released from the adrenal medulla. Catecholamines are stored in inactive form within granular structures in nerve terminals and chromaffin cells [83].

Norepinephrine is synthesized from the amino acid phenylalanine in a stepwise process (scheme 3). The aromatic ring of phenylalanine is hydroxylated by the action of an enzyme, phenylalanine hydroxylase (EC 1.14.16.1). This reaction yields tyrosine, which is converted to dihydroxyphenylalanine (DOPA) by the enzyme tyrosine hydroxylase (EC 1.14.16.2). This reaction involves additional hydroxylation of the benzene ring, and it is believed to represent the rate-limiting step in catecholamine synthesis [84]. DOPA is decarboxylated by the enzyme L-aromatic amino acid decarboxylase (DOPA decarboxylase, EC 4.1.1.28) to dihydroxyphenylethylamine (dopamine). Conversion of tyrosine to DOPA to dopamine is believed to occur within the cytoplasm. Dopamine is taken up into a storage granule. In some central anatomic sites (e.g. the mammalian extrapyramidal system), dopamine seems to act as the primary neurotransmitter rather than its metabolites norepinephrine and epinephrine [85, 86].

In peripheral adrenergic neurons and adrenal medullary chromaffin cells, intragranular dopamine is hydroxylated in the  $\beta$  position of the aliphatic side chain by dopamine  $\beta$ -hydroxylase to form norepinephrine. In the adrenal medulla, norepinephrine is released from the granules of chromaffin cells and is *N*-methylated within the cytoplasm by phenylethanolamine *N*-methyltransferase (EC 2.1.1.28) to form epinephrine. Epinephrine is subsequently localized in what seems to be another type of intracellular storage granule prior to its release from the adrenal medulla.



**Scheme 3** - The biosynthetic pathway of norepinephrine and epinephrine. Adapted from [31].

Catecholamines are taken up from the cytoplasm into granules by an active transport system that is adenosine triphosphate (ATP) and  $Mg^{2+}$  dependent. Storage within the granular vesicles is accomplished by complexation of the catecholamines with ATP and a specific protein, chromogranin. This complexation renders the amines inactive until their release [87]. The intragranular pool of norepinephrine is the principal source of neurotransmitter released upon nerve stimulation. The cytoplasmic amine pool is taken up by the granules for storage or inactivated by a deaminating enzyme, monoamine oxidase (MAO, EC 1.4.3.4), that is located in the neuronal mitochondria.

Excitation-secretion coupling and release of norepinephrine from adrenergic nerve terminals are dependent upon an inward movement of  $Ca^{2+}$ . Released norepinephrine migrates across the synaptic cleft and interacts with specific adrenergic receptor sites on the postjunctional membrane.

A very active amine uptake system is present in the axonal membrane of postganglionic sympathetic nerve terminals. This transport system is  $Na^+$  and energy dependent, and it functions to recapture or reuptake catecholamines that have been released from the nerve [88]. The duration of action of norepinephrine can be terminated by active reuptake into the nerve across the axoplasmic membrane, diffusion from the cleft via extracellular fluid, or metabolic breakdown by an extraneuronal enzyme, catechol-*O*-methyltransferase (COMT, EC 2.1.1.6). Activity of COMT involves methylation of one of the ring hydroxyl groups (3-OH) [31].

Norepinephrine that has been taken back into the nerve may be restored in granules or deaminated by MAO. Deamination of norepinephrine or epinephrine by MAO initially yields the corresponding aldehyde, which in turn is further oxidized to 3,4-dihydroxymandelic acid. Alternatively, the 3-hydroxyl group of norepinephrine and epinephrine can first be methylated by COMT to yield

---

normetanephrine and metanephrine respectively. The *O*-methylated or deaminated metabolites can then be acted upon by the other enzyme to yield 3-methoxy-4-hydroxymandelic acid. The deaminated *O*-methylated metabolites can then be conjugated with sulfate or glucuronide prior to excretion by the kidneys [31].

Physiologic events involved in adrenergic neurotransmission and susceptibility of these events to pharmacologic agents are outlined schematically in Figure 17. The amino acid tyrosine (hydroxyphenylalanine) is present in all food products and can be synthesized from phenylalanine. It enters the neuron by active transport. In the cytoplasm of the dopaminergic neuron, tyrosine is converted into dihydroxyphenylalanine (DOPA) by the tyrosine hydroxylase enzyme. DOPA is converted to dopamine in the cytoplasm by the enzyme aromatic L-amino acid decarboxylase (DOPA-decarboxylase). Dopamine is then actively transported into the storage vesicles by the vesicular transport mechanism. In the dopaminergic neuron, dopamine remains unchanged in the storage vesicles and is ready for release by exocytosis. Dopamine released into the synaptic cleft is actively transported back into the neuronal terminal. This process is called reuptake-1 and is the most important mechanism by which dopamine and other catecholamines are removed from the synaptic cleft. Some of the dopamine entering the neuronal terminal (about 50%) is transported into the vesicles for storage and release. The remaining dopamine that enters the neuronal terminal is destroyed by a mitochondrial enzyme, monoamine oxidase (MAO). Some of the dopamine that is released into the synaptic cleft (about 10%) is actively transported into the effector cells. This process is known as reuptake-2. Dopamine entering the effector cells is inactivated primarily by an enzyme, catechol-*O*-methyltransferase (COMT). Although MAO is also present in the effector cells, its role in the inactivation of dopamine is unclear.

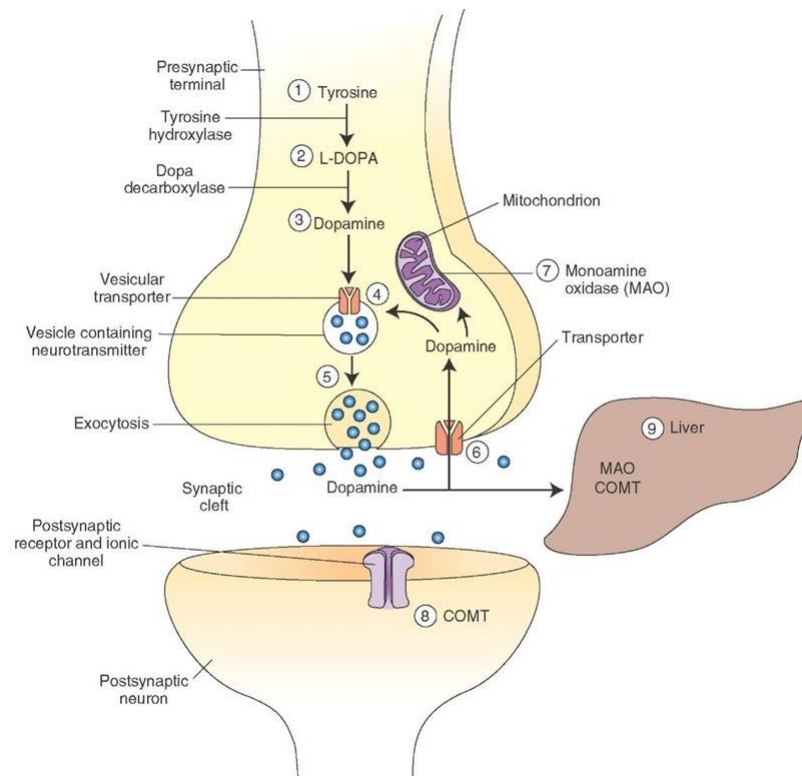


**Figure 17 - Adrenergic neurotransmission:** 1. Tyrosine enters the neuron by active transport; 2. Tyrosine is converted into DOPA by tyrosine hydroxylase; 3. DOPA is converted to dopamine in the cytoplasm by the enzyme DOPA-decarboxylase; 4. Dopamine is then stored in vesicles by the vesicular transport mechanism; 5. Dopamine is ready for release by exocytosis; 6. Dopamine released into the synaptic cleft is actively transported back into the neuronal terminal; 7. Part of the dopamine that enters the neuronal terminal is destroyed by monoamine oxidase (MAO); 8. Some of the dopamine that is released into the synaptic cleft is actively transported into the effector cells and is inactivated primarily by an enzyme, catechol-O-methyltransferase (COMT) [6].

About a million nerve cells contain dopamine. Dopaminergic neurons are found in several main groups including the mesostriatal system and the mesolimbocortical pathway (Fig. 18). As the name indicates the mesostriatal pathway, also called the nigrostriatal pathway, originates in the substantia nigra and nearby areas of the mesencephalon or midbrain and descends as part of the medialforebrain bundle to enervate the striatum, specific the caudate nucleus and the putamen. The mesolimbocortical pathway also originates in the midbrain, in the ventra tegmental area and projects to the limbic system, amygdala, nucleus accumbens, hippocampus and the cortex. The mesostriatal dopamine system normally plays a crucial role in motor control and damage to these neurons results in the resting tremors or even complete paralysis of PD [57].



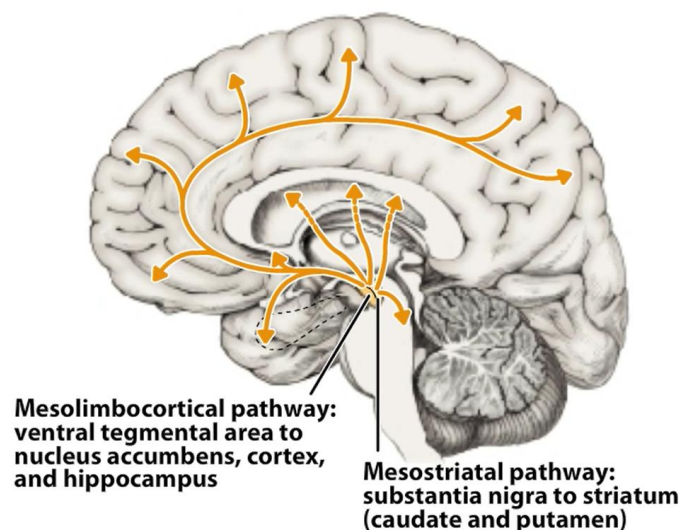


**Figure 18** - Dopaminergic pathway. Adapted from [57].

### 1.3.2.2. Catalytic reaction mechanism of MAO-B

Monoamine oxidase (MAO, E.C. 1.4.3.4) is an outer mitochondrial membrane flavoenzyme and is essential for the enzymatic decomposition of neurotransmitters. Figure 19 shows the three-dimensional structures of monoamine oxidase A (MAO-A) and monoamine oxidase B (MAO-B). Although the crystal structure of human MAO-A is monomeric while MAO-B is dimeric, both enzymes are dimeric in their membrane-bound forms.

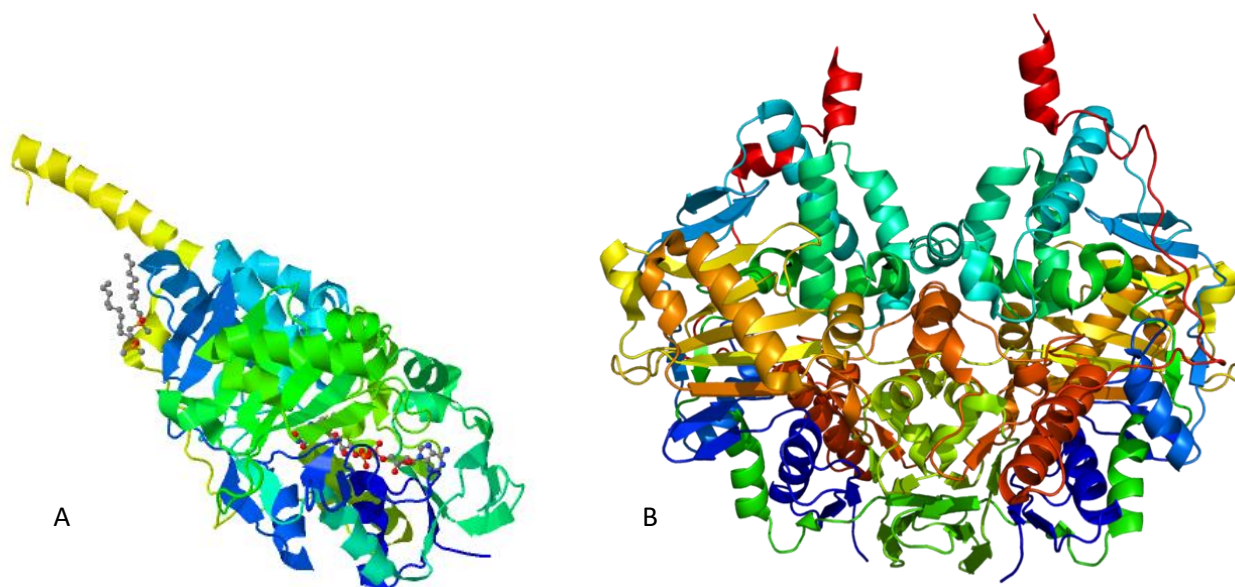


**Figure 19** – Ribbon diagram based on the X-ray crystallography structures of (A) MAO-A (Protein Data Bank ID: 2Z5Y) and (B) MAO-B (Protein Data Bank ID: 1GOS).

Although these two enzymes share 70% sequence identity, have highly conserved chain folds and are structurally identical in their flavin adenine dinucleotide (FAD)-binding sites, they differ considerably in the structures of their active sites opposite the flavin cofactor. MAO-A has a monopartite cavity of approximately 550 cubic angstroms, and MAO-B exhibits a bipartite cavity structure with an entrance cavity of 290 cubic angstroms and a substrate cavity of approximately 400 cubic angstroms (Fig. 20). Ile199 functions as a conformational “gate” separating the two cavities [89]. This amino acid is replaced by Phe208 in MAO-A.

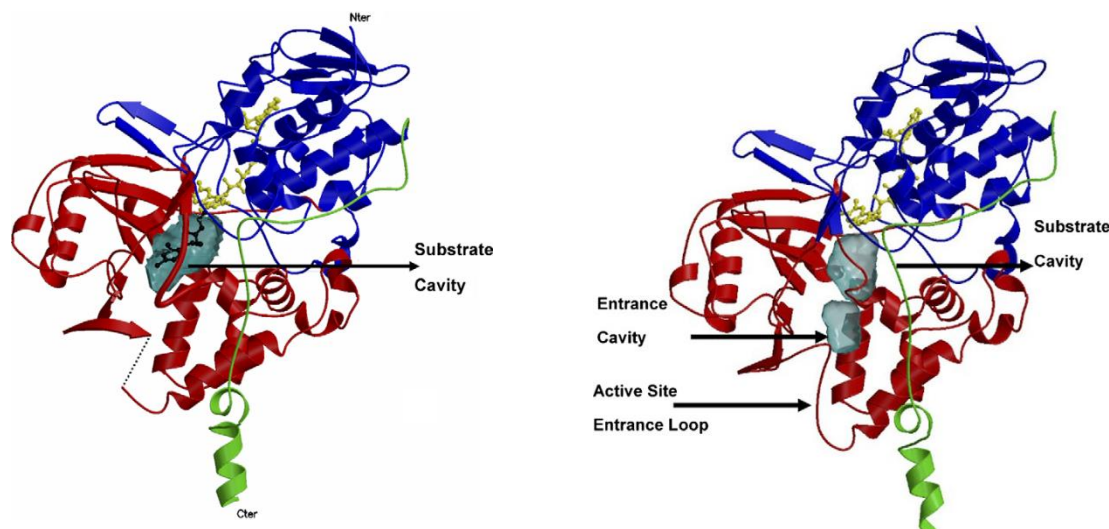


**Figure 20** - Ribbon diagram of (A) human MAO-A structure and (B) human MAO-B structure. The covalent flavin moiety is shown in a ball and stick model in yellow. The flavin binding domain is in blue, the substrate domain in red and the membrane binding domain in green. Adapted from [90].

The substrate-binding sites of MAO-A and MAO-B are both mainly hydrophobic, composed of aromatic and aliphatic residues [91]. An exception is Lys305 in MAO-A (Lys296 in MAO-B) that interacts with a water molecule that also binds the N5 atom of the flavin cofactor [92]. The recognition site for the substrate amino group is an aromatic cage formed by Tyr407 and Tyr444 in MAO-A (Tyr 398 and Tyr 435 in Mao-B) [91, 93, 94]. Another difference in the substrate-binding sites of the two enzymes is caused by the structural differences arising from Ile-335 in MAO-A and Tyr-326 in MAO-B, which contribute to the substrate and inhibitor selectivity of the two enzymes [95].

The two-dimensional representation of the interactions of the covalently-bound FAD (Fig. 21) shows the coenzyme to be in a hydrophobic environment within the enzyme with specific interactions dominated by H bonding to either side chains or peptide bonds in the protein [96].

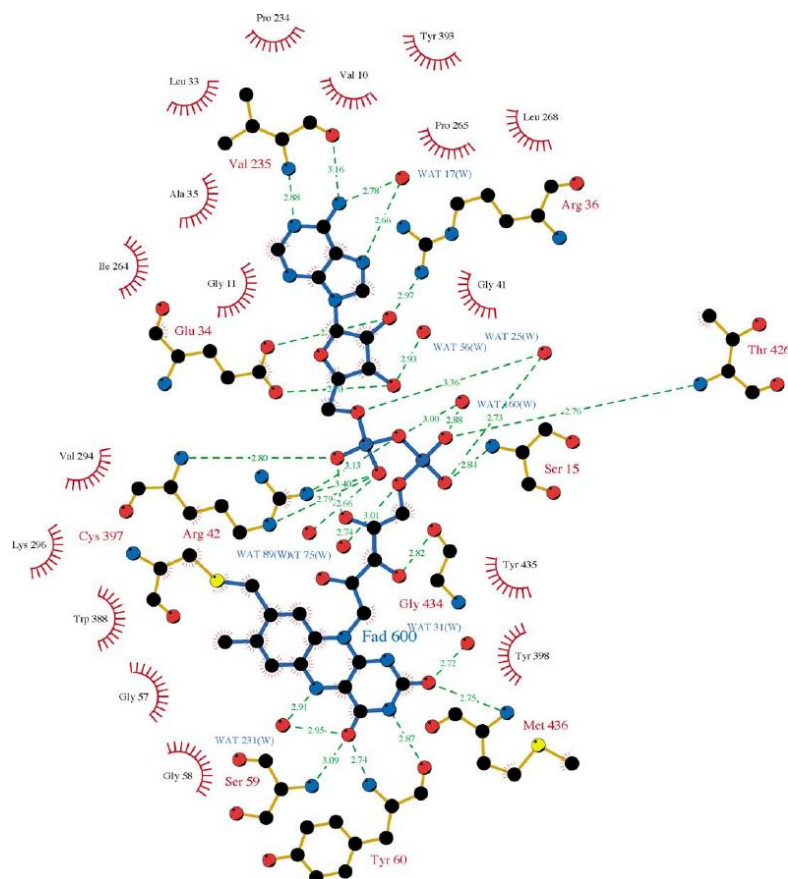
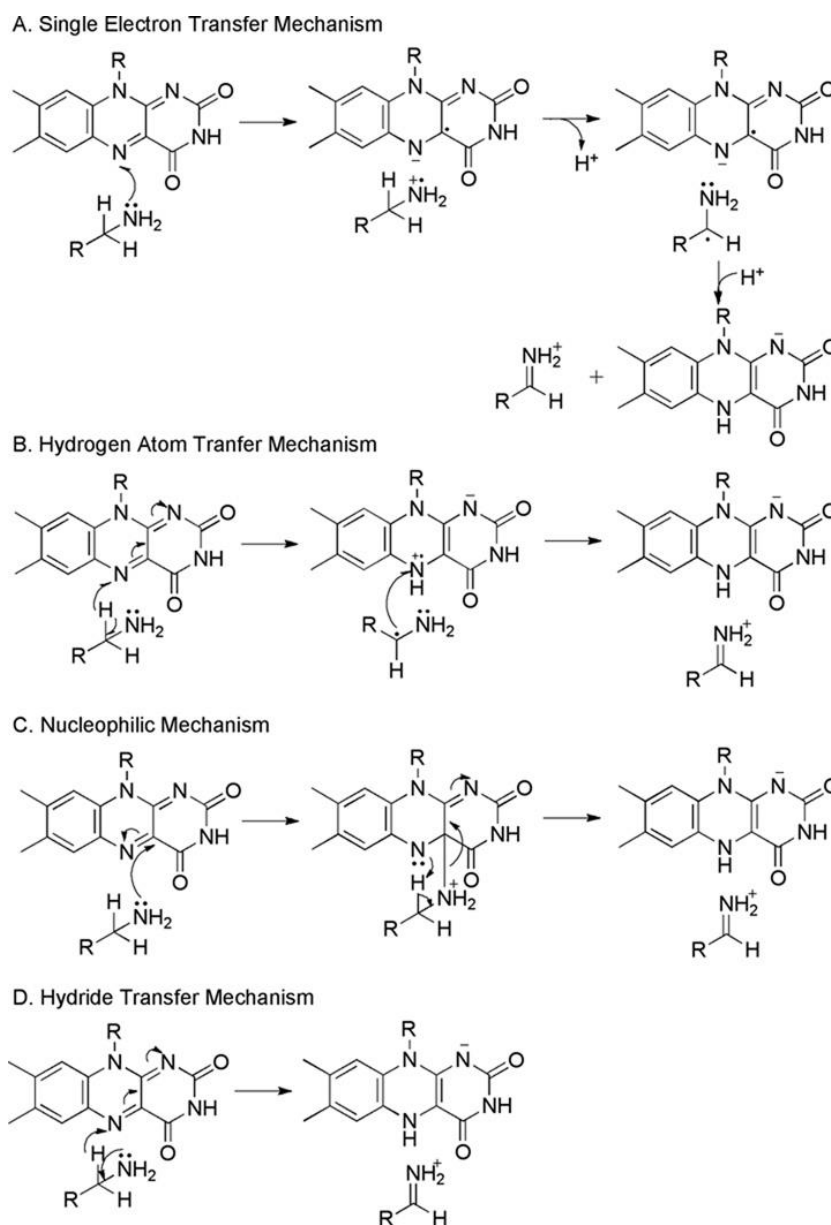


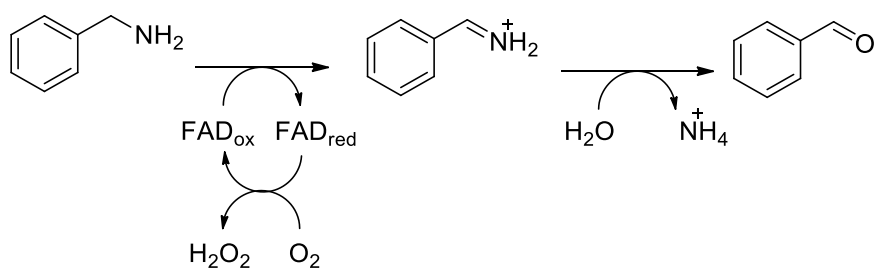
**Figure 21** - Illustration of FAD binding site in MAO-B. Dashed lines indicate H-bonds. Carbons are in black, nitrogens in blue, oxygens in red, and sulfurs are shown as cyan spheres. Adapted from [96].

MAO-A and MAO-B catalyze the oxidation of primary, secondary and tertiary amines to their corresponding imines [97]. While it is commonly accepted that the rate limiting step of the reaction is the stereoselective abstraction of a hydrogen from the substrate, the precise mechanism is unknown [98]. Due to the ability of the flavin cofactor to accept one or two electrons, several mechanisms have been proposed for the transfer of electrons from the substrate to the cofactor (Scheme 4). The single electron transfer mechanism (Scheme 4A) involves formation of semiquinone flavin and aminium cation radical intermediates, with subsequent transfer of a hydrogen atom equivalent [99]. Direct hydrogen atom transfer from the substrate  $\alpha$ -carbon to the flavin either directly or via non-flavin radical (Scheme 4B) is another possible mechanism for substrate oxidation [100]. Variations of a nucleophilic mechanism (Scheme 4C), in which the amino group of the substrate attacks the C4a of the flavin, forming a covalent intermediate, followed by proton abstraction by an active site base, have also been proposed [101]. Finally, the reaction could occur by direct hydride transfer from the substrate to the flavin (Scheme 4D) [102].



**Scheme 4** - Proposed reaction mechanisms for amine deamination by MAO-B in the literature. Adapted from [92].

Notice that scheme 4 doesn't show the next step in the reaction, in which the imine salt is hydrolyzed by water with subsequent aldehyde formation (Scheme 5).



**Scheme 5** – FAD catalyzed deamination of a primary amine to its corresponding aldehyde. Adapted from [92].

### 1.3.2.3. $\alpha$ -Synuclein

$\alpha$ -Synuclein ( $\alpha$ -syn) is a pre-synaptic 14 kDa protein (Fig. 22) that is suggested to play a role in the regulation of neurotransmitter release, synaptic function and plasticity [103].  $\alpha$ -Syn was originally identified in the human brain as the precursor protein of the non- $\beta$ -amyloid component of AD [104]. Although mutations in  $\alpha$ -syn have proved to be extremely rare in familial PD, over 90% of sporadic Parkinsonian disorders are characterized by  $\alpha$ -syn containing Lewy bodies, demonstrating that this protein could be involved in the molecular chain of events leading to the disease [105].

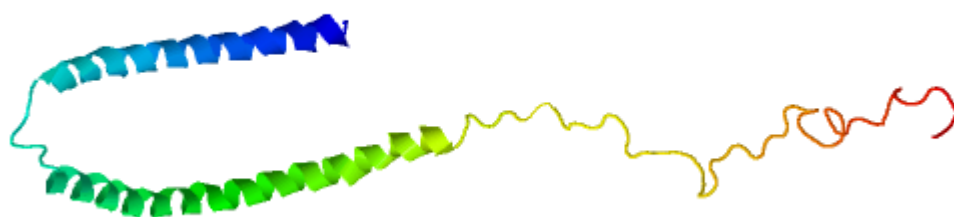


**Figure 22** – Schematic representation of micelle-bound  $\alpha$ -synuclein (Protein Data Bank ID: 1XQ8).

Monomeric, soluble  $\alpha$ -syn is normally present in neurons but misfolding can cause  $\alpha$ -syn to oligomerize, including transient spherical and ring-like oligomers that eventually convert to fibrils. The  $\alpha$ -syn oligomers are in equilibrium with monomers and convert to fibrils by monomer addition via a nucleated polymerization mechanism. These amyloid fibrils are a major component of Lewy bodies, which are intracellular protein aggregates associated with neurodegenerative conditions, such as Parkinson's disease and Lewy body dementia [106]. Membrane-bound monomeric  $\alpha$ -syn adopts a predominantly  $\alpha$ -helical confirmation, but at high concentrations the protein undergoes a conformational change either before or coincident with its oligomerization to form membrane-bound  $\beta$ -sheet-rich structures that self-associate to form oligomers, including trans-membrane amyloid pores and fibrils. Ring-like cytosolic oligomers can also associate with the membrane and form trans-membrane pores [103]. The oligomeric form of  $\alpha$ -syn spreads from neuron to neuron and can seed the formation of protein aggregates in stem cells [106]. This protein enters cells through endocytosis and can be transferred between cells through nanotubes [107]. Other spreading mechanisms could be trans-synaptic transmission, direct penetration or membrane receptors [103] (Fig. 23).

$\alpha$ -syn Oligomers and amyloid fibrils are highly toxic [108], affecting mitochondrial function [109], endoplasmic reticulum–Golgi trafficking [110, 111], protein degradation and/or synaptic

transmission [112], and these intracellular effects are thought to induce neurodegeneration. The transmembrane pores disrupt membrane integrity as well as intracellular calcium homeostasis and signaling, and may also contribute to neuronal toxicity [113].

Despite all the efforts, the exact molecular mechanisms through which  $\alpha$ -synuclein determines the loss of dopaminergic neuronal functions and viability in the context of PD is not clear [114].

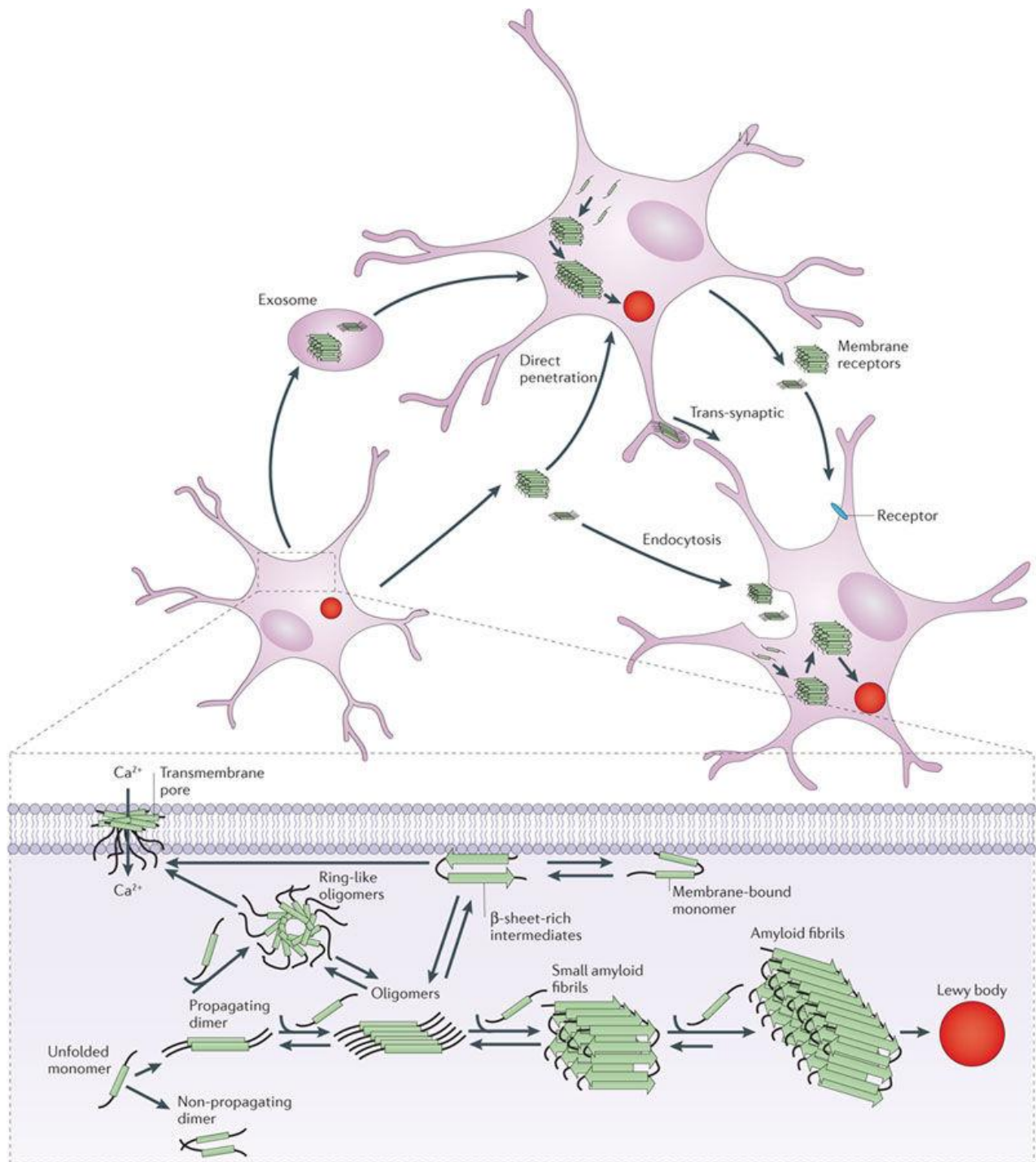


**Figure 23** - Mechanisms of  $\alpha$ -synuclein aggregation and propagation. Adapted from [103].

---

#### 1.3.2.4. Oxidative Stress

A number of studies have suggested the importance of oxidative stress in the pathophysiology of PD [115]. Oxidative stress results from either excess formation of oxidants or a decrease in the amount of function of antioxidants [116]. Oxidative damage in the brain of patients with PD are related with an increase in the amount of lipid peroxidation products such as malondialdehyde and 4-hydroxynonenal, an increase in protein oxidation (cross-linking and fragmentation), and an increase in the concentration of 8-hydroxy-2'-deoxyguanosine, a product of DNA oxidation [117]. There is evidence to suggest that reactive oxygen species (ROS) are derived from dopamine, and that this auto-oxidation may be increased in the early stages of PD when dopamine turnover is increased to compensate for dying dopaminergic neurons [118].

Glutathione, an important reducing agent in the neurons, has been found to be depleted in the brain of PD patients [119] and the amount of the depletion seems to be directly proportional to the severity of the disease and is the earliest known indicator of *substantia nigra* degeneration, even before dopamine losses in the *striatum* [119, 120]. The brain has difficulty withstanding substantial amounts of oxidative stress because of the presence of high amounts of polyunsaturated fatty acids, low levels of antioxidants such as glutathione, and increased iron content in specific areas such as the *globus pallidus* and the *substantia nigra* [117].

An additional component to the relationship between oxidative stress and PD is related to  $\alpha$ -synuclein [121]. Previous studies have implicated the role of oxidative stress in the formation of  $\alpha$ -synuclein aggregates [122, 123]. In addition, several studies have suggested that iron-related oxidative stress can promote  $\alpha$ -synuclein aggregation [124, 125]. Furthermore, soluble nitrated  $\alpha$ -synuclein, which results from interactions with oxidized nitrogen species, appears to activate microglia to produce substantial amounts of ROS through modulation of specific ion channels [126].

### 1.3.3. Therapeutic approaches

Although there are many ongoing research activities in the search of drugs for treating AD [72, 127], only four drugs are currently approved by INFARMED [128], three anti-cholinergic drugs (Donepezil, Rivastigmine and Galantamine) and the NMDA glutamate receptor antagonist, Memantine (Fig. 24).

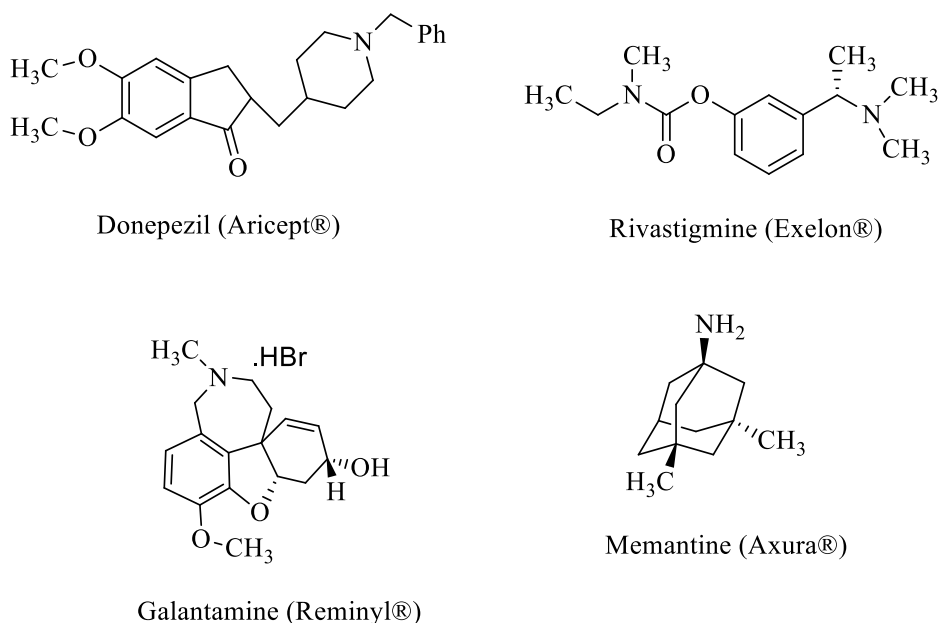


**Figure 24** - Drugs currently approved by INFARMED against Alzheimer's disease.

Donepezil is a piperidine based, reversible and non-competitive cholinesterase inhibitor [129].

Rivastigmine belongs to the carbamate group of cholinesterase inhibitors and is described as a pseudo-irreversible enzyme inhibitor due to its prolonged effect when compared to the drug presence in the plasma [130, 131].

Galantamine is a tertiary alkaloid drug that binds competitively and reversibly to the AChE active site and has proven activity as an allosteric modulator of nicotinic acetylcholine receptors [132].

The treatment with these drugs have resulted in a modest improvement in memory and cognitive function for AD patients, while unable to prevent progressive neurodegeneration [5, 133-138]. This could be due to the multiple pathogenic mechanisms involved in AD including A $\beta$  aggregation to form plaques,  $\tau$  hyperphosphorylation to disrupt microtubule to form neurofibrillary tangles, calcium imbalance, enhanced oxidative stress, impaired mitochondrial function, apoptotic neuronal death, and deterioration of synaptic transmission, particularly at cholinergic neurons [139].



The amyloid- $\beta$  protein was proposed as the trigger for a cascade of events in the brain that lead to Alzheimer's disease [140]. Several anti-A $\beta$  treatments have been developed to short-circuit this cascade [141]. Compounds that are intended to reduce A $\beta$  production, inhibit A $\beta$  aggregation, and promote A $\beta$  clearance are currently in clinical trials [127]. This is the case of the monoclonal antibody aducanumab that selectively binds to soluble A $\beta$  oligomers and insoluble fibrils [142]. This will prevent inflammatory response by  $\tau$  protein and subsequent neuronal loss (Fig. 25).

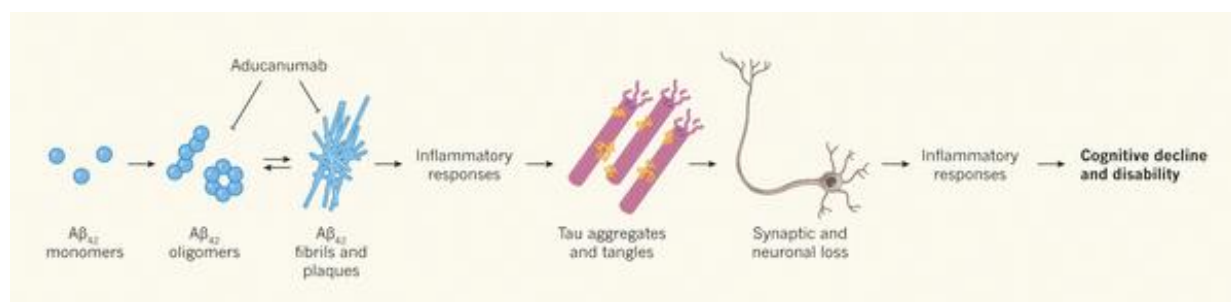


**Figure 25** - The amyloid hypothesis. Adapted from [63].

In addition, there is compelling evidence demonstrated that oxidative stress played an important role in the processes of AD pathogenesis, cellular changes show that it precedes the appearance of two hallmark pathologies of the disease, neurofibrillary tangles and senile plaques [143]. Therefore, compounds with radical scavenging activities (such as melatonin and vitamin E) were supposed to be useful for either the prevention or the treatment of AD [144, 145]. Recently, elevated concentrations of copper, zinc and iron have been detected in amyloid plaques, and in vitro experiments have proved that copper and zinc metals are able to bind to A $\beta$  and promote its aggregation.[146, 147] Moreover, evidence showed that redox-active Cu and Fe contribute to the production of reactive oxygen species (ROS) and oxidative stress [148]. Therefore, modulation of these biometals in the brain may exert potential therapeutic effect on AD, and several metal chelators such as desferrioxamine [149], D-penicillamine [64], clioquinol (PBT1) and PBT2 [150, 151] have been used for the treatment of AD in preclinical or clinical trials, while the poor target specificity and brain barrier permeability limited their widespread use in clinic.

To combat the complex profile of Alzheimer's disease, more attention has been focused on the development of novel multitarget directed ligands (MTDLs), which interacts with multiple targets in the complex neurotoxic cascades would achieve better efficacy by a complementary manner [139, 152-154]. Many MTDLs with a variety of scaffolds have been developed in the past few years, including AChE/BuChE and A $\beta$  aggregation inhibitor memoquin [155], AChE inhibitor and VDCC

antagonist ITH4012 [156] iron chelating agent and MAO-B inhibitor M30 [157]. Especially, an AChE and MAO-B dual inhibitor ladostigil [158, 159] had been advanced into phase II clinical trial in 2011, which confirmed the rationality and feasibility of MTDLs strategy in the treatment of AD (Fig. 26).

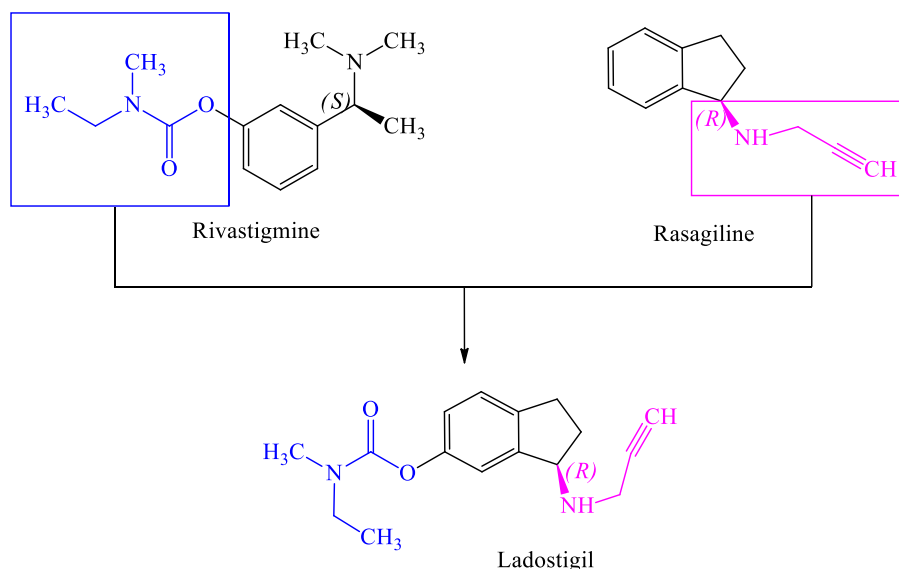


**Figure 26** – The multitarget directed ligand Ladostigil. Adapted from [158]. The carbamate group of Rivastigmine is highlighted in blue and the propargyl group of Rasagiline is highlighted in purple.

Ladostigil comprises the carbamate functional group (blue) of Rivastigmine, which inhibits AChE and the propargyl moiety (purple) of Rasagiline, that inhibits MAO-B (Fig. 26).

In spite of the extensive studies performed on postmortem *substantia nigra* from Parkinson's disease patients, the etiology of the disease has not yet been established. The existing drugs do not prevent or cure the disease, but attenuate the symptoms. INFARMED [128] approved several therapeutic drugs (Table 1) that are divided into two major groups: anticholinergics (Fig. 27) and dopamine mimetics (Fig. 28).

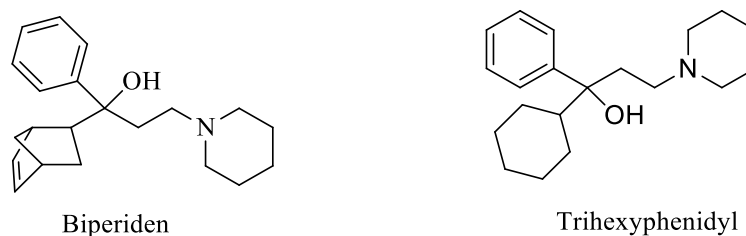


**Figure 27** - Anticholinergic drugs for treating Parkinson's disease.

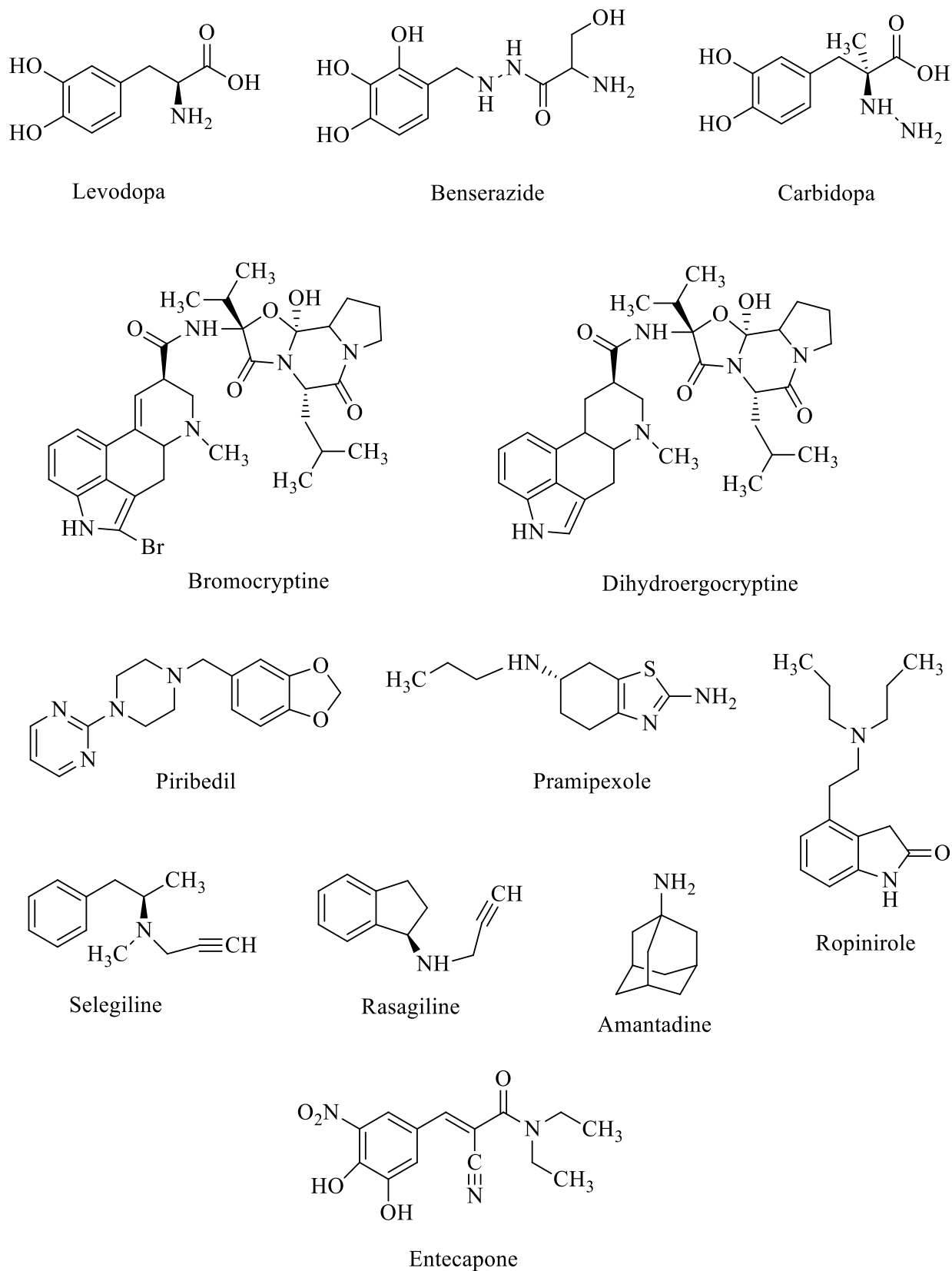


**Figure 28** - Dopamine mimetic drugs used in Parkinson's disease.

**Table 1** - Drugs approved by INFARMED for PD treatment (used individually or as a combination therapy).

<b>Mechanism of action</b>	<b>Drug</b>	<b>Commercial name</b>
<b>Anticholinergics</b>	Biperiden	Akineton®
	Trihexyphenidyl	Artane®
<b>Dopamine precursors</b>	Levodopa+benserazide	Madopar®
	Levodopa+carbidopa	Sinemet®
	Levodopa+carbidopa+entecapone	Stalevo®
<b>Dopamine agonists</b>	Bromocryptine	Parlodel®
	Dihydroergocryptine mesylate	Striatal®
	Piribedil	Trivastal®
	Pramipexol	Pramipexol®
	Ropinirole	Ropinirol®
<b>MAO-B inhibitors</b>	Selegiline (L-deprenyl)	Jumex®
	Rasagiline	Azilect®
<b>COMT inhibitors</b>	Entecapone	Comtan®
<b>Glutamate inhibitors</b>	Amantadine	Parkadina®

There is a growing interest in search for new drugs with neuroprotection effects [160, 161]. Hypothetical mechanisms of neuroprotection include anti-oxidation, anti-apoptosis, anti-inflammation, mitochondrial stabilization, trophic factor action, and *N*-methyl-*D*-aspartate (NMDA)–receptor antagonism [162, 163]. There is also a growing interest in strategies to modify the expression of oligomeric  $\alpha$ -synuclein. One possible strategy is the introduction of short interfering RNA (siRNA) to modify expression of the synuclein [164]. Another approach is to find small molecules that can prevent misfolding of the protein or development of antibodies that could block toxic aggregation.

---

Even with the advent of powerful new tools such as genomics, proteomics, brain imaging, gene replacement therapy and knockout animal models, the desired end result of neuroprotection is still beyond researchers current capability [165].



## *Chapter 2*

# *Methodology optimization for selecting therapeutic targets*

---

*"Anyone who has never made a mistake has never tried anything new."*

Albert Einstein (1879-1955)





## 2.1. Introduction

Acetylcholinesterase (AChE) reversible inhibitors have provided the first-generation drugs for AD treatment in order to increase levels of ACh in the brain [166, 167]. ACh is hydrolyzed by both AChE and butyrylcholinesterase (BuChE). Although little is known about the physiological role of BuChE [168, 169], particularly in the central nervous system, studies have been made in order to determine its influence on the treatment of AD [170, 171]. It was found that in the course of the disease, levels of AChE in the CNS decrease contrary to what happens with BuChE [172]. Both enzymes represent legitimate therapeutic targets for ameliorating the cholinergic deficit characteristic of AD.

The enzyme monoamine oxidase metabolized primary, secondary and tertiary amines, including adrenaline and noradrenaline [173]. The neurotransmitters phenylethylamine and benzylamine were identified as MAO-B substrates [174], while serotonin, adrenaline and noradrenaline are MAO-A substrates [173]. Tyramine and dopamine are substrates for both isoforms [174]. MAO-B not only exists in large quantities in the human brain, but also is related with PD. So, it represents a legitimate therapeutic target for ameliorating the dopaminergic loss characteristic of PD [175, 176].

To evaluate these therapeutic targets, two different techniques were used: UV-Vis molecular absorption spectrometry and fluorescence spectrometry.

*ee*AChE and *eq*BuChE kinetic parameters were evaluate by UV-Vis spectrometry, as well as the specificity of these enzymes for different substrates, namely acetylthiocholine (ATCI) and butyrylthiocholine (BTCI). This approach was also used to evaluate the influence of different assay conditions in the IC<sub>50</sub> determination of the standards donepezil, rivastigmine and galantamine, the active ingredients of some commercial drugs used in AD treatment, such as, Aricept<sup>®</sup>, Exelon<sup>®</sup> and Reminyl<sup>®</sup>.

MAO-B kinetic parameters were determined by two different techniques, UV-Vis and fluorescence spectrometry, to determine which one was more accurate, by determining IC<sub>50</sub> values for pargyline, commercialized as Ethonyl<sup>®</sup>, and rasagiline, the active ingredient of the commercial drug used in PD treatment, Azilect<sup>®</sup>.

## 2.2. Materials and Methods

### 2.2.1. Enzymatic activity quantification for AChE and BuChE by spectrophotometry

#### 2.2.1.1. Chemicals

AChE, BuChE, 5,5-dithio-bis-(2-nitrobenzoic acid) (DTNB), acetylthiocholine iodide (ATCI), butyrylthiocholine iodide (BTCI), rivastigmine tartrate, donepezil hydrochloride and galantamine bromide were purchased from Sigma-Aldrich. AChE used in the assay was from *Electrophorus electricus* (type VI-S lyophilized powder, 518 U mg<sup>-1</sup> solid, 814 U mg<sup>-1</sup> protein), BuChE used in the assay was from equine serum (lyophilized powder, 219.6 U mg<sup>-1</sup> solid, 1830 U mg<sup>-1</sup> protein). The lyophilized enzymes were prepared in 20 mM Tris-HCl pH 7.6 buffer. DTNB was prepared in 50 mM Tris-HCl, 0.1 M NaCl, 0.02 M MgCl<sub>2</sub> buffer (pH 8.0). ATCI and BTCI were prepared in 50 mM Tris-HCl buffer (pH 8.0).

#### 2.2.1.2. Influence of substrate concentration in enzymatic activity

The assay for determining the substrate concentration to be used was modified from the literature [177, 178]. To 75  $\mu$ L of Tris-HCl buffer (50 mM, pH 8) were added 25  $\mu$ L of ATCI or BTCI (with concentrations between 1.25 mM and 25 mM), 125  $\mu$ L of DTNB (with concentrations between 0.25 mM and 5 mM) and 25  $\mu$ L of *ee*AChE or *eq*BuChE (0.3 U mL<sup>-1</sup>), to a final volume of 250  $\mu$ L.

In addition, it was optimized the DTNB concentration ranging from 0.5 mM to 7.5 mM. A concentration of 3 mM was chosen for the assays, not only because of the satisfactory absorbance value obtained, but also because both the substrate and DTNB concentrations would be equimolar in the assay. The molar absorption coefficient of purified TNB<sup>2-</sup> at 405 nm is 13300 M<sup>-1</sup> cm<sup>-1</sup>. Based on the reaction curve it was possible to see that substrate concentrations higher than 1.5 mM gave the same  $V_{max}$ . So 1.5 mM of ATCI was selected as the concentration to determine the enzymatic activity for AChE. In the same way, 1.5 mM of BTCI was chosen as the concentration to determine the enzymatic activity for BuChE.

The microplate was read at 25 °C and 405 nm, with a BIO-TEK ELX800G (with software Gen5 v.1.05) spectrometer during 60 min. The rate of the reaction was measured. All experiments were done in triplicate. A calibration curve for the enzymes was built (Figs. S<sub>1</sub> and S<sub>2</sub>).

### 2.2.1.3. Determination of the kinetic parameters for AChE and BuChE

The assay for measuring cholinesterases kinetic parameters was modified from the literature [177, 178]. To 75  $\mu\text{L}$  of Tris-HCl buffer (50 mM, pH 8) were added 25  $\mu\text{L}$  of ATCI or BTCI (with concentrations between 1,25 mM and 25 mM), 125  $\mu\text{L}$  of DTNB (with concentrations between 0,25 mM and 5 mM) and 25  $\mu\text{L}$  of *ee*AChE or *eq*BuChE ( $0.3 \text{ U mL}^{-1}$ ), to a final volume of 250  $\mu\text{L}$ . The microplate was read at 25 °C and 405 nm, with a BIO-TEK ELX800G (with software Gen5 v.1.05) spectrometer during 60 min. The rate of the reaction was measured. All experiments were done in triplicate. The kinetic parameters were determined with software Hiper 3.2.

### 2.2.1.4. Evaluation of enzymatic selectivity for the substrate

The assay to determine enzymatic selectivity for ATCI and BTCI was modified from the one described in literature.[177, 178] To 75  $\mu\text{L}$  of Tris-HCl buffer (50 mM, pH 8.0) were added 25  $\mu\text{L}$  of ATCI (concentrations between 1.25 mM and 25 mM) or BTCI (concentrations between 1.25 mM and 25 mM), 125  $\mu\text{L}$  of DTNB (concentrations between 0.25 mM and 5 mM) and 25  $\mu\text{L}$  of *ee*AChE ( $0.3 \text{ U mL}^{-1}$ ) or *eq*BuChE ( $0.3 \text{ U mL}^{-1}$ ), to a final volume of 250  $\mu\text{L}$ . The microplate was read at 25 °C and 405 nm, with a BIO-TEK ELX800G (with software Gen5 v.1.05) spectrometer during 60 min. The rate of the reaction was measured. All experiments were done in triplicate. The kinetic parameters were determined with software Hiper 3.2.

### 2.2.1.5. Evaluation of *ee*AChE and *eq*BuChE inhibitory activity of rivastigmine, donepezil and galantamine

To 75  $\mu\text{L}$  of a mixture of different inhibitor concentrations and Tris-HCl buffer (0.05 M, pH 8.0) were added 25  $\mu\text{L}$  of ATCI (15 mM) or BTCI (15 mM), 125  $\mu\text{L}$  of DTNB (3 mM) and 25  $\mu\text{L}$  of *ee*AChE ( $0.3 \text{ U mL}^{-1}$ ) or *eq*BuChE ( $0.3 \text{ U mL}^{-1}$ ), to a final volume of 250  $\mu\text{L}$ . The microplate was read at 25 °C choosing two different wavelengths (405 nm or 412 nm) and at 37 °C using the same wavelengths, with a Thermo Scientific MultiSkan Go spectrophotometer during 15 min. The rate of the reaction was measured. All experiments were done in triplicate. The same assay was done with AChE using phosphate buffer (0.1 M, pH 8.0) instead of Tris-HCl buffer (0.05 M, pH 8.0).

## **2.2.2. Enzymatic activity quantification for MAO-B by spectrophotometry**

### **2.2.2.1. Chemicals**

MAO-B, benzylamine, rasagiline mesylate, pargyline hydrochloride, peroxidase (type II, from horseradish), vanillic acid, 4-aminoantipyrine, resorufin and amplex-red were purchased from Sigma-Aldrich. All samples were prepared in 0.2 M phosphate buffer (pH 7.4).

### **2.2.2.2. Influence of MAO-B concentration**

To determine the optimum concentration of enzyme to use in the assays, the following concentrations were tested: 0.470, 0.705, 0.940 and 1.175 U. To 133-130  $\mu\text{L}$  of phosphate buffer (0.1 M, pH 7.6) were added 2-5  $\mu\text{L}$  of MAO-B, 15  $\mu\text{L}$  of benzylamine (100 mM) and 50  $\mu\text{L}$  of chromogenic solution to a final volume of 200  $\mu\text{L}$ . A negative control without the enzyme was also used. The chromogenic solution contained vanillic acid (1 mM), 4-aminoantipyrine (0.5 mM) and peroxidase (12 U  $\text{mL}^{-1}$ ). The chromogenic solution was prepared on a daily basis and kept at 4  $^{\circ}\text{C}$  until needed. The molar absorption coefficient of the quinoneimine dye at 498 nm is 4654  $\text{M}^{-1} \text{cm}^{-1}$ . The mixture was incubated at 37  $^{\circ}\text{C}$  for 60 min. The reaction was then followed for another 60 minutes at 37  $^{\circ}\text{C}$  and 490 nm, with a Thermo Scientific MultiSkan Go spectrophotometer. The rate of the reaction was measured. All experiments were done in triplicate. A calibration curve for the enzyme was built (Fig. S<sub>3</sub>).

It is important that the enzyme concentration isn't rate limiting so that  $V_{max}$  can be reached, so a MAO-B concentration of 0.940 U was chosen for the assays.

### **2.2.2.3. Influence of substrate concentration in enzymatic activity**

To determine the concentration of benzylamine (substrate) to use in the assay, the following concentrations were tested: 2.5, 5, 7.5 and 10 mM. To 4  $\mu\text{L}$  of MAO-B (0.94 U) were added 5-20  $\mu\text{L}$  benzylamine (100 mM), 50  $\mu\text{L}$  of chromogenic solution and phosphate buffer (0.1 M, pH 7.6) to a final volume of 200  $\mu\text{L}$ . The reaction was then followed for 120 min at 37  $^{\circ}\text{C}$  and 490 nm, in a spectrophotometer Thermo Scientific MultiSkan Go. The rate of the reaction was measured. All experiments were done in triplicate.

The substrate concentration must be high enough to saturate the enzyme, so  $V_{max}$  can be reached. Substrate concentration higher than 7.5 mM give the same  $V_{max}$ . So, 7.5 mM of benzylamine was selected as the concentration to determine the enzymatic activity for MAO-B.

#### **2.2.2.4. Determination of kinetic parameters for MAO-B**

The assay for measuring MAO-B kinetic parameters was modified from the literature [179]. To 4  $\mu\text{L}$  of MAO-B (0.94 U) were added 5-20  $\mu\text{L}$  benzylamine (100 mM), 50  $\mu\text{L}$  of chromogenic solution and phosphate buffer (0.1 M, pH 7.6) to a final volume of 200  $\mu\text{L}$ . The chromogenic solution contained vanillic acid (1 mM), 4-aminoantipyrine (0.5 mM) and peroxidase (12  $\text{U mL}^{-1}$ ). The chromogenic solution was prepared on a daily basis and kept at 4 °C until needed. The reaction was then followed for 60 min at 37 °C and 490 nm, with a Thermo Scientific MultiSkan Go spectrophotometer. The rate of the reaction was measured. All experiments were done in triplicate.

#### **2.2.2.5. Evaluation of MAO-B inhibitory activity of pargyline and rasagiline**

Two different approaches were used to evaluate the inhibitory MAO-B activity for pargyline and rasagiline.

In the first assay (without previous incubation), to a mixture of 131  $\mu\text{L}$  of phosphate buffer (0.2 M, pH 7.4) and pargyline (0.00625-0.2  $\mu\text{M}$ ) or rasagiline (0.0125-0.150  $\mu\text{M}$ ), were added 4  $\mu\text{L}$  of MAO-B (0.94 U), 15  $\mu\text{L}$  of benzylamine (100 mM) and 50  $\mu\text{L}$  of chromogenic solution (to a final volume of 200  $\mu\text{L}$ ). A negative control without the enzyme and a positive control without inhibitor were also done. The mixture was incubated for 30 minutes at 37 °C, after that the reaction was followed for 60 minutes at 37 °C and 490 nm, with a Thermo Scientific MultiSkan Go spectrophotometer. The rate of the reaction was measured. All experiments were done in triplicate.

In the second (with previous incubation), to a mixture of 131  $\mu\text{L}$  of phosphate buffer (0.1 M, pH 7.6) and pargyline (0.00625-0.2  $\mu\text{M}$ ) or rasagiline (0.0125-0.150  $\mu\text{M}$ ), were added 4  $\mu\text{L}$  of MAO-B (0.94 U). This mixture was incubated at 37 °C for 15 minutes. Then 15  $\mu\text{L}$  of benzylamine (100 mM) and 50  $\mu\text{L}$  of chromogenic solution (to a final volume of 200  $\mu\text{L}$ ) were added followed by further incubation at 37 °C for 15 more minutes. A negative control without the enzyme and a positive control without inhibitor were also carried out. The reaction was followed for 60 more

minutes at 37 °C and 490 nm, with a Thermo Scientific MultiSkan Go spectrophotometer. The rate of the reaction was measured. All experiments were done in triplicate.

### **2.2.3. Enzymatic activity determination for MAO-B by fluorometry**

#### **2.2.3.1. Influence of MAO-B concentration**

In order to determinate the optimum excitation and emission wavelengths for resorufin, a solution of 1  $\mu\text{M}$  resorufin was prepared in a 1:10 phosphate buffer (0.1 M, pH 7.6) to a final volume of 900  $\mu\text{L}$ , and was used to determine the excitation and emission  $\lambda_{\text{max}}$  for this compound. The excitation wavelength was kept constant at three different values (560 nm, 570 nm, 580 nm) and the emission wavelength varied from  $580 \pm 10$  nm for each of the excitation wavelength values. The fluorescence was measured with a PerkinElmer LS 55 spectrometer. All the experiments were done in triplicate. The results showed a maximum excitation wavelength of 570 nm and a maximum emission wavelength of 584 nm. These results were in agreement with the ones described in literature [180]. A calibration curve for resorufin was constructed using the following concentrations: 1, 5, 10, 15 and 20  $\mu\text{M}$ . These were diluted 1:100 in a phosphate buffer (0.1 M, pH 7.6) to a final volume of 900  $\mu\text{L}$ . The fluorescence was read with a PerkinElmer LS 55 spectrometer. All the experiments were done in triplicate.

In order to optimize the enzyme activity quantification a set of assays were performed with concentration range from 0.185 U to 5.7872 mU. The enzyme solution was diluted in phosphate buffer (0.1 M, pH 7.6). To the different enzyme concentrations was added the reaction mixture composed of benzylamine (2 mM), amplex red (400  $\mu\text{M}$ ) and HRP (2 U  $\text{mL}^{-1}$ ) and phosphate buffer (0.1 M, pH 7.6) diluting to a final volume of 900  $\mu\text{L}$ . The fluorescence was read with a PerkinElmer LS 55 spectrometer. All the experiments were done in triplicate. A calibration curve for Resorufin was built (Fig. S4).

#### **2.2.3.2. Evaluation of MAO-B inhibitory activity of pargyline and rasagiline**

The assay for measuring the  $\text{IC}_{50}$  for pargyline and rasagiline was modified from the literature [180]. To 5.782 mU of MAO-B were added 0.150, 0.100, 0.050, 0.025 or 0.0125  $\mu\text{M}$  of pargyline or rasagiline and phosphate buffer (0.1 M, pH 7.6) diluting to a final volume of 500  $\mu\text{L}$ . The mixture was incubated for 30 minutes at 25 °C. After which, were added 500  $\mu\text{L}$  of the reaction mixture

and the fluorescence was read with a PerkinElmer LS 55 spectrometer. This mixture was left to incubate at 25 °C for 30 minutes and a second reading was done. A negative control composed of phosphate buffer (0.1 M, pH 7.6) and a positive control without inhibitor were used. All experiments were done in triplicate.

#### 2.2.4. Statistical analysis

All data was expressed as mean  $\pm$  standard deviation of triplicate measurements. The dose-response curve allows to determine the IC<sub>50</sub> value. GraphPad Prism 5<sup>TM</sup> software was used to draw all dose-response curves as well as the corresponding IC<sub>50</sub> for all the samples, following Equation 1:

$$y = \frac{y_{max} - y_{min}}{1 + \left(\frac{[I]}{IC_{50}}\right)} + y_{min} \quad (1)$$

Where  $y$  is the fractional activity of the enzyme in the presence of inhibitor at concentration  $[I]$ ,  $y_{max}$  is the maximum value of  $y$  that is observed at zero inhibitor concentration (for fractional activity, this is 1.0),  $y_{min}$  is the minimum value of  $y$  that can be obtained at high inhibitor concentrations and  $IC_{50}$  is the concentration that inhibits the enzyme by 50%.

The kinetic constants,  $K_m$  and  $V_{max}$ , were determined with the software Hyper 3.2, through the Michaelis-Menten equation (Eq. 2), where the velocity ( $v$ ) of enzyme-catalyzed reactions is hyperbolically related to the substrate concentration ( $[S]$ ):

$$v = \frac{V_{max} \times [S]}{K_m + [S]} \quad (2)$$

Two different linearizations derived from Equation 2 were also presented, namely the Lineweaver-Burk Plot (Eq. 3) and the Eadie-Hofstee Plot (Eq. 4), using software Hyper 3.2:

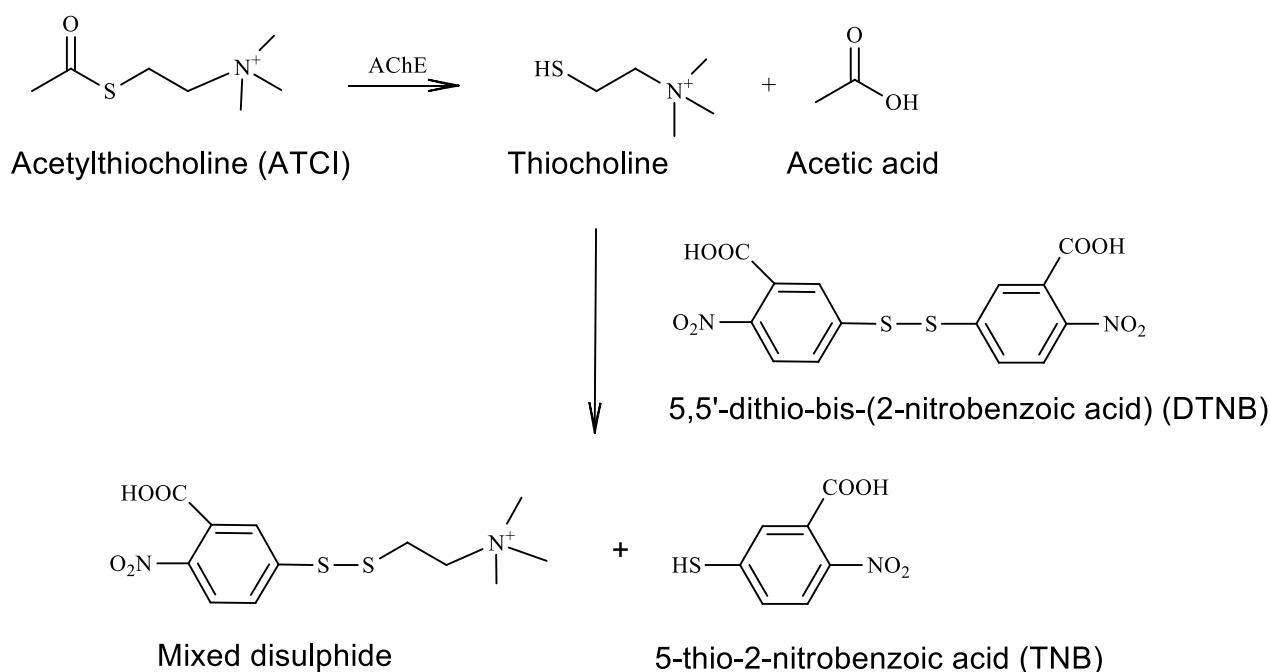
$$\frac{1}{v} = \frac{K_m}{V_{max}} \times \frac{1}{[S]} + \frac{1}{V_{max}} \quad (3)$$

$$v = V_{max} - \frac{v}{[S]} \times K_m \quad (4)$$

## 2.3. Results and Discussion

### 2.3.1 Enzymatic activity of AChE and BuChE by UV-Vis spectrometry

The assays were based on the Ellman method [178], which uses DTNB to quantify the amount of thiocholine (TCh) produced from the hydrolyses of ATCI by *ee*AChE. TCh reacts with DTNB to give a yellow anion, 2-nitro-5-thiobenzoate (TNB<sup>2-</sup>) (Scheme 6).



**Scheme 6** - ATCI hydrolysis by AChE. Adapted from [178].

In a first step, the methodology was optimized taking into account the concentration of both substrate and DTNB (see section 2.2.1.2.).

The study of the effects of substrate concentration is complicated due to the fact, that [S] varies during the course of the reaction, as long as the substrate is converted into product. One way to simplify this problem is to measure  $V_0$ . In a kinetic experiment [S] is always higher than the concentration of the enzyme [E] [181]. The effect on  $V_0$  provoked by the substrate concentration variation when [E] is constant is represented in Figures 29A and 29B.



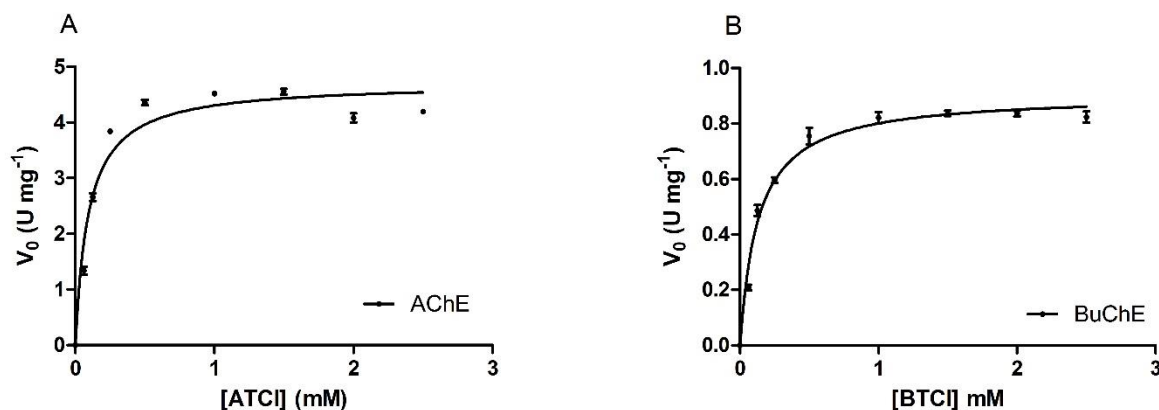


**Figure 29** – Michaelis–Menten curve for (A) *eeAChE* in the presence of ATCI; (B) *eqBuChE* in the presence of BTCI.

The dose-response curve for *eeAChE* using ATCI as substrate and the dose-response curve for *eqBuChE* using BTCI as substrate both followed a Michaelis-Menten kinetics, reaching a maximum concentration for 1.5 mM in both cases.

The kinetic parameters,  $K_m$  and  $V_{max}$ , for *eeAChE* and *eqBuChE* were determined using, respectively, ATCI and BTCI as substrates. The results are presented in Tables 2 and 3.

**Table 2** - Kinetic parameters for *eeAChE* using ATCI as substrate.

	Michaelis-Menten	Eadie-Hofstee	Lineweaver-Burk
$K_m$ (mM)	$0.092 \pm 0.006$	0.109	0.157
$V_{max}$ (U mg <sup>-1</sup> )	$4.697 \pm 0.584$	4.788	5.249

The value of  $K_m$  for *eeAChE* varied between 0.092 mM and 0.157 mM and the  $V_{max}$  ranged from 4.697 to 5.249 U mg<sup>-1</sup> using Michaelis-Menten equation and two different linearization methods.

**Table 3** - Kinetic parameters for *eqBuChE* using BTCI as substrate.

	Michaelis-Menten	Eadie-Hofstee	Lineweaver-Burk
$K_m$ (mM)	$0.132 \pm 0,052$	0.145	0.233
$V_{max}$ (U mg <sup>-1</sup> )	$0.906 \pm 0.074$	0.911	1.062

For *eq*BuChE, the value of  $K_m$  ranged from 0.132 mM to 0.233 mM and  $V_{max}$  varied between 0.906 and 1.062 U mg<sup>-1</sup> using Michaelis-Menten equation and two different linearization methods.

The results obtained for *ee*AChE  $K_m$  parameter is lower than the result obtained for *eq*BuChE, which means that the first needs lower substrate concentration to reach half maximal velocity for the enzymatic reaction. Therefore, if an enzyme has a small value of  $K_m$ , it achieves maximal catalytic efficiency at low substrate concentrations [32]. Actually, Voet *et al.* report for AChE a  $K_m$  value of 0.095 mM and a catalytic efficiency<sup>3</sup> of  $1.5 \times 10^8 \text{ M}^{-1} \text{ s}^{-1}$  under similar conditions as described above (see 2.2.1.3.) [32]. With regards to  $V_{max}$ , AChE (Table 2) presents a result 4 times higher than BuChE (Table 3), which is in concordance with the catalytic efficiency of AChE.

Ramsay *et al.* reported a  $K_m$  value of 0.1 mM for AChE and 0.15 mM for BuChE [35]. In another study Di Giovanni *et al.* presented a  $K_m$  of  $0.12 \pm 0.02$  mM and a  $V_{max}$  of  $1.39 \pm 0.06$  mM min<sup>-1</sup> U<sup>-1</sup> for AChE under similar conditions to the ones used in this thesis, the exception was the 412nm wavelength used by Di Giovanni [182]. Comparing these results with the ones presented in Tables 2 and 3, is possible to assume they are in agreement.

In the case of the Lineweaver-Burk results from both Tables (2 and 3) a big discrepancy is observed, especially for  $K_m$ . Actually, Copeland and coworkers previously mentioned that Lineweaver-Burk plots were not suitable for determining  $K_m$  and  $V_{max}$ , instead they recommended following a non-linear regression analysis of the untransformed data fit to the Michaelis-Menten equation [183]. Dowd and Riggs confirmed this by using a computer program to generate random samples from populations of simulated data (using 500 replicates), and to estimate  $K_m$  and  $V_{max}$  from each sample, by the method of least squares, without weighting, for three different linear transformations, including Lineweaver-Burk. The distribution of the sample estimates of the parameters were then compared with the Michaelis-Menten equation values, and the results depicted by the Lineweaver-Burk equation were the least reasonable [184]. So, it is possible to say that the results obtained with the Lineweaver-Burk linearization method (Tables 2 and 3) are unreliable when compared to Eadie-Hofstee linearization method and to the untransformed data fitted to the Michaelis-Menten equation.

---

<sup>3</sup> Increasing the reaction rate of a chemical reaction allows the reaction to become more efficient, and hence more products are generated at a faster rate. Increase of the reaction rate, will result in a more efficient chemical reaction within a biological system.

### 2.3.1.1. Evaluation of enzymatic selectivity for the substrate

ACh is hydrolyzed by *ee*AChE and *eq*BuChE. An important fact that distinguishes the two enzymes is their kinetic response to different concentrations of the neurotransmitter acetylcholine (ACh), which is reflected by their  $K_m$  and  $V_{max}$  values. The results from this experiment are presented in Figures 30A and 30B and Table 4. Actually, Figure 30A shows the hydrolysis of ATCI for *ee*AChE (dot) and *eq*BuChE (square), where it is clear that ATCI hydrolysis catalyzed by *eq*BuChE is slower than the same substrate hydrolysis by *ee*AChE [185, 186].

In the case of BTCI (synthetic substrate),  $V_{max}$  for *eq*BuChE was 1000 times greater than for *ee*AChE. This, allied to the analysis of Figure 30B, that shows the hydrolysis of BTCI by *ee*AChE (dot) and *eq*BuChE (square), led to the conclusion that *ee*AChE had no affinity for BTCI (see the dot line over the  $xx$  axis), contrary to what was verified for *eq*BuChE, for which this is a specific substrate (Fig. 30B).

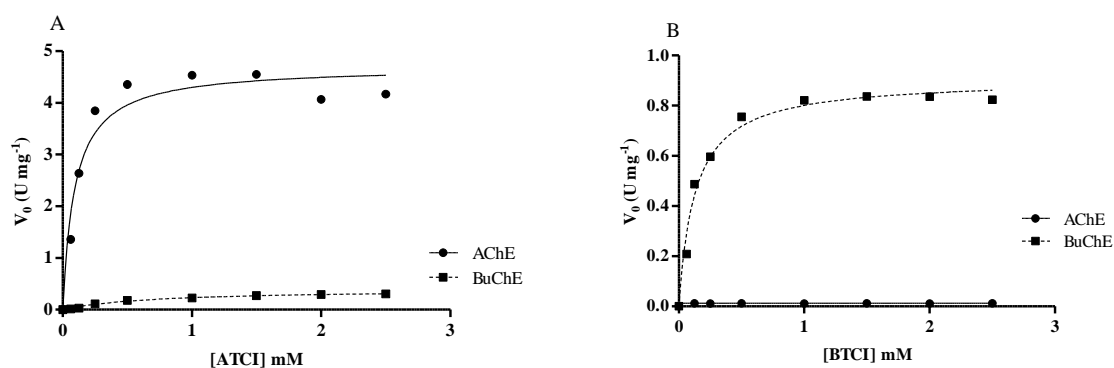


**Figure 30** - Michaelis–Menten curve kinetic representation of *ee*AChE and *eq*BuChE using: (A) ATCI as substrate; (B) BTCI as substrate.

From these results, it's possible to see that both *ee*AChE and *eq*BuChE hydrolyze ATCI, although the affinity of the substrate to *ee*AChE was bigger, showing a  $K_m$  value seven times inferior for this enzyme when compared to *eq*BuChE. It's possible to assume that, if *eq*BuChE hydrolyzes ATCI (the synthetic substitute for ACh) it should also hydrolyze ACh in the brain. In fact, Silver stated that *eq*BuChE could efficiently catalyze ACh hydrolysis [186].

**Table 4** – Kinetic parameters for *ee*AChE (using ATCI as substrate) and *eq*BuChE (using both ATCI and BTCI as substrates) .

	AChE		BuChE
	ATCI	ATCI	BTCI
$K_m$ (mM)	0.092 ± 0.006	0.672 ± 0.033	0.132 ± 0.052
$V_{max}$ (U mg <sup>-1</sup> )	4.697 ± 0.584	0.391 ± 0.07	0.906 ± 0.074

### 2.3.1.2. *ee*AChE and *eq*BuChE inhibitory activity evaluation for rivastigmine, donepezil and galantamine

The variety of different parameters presented in the literature for calculating IC<sub>50</sub> values produces numerous results. These different parameters include temperature, wavelength, buffer, pH value, the source of the enzyme, previous incubation (or not) of the inhibitor with the enzyme and the substrate used. To properly compare the results of existing compounds with new ones, a study of these variables was carried out in this dissertation.

The active ingredients of three commercial compounds used in AD therapy (donepezil, rivastigmine and galantamine) were studied for the effects of different parameters on their IC<sub>50</sub> determination for *ee*AChE and *eq*BuChE. These parameters include: wavelength (405 nm or 412 nm); temperature (25 °C or 37 °C); buffer (Tris-HCl 0.05M, pH 8 or Phosphate 0.1M, pH 8); pre-incubation (or not) of the inhibitor with the enzyme before adding the substrate. The dose-response graphs are presented in Figures 31 to 34 and the IC<sub>50</sub> results are presented in Tables 5 to 8.

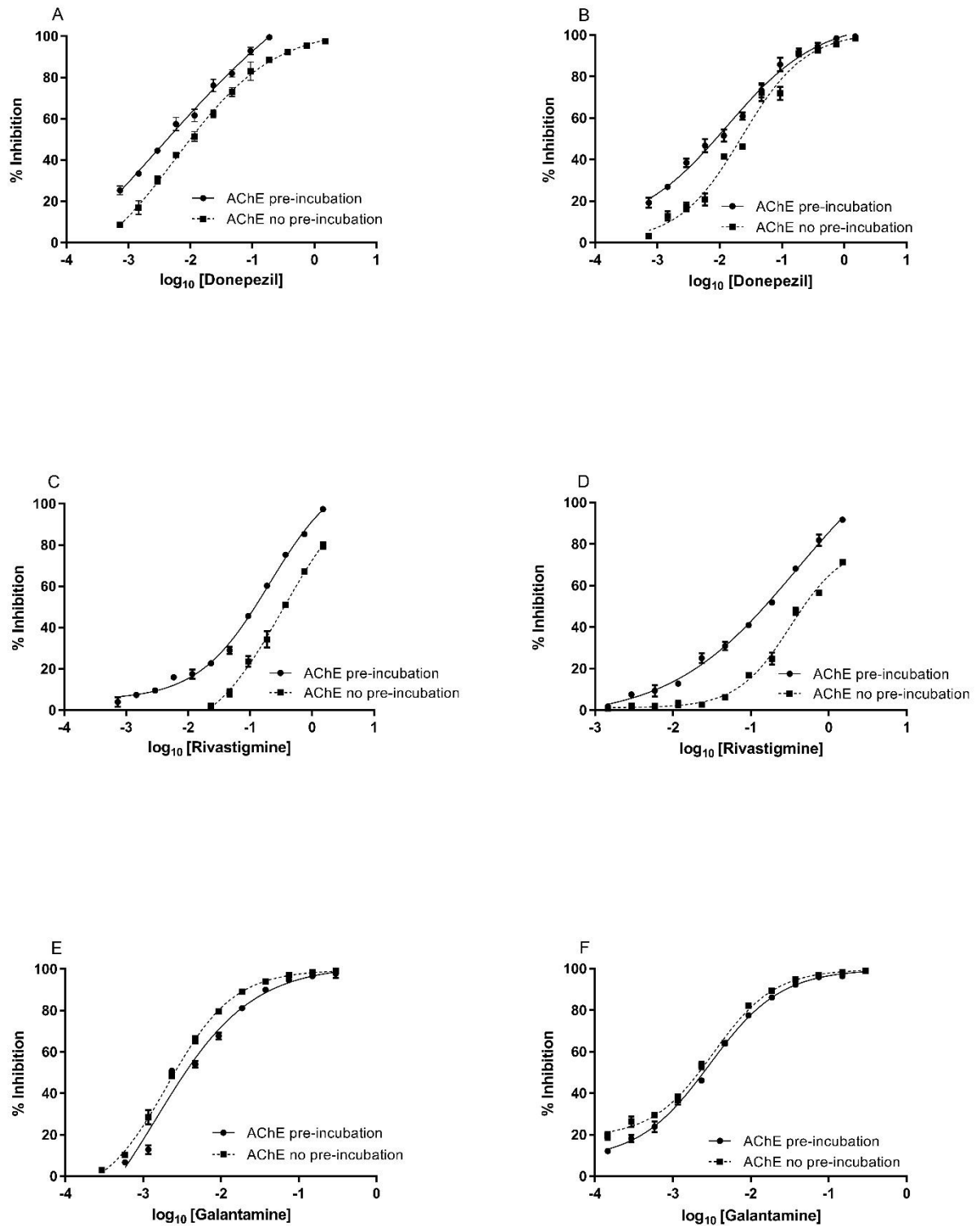


**Figure 31** – *ee*AChE dose-response curves for donepezil, rivastigmine and galantamine in Tris-HCl buffer and 405 nm, at 25 °C (A, C, E) and 37 °C (B, D, F).

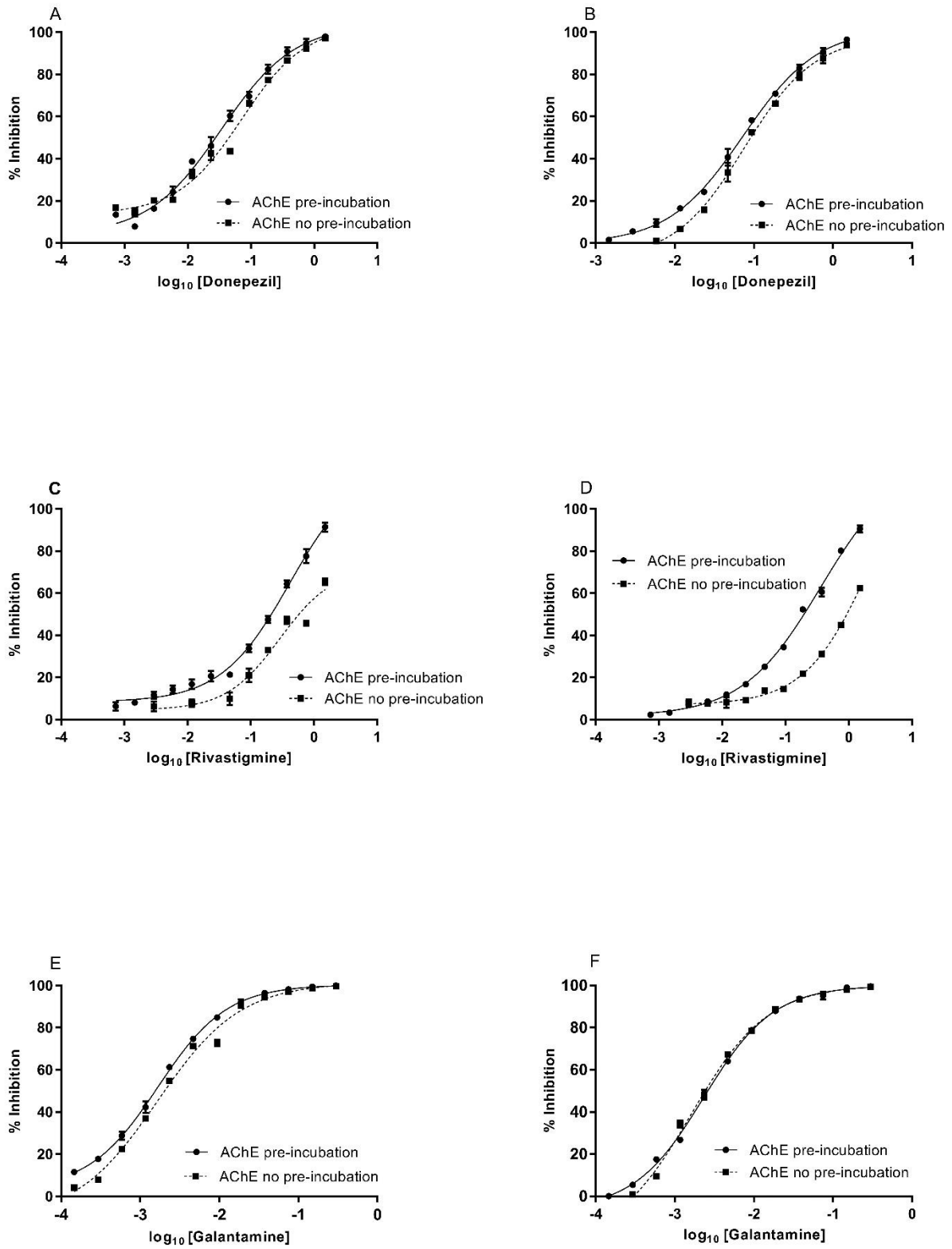


**Figure 32** - *ee*AChE dose-response curves for donepezil, rivastigmine and galantamine in Tris-HCl buffer and 412 nm, at 25 °C (A, C, E) and 37 °C (B, D, F).

**Table 5** - *eeAChE* IC<sub>50</sub> values of the active ingredients of the commercial drugs used in AD treatment with Tris-HCl 0.05 M, pH 8, measured at 25 °C and 37 °C (with/without pre-incubation at 405 nm).

	25°C		37°C	
	No pre-incubation	Pre-incubation	No pre-incubation	Pre-incubation
<b>Donepezil Hydrochloride</b>	14.3 ± 0.1 nM	6.12 ± 0.5 nM	26.9 ± 1.3 nM	11.5 ± 4.0 nM
<b>Rivastigmine Tartrate</b>	342.5 ± 13.0 µM	127.6 ± 5.9 µM	478.0 ± 5.1 µM	163.2 ± 3.9 µM
<b>Galantamine Bromide</b>	2.9 ± 0.2 µM	4.4 ± 0.0 µM	2.0 ± 0.4 µM	2.5 ± 0.0 µM

**Table 6** - *eeAChE* IC<sub>50</sub> values of the active ingredients of the commercial drugs used in AD treatment with Tris-HCl 0.05 M, pH 8, measured at 25 °C and 37 °C (with/without pre-incubation at 412 nm).

	25°C		37°C	
	No pre-incubation	Pre-incubation	No pre-incubation	Pre-incubation
<b>Donepezil Hydrochloride</b>	42.1 ± 1.8 nM	21.5 ± 10.3 nM	73.3 ± 2.9 nM	57.7 ± 4.9 nM
<b>Rivastigmine Tartrate</b>	914.0 µM	228.3 ± 31.6 µM	966.0 µM	199.0 ± 6.2 µM
<b>Galantamine Bromide</b>	2.2 ± 0.4 µM	1.6 ± 0.0 µM	2.2 ± 0.1 µM	2.7 ± 0.2 µM

The results of *eeAChE* activity, with and without incubation at 25 °C and 37 °C using Tris-HCl buffer (tables 5 and 6) showed that the IC<sub>50</sub> values for both donepezil and rivastigmine improved with pre-incubation. For galantamine there was no considerable change. Between the two different temperatures the overall results are better at 25 °C, except for rivastigmine. If the different wavelengths are considered (Tables 5 and 6), the results are similar in the case of galantamine but very different for donepezil and rivastigmine, showing IC<sub>50</sub> results much better for a wavelength of 405 nm (Figs. 31-32).

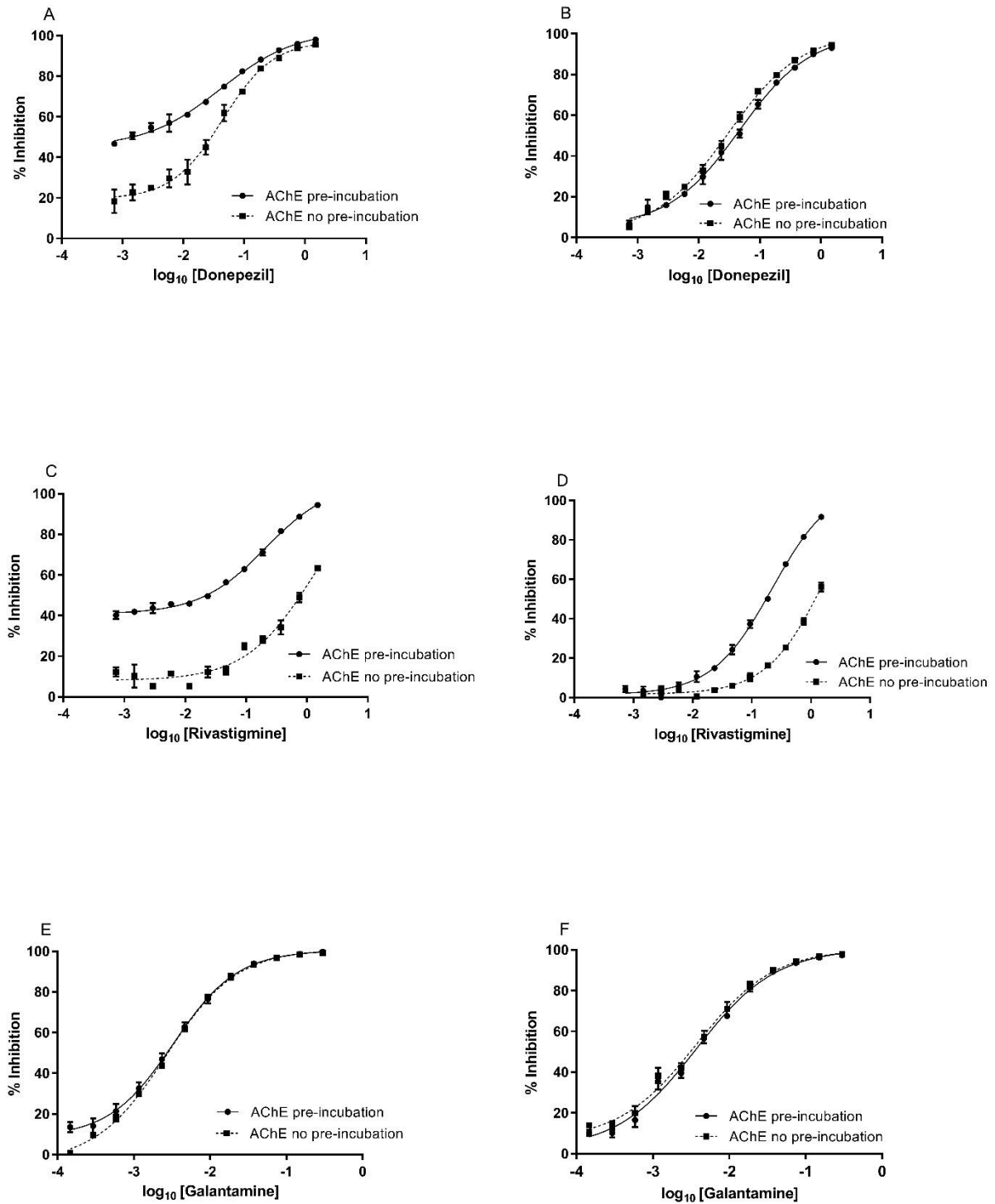


**Figure 33** – *ee*AChE dose-response curves for donepezil, rivastigmine and galantamine in phosphate buffer and 405 nm, at 25 °C (A, C, E) and 37 °C (B, D, F).



**Table 7** – *eeAChE* IC<sub>50</sub> values of the active ingredients of the commercial drugs used in AD treatment with phosphate buffer 0.1 M, pH 8 measured at 25 °C and 37 °C (with/without pre-incubation at 405 nm).

	25°C		37°C	
	No pre-incubation	Pre-incubation	No pre-incubation	Pre-incubation
<b>Donepezil Hydrochloride</b>	32.9 ± 4.5 nM	1.6 ± 0.7 nM	41.9 ± 7.5 nM	28.8 ± 3.4 nM
<b>Rivastigmine Tartrate</b>	789.5 ± 77.9 µM	22.4 ± 1.6 µM	175.4 ± 4.0 µM	78.2 ± 13.8 µM
<b>Galantamine Bromide</b>	2.8 ± 0.0 µM	2.7 ± 0.4 µM	3.1 ± 0.3 µM	3.5 ± 0.3 µM

Comparing the results of the assays, in the presence of *eeAChE*, with and without incubation at 25° C and 37 °C using phosphate buffer (Table 7, Figure 33) shows that, once again, galantamine doesn't change significantly its IC<sub>50</sub> values. On the other hand, donepezil and rivastigmine present better results for incubation at 25 °C in phosphate buffer. Rivastigmine also shows better IC<sub>50</sub> results at 37 °C with and without incubation in phosphate buffer.

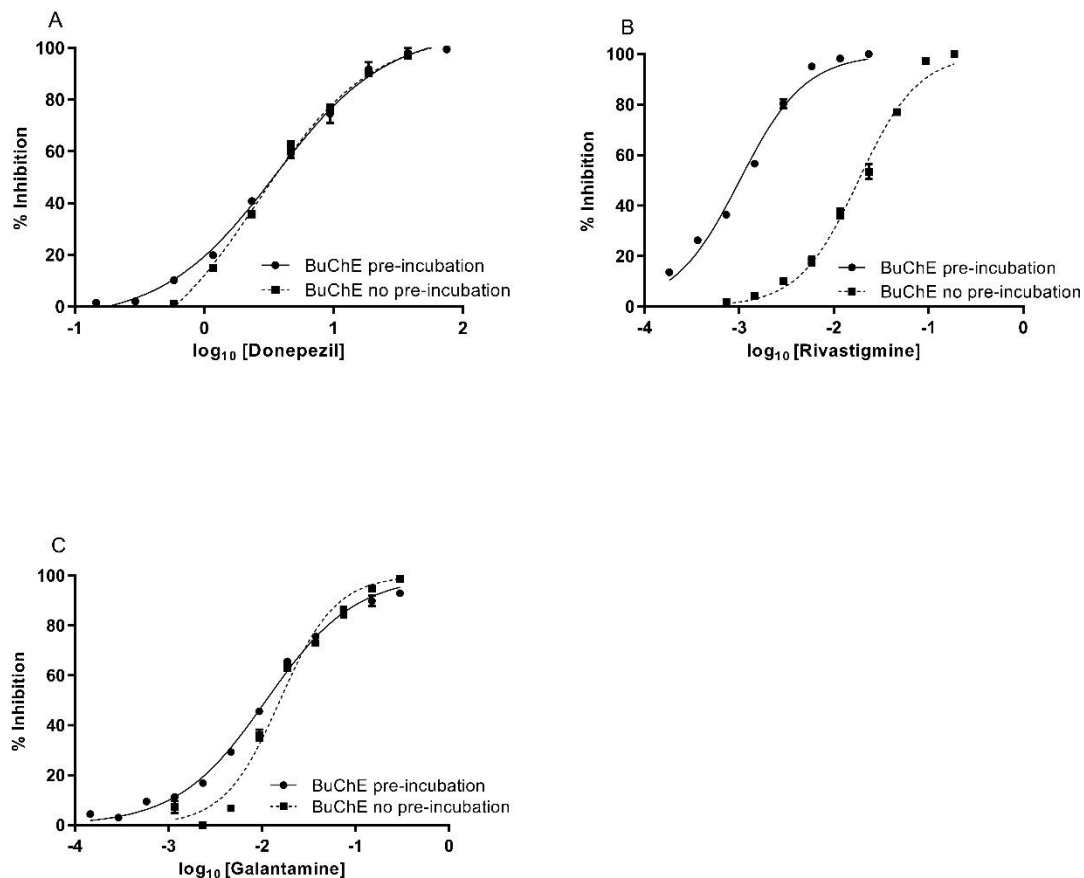


**Figure 34** - *eq*BuChE dose-response curves for donepezil, rivastigmine and galantamine in phosphate buffer and 405 nm, at 25 °C (A, B, C).

**Table 8** - *eq*BuChE IC<sub>50</sub> values of the active ingredients of the commercial drugs used in AD treatment with Tris-HCl 0.05 M, pH 8, measured at 25 °C (with/without pre-incubation at 405 nm).

	25°C	
	No pre-incubation	Pre-incubation
<b>Donepezil Hydrochloride</b>	3.3 ± 0.1 μM	3.4 ± 0.2 μM
<b>Rivastigmine Tartrate</b>	26.7 ± 3.8 μM	1.3 ± 0.0 μM
<b>Galantamine Bromide</b>	14.9 ± 0.7 μM	10.9 ± 0.2 μM

Analyzing the results on Table 8, only rivastigmine presented considerable changes in activity against *eq*BuChE, with better results when incubated at 25 °C. When compared, Tables 5 and 8 show that the both donepezil and galantamine were better inhibitors against *ee*AChE and rivastigmine was a better inhibitor against *eq*BuChE.

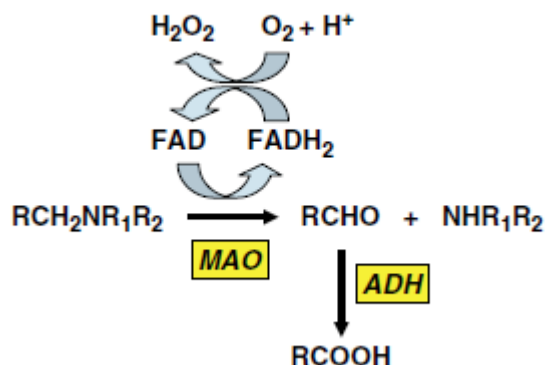
The overall results (Tables 5-8 and Figs. 31-34) show donepezil as the best inhibitor for *ee*AChE. Anand and Gharabawi describe Rivastigmine as a “pseudo-irreversible” enzyme inhibitor (dissociates more slowly) that undergoes hydrolysis by AChE [131].

Enz and coworkers reported that the activity of Rivastigmine against AChE is 100 to 1000 times less potent *in vitro* (without previous incubation) than that of tacrine or physostigmine, but only 10-fold lower *in vivo* [187]. This can explain the discrepancy of IC<sub>50</sub> results against *ee*AChE, between rivastigmine and the other two inhibitors, donepezil and galantamine.

As stated earlier, IC<sub>50</sub> values can suffer slight to major variation, depending on the inhibitor and on the assay conditions. For instance, galantamine presents an activity against AChE that ranges from 0.55 μM to 6.60 μM [167, 182, 188-190], and is of 7.3 μM for BuChE [171]. The activity of donepezil against AChE varies between 11 nM and 7.61 μM [35, 182, 191-194], and against BuChE ranges from 4.1 μM to 7.3 μM [35, 191-193]. The lower IC<sub>50</sub>'s presented for these compounds were achieved with pre-incubation of the enzyme, which show its importance on the assay conditions.

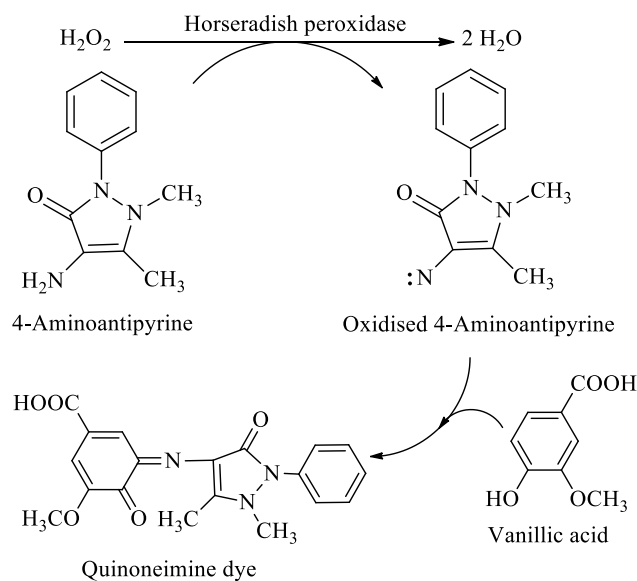
### 2.3.2. Enzymatic activity for MAO-B

The assays were based on the method described by Holt *et al.*[179]. The reaction mechanism of MAO involves oxidative deamination of primary, secondary and tertiary amines to the corresponding aldehyde and free amine, with the generation of hydrogen peroxide (Scheme 7). In this case, the substrate benzylamine (which is specific for MAO-B) is deaminated by the enzyme to form benzaldehyde. The aldehyde is rapidly metabolized by aldehyde dehydrogenase to acidic metabolites [195]. The aldehyde formed can be detected by spectrophotometry [179]. It is also possible to detect the amount of hydrogen peroxide formed during the reaction.



**Scheme 7** - Reaction pathway of monoamine metabolism by oxidative deamination by mitochondrial MAO. Adapted from [195].

In this test reaction, the  $\text{H}_2\text{O}_2$  formed is detected instead of the aldehyde. 4-Aminoantipyrine acts as the proton donor in the peroxidase reaction and then condenses with vanillic acid to afford the quinoneimine dye (Scheme 8) [179].



**Scheme 8** - Peroxidase assay for MAO-B activity determination. Adapted from [179].

Results show that MAO-B follows a Michaelis-Menten kinetic (Fig. 35) with a maximum concentration of 7.5 mM.

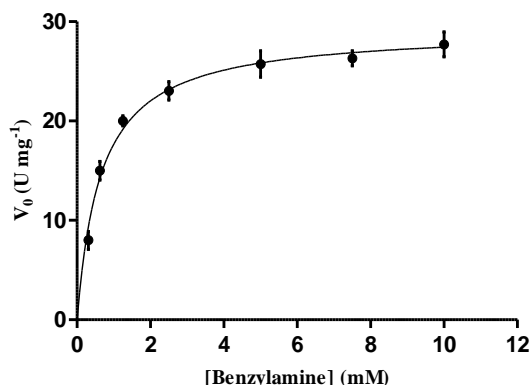


Figure 35 - Determination of kinetic parameters for MAO-B.

Table 9 presents  $K_m$  and  $V_{max}$  values for Michaelis-Menten and two different linearization methods (Eadie-Hofstee and Lineweaver-Burk).

Table 9 - Kinetic parameters for MAO-B using benzylamine as substrate.

	Michaelis-Menten	Eadie-Hofstee	Lineweaver-Burk
$K_m$ (mM)	$0.675 \pm 0.044$	0.668	0.665
$V_{max}$ (U mg <sup>-1</sup> )	$29.180 \pm 2.374$	29.150	29.130

The value of  $K_m$  for MAO-B varied between 0.665 mM and 0.675 mM and the  $V_{max}$  ranged from 29.130 to 29.180 U mg<sup>-1</sup> using different linearization methods.

Finberg *et al.* reported for MAO-B a  $K_m$  of 0.305 mM and a catalytic efficiency of  $4.9 \times 10^4$  M<sup>-1</sup>s<sup>-1</sup> [196]. When comparing these results with the ones for *ee*AChE or *eq*BuChE (Tables 2 and 3) the difference in  $K_m$  and  $V_{max}$  is significant, showing that MAO-B is an enzyme that needs a higher substrate concentration to reach half-maximum velocity and presents a catalytic efficiency  $10^4$  lower than *ee*AChE.

To determine the IC<sub>50</sub> values for pargyline and rasagiline by UV/Vis absorption spectrometry, two different approaches were used, with or without inhibitor pre-incubation before substrate addition (see Section 2.2.2.5.).

In the first approach, without inhibitor incubation with the enzyme before substrate addition, there was no variation in the percentage of inhibition of the enzymatic activity with the variation of

substrate concentration (results not shown). On the other hand, in the second approach, when the inhibitor was previously incubated with the enzyme prior to substrate addition followed by addition of the other reagents, it was possible to build a dose-response curve for both inhibitors (Fig. 36).

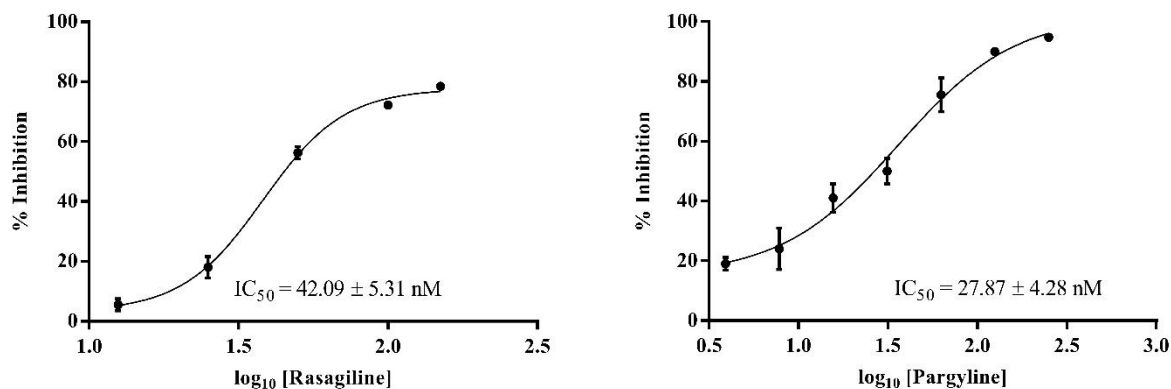


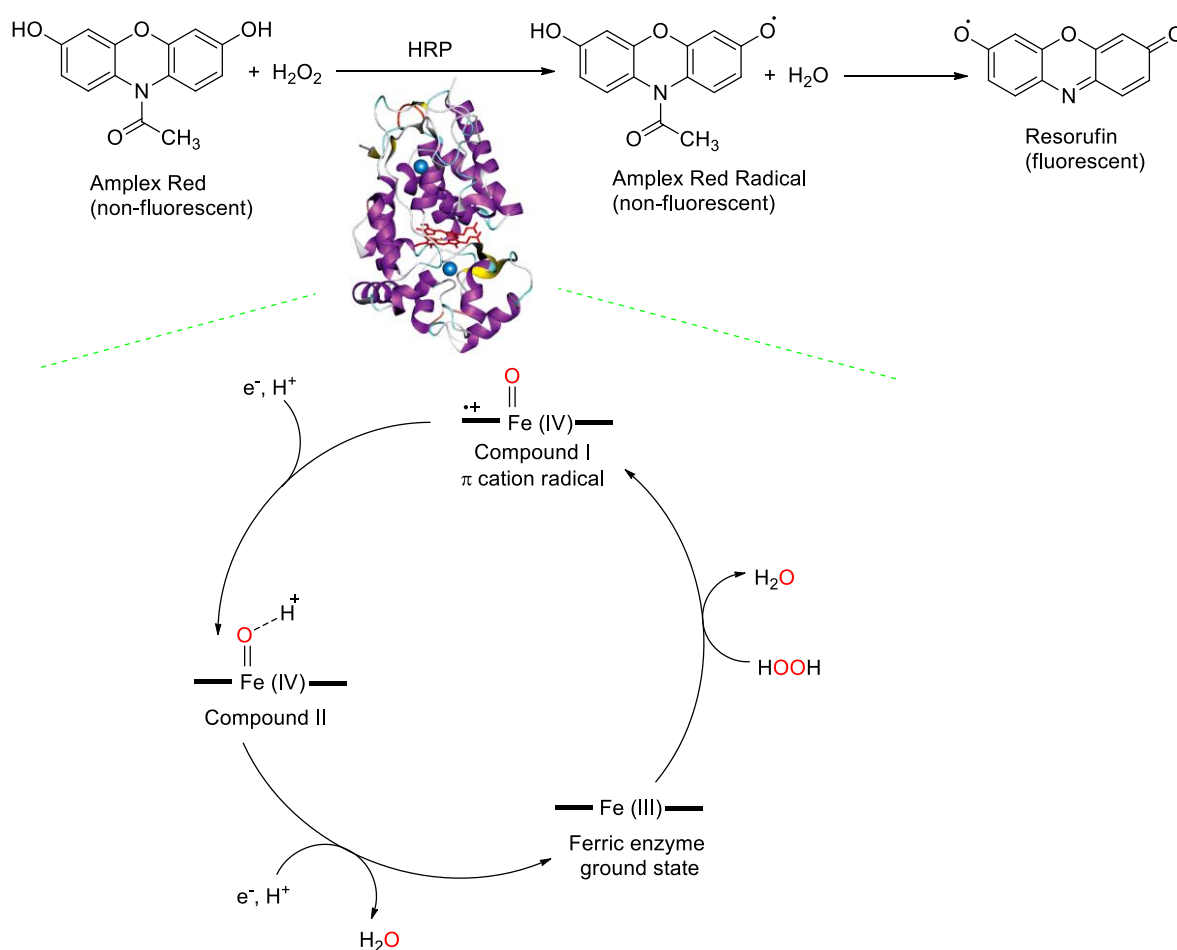
**Figure 36** - Dose-response graph of MAO-B activity against rasagiline and pargyline.

Based on the pargyline concentrations, that varied between 3.9 and 250 nM, it was possible to observe a variation in MAO-B inhibition between 19% and 95%, with an IC<sub>50</sub> of 27.87 nM. For rasagiline, the concentrations varied between 12.5 and 150 nM showing a variation in MAO-B inhibition between 18% and 78%, with an IC<sub>50</sub> of 42.09 nM.

The first approach wasn't suitable for determining MAO-B enzymatic activity. It was possible that these irreversible inhibitors (also called suicide inhibitors) didn't have enough time to out-compete the substrate for the enzyme active center. On the other hand, the second approach gave similar results to those from the literature, leading to the use of this method for further assays. In fact, according to Fowler *et al.*, pargyline inhibits phenylethylamine (PEA) deamination in human brain *in vitro* with an IC<sub>50</sub> of 40 nM [197], whilst Usdin reported an IC<sub>50</sub> for pargyline of 30 nM [198]. Regarding rasagiline, our results are somewhat different from those published by Youdim *et al.*, 4.43 nM for rat brain and 14 nM for human brain *in vitro* [199]. This discrepancy could be due to the different methods used to determine MAO-B activity, since Youdim *et al.* used a liquid scintillation counting technique, with selegiline as substrate and a 60 min pre-incubation at 37 °C, as we used spectrometry UV-Vis, with benzylamine as substrate and 30 min pre-incubation at 37 °C.

Another assay method used for determining the enzymatic activity of MAO-B is based on the detection of hydrogen peroxide ( $\text{H}_2\text{O}_2$ ) in a horseradish peroxidase-coupled reaction using *N*-acetyl-3,7-dihydroxyphenoxazine (Amplex Red), a highly sensitive and stable probe for  $\text{H}_2\text{O}_2$ . HRP (E.C. 1.11.1.7.) is a metalloenzyme with a heme group and two calcium ions located at the distal and proximal regions of the enzyme. These calcium ions confer stability to the enzyme [200].

Hydrogen peroxide is the oxidizing agent of HRP reaction and is produced from the oxidative-deamination of the substrate, which is then followed by hydrolysis of the iminium ion to the corresponding aldehyde by MAO-B (see scheme 5).  $\text{H}_2\text{O}_2$  then reacts with amplex red (non-fluorescent) in the presence of HRP producing resorufin (fluorescent). The stoichiometry of the reaction is 1:1 [201]. By measuring the fluorescence it is possible to calculate the product concentration (scheme 9). HRP (purple) catalyzes a one-electron oxidation of non-fluorescent Amplex Red to the non-fluorescent Amplex Red radical. The formation of fluorescent resorufin from the Amplex Red radical is an enzyme independent reaction. The overall reaction stoichiometry between Amplex Red and  $\text{H}_2\text{O}_2$  (red) is 1 : 1 [202].



**Scheme 9** – Horseradish peroxidase assay (showing the catalytic cycle of peroxidase) for MAO-B activity determination by tracing hydrogen peroxide. Adapted from [202].

In scheme 9, HRP first oxidizes Amplex Red to non-fluorescent radical intermediates, which subsequently undergo an enzyme independent reaction to form fluorescent resorufin [202]. In the peroxidase cycle, hydrogen peroxide binds to the iron atom on the distal side of the ferric enzyme which forms a peroxide adduct, that upon elimination of water, forms an oxoferryl species plus a porphyrin-based  $\pi$  cation radical, compound I. Reduction of compound I by elimination of the  $\pi$  cation radical forms compound II which is reduced to return the enzyme to the resting state [200, 203].

To determine the  $IC_{50}$  for pargyline and rasagiline, the fluorescence was measured at the initial time and after 30 minutes. By applying the calibration curve equation, a dose-response graph was drawn for each inhibitor (Fig. 37), which allowed to determine the corresponding  $IC_{50}$  values.

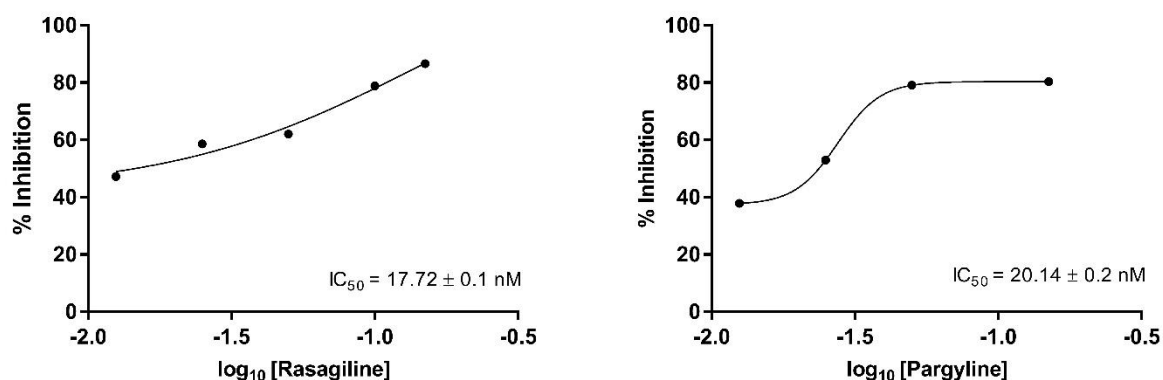


**Figure 37** - Dose-response curves and  $IC_{50}$  values for pargyline and rasagiline by fluometry.

The  $IC_{50}$  for both inhibitors were very similar (20.14 nM and 17.72 nM), but the value for pargyline was greater. When we compared these results with the ones obtained by the spectrometric method (28.70 nM and 40.72 nM), we observed that these results were lower. In a study by Zhou and coworkers, they used a fluorometric method to measure MAO-B with a sensitivity 10-fold higher than the conventional spectrophotometric assay method, and were able to detect MAO-B activity as low as  $1.2 \times 10^{-5}$  U/mL [180]. Another point favorable to the fluorometric method is the use of much lower amounts of enzyme, making this method much more sensitive (and less expensive) than the previous one. This makes it a reliable method for a bioassay screening test.



---

### 2.3. Conclusions

The kinetic parameters for *ee*AChE, *eq*BuChE and MAO-B were optimized. *ee*AChE was the most efficient of the three enzymes studied. Both *ee*AChE and *eq*BuChE presented selectivity for ATCI, but only *eq*BuChE presented selectivity for BTCl.

The lack of information in terms of comparison of the three major commercial drugs used in AD led to their study under different assay conditions. The IC<sub>50</sub> values of Donepezil, Rivastigmine and Galantamine, suffered slight to major variation, depending on the assay conditions. According to the results obtained (see Section 2.3.1.2.) the following conditions were chosen for the proceeding assays: no incubation at 25 °C with a wavelength of 405 nm and Tris-HCl 0.05 M, pH 8 buffer.

The comparative study of rasagiline and pargyline was made using two different methods, to determine their accuracy. UV-Vis molecular absorption spectrometry and fluorometric methods were compared, and although the fluorometric method was much more sensitive, a good correlation in the bioassay screening test was achieved with the UV-Vis molecular absorption spectrometry method, allowing this technique to be used in a simpler and less expensive way.



## ***Chapter 3***

# ***Screening therapeutic target molecules for neurodegenerative diseases***

---

*“One never notices what has been done;  
One can only see what remains to be done.”*

Marie Curie (1867-1934)

The studies made in this chapter originated the following publications:

1. Bacalhau, P., San Juan, A., Marques, C., Peixoto, D., Burke, A.J., Caldeira, A., Martins, M.R. *The role of cholinesterases in Alzheimer's disease: screening of target compounds*. *Neurodegener Dis.* **15(suppl 1)**, 741 (2015).
2. Bacalhau, P., San Juan, A., Marques, C., Peixoto, D., Goth, A., Guarda, C., Silva, M., Arantes, S., Caldeira, A. T., Martins, M. R., Burke, A. J. New cholinesterase inhibitors for Alzheimer's disease: Structure Activity Studies (SARs) and molecular docking of isoquinolone and azepanone derivatives. *Bioorg. Chem.* **67**, 1–8 (2016).
3. Viana, H., Carreiro, E. P., Goth, A., Bacalhau, P., Caldeira, A. T., Martins, M. R. and Burke, A. J., ChemInform Abstract: Sequential Alcohol Oxidation/putative Homo Claisen—Tishchenko-Type Reaction to Give Esters: A Key Process in Accessing Novel Biologically Active Lactone Macrocycles. *ChemInform*, **47** (47) (2016).
4. Viana, H., Carreiro, E., Goth, A., Bacalhau, P., Caldeira, A.T., Martins, M. R., Burke, A. J. Sequential Alcohol Oxidation/putative Homo Claisen-Tishchenko-Type Reaction to give esters: A Key process in accessing novel biologically active lactone macrocycles. *RSC Adv.* **6**, 63214-63223 (2016).
5. Totobenazara, J., Bacalhau, P., San Juan, A., Marques, C. S., Fernandes, L., Goth, A., Caldeira, A. T., Martins, R., Burke, A. J., Design, Synthesis and Bioassays of 3-Substituted-3-Hydroxyoxindoles for Cholinesterase Inhibition. *Chemistry Select*, **1**, 3580 – 3588 (2016).

### 3.1. Introduction

In the healthy human brain, AChE activity is greater than BuChE activity. One of the hallmarks of AD is the significant loss of cholinergic neurons, accompanied by the decline of ACh available in the brain [204]. During AD progression AChE levels in the CNS decrease contrary to what occurs with BuChE [172]. Based on the cholinergic hypothesis (see section 1.3.1.3), targeting these enzymes will help increase the neurotransmitter ACh levels.

PD is associated with the loss of dopaminergic neurons resulting in dopamine decrease by MAO-B, by oxidative deamination [76]. One of the promise strategy to delay PD symptoms is based on targeting MAO-B (see section 1.3.2.5).

The increasing mortality rate of AD, PD and the reduced therapeutic potential of the currently available options have led to focus these research activities on the development of MTDLs as potential cholinesterase and monoamine oxidase inhibitors. This research led to the screening of a wide range of structurally diverse small molecules, in an *in vitro* bioassay which involved the search for “hits”, which are active substances having a preferential activity for the target [205].

All the compounds, except stated otherwise were tested as a racemic mixture. Many drugs having a center of asymmetry are still used in clinical practice as racemates. Often, racemic drugs were introduced in clinical practice because the animal and the clinical pharmacology, the toxicology, and the teratology were performed with the racemates [206]. A large proportion of therapeutic agents are chiral molecules, being single enantiomer or racemic mixtures. The best and most simple definition to date for chirality is that given by Mislow, which states: “An object is chiral if and only it is not superimposable on its mirror image; otherwise it is achiral” [207]. This term describes the nature of the molecule but does not refer to its stereochemical composition [208].

There is a large number of natural occurring molecules that are pharmacologically active substances with a broad spectrum, i.e., antimicrobial, antineoplastic, CNS-active, anti-inflammatory and cardiovascular [209]. Most compounds in nature present the same sense of chirality, for instance, with rare exceptions  $\alpha$ -aminoacids occurring in nature consistently have the L configuration; similarly, monosaccharides are of the D configuration. Closely related molecules usually have the same sense of chirality. Specific interaction of the chiral drug with the chiral space of the biological receptor is preferential for only one of the enantiomers. So, it is not surprising that many of the compounds that are used as therapeutic agents are chiral and present a specific enantiomeric form [208].

The screening methods used were as described in chapter 2.

## 3.2. Materials and methods

### 3.2.1. Chemicals

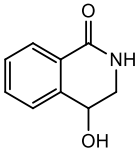
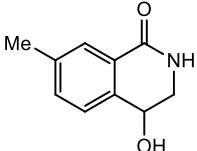
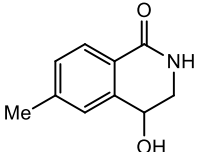
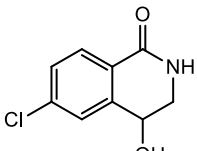
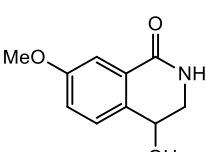
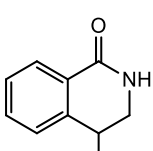
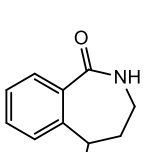
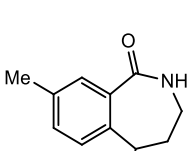
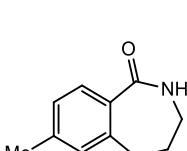
*ee*AChE, *eq*BuChE, 5,5-dithio-bis-(2-nitrobenzoic acid) (DTNB), acetylthiocholine iodide (ATCI) and butyrylthiocholine iodide (BTCI) were purchased from Sigma-Aldrich. AChE used in the assay was from *Electrophorus electricus* (type VI-S lyophilized powder, 814 U mg<sup>-1</sup> protein), BuChE used in the assay was from equine serum (lyophilized powder, 1830 U mg<sup>-1</sup> protein). The lyophilized enzymes were prepared in 20 mM Tris-HCl pH 7.6 buffer. DTNB was prepared in 50 mM Tris-HCl, 0.1 M NaCl, 0.02 M MgCl<sub>2</sub> buffer (pH 8.0). ATCI and BTCI were prepared in 50 mM Tris-HCl buffer (pH 8.0).

### 3.2.2. Compound Screening

All synthesized compounds were developed by the Group of Medicinal Chemistry/Organic Synthesis of Prof. Anthony Burke. The isoquinolinone and azepanone derivatives were synthesized by Dr. Daniela Peixoto and Dr. Carolina Marques [210]. The indolinone derivatives were synthesized by Dr. Jane Totobenazara, Dr. Carolina Marques and Luís Fernandes [211]. The diether-ester derivatives as well as the chromanone and chromanol derivatives were synthesized by Dr. Hugo Viana [212]. Compounds **17a** and **17b** were enantiomers of compound **17** (racemate). All the other compounds were racemic. Compounds **48a** and **48b** were presented in the form of salt.

The rivastigmine derivatives were synthesized by Prof. Maurizio Benaglia Chemistry Group in the context of the bilateral project, FCT/ITALIA CNR - 2015/2016 (Ref. 441.00), “*Using enantioselective reductions with organocatalysts as a means to obtaining key drugs for neurodegenerative diseases*”. These compounds were enantiomerically pure and presented in the form of salt. Table 10 shows the name, structure and family of the compounds tested in this chapter.

Table 10 - Compounds in study.

Family	Compound structure	Compound name	Number
Isoquinolinone		4-hydroxy-3,4-dihydroisoquinolin-1(2H)-one	1
Isoquinolinone		4-hydroxy-7-methyl-3,4-dihydroisoquinolin-1(2H)-one	2
Isoquinolinone		4-hydroxy-6-methyl-3,4-dihydroisoquinolin-1(2H)-one	3
Isoquinolinone		6-chloro-4-hydroxy-3,4-dihydroisoquinolin-1(2H)-one	4
Isoquinolinone		4-hydroxy-7-methoxy-3,4-dihydroisoquinolin-1(2H)-one	5
Isoquinolinone		4-methoxy-3,4-dihydroisoquinolin-1(2H)-one	6
Isoquinolinone		5-hydroxy-2,3,4,5-tetrahydro-1H-benzo[c]azepin-1-one	7
Isoquinolinone		5-hydroxy-8-methyl-2,3,4,5-tetrahydro-1H-benzo[c]azepin-1-one	8
Azepanone		-hydroxy-7-methyl-2,3,4,5-tetrahydro-1H-benzo[c]azepin-1-one	9

**Table 10** – (continued).

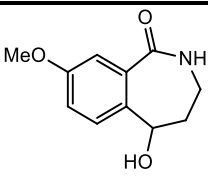
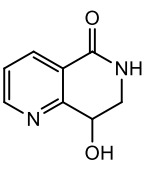
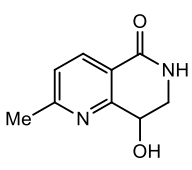
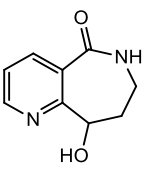
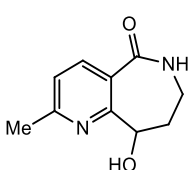
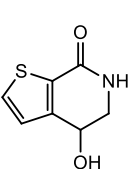
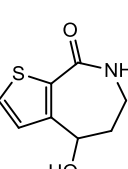
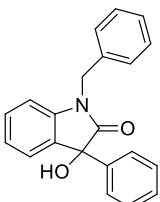
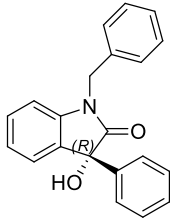
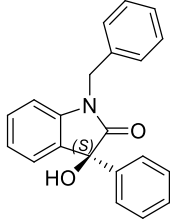
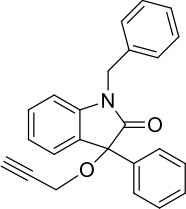
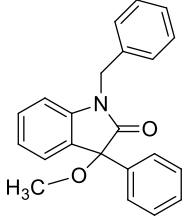
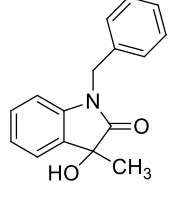
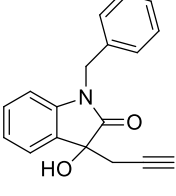
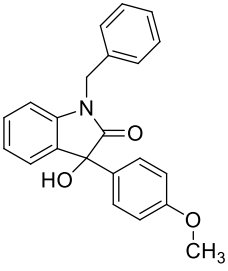
Azepanone		5-hydroxy-8-methoxy-2,3,4,5-tetrahydro-1H-benzo[c]azepin-1-one	10
Azepanone		8-hydroxy-7,8-dihydro-1,6-naphthyridin-5(6H)-one	11
Azepanone		8-hydroxy-2-methyl-7,8-dihydro-1,6-naphthyridin-5(6H)-one	12
Azepanone		9-hydroxy-6,7,8,9-tetrahydro-5H-pyrido[3,2-c]azepin-5-one	13
Azepanone		9-hydroxy-2-methyl-6,7,8,9-tetrahydro-5H-pyrido[3,2-c]azepin-5-one	14
Azepanone		4-hydroxy-5,6-dihydrothieno[2,3-c]pyridin-7(4H)-one	15
Azepanone		4-hydroxy-6,7-dihydro-4H-thieno[2,3-c]azepin-8(5H)-one	16
Indolinone		1-benzyl-3-hydroxy-3-phenylindolin-2-one	17



Table 10 – (continued).

Indolinone		(R)-1-benzyl-3-hydroxy-3-phenylindolin-2-one	17a
Indolinone		(S)-1-benzyl-3-hydroxy-3-phenylindolin-2-one	17b
Indolinone		1-benzyl-3-phenyl-3-(prop-2-yn-1-yloxy)indolin-2-one	18
Indolinone		1-benzyl-3-methoxy-3-phenylindolin-2-one	19
Indolinone		1-benzyl-3-hydroxy-3-methylindolin-2-one	20
Indolinone		1-benzyl-3-hydroxy-3-(prop-2-yn-1-yl)indolin-2-one	21
Indolinone		1-benzyl-3-hydroxy-3-(4-methoxyphenyl)indolin-2-one	22

**Table 10** – (continued).

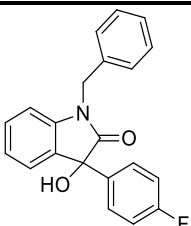
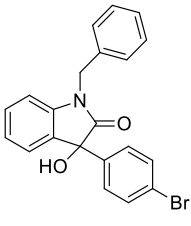
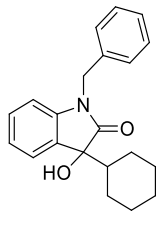
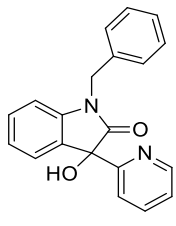
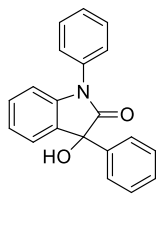
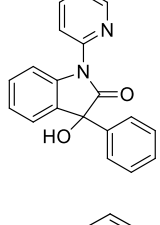
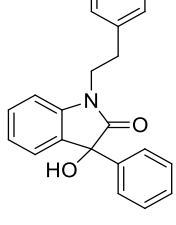
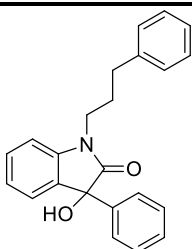
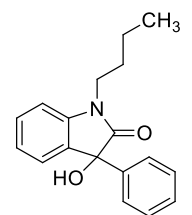
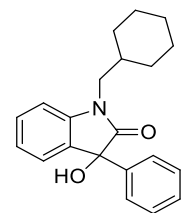
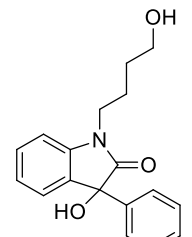
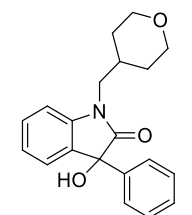
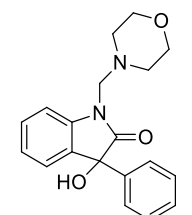
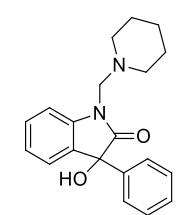
Indolinone		1-benzyl-3-(4-fluorophenyl)-3-hydroxyindolin-2-one	23
Indolinone		1-benzyl-3-(4-bromophenyl)-3-hydroxyindolin-2-one	24
Indolinone		1-benzyl-3-cyclohexyl-3-hydroxyindolin-2-one	25
Indolinone		1-benzyl-3-hydroxy-3-(pyridin-2-yl)indolin-2-one	26
Indolinone		3-hydroxy-1,3-diphenylindolin-2-one	27
Indolinone		3-hydroxy-3-phenyl-1-(pyridin-2-yl)indolin-2-one	28
Indolinone		3-hydroxy-1-phenethyl-3-phenylindolin-2-one	29

Table 10 – (continued).

Indolinone		3-hydroxy-3-phenyl-1-(3-phenylpropyl)indolin-2-one	30
Indolinone		1-butyl-3-hydroxy-3-phenylindolin-2-one	31
Indolinone		1-(cyclohexylmethyl)-3-hydroxy-3-phenylindolin-2-one	32
Indolinone		3-hydroxy-1-(4-hydroxybutyl)-3-phenylindolin-2-one	33
Indolinone		3-hydroxy-3-phenyl-1-((tetrahydro-2H-pyran-4-yl)methyl)indolin-2-one	34
Indolinone		3-hydroxy-1-(morpholinomethyl)-3-phenylindolin-2-one	35
Indolinone		3-hydroxy-3-phenyl-1-(piperidin-1-ylmethyl)indolin-2-one	36

**Table 10** – (continued).

Indolinone		tert-butyl 4-((3-hydroxy-2-oxo-3-phenylindolin-1-yl)methyl)piperidine-1-carboxylate	37
Indolinone		tert-butyl 4-((3-hydroxy-2-oxo-3-phenylindolin-1-yl)methyl)piperazine-1-carboxylate	38
Indolinone		3-hydroxy-3-phenyl-1-(pyridin-2-ylmethyl)indolin-2-one	39
Indolinone		3-hydroxy-3-phenyl-1-(pyridin-4-ylmethyl)indolin-2-one	40
Indolinone		3-hydroxy-1-(4-methoxybenzyl)-3-phenylindolin-2-one	41
Indolinone		1-(4-fluorobenzyl)-3-hydroxy-3-phenylindolin-2-one	42

Table 10 – (continued).

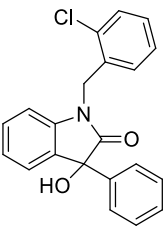
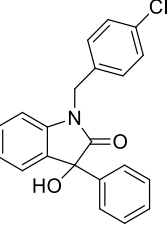
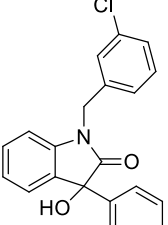
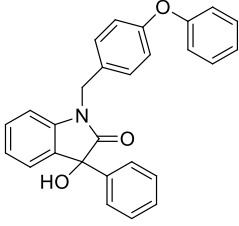
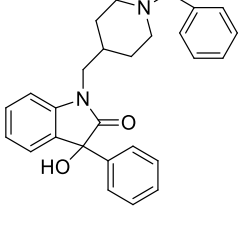
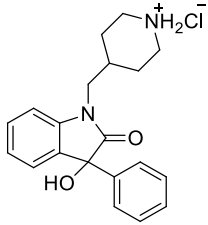
Indolinone		1-(2-chlorobenzyl)-3-hydroxy-3-phenylindolin-2-one	43
Indolinone		1-(4-chlorobenzyl)-3-hydroxy-3-phenylindolin-2-one	44
Indolinone		1-(3-chlorobenzyl)-3-hydroxy-3-phenylindolin-2-one	45
Indolinone		3-hydroxy-1-(4-phenoxybenzyl)-3-phenylindolin-2-one	46
Indolinone		1-((1-benzylpiperidin-4-yl)methyl)-3-hydroxy-3-phenylindolin-2-one	47
Indolinone		4-((3-hydroxy-2-oxo-3-phenylindolin-1-yl)methyl)piperidin-1-ium chloride	48a

Table 10 – (continued).

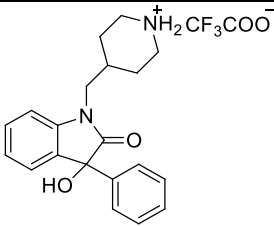
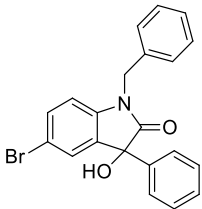
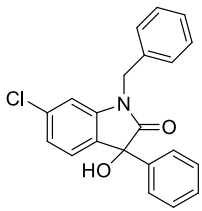
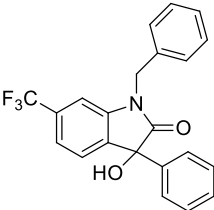
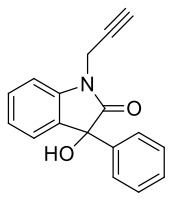
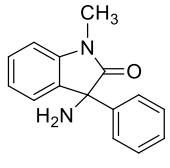
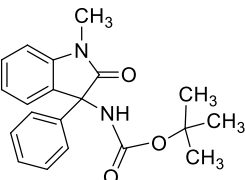
Indolinone		4-((3-hydroxy-2-oxo-3-phenylindolin-1-yl)methyl)piperidin-1-ium 2,2,2-trifluoroacetate	48b
Indolinone		1-benzyl-5-bromo-3-hydroxy-3-phenylindolin-2-one	49
Indolinone		1-benzyl-6-chloro-3-hydroxy-3-phenylindolin-2-one	50
Indolinone		1-benzyl-3-hydroxy-3-phenyl-6-(trifluoromethyl)indolin-2-one	51
Indolinone		3-hydroxy-3-phenyl-1-(prop-2-yn-1-yl)indolin-2-one	52
Indolinone		3-amino-1-methyl-3-phenylindolin-2-one	53
Indolinone		tert-butyl(1-methyl-2-oxo-3-phenylindolin-3-yl)carbamate	54

Table 10 – (continued).

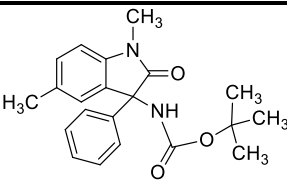
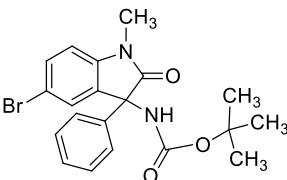
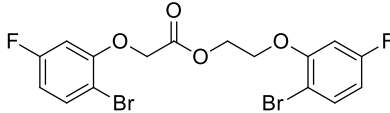
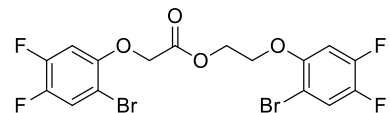
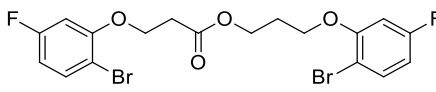
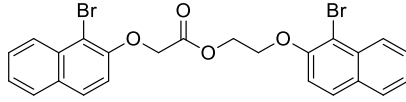
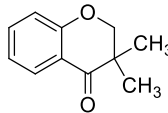
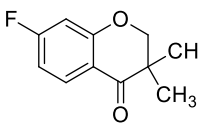
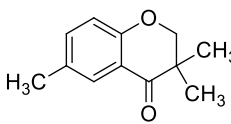
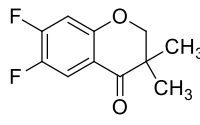
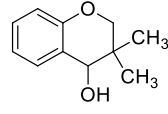
Indolinone		tert-butyl(1,5-dimethyl-2-oxo-3-phenylindolin-3-yl) carbamate	55
Indolinone		tert-butyl(5-bromo-1-methyl-2-oxo-3-phenylindolin-3-yl)carbamate	56
Diether-ester		2-(2-bromo-5-fluorophenoxy)ethyl-2-(2-bromo-5-fluorophenoxy)acetate	57
Diether-ester		2-(2-bromo-4,5-difluorophenoxy)ethyl-2-(2-bromo-4,5-difluorophenoxy)acetate	58
Diether-ester		3-(2-bromo-5-fluorophenoxy)propyl-3-(2-bromo-5-fluorophenoxy)propanoate	59
Diether-ester		2-((1-bromonaphthalen-2-yl)oxy)ethyl 2-((1-bromonaphthalen-2-yl)oxy)acetate	60
Chromanone		3,3-dimethylchroman-4-one	61
Chromanone		7-fluoro-3,3-dimethylchroman-4-one	62
Chromanone		3,3,6-trimethylchroman-4-one	63
Chromanone		6,7-difluoro-3,3-dimethylchroman-4-one	64
Chromanol		3,3-dimethylchroman-4-ol	65

Table 10 – (continued).

Chromanol		3,3-dimethyl-3,4-dihydro-2H-benzo[g]chromen-4-ol	66
$\alpha$ -Methylbenzylamine		( <i>S</i> )-bis(( <i>S</i> )-1-phenylethyl)ammonium chloride	67
$\alpha$ -Methylbenzylamine		( <i>R</i> )-bis(( <i>R</i> )-1-phenylethyl)ammonium chloride	68
$\alpha$ -Methylbenzylamine		( <i>S</i> )-1-(3-methoxyphenyl)- <i>N</i> -(( <i>S</i> )-1-phenylethyl) ethanaminium chloride	69
$\alpha$ -Methylbenzylamine		( <i>R</i> )-1-(3-methoxyphenyl)- <i>N</i> -(( <i>R</i> )-1-phenylethyl) ethanaminium chloride	70
$\alpha$ -Methylbenzylamine		( <i>S</i> )-1-(3-(benzyloxy)phenyl)- <i>N</i> -(( <i>S</i> )-1-phenylethyl) ethanaminium chloride	71
$\alpha$ -Methylbenzylamine		( <i>R</i> )-1-(3-(benzyloxy)phenyl)- <i>N</i> -(( <i>R</i> )-1-phenylethyl) ethanaminium chloride	72
Carbamate substituted $\alpha$ -Methylbenzylamine		( <i>S</i> )-1-(3-((ethyl(methyl)carbamoyloxy)phenyl)- <i>N</i> -(( <i>S</i> )-1-phenylethyl)ethanaminium chloride	73
Carbamate substituted $\alpha$ -Methylbenzylamine		( <i>R</i> )-1-(3-((ethyl(methyl)carbamoyloxy)phenyl)- <i>N</i> -(( <i>R</i> )-1-phenylethyl)ethanaminium chloride	74



### 3.2.2. *eeAChE* and *eqBuChE* IC<sub>50</sub> evaluation of isoquinolinone, azepanone, indolinone, diether ester, chromanone, chromanol and rivastigmine derivatives

To 75  $\mu\text{L}$  of a mixture of different inhibitor concentrations and Tris-HCl buffer (50 mM, pH 8.0) were added 25  $\mu\text{L}$  of ATCI (15 mM) or BTCI (15 mM), 125  $\mu\text{L}$  of DTNB (3 mM) and 25  $\mu\text{L}$  of *eeAChE* (0.3 U mL) or *eqBuChE* (0.3 U mL<sup>-1</sup>), to a final volume of 250  $\mu\text{L}$ . The synthesized compounds were dissolved in the reaction buffer with a maximum of 5% DMSO.

The microplate was read at 25 °C and 405 nm, in a spectrophotometer Thermo Scientific MultiSkan Go, during 15 min. The rate of the reaction was measured. All experiments were done in triplicate.

### 3.2.3. MAO-B IC<sub>50</sub> evaluation of isoquinolinone, azepanone, indolinone, diether ester, chromanone, chromanol and rivastigmine derivatives

To a mixture of 131  $\mu\text{L}$  of phosphate buffer (0.1 M, pH 7.6) and several concentrations of the synthesized compounds (0.04883-100  $\mu\text{M}$ ), were added 4  $\mu\text{L}$  of MAO-B (0.94 U). This mixture was incubated at 37 °C for 15 minutes. Then 15  $\mu\text{L}$  of benzylamine (100 mM) and 50  $\mu\text{L}$  of chromogenic solution (to a final volume of 200  $\mu\text{L}$ ) were added, followed by 15 more minutes of incubation at 37 °C. A negative control without the enzyme and a positive control without inhibitor were also conducted. The reaction was followed for a further 60 minutes at 37 °C and 490 nm, in a Thermo Scientific MultiSkan Go spectrophotometer. The rate of the reaction was measured. All experiments were done in triplicate.

### 3.2.4. Statistical analysis

All data was expressed as mean  $\pm$  standard deviation of triplicate measurements. Statistical analysis of data was performed using one-way ANOVA. A probability value of  $p < 0.05$  was considered statistically significant. Multiple comparisons of means were analyzed using the b-Tukey test. Analyses were performed using SPSS<sup>®</sup> 22 Windows, IBM. The dose-response curves were built with the software GraphPad Prism 5<sup>TM</sup> and the IC<sub>50</sub> for all the samples was determined with the software OriginPro<sup>®</sup> 8. The selectivity index (S.I.) for *eeAChE* is calculated by using Equation 5.

$$S.I. = \frac{IC_{50}BuChE}{IC_{50}AChE} \quad (5)$$

### 3.3. Results and discussion

#### 3.3.1. *ee*AChE and *eq*BuChE IC<sub>50</sub> evaluation

##### 3.3.1.1. Isoquinolinone and Azepanone derivatives

Considering their broad biological activity spectrum, the isoquinolinone scaffold is a privileged-scaffold lead for targeting various diseases. Isoquinolines are alkaloids found in several bioactive natural products [213-216]. These molecules are derived from phenylalanine [217], and exhibit antidepressant [218], anti-inflammatory [219] and analgesic [220, 221] characteristics. For this reason, this family was chosen for evaluating their inhibitory properties against AChE and BuChE. The azepanone family was chosen on the basis of their analogy with galantamine which contains an azepane ring, and it is the azepane ring which is recognized as the important pharmacophore element for AChE inhibition.

A library of 16 isoquinolinone and azepanone derivatives with benzyl, pyridyl and thiophene cores (Fig. 38) was tested for *ee*AChE and *eq*BuChE inhibition [210].

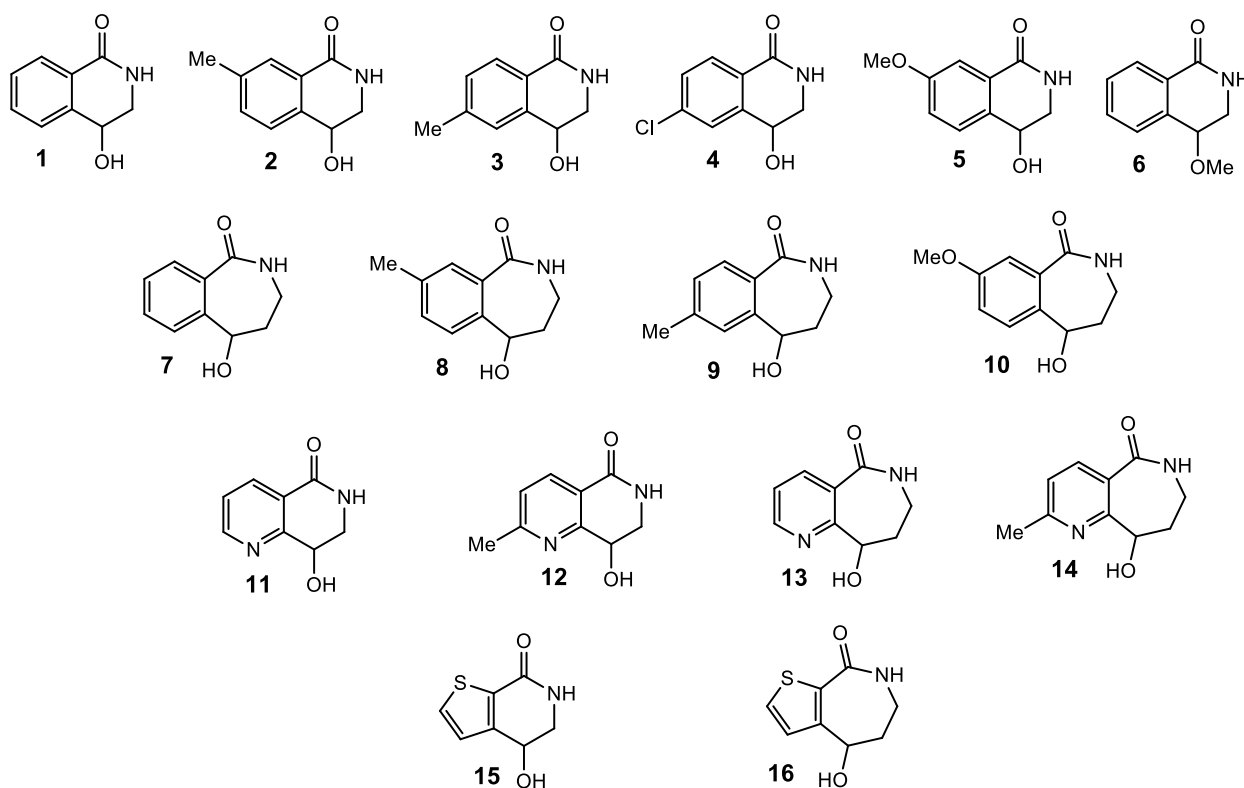
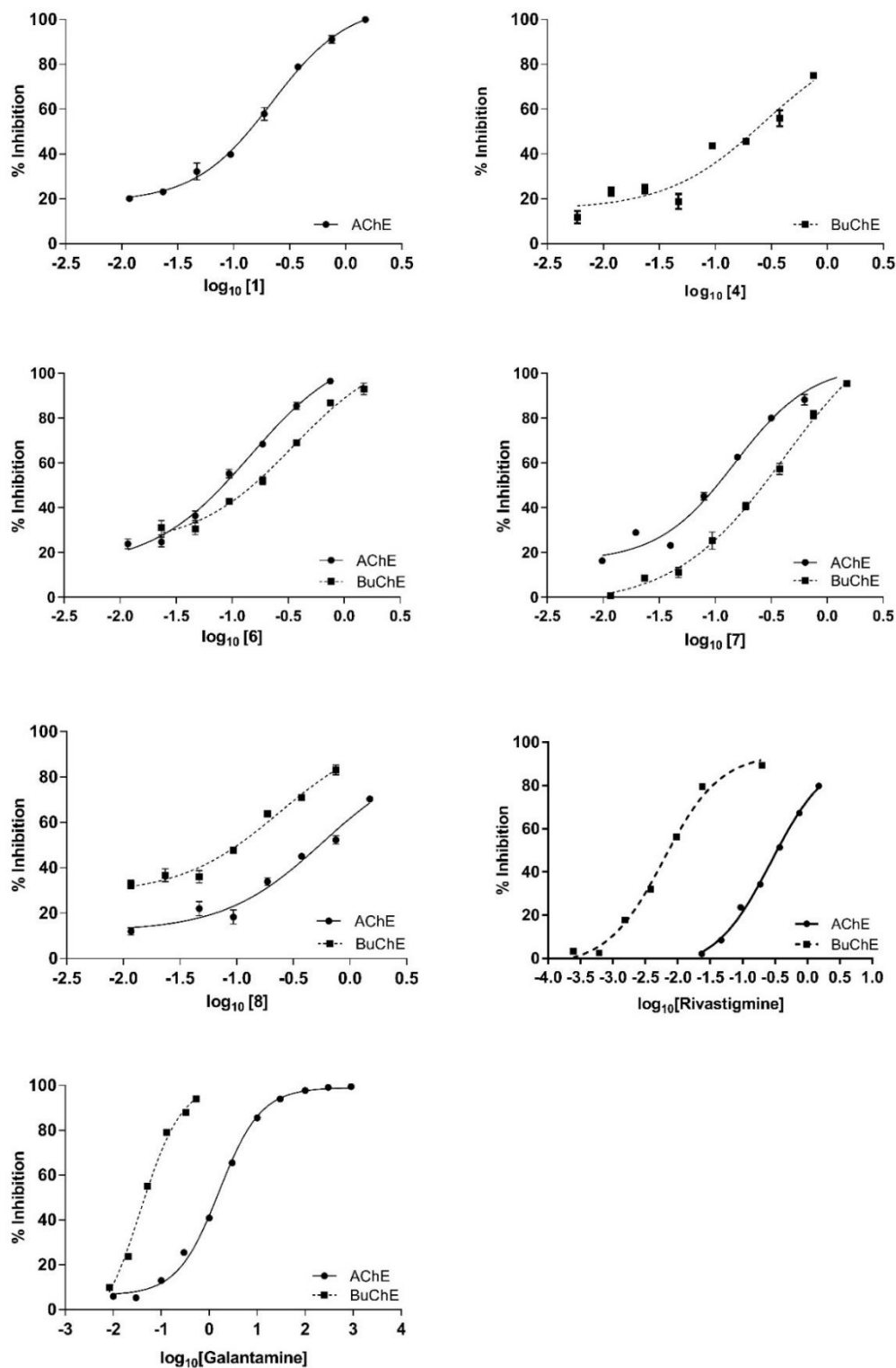
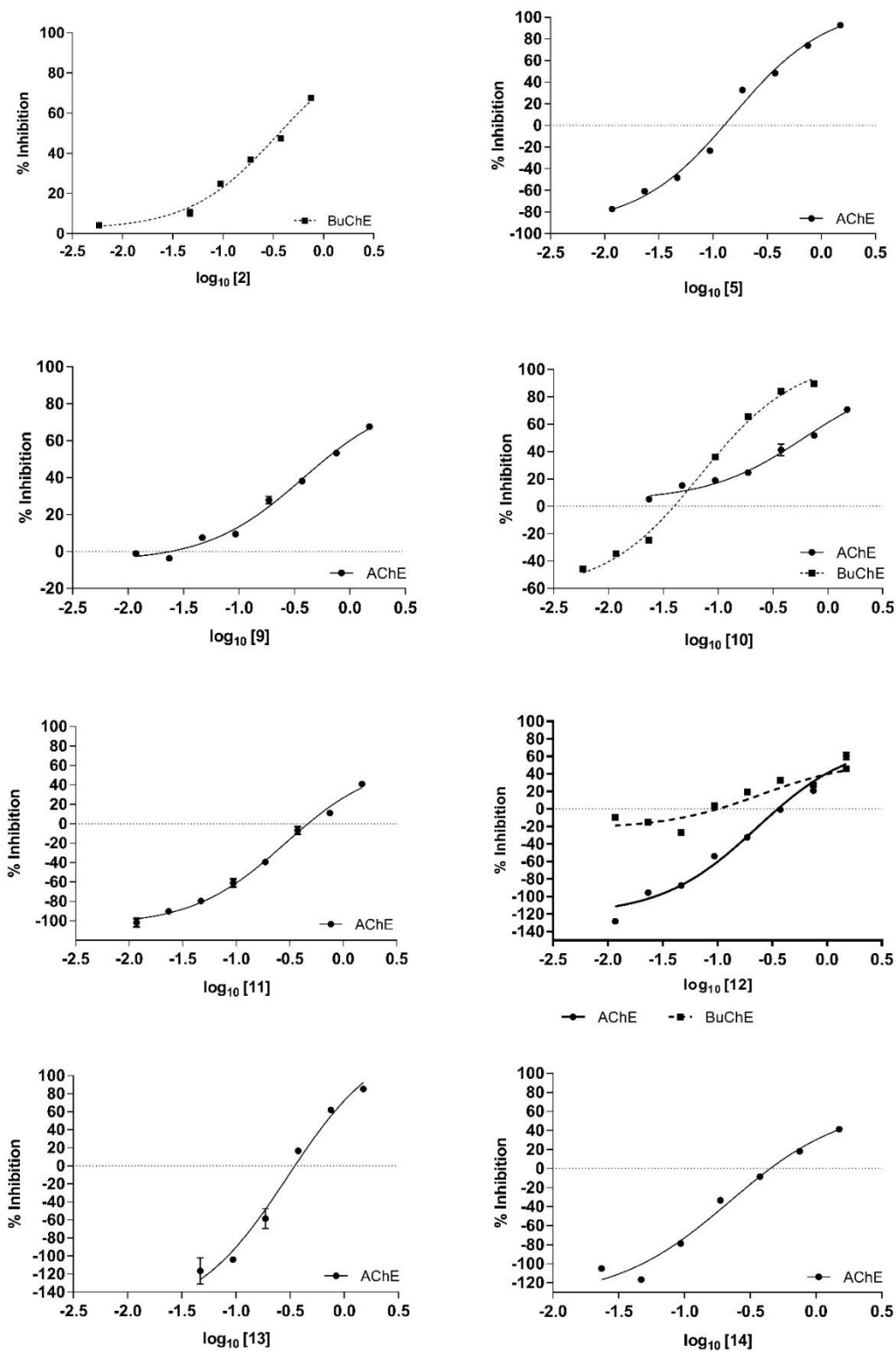


Figure 38 – Isoquinolinone and azepanone derivatives.

The dose-response curves of both *ee*AChE and *eq*BuChE are presented in Figures 39 and 40. The results of these inhibition studies are shown in Table 11 and the corresponding statistical analysis is shown in Figures 41(for *ee*AChE) and 42 (for *eq*BuChE), as well as in Table A1.



**Figure 39** - Dose-response curves for compounds **1**, **6**, **7**, **8** and rivastigmine for *ee*AChE inhibition; and of compounds **4**, **6**, **7**, **8**, galantamine and rivastigmine for *eq*BuChE inhibition.



**Figure 40** - Dose-response curves for compounds **5**, **9**, **10**, **11**, **12**, **13**, **14**, **15** and **16** for *ee*AChE inhibition; and of compounds **2**, **10**, **12**, **15** and **16** for *eq*BuChE inhibition (continues next page).

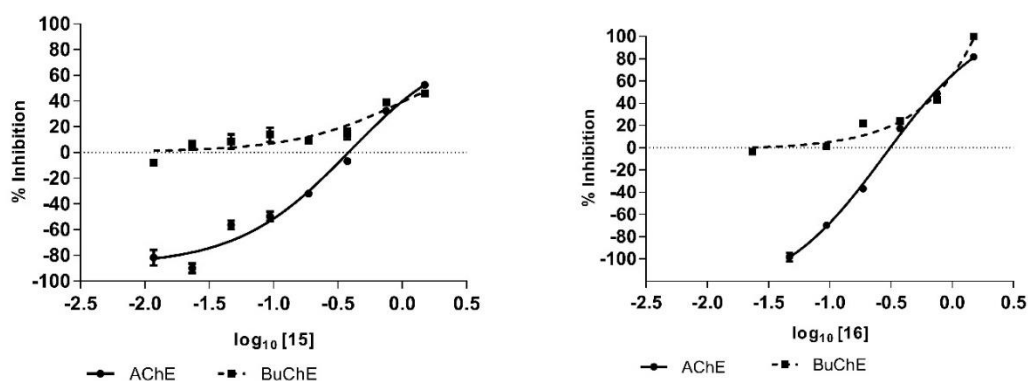


**Figure 40** - Dose-response curves for compounds **5**, **9**, **10**, **11**, **12**, **13**, **14**, **15** and **16** for *ee*AChE inhibition; and of compounds **2**, **10**, **12**, **15** and **16** for *eq*BuChE inhibition (continued).

Analysis of the dose-response curves (Fig. 39) revealed some interesting insights. Both compounds **6** and **7** showed similar behavior for *ee*AChE and *eq*BuChE inhibition (Fig. 39), this along with the respective IC<sub>50</sub> values (Table 11), made these compounds potential target inhibitors for both enzymes, and a structural basis for lead development design. Compound **1** presented a good sigmoidal shape dose-response curve, and along with it the corresponding IC<sub>50</sub> value showed potential to be a target drug for AChE (Fig. 39). Compounds **5**, **11**, **12**, **13**, **14**, **15** and **16** acted as *ee*AChE activators, which means that they increased AChE activity, at concentrations lower than 120.2, 426.6, 346.7, 331.1, 446.7, 363.1 and 190.5  $\mu$ M, respectively (Fig. 40). It is not yet clear why these compounds presented this behavior. For higher concentrations, they acted as inhibitors. The same was true for the *eq*BuChE inhibitors **10** and **12** that acted as activators for concentrations lower than 61.7 and 93.8  $\mu$ M, respectively. For concentrations above 61.7  $\mu$ M, compound **10** showed good inhibition of *eq*BuChE (Fig. 40). In the case of compound **4**, for *eq*BuChE it presented an IC<sub>50</sub> of 226.1  $\mu$ M, but at half this concentration (108  $\mu$ M) it presented a significant 40% inhibition and at a quarter the IC<sub>50</sub> concentration (54  $\mu$ M), 30% inhibition (Fig. 39). Compound **9** presented an IC<sub>50</sub> of 564.4  $\mu$ M for *ee*AChE, but at a concentration 2.5 times lower (226  $\mu$ M) it gave a significant 30% inhibition. The same behavior was observed for compound **10** in the case of *ee*AChE inhibition (Fig. 40).

**Table 10** – Inhibition studies for *ee*AChE and *eq*BuChE activities.

<b>Compound</b>	<b>IC<sub>50</sub> <i>ee</i>AChE (μM)<sup>a</sup></b>	<b>IC<sub>50</sub> <i>eq</i>BuChE (μM)<sup>a</sup></b>	<b>Selectivity Index (IC<sub>50</sub> <i>eq</i>BuChE/ IC<sub>50</sub> <i>ee</i>AChE)</b>
<b>1</b>	136.0 ± 8.8	807.5 ± 1.9	5.938
<b>2</b>	N.D.	352.1 ± 17.7	N.D.
<b>3</b>	N.D.	N.D.	N.D.
<b>4</b>	N.D.	226.1 ± 20.8	N.D.
<b>5</b>	311.3 ± 2.3	N.D.	N.D.
<b>6</b>	89.5 ± 2.0	153.8 ± 2.6	1.718
<b>7</b>	108.4 ± 3.4	277.8 ± 7.7	2.563
<b>8</b>	536.3 ± 37.7	108.0 ± 8.1	0.201
<b>9</b>	564.4 ± 21.8	269.4 ± 6.5	0.477
<b>10</b>	585.1 ± 23.6	108.6 ± 15.7	0.186
<b>11</b>	1296.7 ± 22.8	N.D.	N.D.
<b>12</b>	1251.7 ± 80.9	N.D.	N.D.
<b>13</b>	550.4 ± 17.8	N.D.	N.D.
<b>14</b>	> 1500	N.D.	N.D.
<b>15</b>	1366.2 ± 48.9	N.D.	N.D.
<b>16</b>	756.4 ± 24.4	825.6 ± 16.1	1.091
Rivastigmine	342.5 ± 13.0	5.1 ± 0.9	0.015
Galantamine	2.9 ± 0.2	14.9 ± 0.7	5.138

<sup>a</sup> IC<sub>50</sub> values are expressed as mean ±SD (n =3) based on dose-response curves, using the Origin 8.0 Pro.

N.D. – Not determined in the tested concentrations (because the inhibitory activities were too weak to permit an IC<sub>50</sub> determination).

From the analysis of *ee*AChE activity, compound **6** provided a good inhibition value (Table 11), showing the importance of the methoxy group in position-4 (compare compound **1** and **6**, Table 11). The presence of electron withdrawing and electron donor substituents in the aryl ring of isoquinolin-1(2*H*)-ones derivatives does not affect the IC<sub>50</sub> value considerably (compounds **2** to **4**, Table 11), with the exception of compound **5** – a compound bearing a methoxy group in the 8-position) showing an IC<sub>50</sub> of 311.3 μM (Table 11), once again demonstrating the importance of the methoxyl group for binding to the enzyme active site. Comparing the azepanone compounds with their isoquinolinone counterparts it was noticed that compounds **8-10** gave better inhibition values than **2- 4** (Table 11), although they're still very high when compared to the benchmarks rivastigmine and galantamine. Compound **7** was the exception since it had a similar value to compound **1** (Table 11). Isoquinolinones and azepin-1(2*H*)-ones with pyridyl cores, independently of having, or not, electron donor groups in the aryl ring gave similar IC<sub>50</sub> values for *ee*AChE (Table 11, compounds **11**, **12** and **14**), compound **13** (IC<sub>50</sub> of 550 μM) was the best candidate (Table 11), but still with no significant inhibition properties. There was a big difference observed in the two molecules containing a thiophene core, for instance, isoquinolin-1(2*H*)-one (**15**) had an IC<sub>50</sub> almost twice that of azepin-1(2*H*)-one (**16**) (Table 11). When compared to the rivastigmine benchmark, all compounds (except **1**, **5**, **6** and **7**) showed higher IC<sub>50</sub> values for *ee*AChE and when compared to the galantamine benchmark, all compounds showed higher IC<sub>50</sub> values for *ee*AChE.

Analyzing *eq*BuChE activity, the azepin-1(2*H*)-one compounds gave better results than their isoquinolin-1(2*H*)-one counter-parts, independently of the type of substituent in the aryl ring. Compounds **8** and **10** gave the best results, with moderately good IC<sub>50</sub> values, 108.0 μM and 108.6 μM, respectively (Table 11). Higher IC<sub>50</sub> values were obtained for the isoquinolin-1(2*H*)-ones, as compound **6** gave an IC<sub>50</sub> value of 153.8 μM (Table 11), which was the best result for these compounds with this enzyme. Moreover, the pyridyl and thiophene containing derivatives, regardless of the ring size, did not present any major differences in their IC<sub>50</sub> values (Table 11, compounds **11** to **15**), and displayed poor inhibition. Unfortunately, all these compounds were less active with *eq*BuChE than the benchmarks (all presented higher IC<sub>50</sub> values). Compound **8** gave the lowest value of 108.0 μM. As can be seen from Table 11, and the selectivity indexes, the isoquinolin-1(2*H*)-ones and azepin-1(2*H*)-ones with no substituents in the aryl ring, and the isoquinolinones and azepin-1(2*H*)-ones with pyridyl and thiophene units were selective for *ee*AChE, whilst isoquinolin-1(2*H*)-ones and azepin-1(2*H*)-ones with substituents in the aryl ring were selective for *eq*BuChE.

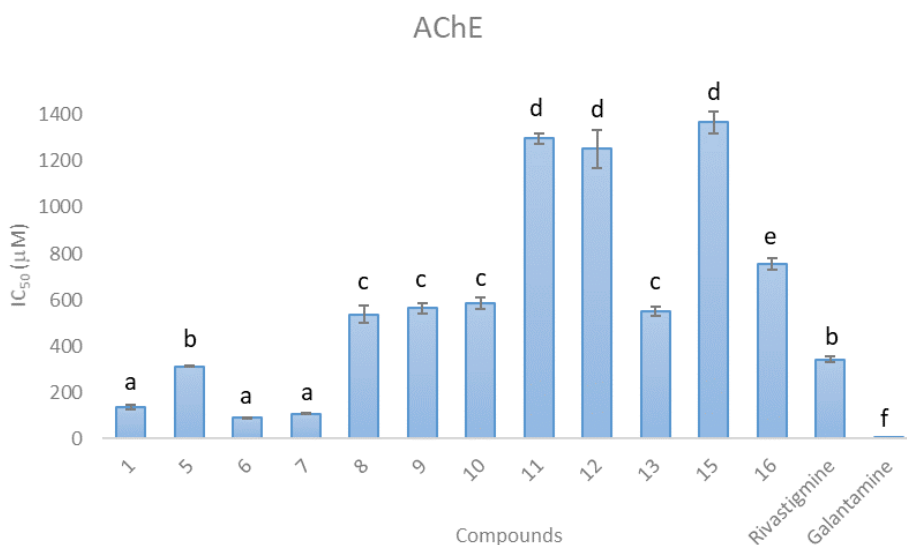


**Figure 41** – *In vitro* eeAChE activity, in the presence of rivastigmine, galantamine and compounds **1**, **5-13** and **15-16**. Different letters represent values significantly different ( $p < 0.05$ ).

The statistical analysis for AChE inhibitory activity in the presence of isoquinolinone and azepanone derivatives (Fig. 41) shows that galantamine is significantly different from all the compounds. Compounds **1**, **6** and **7** aren't significantly different from each other, and present the best IC<sub>50</sub> values, although higher than galantamine they are lower than the benchmark rivastigmine. Compound **5** is not significantly different from rivastigmine but differs significantly from galantamine. Compounds **8-10** and **13** are not significantly different from each other, and the same applies for compounds **11-12** and **15**. As for compound **16**, it is significantly different from all others.

The statistical analysis for *eq*BuChE activity in the presence of isoquinolinone and azepanone derivatives (Fig. 42) shows that all the compounds are significantly different from the benchmarks. Compounds **8** and **10** aren't significantly different from each other, as well as compounds **7** and **9** and compounds **1** and **16** ( $p > 0.05$ ). Compounds **2**, **4** and **6** are significantly different from all others ( $p < 0.05$ ). The compounds that showed higher activity were the azepanones **8** and **10**, although lower than the benchmarks.



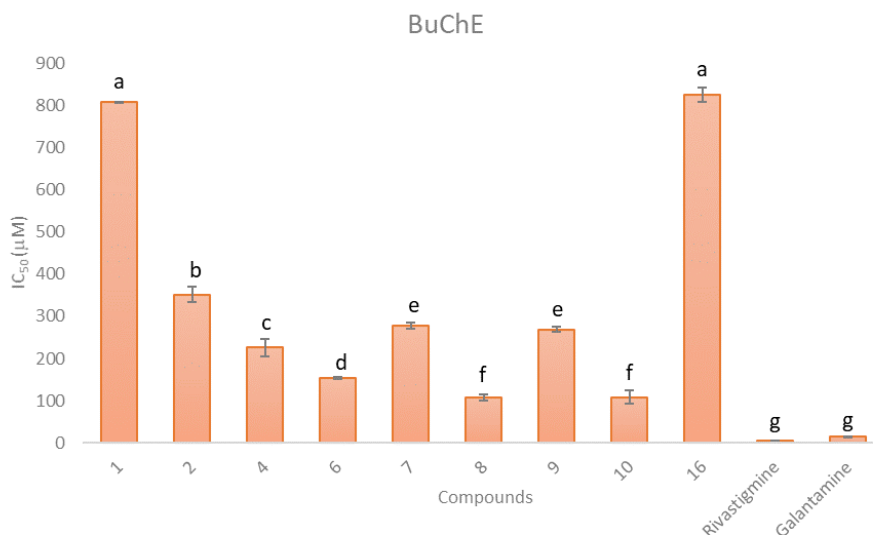
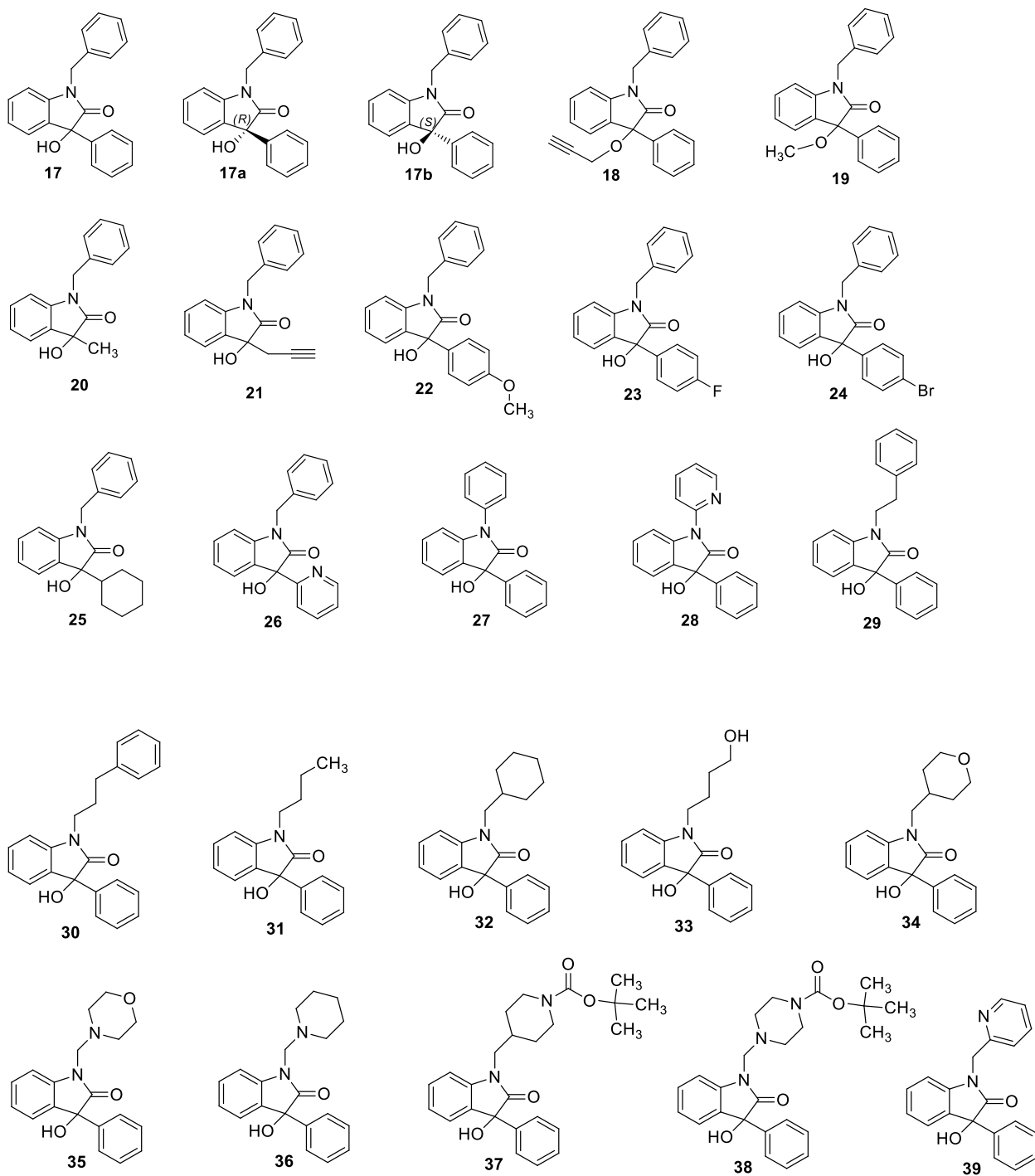


**Figure 42** – *In vitro* eqBuChE activity, in the presence of rivastigmine, galantamine and compounds **1**, **2**, **4**, **6-10** and **16**. Different letters represent values significantly different ( $p < 0.05$ ).

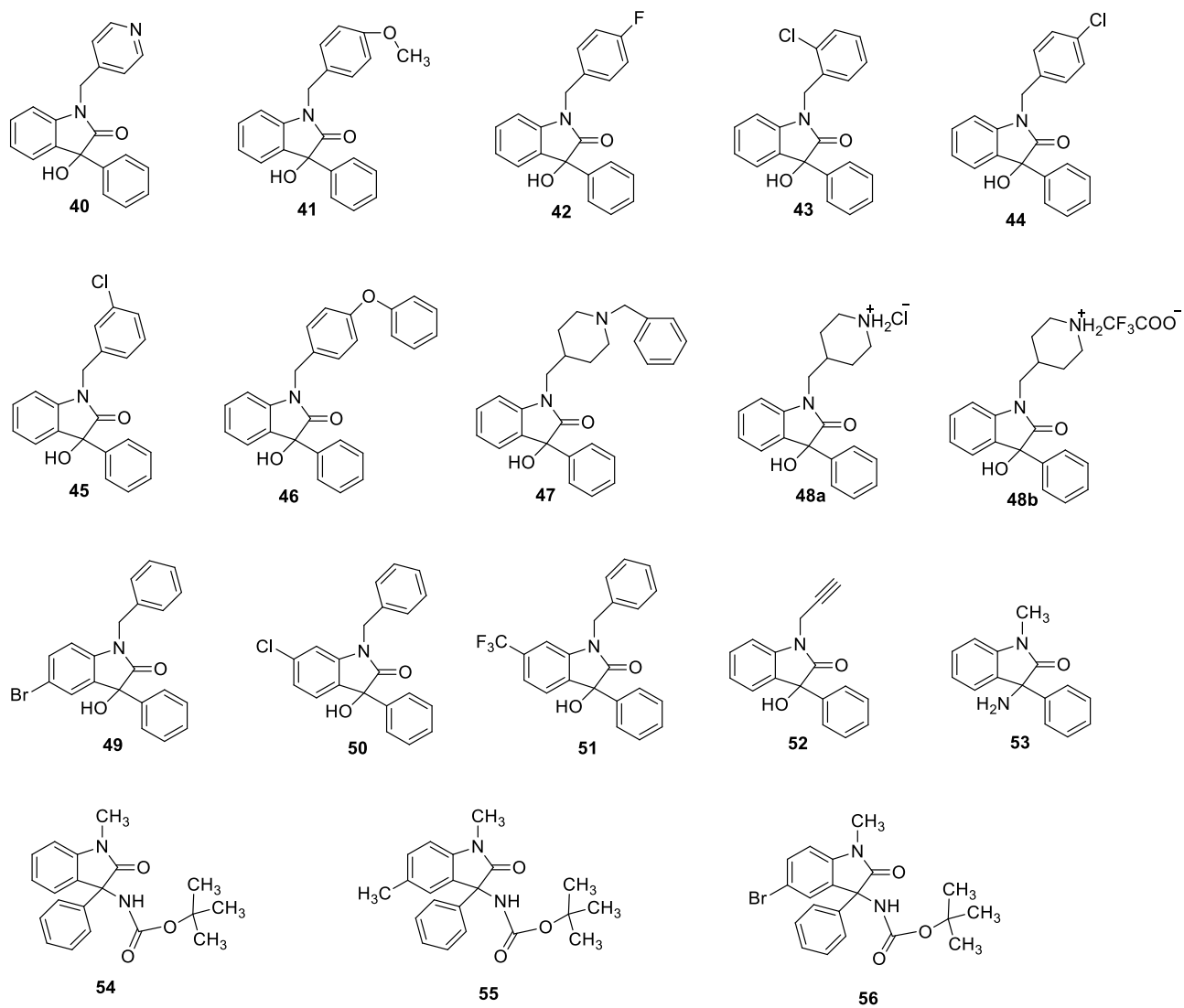
### 3.3.1.2. Indolinone derivatives

Oxindole is a core unit present in many natural product and bioactive compounds [222-227]. The structural analogy between oxindoles and donepezil specifically in regard to the indanone unit, make these compounds of interest for AChE and BuChE inhibition [228]. With this in mind, a library of 43 compounds was tested for their inhibition ability of these enzymes (Fig. 43).

The dose-response curves of both *ee*AChE and *eq*BuChE are presented in Figure 44. The results of these inhibition studies are shown in Table 12 and the corresponding statistical analysis is shown in Figures 45 (for *ee*AChE) and 46 (for *eq*BuChE), as well as in Table A1.



**Figure 43** - Indolinone derivatives (continued in next page).

**Figure 43** - Indolinone derivatives (continued).

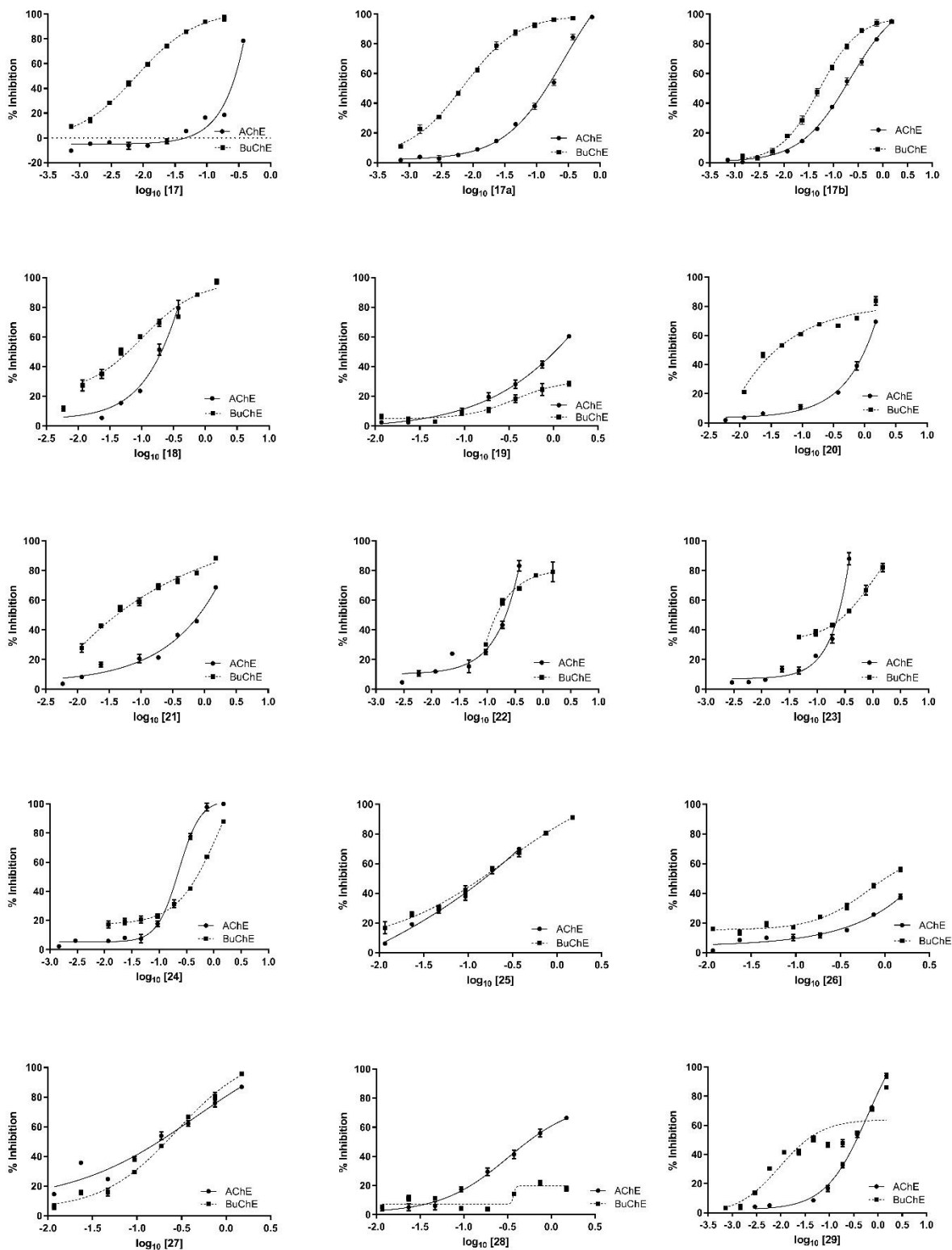


Figure 44 – Dose-response curves for compounds (17)-(56) for *ee*AChE and *eq*BuChE (continued in next page).

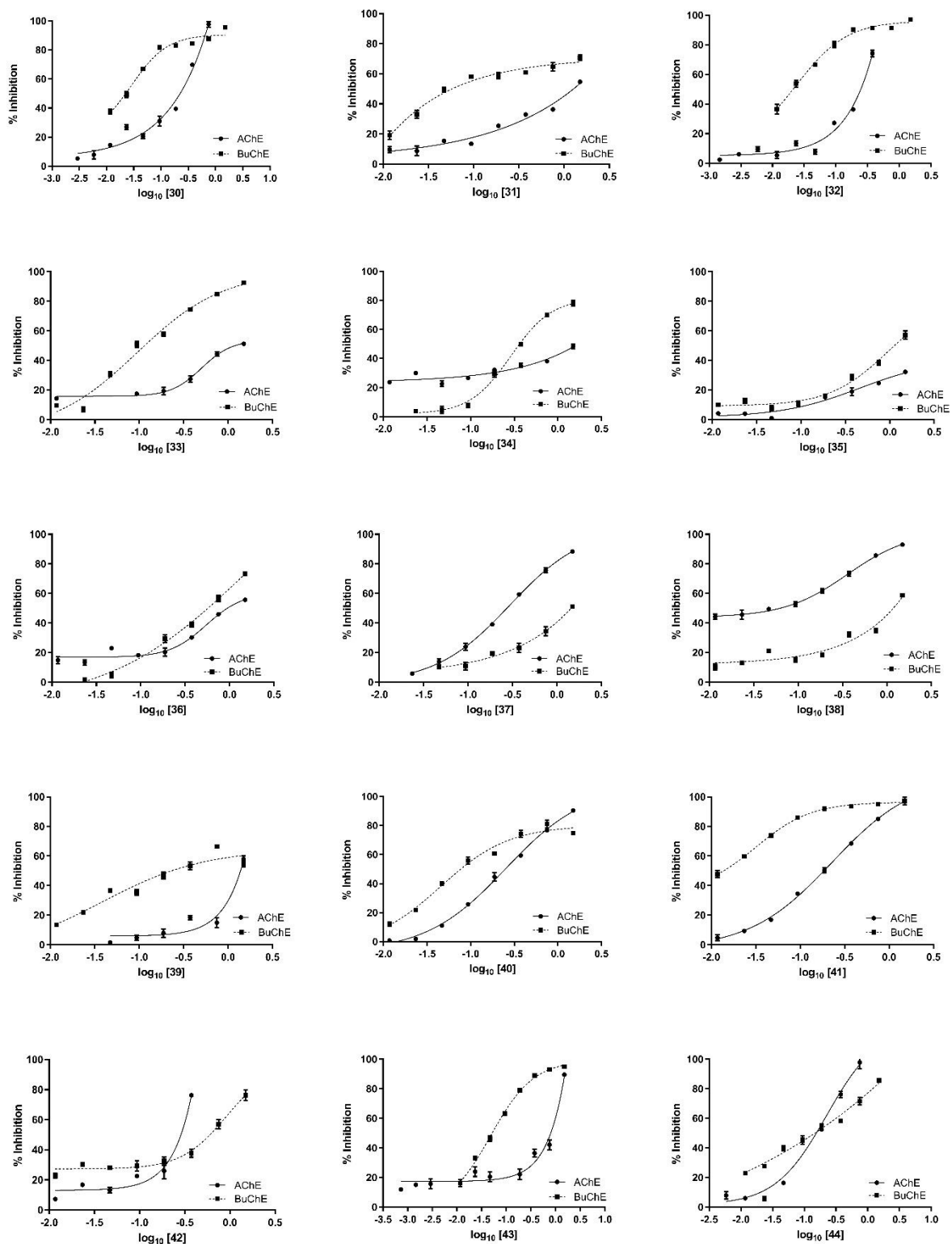


Figure 44 – Dose-response curves of compounds (17)-(56) for *ee*AChE and *eq*BuChE (continued).

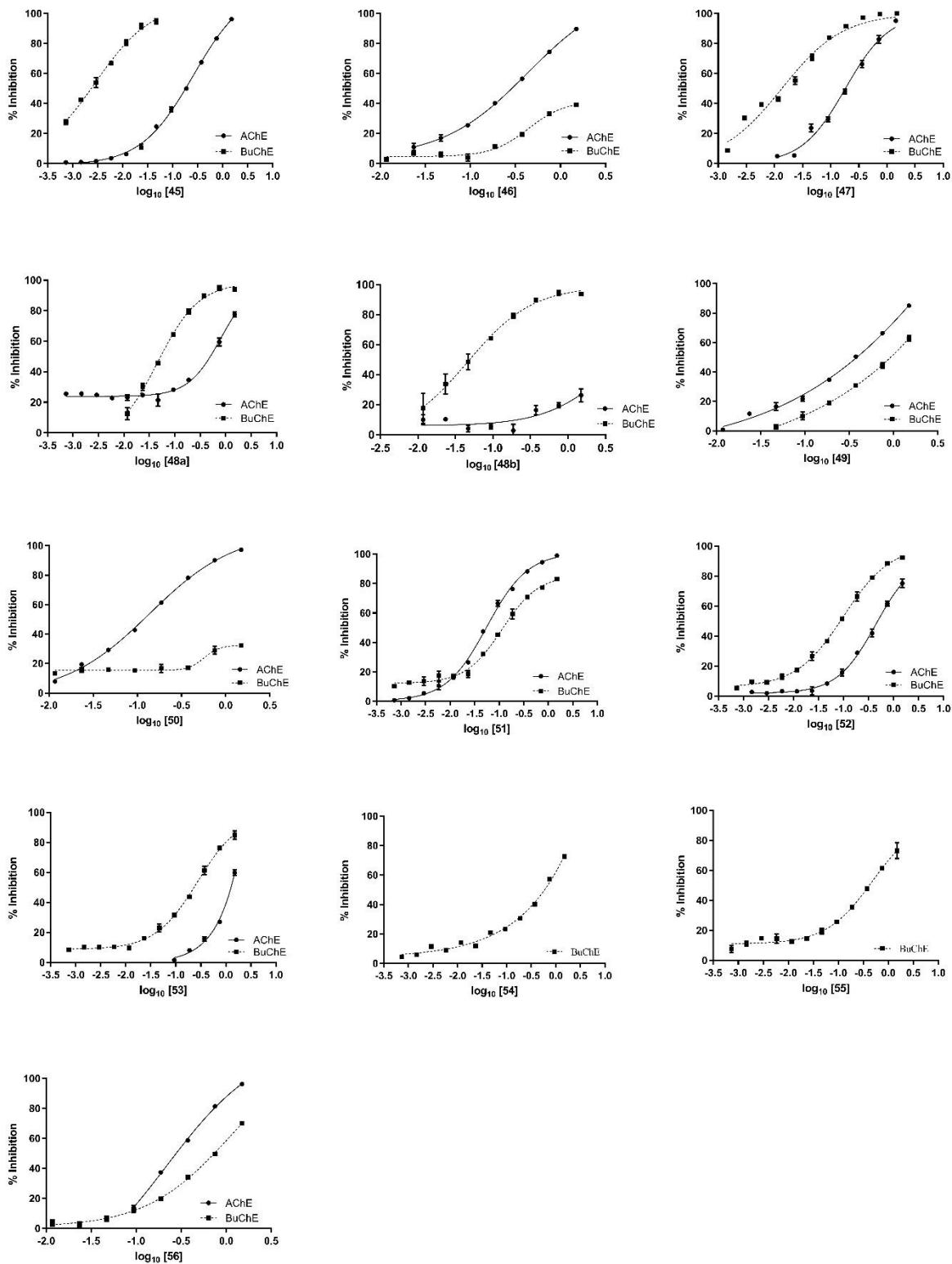


Figure 44 – Dose-response curves of compounds (17)-(56) for *ee*AChE and *eg*BuChE (continued).

**Table 11** - Inhibition studies for *ee*AChE and *eq*BuChE activities with oxindole derivatives (continued next page).

<b>Compound</b>	<b>IC<sub>50</sub> <i>ee</i>AChE (μM)</b>	<b>IC<sub>50</sub> <i>eq</i>BuChE (μM)</b>	<b>Selectivity Index (IC<sub>50</sub> <i>eq</i>BuChE/IC<sub>50</sub> <i>ee</i>AChE)</b>
<b>17</b>	237.18 ± 6.97	7.41 ± 0.001	0.03
<b>17a</b>	143.13 ± 2.09	6.19 ± 0.88	0.04
<b>17b</b>	160.01 ± 23.08	53.95 ± 3.78	0.34
<b>18</b>	N.D.	71.32 ± 8.40	N.D.
<b>19</b>	392.05 ± 46.88	69.03 ± 1.69	0.18
<b>20</b>	640.85 ± 34.41	26.44 ± 1.51	0.04
<b>21</b>	315.68 ± 19.64	53.52 ± 10.11	0.17
<b>22</b>	154.77 ± 11.08	147.12 ± 7.97	0.95
<b>23</b>	203.32 ± 12.27	315.30 ± 14.60	1.55
<b>24</b>	171.04 ± 12.93	484.09 ± 6.34	2.83
<b>25</b>	59.62 ± 5.77	60.30 ± 6.37	1.01
<b>26</b>	N.D.	126.53 ± 13.59	N.D.
<b>27</b>	179.21 ± 4.42	217.31 ± 8.24	1.21
<b>28</b>	206.09 ± 23.94	N.D.	N.D.
<b>29</b>	227.37 ± 49.34	11.20 ± 0.21	0.05
<b>30</b>	229.25 ± 9.35	23.11 ± 1.99	0.10
<b>31</b>	1275.76 ± 33.60	15.30 ± 0.28	0.01
<b>32</b>	170.58 ± 2.11	23.12 ± 1.95	0.14
<b>33</b>	881.63 ± 71.43	103.86 ± 3.88	0.12
<b>34</b>	N.D.	392.17 ± 22.94	N.D.
<b>35</b>	N.D.	1158.95 ± 51.93	N.D.
<b>36</b>	901.29 ± 52.74	264.06 ± 23.05	0.29

**Table 12** - (continued).

<b>37</b>	273.92 ± 9.07	265.78 ± 54.00	0.97
<b>38</b>	61.26 ± 3.70	1127.43 ± 78.85	18.40
<b>39</b>	1037.78 ± 112.64	22.67 ± 2.28	0.02
<b>40</b>	192.45 ± 16.86	39.82 ± 2.24	0.21
<b>41</b>	185.21 ± 7.19	13.52 ± 1.33	0.07
<b>42</b>	218.30 ± 32.45	600.41 ± 69.08	2.75
<b>43</b>	813.53 ± 96.85	51.60 ± 2.42	0.06
<b>44</b>	154.88 ± 4.59	146.33 ± 1.44	0.94
<b>45</b>	128.62 ± 18.48	1.02 ± 0.001	0.01
<b>46</b>	181.35 ± 2.92	N.D.	N.D.
<b>47</b>	193.09 ± 10.12	6.61 ± 0.26	0.03
<b>48a</b>	500.21 ± 62.01	18.26 ± 0.75	0.04
<b>48b</b>	N.D.	47.07 ± 3.89	N.D.
<b>49</b>	215.15 ± 9.31	363.07 ± 8.39	1.69
<b>50</b>	96.19 ± 0.95	N.D.	N.D.
<b>51</b>	53.80 ± 2.47	108.00 ± 7.22	2.01
<b>52</b>	462.39 ± 13.53	111.18 ± 8.32	0.24
<b>53</b>	609.03 ± 1.69	141.24 ± 5.99	2.24
<b>54</b>	1046.23 ± 12.46	692.06 ± 76.79	0.60
<b>55</b>	1083.64 ± 25.83	555.61 ± 13.17	0.51
<b>56</b>	299.99 ± 32.77	678.76 ± 85.22	2.26
<b>Donepezil</b>	0.014 ± 0.0001	3.3 ± 0.1	235.71

N.D. – Not determined in the tested concentrations (because the inhibitory activities were too weak to permit an IC<sub>50</sub> determination).



Although compound **17** showed good inhibitory activity, particularly for *eq*BuChE (Table 12), the (*R*)-enantiomer (compound **17a**) presented better inhibitory activity for both *ee*AChE and *eq*BuChE. The (*S*)-enantiomer (compound **17b**) presented better inhibition results for *ee*AChE but not for *eq*BuChE when compared to the racemate (compound **17**). In the case of the two enantiomers, **17a** and **17b**, it was the (*R*)-enantiomer that presented the best results, especially for *eq*BuChE. Compounds **18** and **19** presented lower inhibition activity compared to compound **17** (Table 12), showing the importance of the free alcohol as a hydrogen bond donor in the ligand-protein interaction. This seems to be the case for *ee*AChE.

In the case of *eq*BuChE, substitution of the phenyl group by an alkyl (compound **20**) or a propargyl group (compound **21**), presents better inhibition results than the substitution of the phenyl group in the *para*-position with a halogen (F, Br) or a OMe (compounds **22-24**) as seen in Table 12.

Interesting, the isosteric replacement of the substituted phenyl by a cyclohexyl (compound **25**) or a pyridine (compound **26**) gave better results for *eq*BuChE than compounds **22** to **24**. Actually, the non-aromatic units of compounds **20**, **21** and **25**, most probably developed CH/ $\pi$  interactions with the aromatic ring of the enzymes gorge. None of these compounds (**20-26**) was a better inhibitor than compound **17**. In the case of *ee*AChE, compounds **22** to **25** gave better inhibition results than compound **17**, with compound **25** being the best in this group. Although the presence of a 3-Ph group is desirable for *eq*BuChE inhibition, the presence of a 3-cyclohexyl should give better inhibition in the case of *ee*AChE.

Analyzing the results for BuChE inhibition of compounds **27** to **48b**, the lower inhibition of compound **27** – with a phenyl group directly attached to the oxindole nitrogen – and for compound **28** – with a 2-pyridyl unit – were noteworthy. Compounds **29** to **32** presented much better inhibitory activities for BuChE than for AChE. Extending the side chain by one methylene unit (compound **30**) decreased BuChE inhibition by half, but didn't affect AChE inhibition. In the case of compound **33**, the OH group of the side chain didn't improve the inhibition of the enzyme. The attachment of a cyclohexylmethyl unit as in the case of compound **32** gave an IC<sub>50</sub> of 170.58  $\mu$ M, this was probably due to the lack of  $\pi$ - $\pi$  stabilizing interactions. The replacement of the phenyl group of compound **17** with an acyclic unit, like in the case of compounds **31** and **33** gave very poor inhibitions for *ee*AChE. The alicyclic terminal units incorporated into the molecule in the case of compounds **34-36**, failed to improve the inhibition with either AChE or BuChE. Compounds **37** and **38** were poor inhibitors for BuChE. None the less, compound **38** presented good results for AChE. On the other hand, the pyridine substituted analogues (compounds **30** and **40**) proved to be good inhibitors for BuChE. Compound **40** also presented better inhibition results for AChE than compound **17**. In the case of electron-donor compounds, as **41** and **46**, very different

results were obtained. Compound **41** presented a good inhibition to BuChE, but compound **46** didn't inhibit the enzyme. Electron-withdrawing substituents, like compound **45**, gave a very good inhibition result for BuChE, and a good result for AChE (Table 12). A good result was also obtained by compound **43** for BuChE, but when these substituents were placed into the *para*-position (compounds **42** and **44**) much lower inhibitions were obtained. So it would seem that both steric and electronic factors can influence the inhibitor activity in the case of BuChE.

Compound **47** gave the second best inhibition for BuChE ( $IC_{50}=6.61 \mu M$ ). This was expected on the basis of the molecular docking studies [211]. The benzene A-ring of compound **17** was substituted with halogens in different positions, to give compounds **49** and **50**, but none of these compounds showed significant inhibition, with either enzyme (Table 12).

By looking at the results on Table 12 it's interesting to see that almost all the compounds were selective for BuChE. The exceptions were compounds **23**, **24**, **27**, **28**, **38**, **42**, **46**, **49**, **50** and **51**.

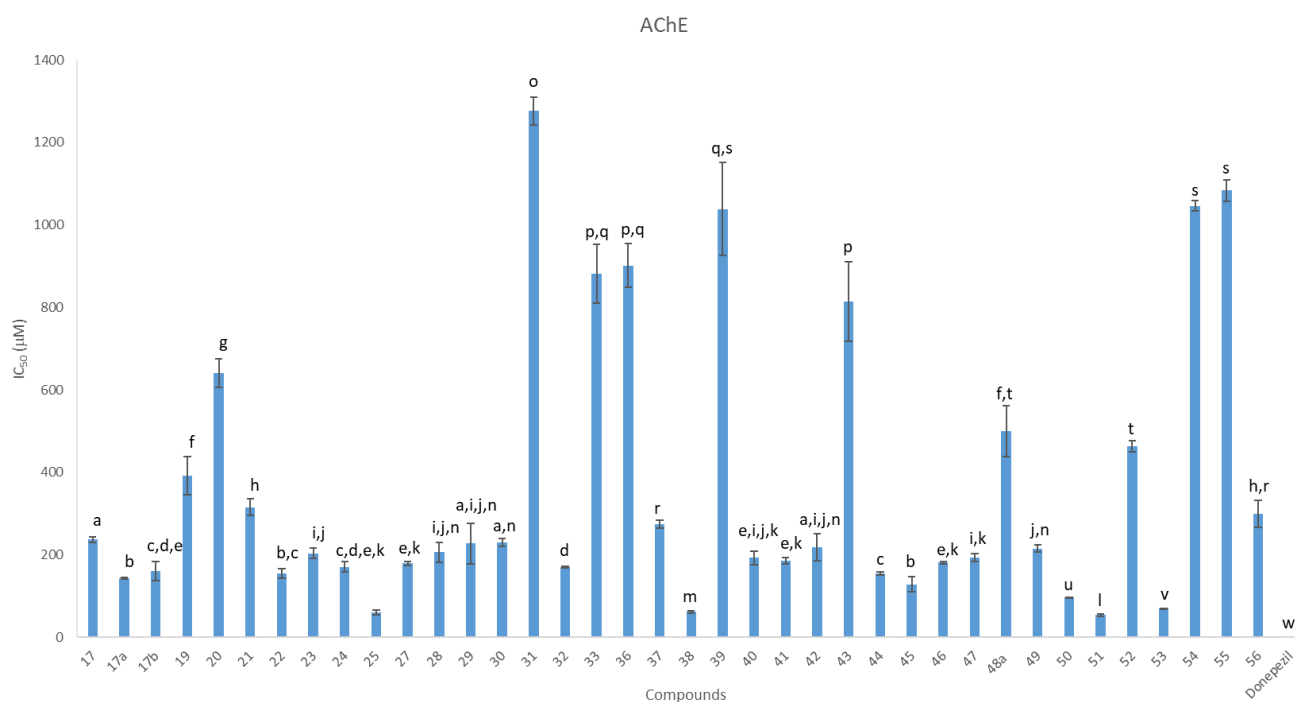


**Figure 45** - *In vitro* eeAChE activity, in the presence of donepezil and compounds **17-17b**, **19-33** and **36-56**. Different letters represent values significantly different ( $p < 0.05$ ).

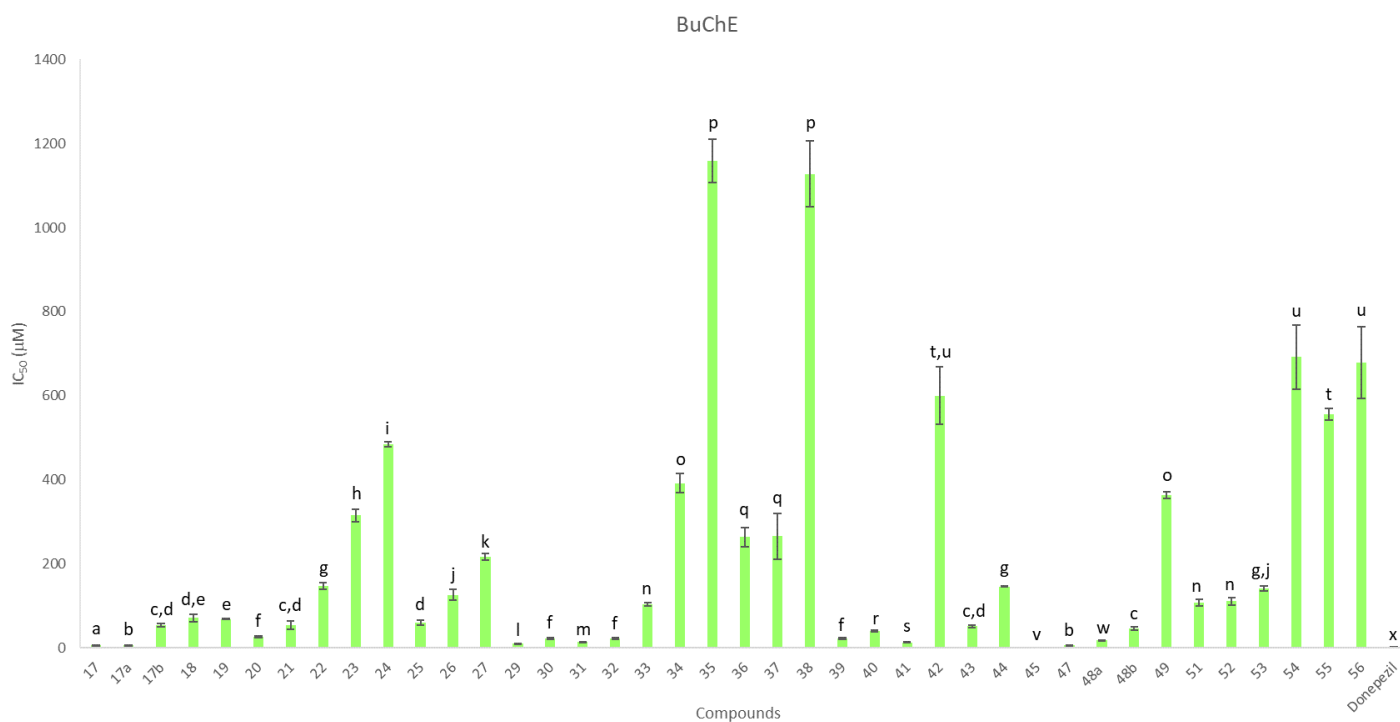


**Figure 46** - *In vitro* eqBuChE activity, in the presence of donepezil and compounds **17-27**, **29-45**, **47-49** and **51-56**. Different letters represent values significantly different ( $p < 0.05$ ).

All the compounds are significantly different from donepezil. In the case of *ee*AChE, the best results were obtained with compounds **25**, **38** and **51**, although they are all significantly different from each other (Fig. 45). In the of *eq*BuChE, the best results were given by compounds **17**, **17a**, **45** and **47**, with **17a** and **47** not significantly different from each other (Fig. 46).

### 3.3.1.3. Diether-ester derivatives

The diether ester compounds **57-60** (Fig. 47) had structural characteristics that suggested they could potentially inhibit both AChE and BuChE [229]. They could interact favorably in the active site, especially through aromatic  $\pi$ - $\pi$  interactions with the active site aromatic amino acid residues and via H-bonding interactions of the ester group with the catalytic triad residues [212]. So, these four compounds were evaluated for their inhibition of *ee*AChE and *eq*BuChE. The dual inhibitor Rivastigmine was used as a standard. Dose-response curves for *ee*AChE and *eq*BuChE are presented in Figure 48. The results of these inhibition studies are shown in Tables 13 and 14 as well as in Figures 49 and 50 (see also Table A1).

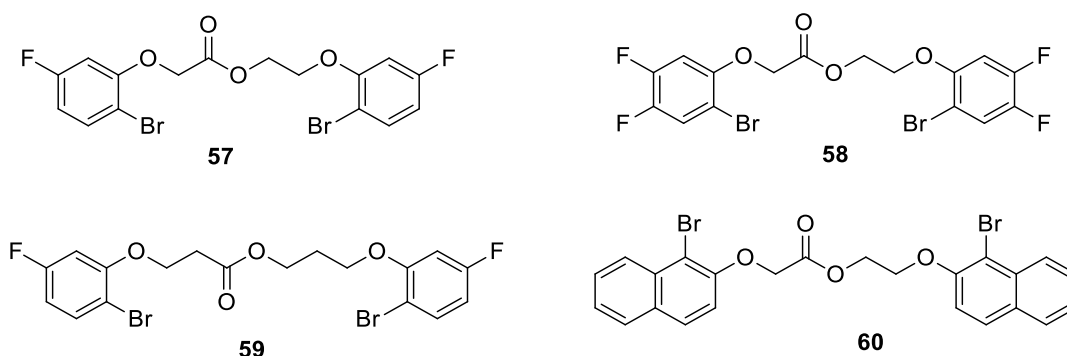


Figure 47 – Diether-ester derivatives.

By analysing the dose-response curves for *ee*AChE and *eq*BuChE (Fig. 48), it is possible to determine the corresponding  $IC_{50}$  values. All the curves present a sigmoidal shape and are very similar for *ee*AChE, reaching 100% inhibition for all compounds, except **60**, that with pre-incubation reached a maximum of 80% inhibition. All the compounds presented better results with pre-incubation. For *eq*BuChE inhibition, none of the compounds reached 100 % inhibition, although the results were better with pre-incubation.

Table 13 - Inhibition studies for *ee*AChE and *eq*BuChE with diether-ester derivatives.

Compound	$IC_{50}$ <i>ee</i> AChE <sup>a</sup> ( $\mu$ M)		$IC_{50}$ <i>eq</i> BuChE <sup>a</sup> ( $\mu$ M)	
	No pre-incubation	Pre-incubation	No pre-incubation	Pre-incubation
<b>57</b>	146.65 $\pm$ 2.68	67.95 $\pm$ 8.21	863.12 $\pm$ 12.55	664.10 $\pm$ 11.76
<b>58</b>	188.24 $\pm$ 3.79	107.25 $\pm$ 0.69	951.31 $\pm$ 12.90	481.79 $\pm$ 20.09
<b>59</b>	191.66 $\pm$ 5.78	103.67 $\pm$ 1.48	836.11 $\pm$ 8.91	335.76 $\pm$ 10.70
<b>60</b>	145.21 $\pm$ 13.36	38.37 $\pm$ 1.38	> 1500	437.85 $\pm$ 10.15
<b>Rivastigmine</b>	342.50 $\pm$ 13.00	127.60 $\pm$ 5.90	26.71 $\pm$ 3.77	1.3 $\pm$ 0.0

<sup>a</sup>  $IC_{50}$  values are expressed as mean  $\pm$ SD (n=3) based on dose-response curves, using the Origin 8.0 Pro.

The incubation time was studied for the compounds with both enzymes, and was found to be crucial to the inhibition process (Table 13). All the compounds showed higher inhibition for *ee*AChE than for *eq*BuChE, thus being more selective for this enzyme (Table 14).

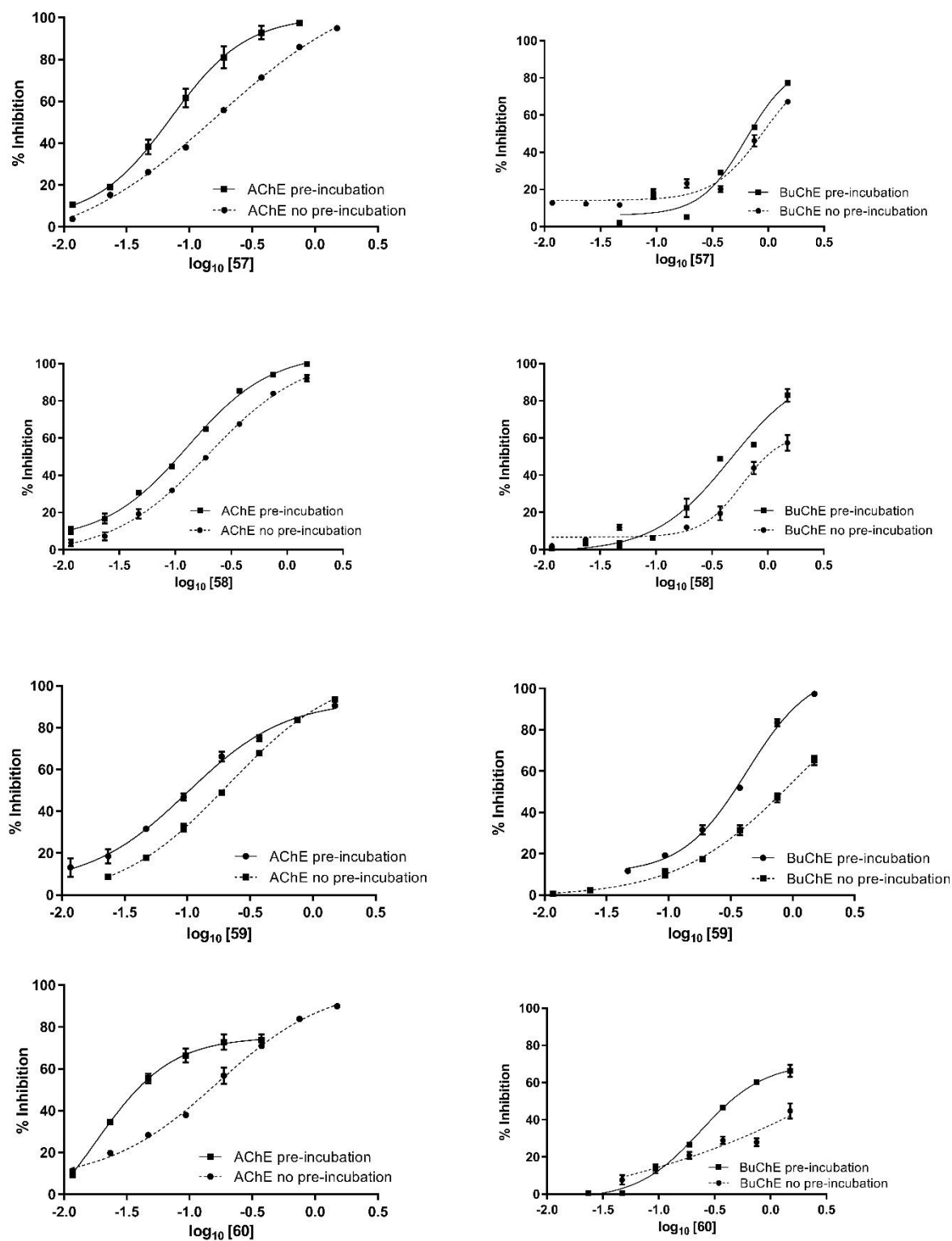
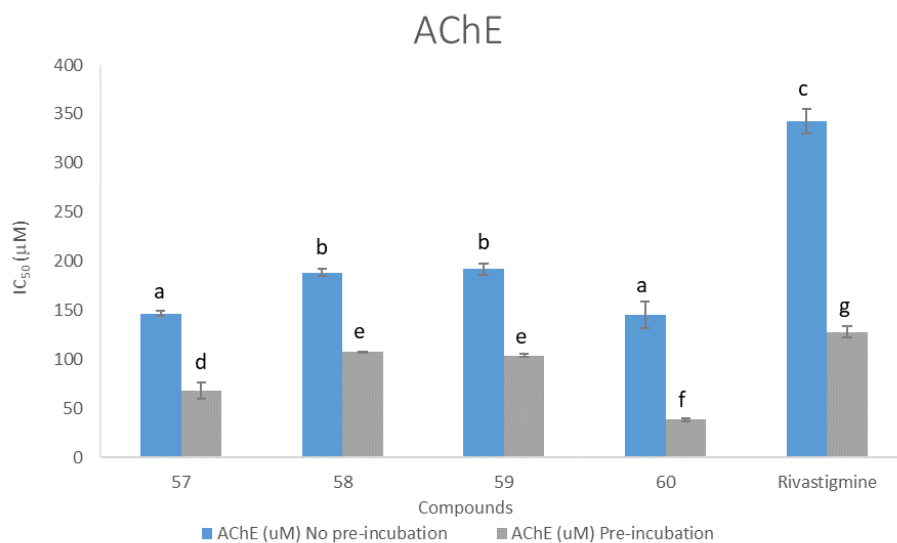
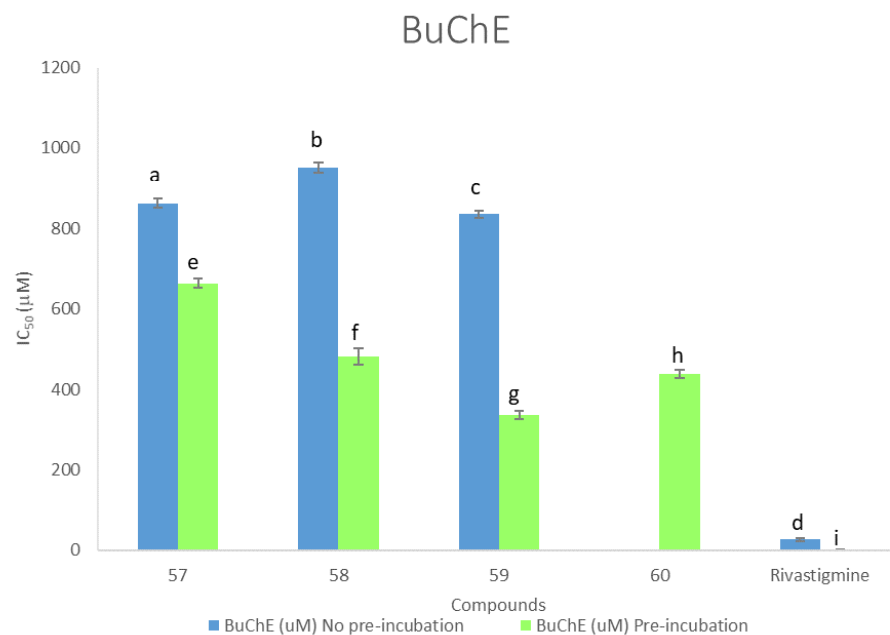


Figure 48 - Dose-response curves with and without incubation, for *ee*AChE and *eq*BuChE with diether-ester derivatives.



**Figure 49** - *In vitro* *ee*AChE activity, in the presence of rivastigmine and compounds **57** to **60**. Different letters represent values significantly different ( $p < 0.05$ ).

In the case of *ee*AChE, all compounds presented higher inhibition than the standard, Rivastigmine. Compound **60** provided the best IC<sub>50</sub> value, 38.37 µM, showing the importance not only of the aromatic rings in this process, with putative  $\pi$ - $\pi$  interactions, but also the ester group that perhaps was hydrolyzed by the catalytic triad in the enzymes' active site. This result for compound **60** was significantly different from all others ( $p < 0.05$ ) in the case of pre-incubation with *ee*AChE, but not in the absence pre-incubation, where compounds **57** and **60** are not significantly different ( $p > 0.05$ ). On comparing the IC<sub>50</sub> values for **57** and **58** it's clear that the *p*-fluorine atoms didn't favour *ee*AChE inhibition (Table 14) with values significantly different (Fig. 49). Compounds **58** and **59** didn't present any significant difference with or without pre-incubation with *ee*AChE (Fig. 49), which led us to believe that the elongation of the chain wasn't the principal factor for better *ee*AChE inhibition with these compounds. In the case of *eq*BuChE, compound **59** gave the best IC<sub>50</sub> value, 335.76 µM (with pre-incubation) and this value was significantly different from all others ( $p < 0.05$ ). Without pre-incubation all of the compounds showed significantly different inhibitory results to Rivastigmine and to each other (Fig. 50). Contrary to *ee*AChE, the presence of different substituents in the aryl ring favours *eq*BuChE inhibition (Table 14, with incubation).



**Figure 50** - *In vitro* eqBuChE activity, in the presence of rivastigmine and compounds **57** to **60**. Different letters represent values significantly different ( $p < 0.05$ ).

In the case of the eqBuChE inhibition, although the IC<sub>50</sub> values with pre-incubation are far better than without pre-incubation, they were all significantly different from each other (Fig. 50), and besides, the inhibition was very low compared to the standard. Actually, compound **60** didn't inhibited eqBuChE without pre-incubation. Ultimately, these results showed that these compounds were unsuitable for inhibiting eqBuChE, as we can see from Table 14 (higher values indicate selectivity towards eeAChE).

**Table 14** – Selectivity index for cholinesterase studies with diether-ester derivatives.

Compound	Selectivity Index (IC <sub>50</sub> eqBuChE / IC <sub>50</sub> eeAChE)	
	No pre-incubation	Pre-incubation
<b>57</b>	5.89	9.77
<b>58</b>	5.05	4.49
<b>59</b>	4.36	3.24
<b>60</b>	N.D.	11.41
<b>Rivastigmine</b>	0.08	0.05

Interestingly, unlike rivastigmine, the diether-ester **57-60** were highly selective for eeAChE, especially with previous incubation (Table 14).

### 3.3.1.4. Chromanone and chromanol derivatives

The structural analogy between chromanones and donepezil - specifically in regard to the chromanone unit - made these compounds of interest for AChE and BuChE inhibition. With this in mind, 6 compounds were tested for the inhibition ability of these enzymes (Fig. 51). Donepezil was used as standard.

The dose-response curves are presented in Figure 52 and the corresponding  $IC_{50}$  results of these studies are presented in Table 15. Figure 53 (and Table A2) shows the statistical analysis for *ee*AChE and *eq*BuChE inhibition in the presence of compounds **61-66** and donepezil.

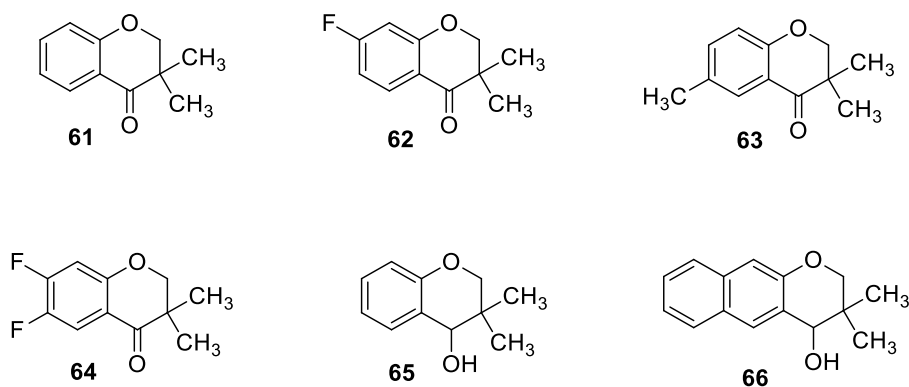
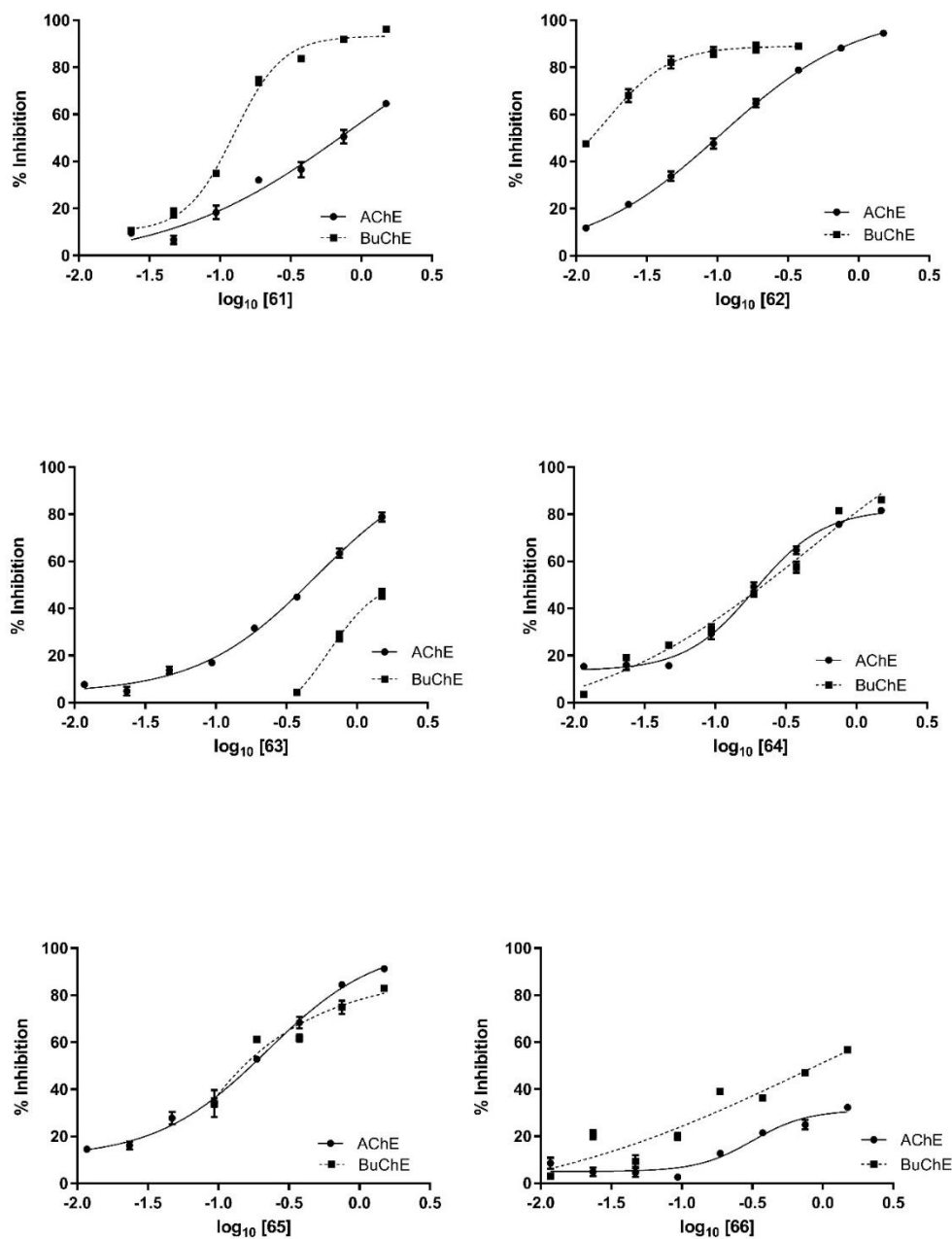


Figure 51 - Chromanone and chromanol derivatives.

In the case of *ee*AChE, compound **62** had the higher inhibition, probably due to the existence of electron withdrawing substituents in the *m*-position of the aryl ring. Compound **61** showed a very weak interaction, contrary to compounds **62-64**, which led to the conclusion that the existence of substituents in the aryl ring potentiates *ee*AChE inhibition. None the less, substitution in both *m*- and *p*-position wasn't so favorable (Table 15, compound **64**). The existence of an electron donor group in the *p*-position of the aryl ring (compound **63**) also showed a weak interaction with the enzyme. Interestingly, compounds **65** and **66** presented similar inhibition values for *ee*AChE (Table 15). When compounds **61** ( $IC_{50}$ = 692.60  $\mu$ M) and **65** ( $IC_{50}$ = 181.60  $\mu$ M) were compared, there was a significant preference of compound **65** for *ee*AChE, most likely due to hydrogen bonding between the alcohol group and enzyme catalytic triad.





**Figure 52** - Dose-response curve for *ee*AChE and *eq*BuChE with chromanone and chromanol derivatives.

In the case of *eq*BuChE, compounds **61**, **65** and **66** had similar inhibition values (Table 15). Compound **63** didn't inhibit the enzyme and compound **64** presented a weak inhibition, similar to the one it had for *ee*AChE (Table 15). On the other hand, compound **62** showed the lower IC<sub>50</sub> (12.00  $\mu$ M), suggesting that electron withdrawing substituents in the *m*-position were favorable to *eq*BuChE inhibition. Compounds **61**, **62** and **65** were selective for *eq*BuChE, whilst compounds **64** and **66** were slightly selective for *ee*AChE. Compound **63** was selective for *ee*AChE (Table 15).

**Table 15** – Inhibition studies for *ee*AChE and *eq*BuChE activities with chromanone and chromanol derivatives.

Compound	IC <sub>50</sub> <i>ee</i> AChE <sup>a</sup> (μM)	IC <sub>50</sub> <i>eq</i> BuChE <sup>a</sup> (μM)	Selectivity Index (IC <sub>50</sub> <i>eq</i> BuChE/ IC <sub>50</sub> <i>ee</i> AChE)
<b>61</b>	692.60 ± 22.00	123.30 ± 6.10	0.18
<b>62</b>	100.00 ± 1.79	12.00 ± 0.02	0.12
<b>63</b>	380.00 ± 5.78	N.D.	N.D.
<b>64</b>	215.14 ± 10.40	249.00 ± 17.8	1.16
<b>65</b>	181.60 ± 10.10	147.00 ± 10.10	0.81
<b>66</b>	160.67 ± 8.47	163.72 ± 12.44	1.02
<b>Donepezil</b>	0.014 ± 0.0001	3.3 ± 0.1	235.71

<sup>a</sup> IC<sub>50</sub> values are expressed as mean ±SD (n =3) based on dose-response curves, using the Origin 8.0 Pro.

N.D. – Not determined in the tested concentrations (because the inhibitory activities were too weak to permit an IC<sub>50</sub> determination).

From Figure 53 it is possible to see that for *ee*AChE, all the compounds showed inhibitions significantly different from donepezil, and besides the results obtained for **65** and **66** were rather similar. Compound **62** didn't present significantly different results from donepezil for *eq*BuChE and **65** and **66** were not significantly different from each other.

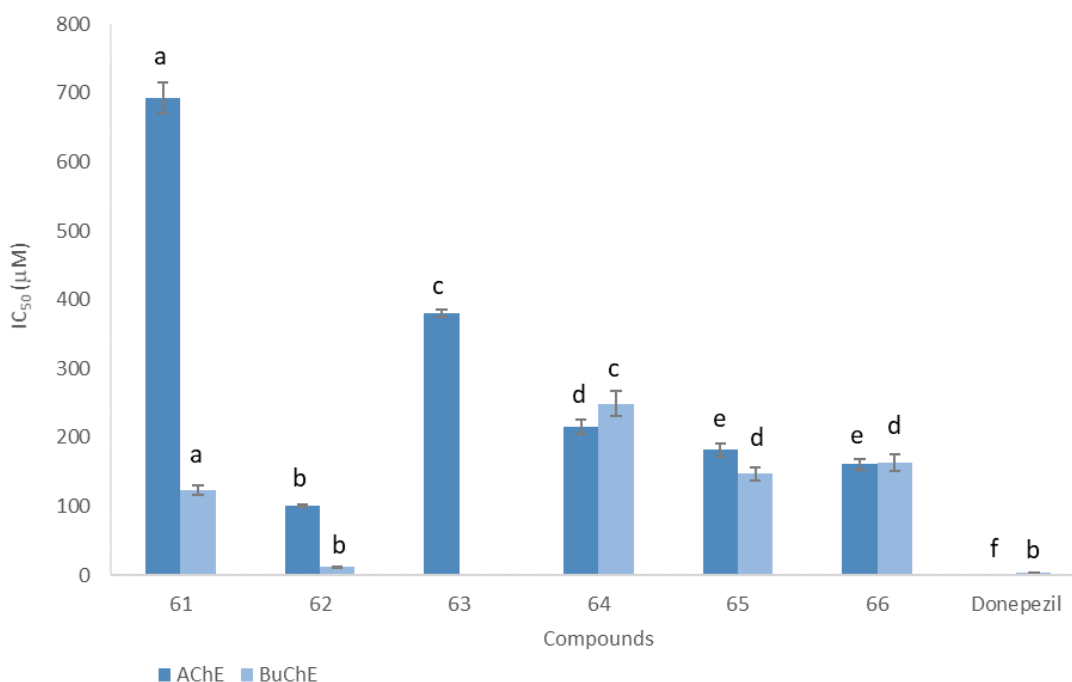
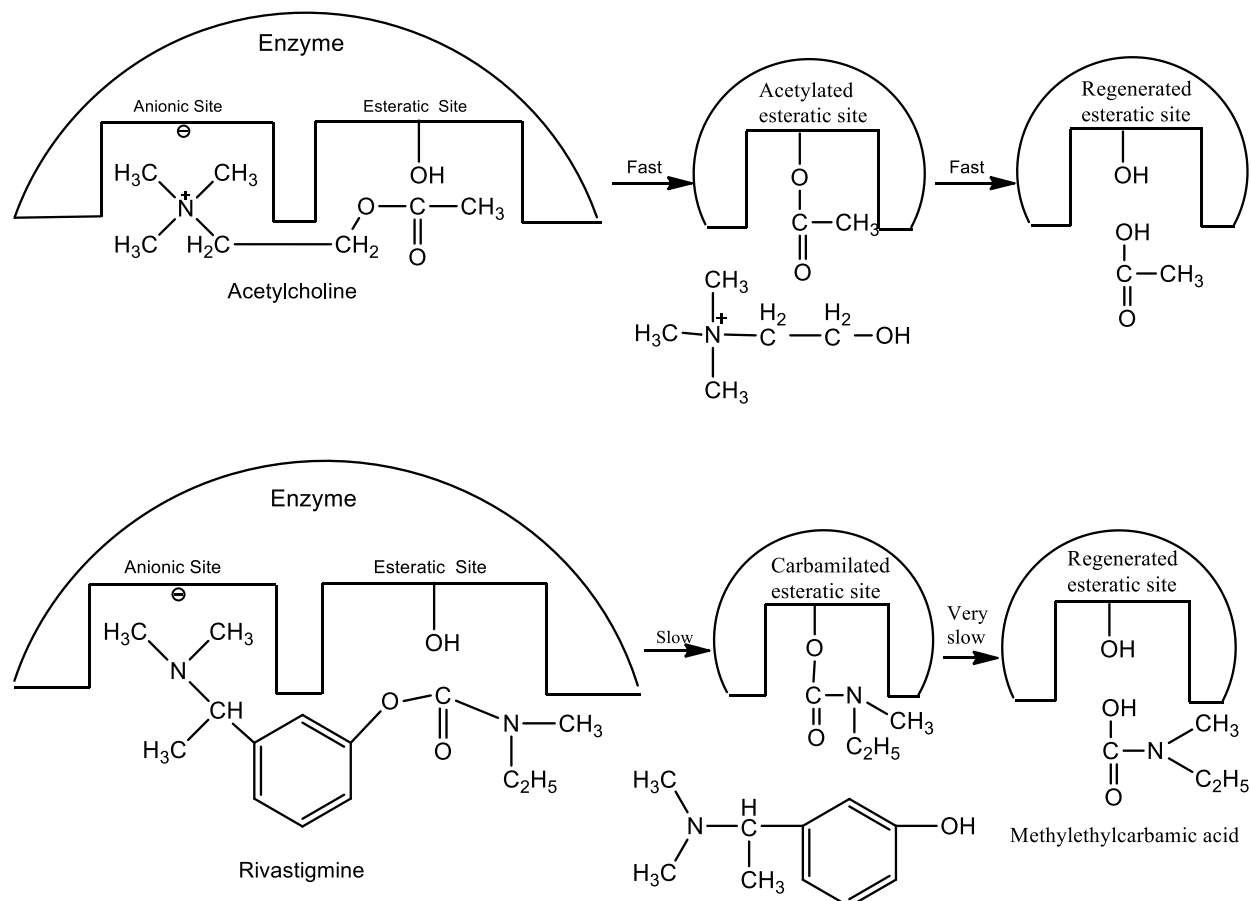


**Figure 53** - *In vitro* *ee*AChE and *eq*BuChE activity, in the presence of donepezil and compounds **61** to **66**. Different letters represent values significantly different for each enzyme experiment (p<0.05).

### 3.3.1.5. Rivastigmine analogues

Rivastigmine is a carbamate derivative used in the treatment of initial to mild forms of AD. It binds to both ionic and esteratic sites of AChE in a similar way to ACh [36]. Just like the natural substrate, rivastigmine undergoes hydrolysis by the enzyme, in this case, to produce a phenolic derivative and a carbamic acid (Scheme 11).



**Scheme 10** – Mechanism of action of Rivastigmine on AChE. Adapted from [36].

The possibility of developing new and better dual ChE inhibitors led to the study of 8 analogues of this commercial drug (Fig. 54). The dose-response curves are presented in Figure 55 and the corresponding  $\text{IC}_{50}$  results of these studies are presented in Table 16. Figure 56 (and Table A2) shows the statistical analysis for *ee*AChE and *eq*BuChE inhibitory activity in the presence of compounds **67-74** and rivastigmine.

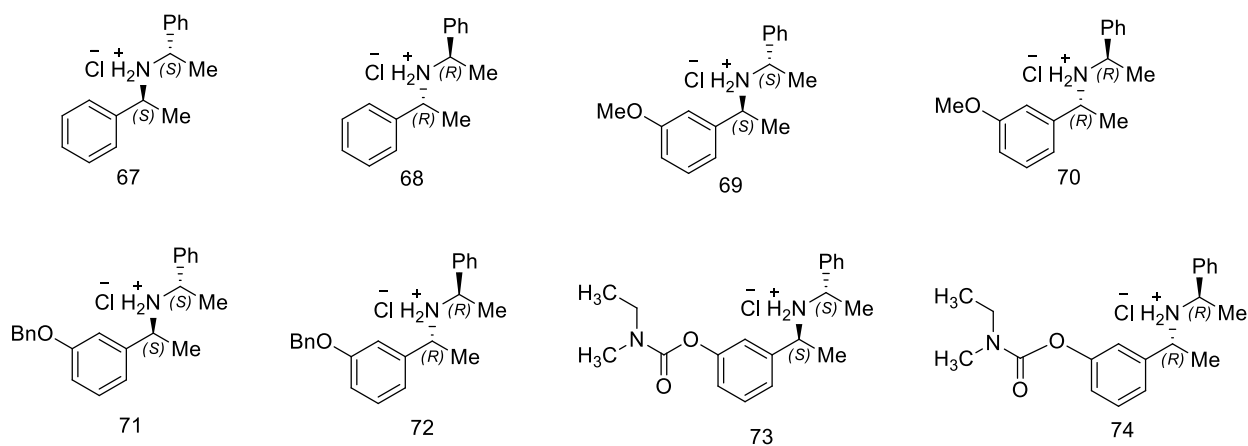
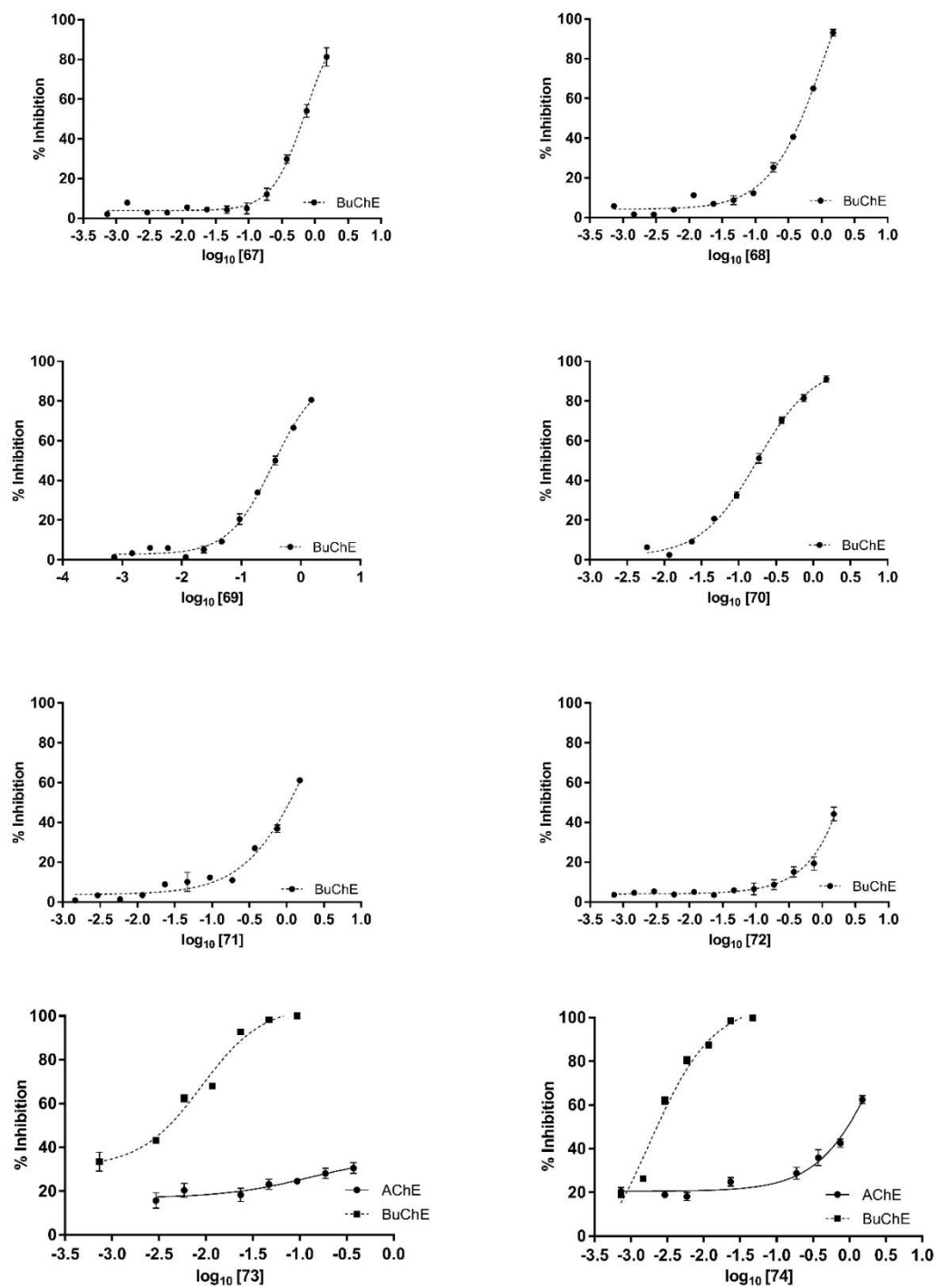


Figure 54 - Rivastigmine analogues.

None of the tested compounds inhibited *ee*AChE. For compounds **67** to **72**, the absence of the carbamate group was associated with the lack of inhibition. In the case of compounds **73** and **74**, which contained a carbamate group, the lower inhibition, when compared to rivastigmine, could be related to the substitution of the ethyl group by a phenyl group, although there is a difference in the results between compounds **73** and **74**, which is probably due to enantiomeric selectivity. Compounds **71** and **72** failed to show any significant inhibition of *eq*BuChE (Table 16), which might be related to the presence of the *m*-benzyloxy group. (Fig. 54).

For *eq*BuChE, compounds **67** and **68** showed very weak inhibition and compounds **69** and **70** showed moderately weak inhibition. Contrary to these results, compounds **73** and **74**, which were highly selective for *eq*BuChE, presented very good inhibition for this enzyme, with an IC<sub>50</sub> that was, respectively, 15 and 6 times lower than rivastigmine (Table 16). This was in some ways to be expected, since the bioactive form of rivastigmine has the (*S*) configuration [36]. None the less, what was surprising was that compound **70** and not **69** (with the (*S*) configuration) presented the lower IC<sub>50</sub> (Table 16). The same applied to compounds **68** and **67**. The preference for the (*R*) enantiomer changed with the introduction of the carbamate group (compounds **73** and **74**) (Table 16). These two compounds were selective for BuChE, and when compared to rivastigmine, the selectivity was almost 20 times higher.



**Figure 55** – Dose-response curves of compounds **73** and **74** for *ee*AChE, and of compounds **67**, **68**, **69**, **70**, **71**, **73** and **74** for *eq*BuChE activities.

**Table 16** - Inhibition studies of *ee*AChE and *eq*BuChE activities with rivastigmine analogues.

Compound	IC <sub>50</sub> <i>ee</i> AChE (μM)	IC <sub>50</sub> <i>eq</i> BuChE (μM)	Selectivity Index (IC <sub>50</sub> BuChE/IC <sub>50</sub> AChE)
<b>67</b>	N.D.	515.92 ± 50.62	N.D.
<b>68</b>	N.D.	499.60 ± 11.53	N.D.
<b>69</b>	N.D.	247.38 ± 18.44	N.D.
<b>70</b>	N.D.	177.99 ± 15.19	N.D.
<b>71</b>	N.D.	1124.54 ± 18.16	N.D.
<b>72</b>	N.D.	N.D.	N.D.
<b>73</b>	913.58 ± 87.79	1.72 ± 0.12	0.002
<b>74</b>	1286.78 ± 70.47	4.04 ± 0.29	0.003
<b>Rivastigmine</b>	342.50 ± 13.00	26.71 ± 3.77	0.08
<b>Rivastigmine<sup>a</sup></b>	3.12 ± 0.46	0.38 ± 0.02	0.12

N.D. – Not determined in the tested concentrations (because the inhibitory activities were too weak to permit an IC<sub>50</sub> determination).

<sup>a</sup>Results from the literature for human AChE and BuChE [230].

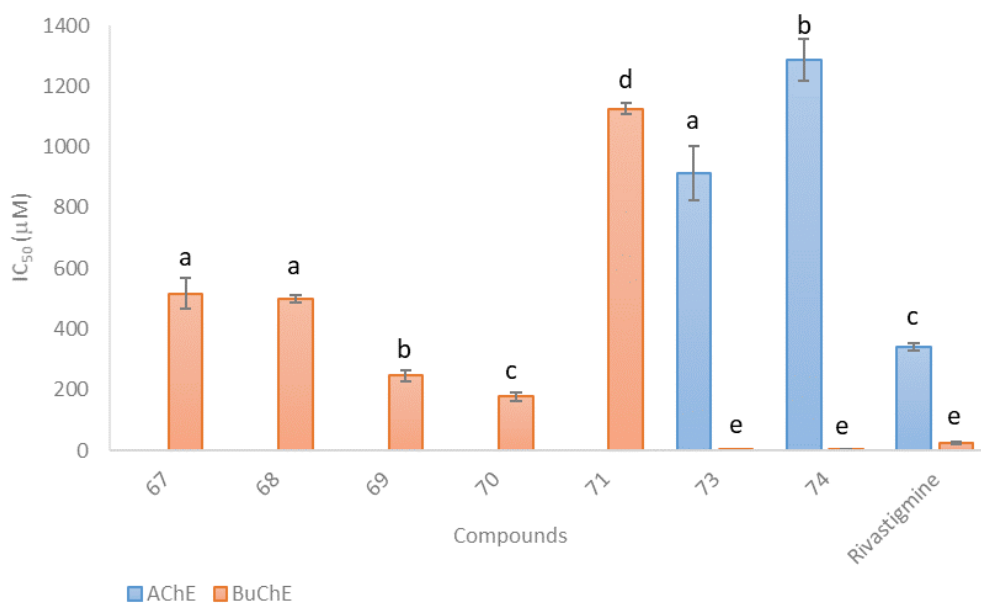


**Figure 56** - *In vitro* AChE and BuChE activity, in the presence of rivastigmine, compounds **67** to **71** and **73-74**. Different letters represent values significantly different for each enzyme experiment ( $p < 0.05$ ).

The statistical analysis presented in Figure 56 reveals significantly different results for AChE. With regards to BuChE, compounds **73** and **74** didn't present significantly different results from rivastigmine, contrary to the rest of the compounds, and **67** and **68** are not significantly different from each other.

Mustazza *et al.* [231] synthesized a variety of dimethyl, diethyl and *n*-hexylcarbamates related to Rivastigmine, that showed IC<sub>50</sub> values ranging from 7 to >1000 nM (for rat brain AChE) and of 8 to >1000 nM (for rat plasma BuChE), which are far better results than the ones presented for rivastigmine. When comparing the result obtained for rivastigmine with AChE from two sources: *ee*AChE (342.50 μM, Table 16) and *h*AChE (3.12 μM) the difference is striking. The same is true for BuChE: *eq*BuChE (26.71 μM) and *h*BuChE (0.38 μM). This leads to the conclusion that rivastigmine is a better inhibitor for human ChEs than for other species. With this in mind, we might speculate that in the case of compounds **67** to **74**, it is quite possible that better inhibitions might be obtained for both *h*AChE and *h*BuChE. Curiously, the selectivity index for both Rivastigmine entries is similar, meaning that this compound is a better inhibitor for BuChE than for AChE, independently of the enzyme source.

### 3.3.2. MAO-B IC<sub>50</sub> evaluation

Some of the compounds tested for *ee*AChE and *eq*BuChE were also tested for hMAO-B inhibition, namely, compounds **21** and **68** to **75**. Unfortunately, none of these compounds presented inhibitory properties for MAO-B in the tested concentrations. Crucial insightful molecular docking studies were conducted by Luís Fernandes in order to understand what was happening and to explain the lack of activity in the case of these compounds (Fig. 57). These simulations revealed that the interaction of compound **21** with MAO-B, involved  $\pi$ - $\pi$  stacking with the Tyr 398 and Tyr 435 residues, respectively. However, these calculations also showed the presence of a hydrogen-bonded water network that stabilizes the FAD moiety, but on the other hand, the water molecules clash with the phenyl and benzyl group in positions 1 and 3 of the inhibitor (Fig. 57B), making it very difficult for the inhibitor to be reasonably accommodated within the enzyme active site.

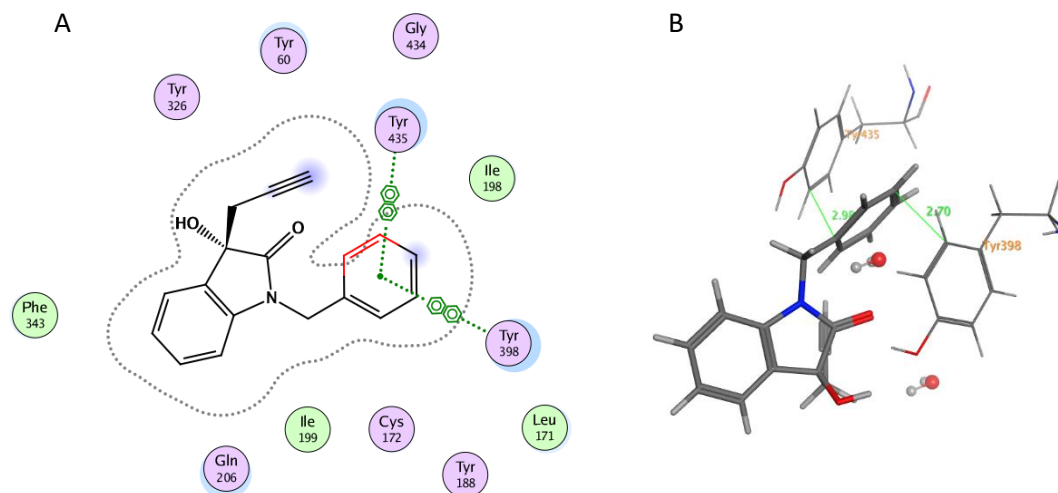


**Figure 57** - Binding mode of compound (**21**) obtained by docking with *h*MAO-B (1OJA, resolution 1.7 Å). Water molecules in the active site are represented as red and grey spheres. (A) Scheme and (B) Catalytic site view.

### 3.4. Conclusions

In this chapter were tested seven different families of compounds to determine which one presented the best inhibition for the enzymes *ee*AChE, *eq*BuChE and MAO-B. Those families were: isoquinolinone, azepanone, indolinone, diether-ester, chromanol, chromanone and rivastigmine derivatives.

Considering the totality of the compounds studied in this thesis, the one that presented the best inhibitory capability for AChE was compound **60**, and compound **45** for BuChE, with similar results for compound **74**. Unfortunately, none of these compounds showed inhibition of MAO-B. As regards dual inhibition of cholinesterases, both **25** and **62** showed favorable inhibitory profiles. In order to better understand how the different families of compounds bind to the target enzymes, a Saturation Transfer Difference-NMR (STD-NMR) study was carried out, which is discussed in Chapter 4.







## ***Chapter 4***

# ***Studying Inhibitor-Enzyme Interactions: Saturation Transfer Difference NMR (STD-NMR) and molecular docking***

---

“Absence of evidence is not evidence of absence.”

(Carl Sagan, 1934-1996)

The studies discussed in this chapter led to the following publication:

1. Bacalhau, P., San Juan, A., Goth, A., Caldeira, A. T., Martins, M. R., Burke, A. J. Insights into (S)-rivastigmine inhibition of butyrylcholinesterase (BuChE): Molecular docking and saturation transfer difference NMR (STD-NMR). *Bioorg. Chem.* **67**, 105–109 (2016).

## 4.1. Introduction

Nuclear magnetic resonance (NMR) is a spectroscopic method capable of yielding information on the structure of molecules, interactions between molecules and molecular motion. This method is based upon the principle that a spinning charge (i.e., the nucleus) generates a magnetic field. In the context of protein-ligand interactions, their kinetic properties (typically medium-weak binding affinities) make them very suitable to be studied by NMR techniques based on the observation of the ligand. Therefore, STD-NMR experiments represent a very robust and powerful ligand-based NMR technique to study, at atomic resolution, the hot spots of ligand-receptor interactions, without any need for processing NMR information about the receptor and at the same time only using small quantities of non-labeled macromolecule [232].

A sample containing the receptor at low concentration and a large molar excess of the ligand (ranging from 1:50 to 1:1000) is usually employed in STD NMR experiments. This precludes the perturbations of absolute STD intensities due to rebinding effects (i.e, a ligand already saturated experiences another association process, without previous full relaxation), thus hindering a correct group epitope mapping assignment [233].

The shorter the protein-ligand proton-proton distance (bound state), the stronger the intensity of the corresponding STD signal. So, by normalizing all the measured STD intensities ( $I_0 - I_{sat}/I_0$ ) against the most intense signal (which is arbitrarily assigned a value of 100%), the so-called “group epitope mapping” is obtained (expressed as percentages). This represents the fingerprint of protein-ligand contacts in the bound state, such that it shows which of the units of the ligand are key for molecular recognition in the binding site [234].

Some STD studies were carried out for AChE, BuChE and MAO-B. Donepezil hydrochloride and galantamine bromide were used as benchmarks and tested with AChE, rivastigmine tartrate was used for both AChE and BuChE, and rasagiline mesylate was the benchmark for MAO-B.

Key STD-NMR experiments were also performed to map the ligand-protein interactions for compounds **6** and **47a** with both AChE and BuChE and compound **17** with BuChE. The selection of these compounds for this study was based on their inhibition profiles, and the necessity to understand their mechanism of inhibition.

The molecular modeling determinations and their figures presented in this section were courtesy of Luís Fernandes.

## 4.2. Materials and methods

### 4.2.1. Chemicals

AChE, BuChE, MAO-B, rivastigmine tartrate, donepezil hydrochloride, galantamine bromide and rasagiline mesylate were purchased from Sigma-Aldrich. AChE used in the assays was from *Electrophorus electricus* (VI-S lyophilized powder, 814 U mg<sup>-1</sup> protein), BuChE used in the assays was from equine serum (lyophilized powder, 1830 U mg<sup>-1</sup> protein). The lyophilized enzymes were prepared in 20 mM Tris-HCl D<sub>2</sub>O pH 7.6 buffer. MAO-B used in the assays was human recombinant expressed in baculovirus infected BTI insect cells (1U mg<sup>-1</sup> protein, 2.5 mg protein mL<sup>-1</sup> in 0.5 mL solution of 100 mM potassium phosphate, pH 7.4, 0.25 M sucrose, 0.1 mM EDTA, and 5% glycerol). Rivastigmine tartrate and donepezil hydrochloride were prepared in DMSO-d<sub>6</sub>, galantamine bromide, MAO-B and rasagiline mesylate were prepared in D<sub>2</sub>O to the desired concentrations.

### 4.2.2. Conducting the STD experimente

The NMR spectroscopy experiments were performed on a Bruker Avance III 400 MHz HD spectrometer equipped with a 5 mm broadband (PABBO BB/19F-1H/D Z-GRD) resonance probe head. STD NMR experiments were carried out with solvent suppression and a 10 ms spin-lock filter after the 90° pulse to reduce residual signals from the protein. For selective saturation, cascades of Gaussian pulses with a length of 50 ms and 40 - 60 dB of attenuation were employed, with an interpulse delay of 1 ms [234, 235]. The *on-resonance* and *off-resonance* frequencies were set to 0 and 12000 Hz, respectively. STD-NMR controls were performed using the ligand itself. Blank experiments were performed to guarantee the absence of direct saturation of the ligand proton signals. The relaxation delay was properly adjusted so that the experiment time length was kept constant at 6.5 s. Water suppression at 1880 Hz (4.7 ppm) was conducted. A sweep-width of 8012.82 Hz (20.03 ppm) was employed. Specifically, the saturation time to obtain the STD buildup curves were recorded at 0.25, 0.5, 1, 2, 3, 4, and 5 s [233, 236].

A 5 μM *eq*BuChE or *ee*AChE solution was prepared in a Tris-HCl buffer in 99.9 % D<sub>2</sub>O (20 mM at pH 7.4). A 5 mM stock solution was prepared for each compound (ligand). Samples for NMR analysis were prepared by adding 100 μL of the ligand to a 500 μL of enzyme solution.

---

Donepezil hydrochloride, galantamine bromide, rivastigmine tartrate and rasagiline mesylate were used as benchmarks for these experiments.

### 4.2.3. Calculation of the STD Amplification factor

For comparing the relative STD effects, the STD amplification factor ( $A_{STD}$ ) was calculated according the Equation 5 [232]:

$$A_{STD} = \frac{I_0 - I_{SAT}}{I_0} \times L/P \text{ molar ratio} = \frac{I_{STD}}{I_0} \times L/P \text{ molar ratio} \quad (5)$$

where  $I_0$  and  $I_{SAT}$  are the intensity of the signals in the reference and saturated spectra, respectively.

### 4.2.4. Mapping of the binding moieties

The  $A_{STD}$  allows the mapping of the ligand hydrogen's that are closer to the protein, by choosing a saturation time that allows a good distinction between the different  $A_{STD}$ . For all the experiments the saturation time chosen was of 3s. The STD signal with the highest intensity was set to 100 % and all the signal percentages were calculated accordingly [232].

## 4.3. Results and discussion

### 4.3.1. Protein-ligand interaction studies by STD-NMR

Cholinesterases are among the most efficient enzymes known. The active site of AChE comprises 2 subsites - the anionic subsite and the esteratic subsite at the gorge rim. The anionic subsite accommodates the positively charged quaternary amine of acetylcholine as well as other cationic substrates and inhibitors. X-ray crystallography studies of AChE and BuChE [237] show an identical catalytic triad of amino acid residues in the esteratic subsite (serine, histidine and glutamate), where ACh is hydrolyzed to acetate and choline, but significant differences at the peripheral anionic site (PAS). The PAS in both AChE and BuChE is essentially composed of

aromatic amino acids, however, six aromatic residues in human AChE (*hAChE*) (Tyr72, Tyr124, Trp286, Phe295, Tyr337, and Tyr341) are replaced by polar and mostly aliphatic residues in human BuChE (*hBuChE*) (Asn68, Gln119, Val279, Val288, Leu330, and Ala334). Due to their large catalytic site, ChE tolerate a wide variety of substrates from small natural or synthesized heterocycles to larger molecules like donepezil-tacrine hybrids [238].

*eeAChE* possesses the three amino acids of the catalytic triad Ser203, Glu334 and His447, the aromatic residues Phe295 and Phe297, which define an acetylcholine-specific acyl pocket, the tryptophan residue Trp86, which interacts with the choline moiety in the active site, Gly121 and Gly122 as well as the 14 aromatic residues lining the walls of the gorge [239]. All 14 amino acids in the aromatic gorge are highly conserved across different species. Together with Trp86, Tyr337 constitutes the choline-binding subsite of the catalytic site [240]. 13 residues of the gorge are identical to *Torpedo californica* (*ray*) AChE (*tcAChE*), only Tyr330 of *EeAChE* is replaced by Phe330 in *tcAChE* [239]. The X-ray crystallographic analysis of *tcAChE* showed that it consists of a catalytic triad (Ser200-His440-Glu327) which lies close to the bottom of the deep and narrow gorge, which is lined with 14 aromatic amino acid residues [42, 241].

*hBuChE* and *hAChE* share 65% amino acid sequence homology [242]. The crystal structure of *hBuChE* has already been solved [39]. This enzyme can hydrolyze toxic esters such as cocaine and scavenge organophosphorous pesticides and nerve agents [39]. It is characterized by possessing the catalytic triad which is constituted by Ser198, Glu325 and His438, and the hydrophobic residues Leu286 and Val288, which define the acyl pocket. These changes make the binding with the bulkier butyrate substrate possible [39]. The tryptophan residue Trp82, which interacts with the choline moiety in the catalytic active site via a cation- $\pi$  interaction, the residues Asp70, Tyr332 and Asn83 constitute the peripheral anionic site [39].

When compared, both *eeAChE* and *eqBuChE* have the catalytic triad at the bottom of the gorge (20 Å deep). In the case of *eeAChE* the gorge consists of aromatic residues and in the case of *eqBuChE* the gorge has hydrophobic residues. In contrast to *eeAChE*, the *eqBuChE* acyl pocket (PAS) has smaller, hydrophobic, amino acid residues, so it can accommodate bulkier substrates. In both enzymes, the PAS is located at the outer rim of the gorge, and is an attraction center for substrates. The anionic site for both *eeAChE* and *eqBuChE* is found half-way down the gorge, between the peripheral and the acylation sites.



### 4.3.1.1. STD-NMR of AChE-Donepezil hydrochloride

Donepezil is a reversible and selective AChE inhibitor and is administered as a racemic mixture [243]. In the interest of developing more potent analogues of donepezil for *h*AChE inhibition, and for refining screening methods, it was undertaking a detailed study of the key interactions between AChE and donepezil using the STD-NMR technique [232-236].

It should be noted that as donepezil hydrochloride was used for the experiment, certain ion-dipole interactions in the vicinity of the piperidine unit would be expected (Fig. 58).

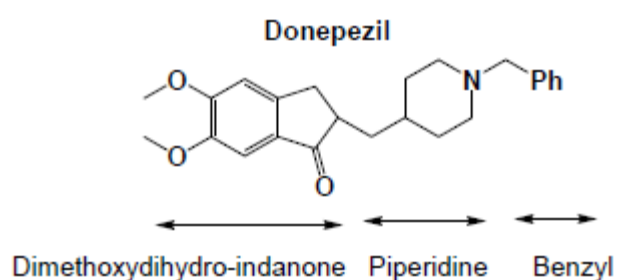


**Figure 58** -Key binding regions of donepezil. Adapted from [243].

To precisely map ligand epitopes in close contact with the protein, STD build up curves were acquired by collecting spectra at different saturation times [232, 233, 236, 244]. The observed STD amplification (ASTD) is not the same for all the hydrogen atoms in donepezil (Figs. 59). This is due to the fact that not all the proton signals in the STD-NMR spectrum received the same amount of saturation [232, 233].

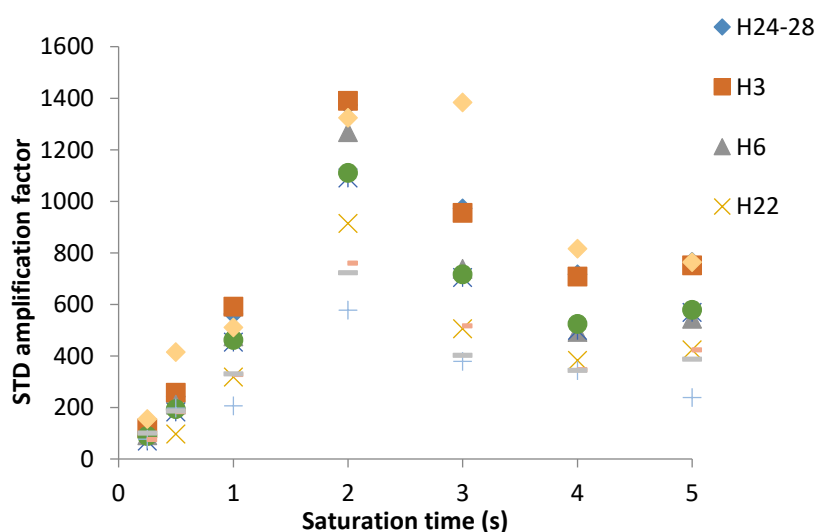


**Figure 59** - STD-AF values of selected protons of donepezil as a function of saturation time for a 200-fold ligand excess.

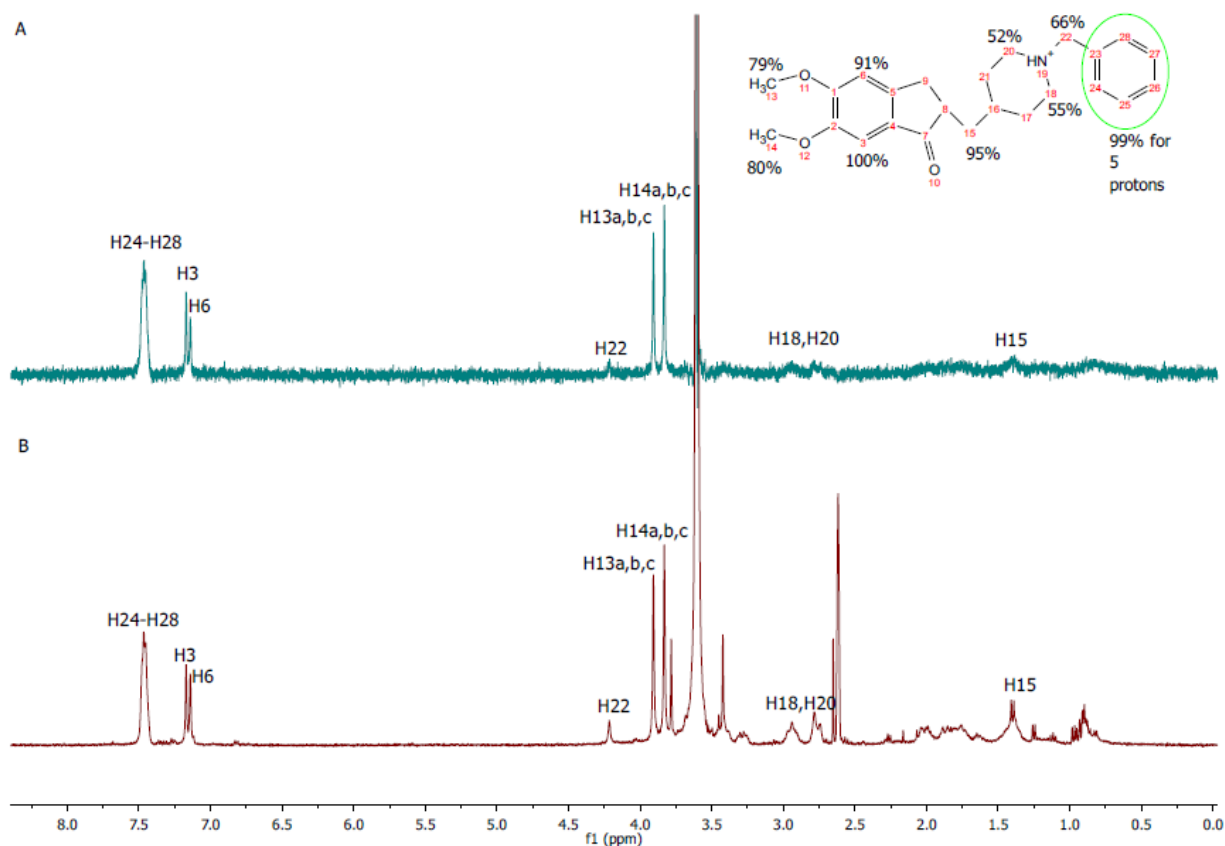


**Figure 60** - STD-NMR of donepezil with *eeAChE*, performed at 400 MHz, 15 °C, and 3 s saturation time. (A) STD of donepezil (0.8 mM) with *eeAChE* enzyme (4  $\mu$ M) and binding epitope of donepezil from STD NMR experiment. The numerical values designate the fraction of saturation as percentage, between the ligand protons and the protein active site, based on the maximum ligand STD signal (H3; 100%). Percentage saturation (75–100%) signifies strong interatomic contacts to the *eqBuChE* active site.; (B) Reference of donepezil (0.8 mM) with *eeAChE* enzyme (4  $\mu$ M).

The phenyl showed excellent interaction with an STD signal of 99% for 5 hydrogens (Fig. 60), probably due to a  $\pi$ - $\pi$  interaction with Trp86 near the bottom of the gorge. It occupies the binding site for quaternary ligands [40, 245], which was also modeled for the quaternary group of the natural substrate, ACh [42, 246]. There is kinetic evidence showing that donepezil binds to the free and the acylated forms of AChE [247] demonstrating that donepezil does not interact with the catalytic triad [243]. In the constricted region, halfway up the gorge, the charged nitrogen of the piperidine ring makes a cation- $\pi$  interaction with the phenyl ring of Tyr 330 [248]. The methylene hydrogens of the piperidine showed an enhancement of 95%, and the methylene hydrogens adjacent to the piperidine nitrogen showed enhancements of 55% and 52% respectively, most probably due to CH/ $\pi$  interactions with aromatic groups that would include the imidazole unit of H447. The same goes for the benzyl methylene hydrogens that showed an enhancement in

the order of 66% again due to possible CH/ $\pi$  interactions with the H447 imidazole unit. As already mentioned, the indole ring of Trp 86 is the binding site for the quaternary nitrogen of ACh, which suggest that Tyr 330 may serve as an additional quaternary binding site, midway down the gorge, between the peripheral site and the anionic subsite of the active site [243].

At the top of the gorge the indanone ring stacks against the indole ring of Trp 285, with enhancement in the signals of the aromatic hydrogens (100% and 91%, respectively) that is possibly due to  $\pi$ - $\pi$  interactions [211]. Both the methoxy hydrogens of the dimethoxyindanone moiety also show significant interaction with enhancements of 79% and 80%, respectively. This is probably due to CH/ $\pi$  interactions [249] with the tryptophan residue Trp 285. The enhancement in the signal for the dimethoxyindanone methane hydrogen of 42% is most probably due to van der Waals contacts with the aromatic rings of Phe 331 and Phe 290. Curiously, a homolog of donepezil, which lacks this carbonyl, was reported to be inactive [250]. It's suggested that the van der Waals contacts made by the carbonyl function help orient the indanone moiety to make a favorable interaction with the indole ring of Trp285. In the homolog which lacks this carbonyl function, the indanone moiety would be less constrained and would consequently make a poorer interaction with Trp 285 [243].

From the STD results (Fig. 60), it can be seen that overall the 3-main regions interact with the enzyme active site, corroborating the evidence obtained from both X-ray crystallography and molecular docking [211, 243], which essentially indicates what is happening in the liquid state.

#### 4.3.1.2. STD-NMR of AChE-Galantamine bromide

To precisely map ligand epitopes in close contact with the protein, STD build up curves were acquired by collecting spectra at different saturation times [232, 233, 236, 244]. The observed STD amplification (ASTD) is not the same for all the hydrogen molecules in galantamine (Figs. 61). This is due to the fact that not all the proton signals in the STD-NMR spectrum received the same amount of saturation [232, 233].

Galantamine is a selective AChE inhibitor containing an azepane ring, and is known to form a tight complex with *Tc*AChE [251-253]. In the galantamine-*Tc*AChE case, the amino acids residues that are within close proximity (i.e. defined as less than 5 Å) were Glu199, Phe330, Trp84, His440, Phe288, Phe290, Tyr121, Phe331, Gly119, Ser200, Gly118, and Gly117 [251-253]. It binds principally with Trp84 (but not via the amine nitrogen N-10 [253]) in the anionic binding site and

Phe288 and Phe290 of the peripheral anionic site (PAS) at the entrance to the gorge. The crystal structure of galantamine-*RhAChE* was also determined and the binding was deemed to be similar to that of galantamine-*TcAChE* [253]. However, an additional hydrogen bond was formed between the galantamine N-10 and Tyr337, which was in a different orientation than the corresponding Phe330 of *TcAChE* [254].

An STD-NMR study of the complex formed between *eeAChE* and galantamine was conducted (Fig. 62). It showed important interactions between the aromatic ring protons (H6, 100% and H5 68%) and the enzyme, with the stronger interaction coming from H6. On comparing this with the report by Greenblatt *et al.* [252], this was presumably a  $\pi$ - $\pi$  interaction with most likely Phe295 or Phe297 of *eeAChE* (in the report by Greenblatt *et al.* [252] a proximity of these protons with the Phe331 residue was observed). The methoxy group and the methyl group attached to N10 also showed significant interaction (62% and 51%, respectively). In the case of the methoxy group this was probably due to H-bonding with His447 (in the study by Greenblatt *et al.* [252] there was a close approximation of His440 with the MeO group). The significant values of 37% and 30% observed for H-14 and H-8, could probably be due to a  $\pi$ - $\pi$  and CH/ $\pi$  interaction [249] with Trp86. As in the X-ray crystal structure the Trp84 indole was observed very close to this region of the molecule [252].

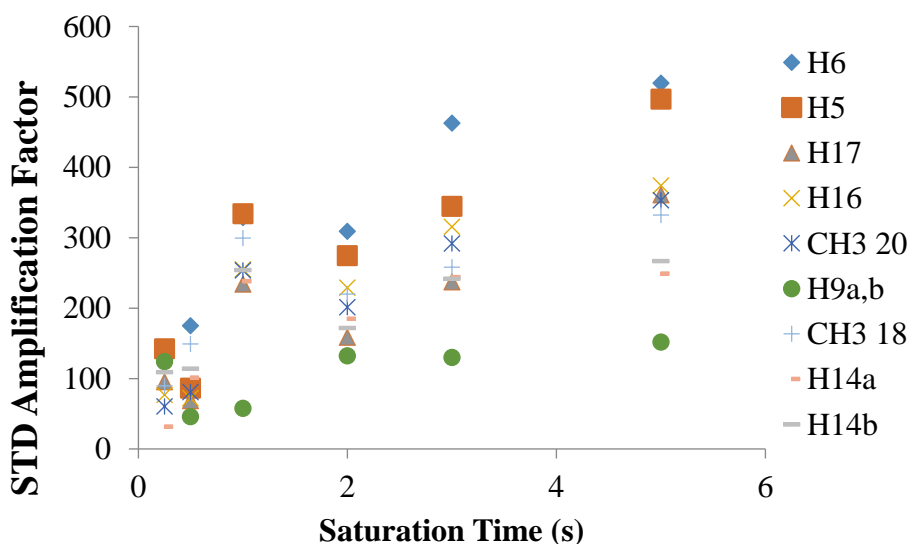


**Figure 61** - STD-AF values of selected protons of galantamine as a function of saturation time. The sample contained 0.8 mM of ligand and 4  $\mu$ M of *eeAChE*.

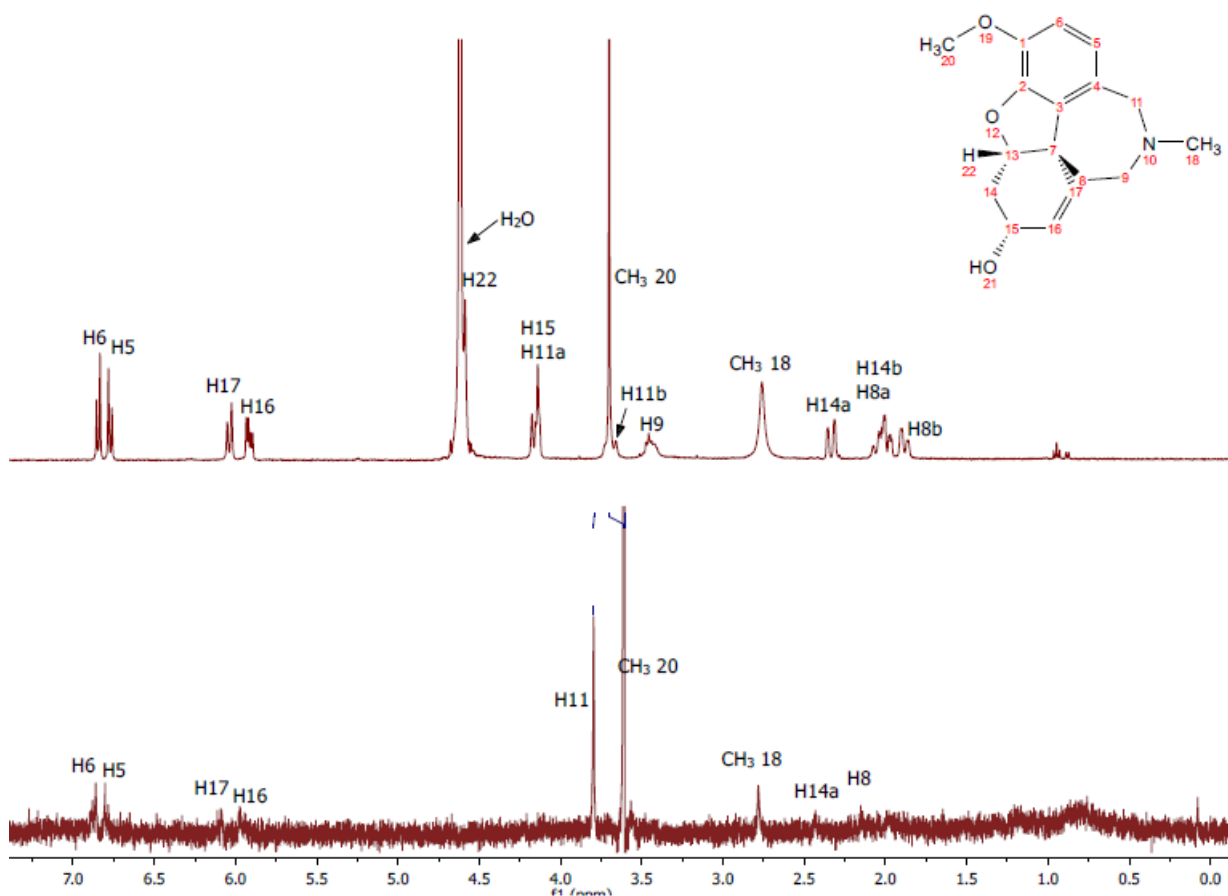


**Figure 62** - STD-NMR of galantamine with *eeAChE*: (A) reference  $^1\text{H}$  spectrum of galantamine with *eeAChE* and (B) STD spectrum of the solution of galantamine (0.8 mM) with *eeAChE* (4  $\mu\text{M}$ ) (3s of saturation time). The relative degree of saturation of the individual hydrogens are mapped into the structure and normalized to that of hydrogen H6. Percentage saturation (75–100%) signifies strong interatomic contacts to the *eeAChE* active site.

#### 4.3.1.3. STD-NMR of BuChE-Rivastigmine tartrate

A key STD-NMR experiment to map the ligand-protein interaction of rivastigmine (as its tartrate salt) with *EqBuChE* was performed. To precisely map ligand epitopes in close contact with the protein, STD build up curves were acquired by obtaining spectra at different saturation times [232, 233, 236, 244]. The observed STD amplification (ASTD) is not the same for all the hydrogens in rivastigmine (Fig. 63). This is due to the fact that not all the proton signals in the STD-NMR spectrum received the same amount of saturation [232, 233]. Thus, the distribution of saturation transferred among the different compound protons indicates spatial proximities between the protons of the compound molecule and the enzyme in the bound state [234]. As stated above, to quantitatively express the relative STD effects at a given saturation time, all of the STD signals are normalized against the most intense signal, which is arbitrarily assumed to be 100% [234]. It

can be concluded that protons with relative STD values close to 100% belong to parts of the ligand that are very intimately recognized by the receptor binding-pocket, and hence must be regarded as significant for the interaction.

In the case of rivastigmine the aromatic group of the NAP unit showed high STD enhancement in agreement with both X-ray crystallography and with docking study [255] which was most likely to be due to both  $\pi$ - $\pi$  and CH/ $\pi$  interactions with the tryptophan residue in the choline binding pocket and the hydrophobic residues in the PAS. The CH/ $\pi$  interactions are a form of weak hydrogen bond, that can be described as a non covalent interaction between CH groups (proton donor) and  $\pi$  electron density of the aromatic ring (proton acceptor). In addition, both the benzylic methyl group (93%) and the *N*-methyl groups (38% each) of the NAP unit showed significant enhancements supporting again CH/ $\pi$  interactions with hydrophobic residues in the PAS. The *N*-ethyl group of the carbamate unit showed an intensification of almost 49%, most probably due to approximation to Tyr120. As a final note, the tartrate moiety of the rivastigmine also showed some significant enhancement at the H-19 and H-21 (74% and 68%, respectively, Fig. 64). However, it is unknown whether this plays a role in the rivastigmine-enzyme binding.

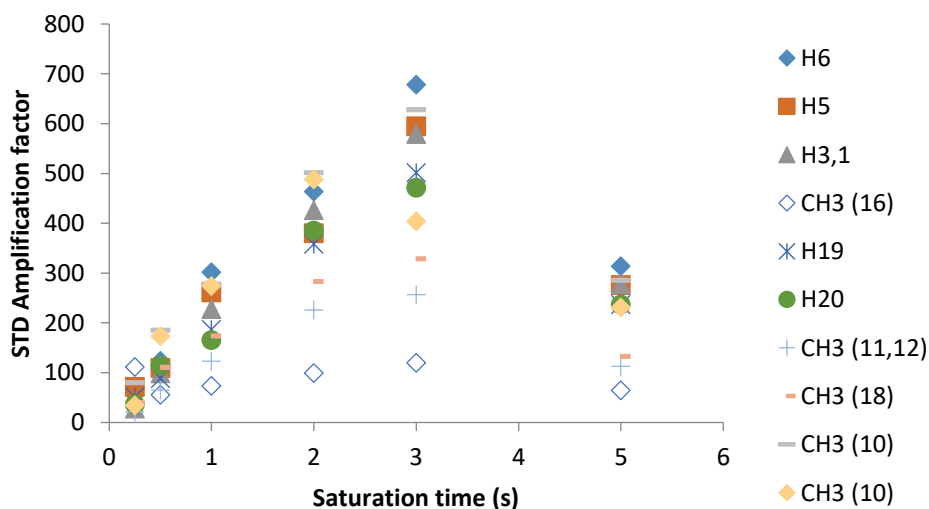


**Figure 63** - STD-AF values of selected protons of rivastigmine as a function of saturation time for a 200-fold ligand excess.

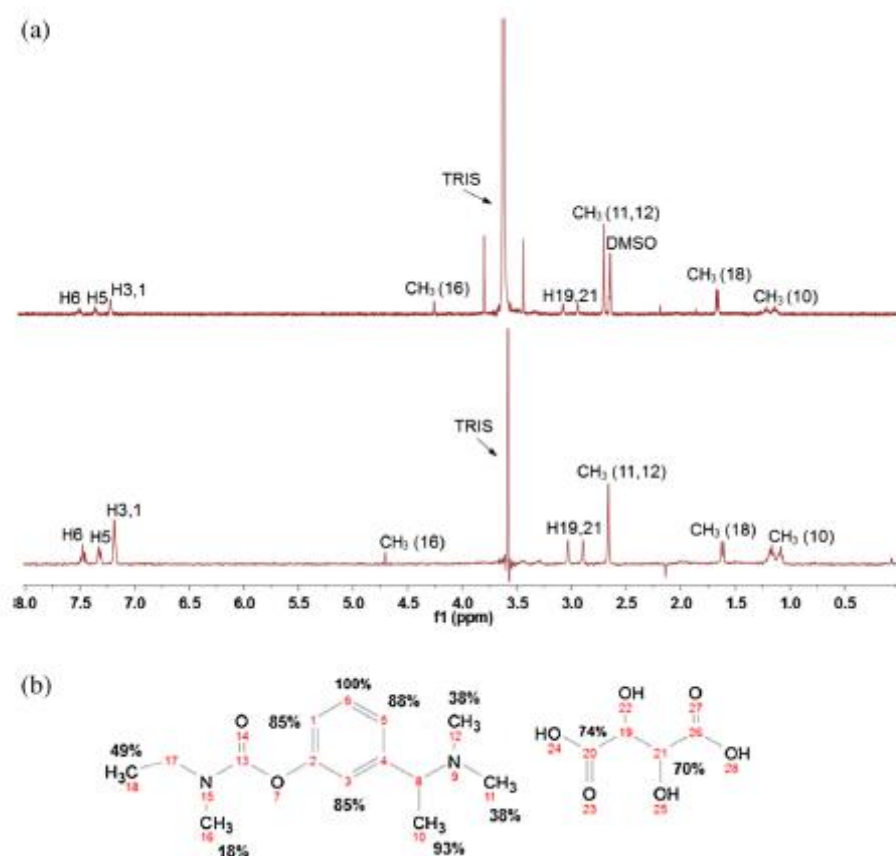


**Figure 64** - STD-NMR of rivastigmine with *EqBuChE*, performed at 400 MHz, 15 °C, and 3 s saturation time. (a) Reference (top) and STD (bottom) of the rivastigmine (0.8 mM) with *EqBuChE* enzyme (4 μM). (b) Binding epitope of rivastigmine from STD NMR experiment. The numerical values designate the fraction of saturation as percentage, between the ligand protons and the protein active site, based on the maximum ligand STD signal (H6; 100%). Percentage saturation (75–100%) signifies strong interatomic contacts to the *EqBuChE* active site.

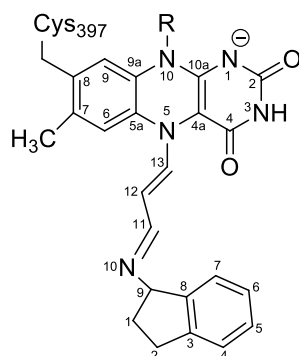
#### 4.3.1.4. STD-NMR MAO-B-Rasagiline mesylate

Rasagiline (*N*-propargyl-1(*R*)-aminoindan) is currently used for PD treatment. It's a selective inhibitor for MAO-B [256] and has been shown to have neuroprotective properties [256, 257].

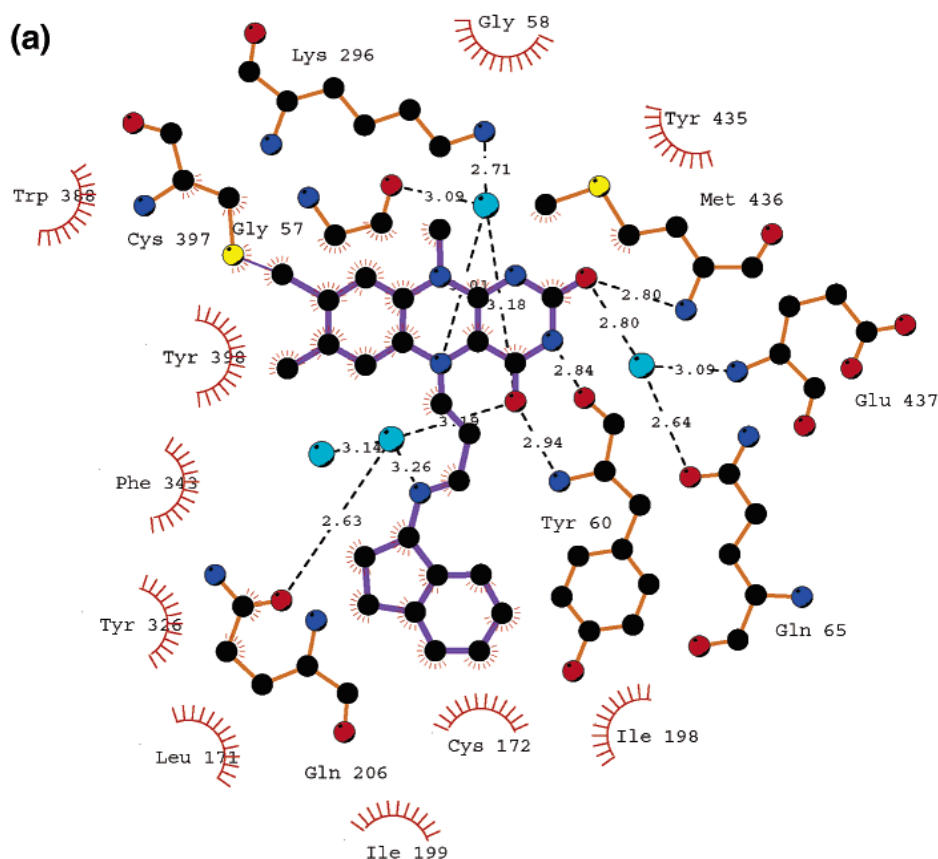
We performed a key STD-NMR experiment to map the key ligand-protein interactions of rasagiline with MAO-B. The binding epitope of rasagiline was calculated as previously described (2.3.3.1.).

The STD-NMR results obtained were actually very different from what it was expected, since rasagiline is an irreversible inhibitor of MAO-B. It binds covalently to N5 of the flavin moiety (Fig. 65) [258] – which is located between two tyrosine residues (Tyr 398 and Tyr 435) – and are found in a conformation approximately perpendicular to the *re* face of the flavin ring (Fig. 66).

The adjacent Cys 397 residue forms a covalent thioether linkage to the 8 $\alpha$  position of the flavin ring [259]. The indan group is oriented perpendicular to the FAD unit so that its projection onto the flavin plane falls into the flavin central pyrazine ring (Fig. 66) [94].



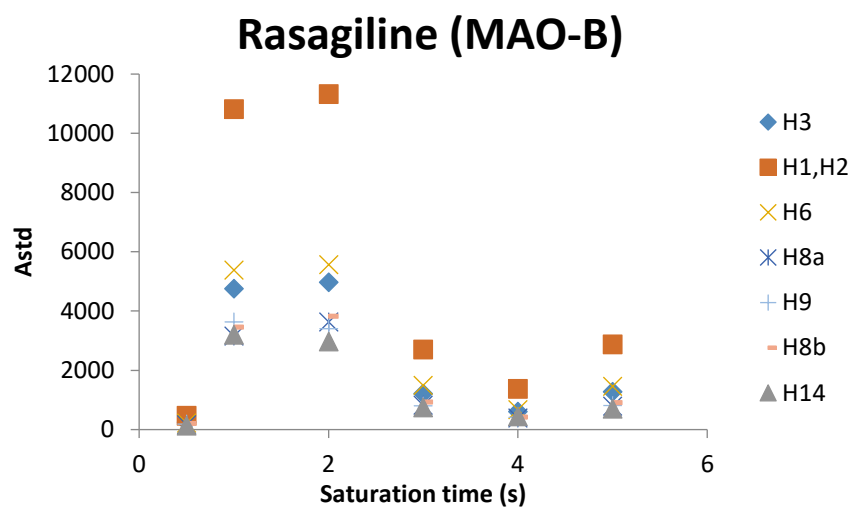
**Figure 65** – Chemical formula of the covalent adduct formed between rasagiline and FAD. The atomic numberings of the flavin and the covalently bound rasagiline are shown. Adapted from [258].



**Figure 66** - Ligplot schematic drawings showing the interactions of Rasagiline with MAO-B. Carbon atoms are in black, oxygen atoms are in red, nitrogen atoms are in blue, and sulfur atoms are in yellow. Water molecules are shown as cyan spheres. Dashed lines indicate all potential H bonds. “Radiating” spheres indicate hydrophobic contacts between carbon atoms of the inhibitor and the neighboring residues. Adapted from [94].

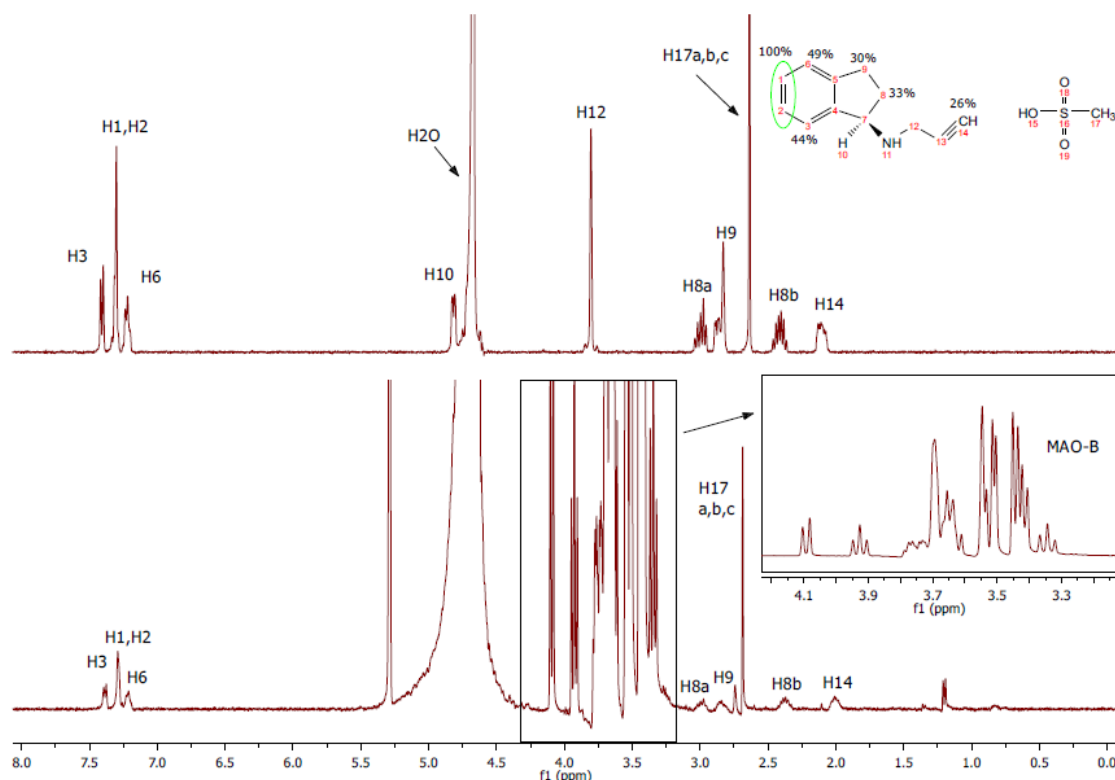


Figure 67 show the STD amplification factor ( $A_{STD}$ ), derived from the buildup saturation spectra, allowing the assignment of the epitope map.



**Figure 67** - STD-AF values of selected protons of rasagiline as a function of saturation time.

The aromatic ring presented the best interaction, with both H1 and H2 showing 100% attenuation respectively (see Fig. 68), whilst both H3 and H6 showed attenuations of 44% and 49%, respectively, possible due to  $\pi$ - $\pi$  interaction with Tyr 326 in both cases. The hydrogens of the indan ring showed attenuations of 30% and 33%, respectively, and we attribute this again to  $\pi$ - $\pi$  interactions with the aromatic residues of the catalytic site. H14 showed a lower attenuation of 24% (Fig. 68). The fact that it was possible to obtain any results in this experiment could be explained by the lack of covalent bonding between C13 and N5 of the FAD unit, as it was expected. The reasons for this could be due to the pH of the solution, or the temperature used in the experiment (25 °C).



**Figure 68** - STD-NMR of rasagiline with MAO-B, performed at 400 MHz, 15 °C, and 3 s saturation time. (A) reference  $^1\text{H}$  spectrum of rasagiline with MAO-B and (B) STD spectrum of the solution of rasagiline (5 mM) with MAO-B (5  $\mu\text{M}$ ) (3s of saturation time). The relative degree of saturation of the individual hydrogens are mapped into the structure and normalized to that of hydrogens H1 and H2. (a) Reference (top) and STD (bottom) of the rivastigmine (0.8 mM) with *Eq*BuChE enzyme (4  $\mu\text{M}$ ). (b) Binding epitope of rivastigmine from STD NMR experiment. The numerical values designate the fraction of saturation as percentage, between the ligand protons and the protein active site, based on the maximum ligand STD signal (H1,H2; 100%). Percentage saturation (75–100%) signifies strong interatomic contacts to the *Eq*BuChE active site.

#### 4.3.1.5. STD - NMR study of the interaction of AChE with 4-methoxy-3,4-dihydroisoquinolin-1(2H)-one (6) and 4-methoxy-3,4-dihydroisoquinolin-1(2H)-one (6) with BuChE

To precisely map ligand epitopes in close contact with the protein, STD build up curves were acquired by collecting spectra at different saturation times.[260-263] The observed STD amplification ( $A_{\text{STD}}$ ) is not the same for all the hydrogen atoms in compound **6** (Figs. 69, 70,  $S_5$  and  $S_6$ ), as well as for Galantamine and Rivastigmine [264]. This is due to the fact that not all the proton signals in the STD-NMR spectrum received the same amount of saturation [260, 261]. Thus, the distribution of saturation transferred among the different compound protons indicates spatial proximities between the protons of the compound molecule and the enzyme in the bound

state [265]. Qualitatively, it can be assumed that a stronger intensity of a compound signal in the STD-NMR spectrum indicates closer inter-hydrogen distances between the compound proton and the receptor surface in the bound state [261]. To quantitatively express the relative STD effects at a given saturation time, all of the STD signals are normalized against the most intense signal, which is arbitrarily assumed to be 100% [265].

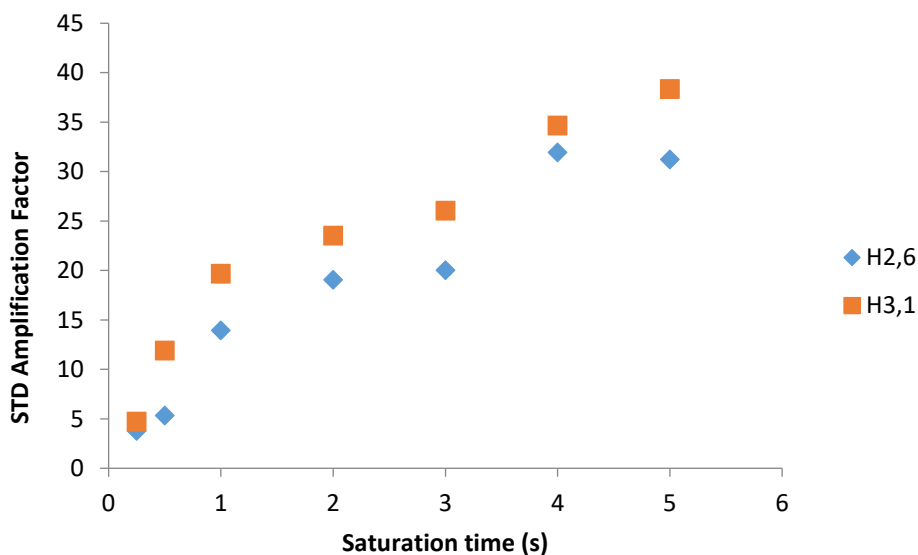


Figure 69 - STD amplification factor of compound 6 interaction with AChE as a function of saturation time.

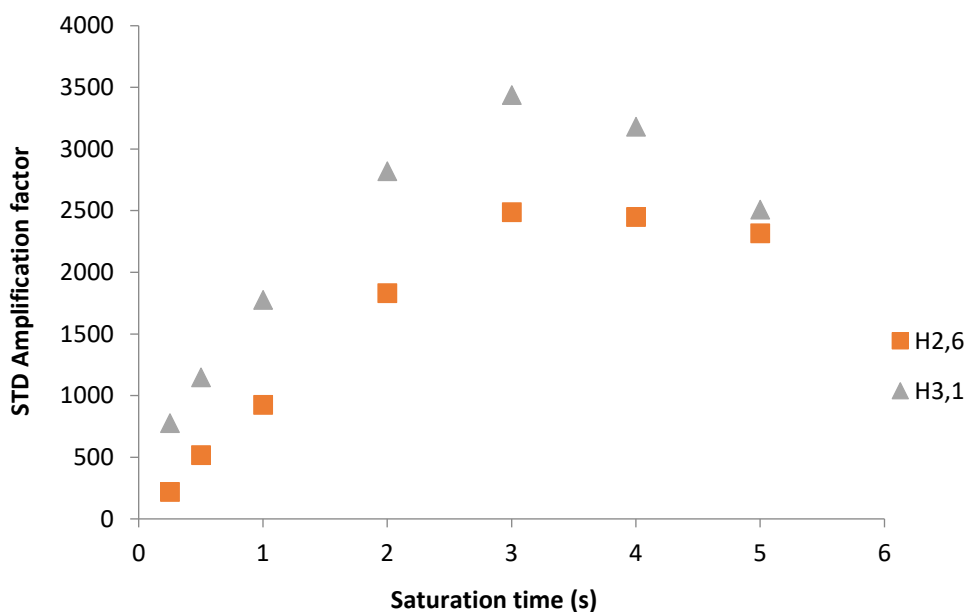


Figure 70 - STD amplification factor of compound 6 with BuChE as a function of saturation time.

It can be concluded that protons with relative STD values close to 100% belong to parts of the compound that are very intimately recognized by the receptor binding-pocket, and hence must be regarded as important for the interaction.

In the case of compound **6**, it was inferred that the hydrogen atoms namely, H1 and H3 were directly involved in the binding to the AChE and BuChE active sites (Fig. 71B and C). According to this qualitative analysis, the aromatic hydrogens (Fig. 71B and C) and the hydrogens from the methoxy group (Fig. 71C), were observed to be strongly involved in the binding. In contrast, the hydrogens H7, H8a, H8b and H11 showed a relatively lower STD value, indicating that they were probably more distant from the active site residues for both enzymes [251].

It wasn't possible to localize the NH peak in the  $^1\text{H}$  NMR spectrum, which made it impossible to confirm if there was an interaction of the NH proton with the enzyme.

These results were in agreement with the molecular docking reported by Bacalhau et al. [210]. Even though in the case of the docking study a single enantiomer was used, in the STD-NMR <sup>4</sup> compound **6** was used in racemic form.

---

<sup>4</sup> Due to purification issues it was not possible to isolate these derivatives in pure form.

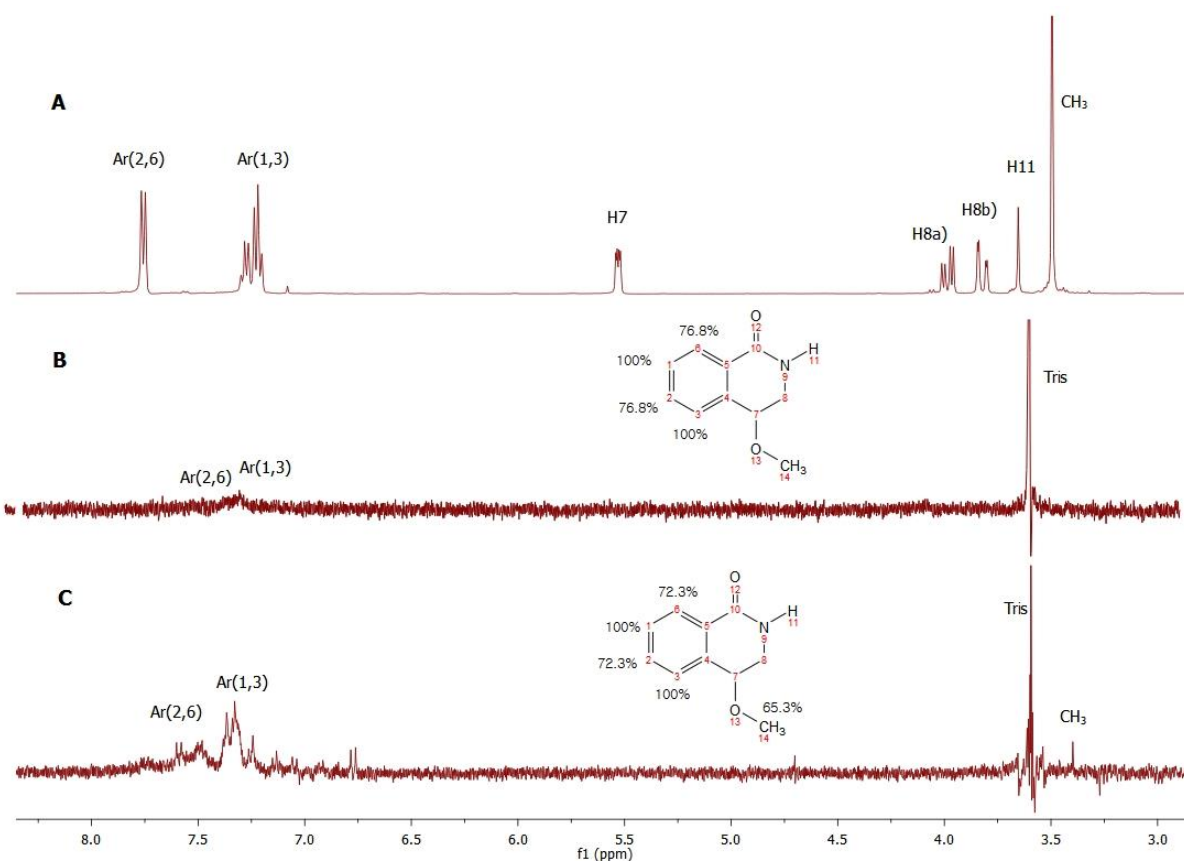


**Figure 71** - STD-NMR of 4-methoxy-3,4-dihydroisoquinolin-1(2H)-one (**6**) with both AChE and BuChE, performed at 400 MHz, 15°C, and 3 s saturation time. (A) reference spectrum, (B) STD spectrum of compound **6** (0.8 mM) with AChE enzyme (4 μM) and (C) STD spectrum of compound **6** (0.8 mM) with BuChE enzyme (4 μM). Binding epitope of **6** from the STD NMR experiment. The numerical values designate the fraction of saturation as a percentage, between the ligand protons and the protein active site, based on the maximum ligand STD signal (H1,3 of Ar; 100%).

With regards to AChE and according to the molecular modelling study that was performed by our group [210], compound **6** showed H-bonding with the oxyanion pocket residues Gly121 and Gly122. Furthermore, the carbonyl oxygen formed a H-bond with Ser203 while the hydroxyl group formed a H-bond with Tyr124. Interesting, a  $\pi$ - $\pi$  stacking interaction formed between the aromatic ring of **6** and the Trp86 of the catalytic site stabilized the interactions between the ligand-protein complex (Fig. 72).

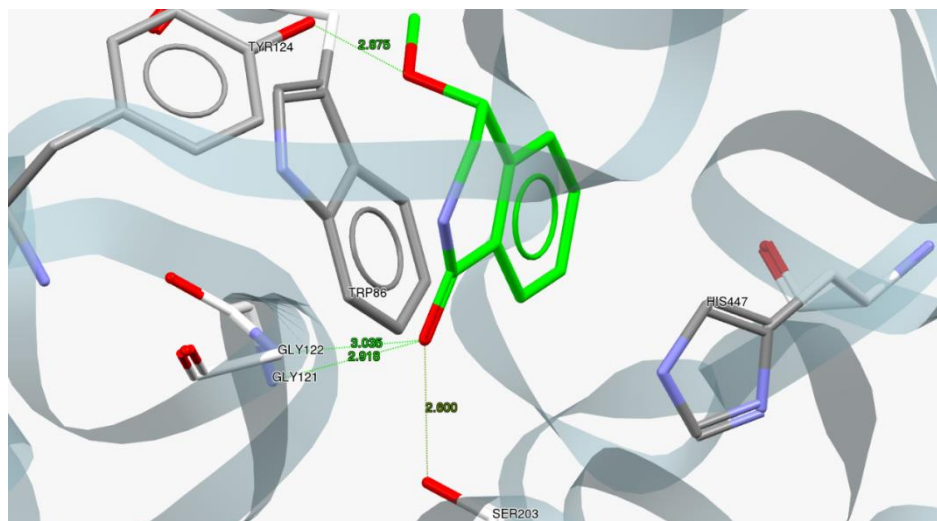


**Figure 72** - Binding mode of compound **6** obtained by docking with *hAChE*. Hydrogen bonds are shown as green dotted lines, formed between the ligand **6** (green color) with the residues in the active site (grey color). Water molecules in the active site are represented as red spheres. Adapted from [210].

In the case of BuChE, and based on molecular docking studies performed by our group, the amide nitrogen of compound **6** is predicted to interact with Ser79 and Asp70, mediated by a water molecule, whereas, Thr120 formed another H-bond interaction with another water molecule. In addition, the hydroxyl group O3 of Tyr332 formed two H-bonds, one with the amide nitrogen and other with carbonyl O2 of compound **6** (Fig. 73).

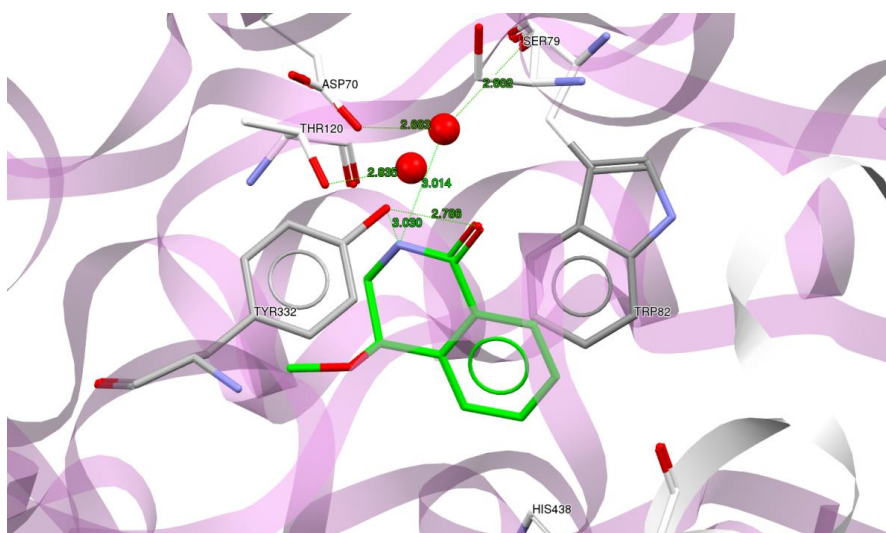


**Figure 73** - Binding mode of compound **6** obtained by docking with *hBuChE*. Hydrogen bonds are shown as green dotted lines, formed between the ligand **6** (green color) with the residues in the active site (grey color). Water molecules in the active site are represented as red spheres. Adapted from [210].

#### 4.3.1.6. STD-NMR study of the BuChE-1-benzyl-3-hydroxy-3-phenylindolin-2-one (**17**) interaction

Some good interactions between compound **17** and the protein (Fig. 74 and S<sub>7</sub>) were observed, as indicated by several significant STD-enhancements.

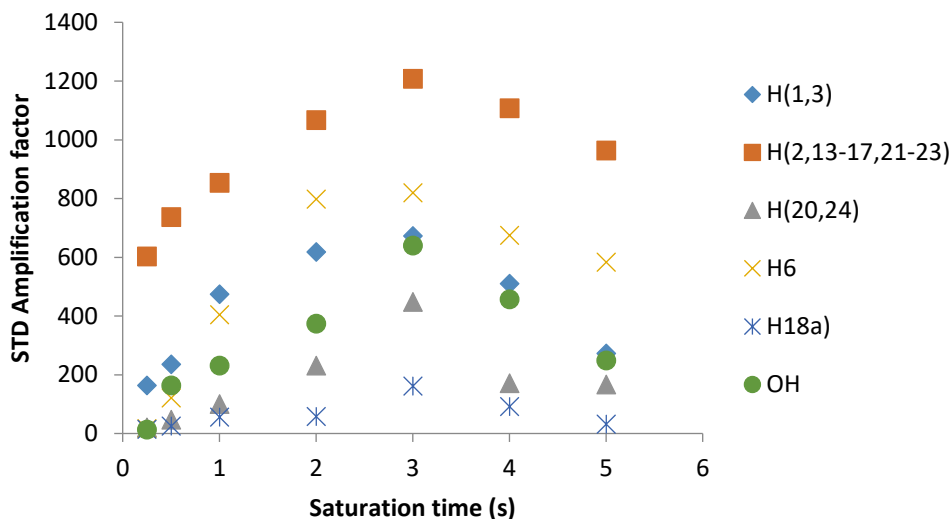


**Figure 74** - STD amplification factor of selected protons of compound **17** as a function of saturation time.

H6 showed the higher interaction with the protein (100%), followed by H1 and H3 (Fig. 75). The interactions of Ar1 are probably due to  $\pi$ - $\pi$  stacking with Phe329. Ar2 presented 125% attenuation, which could be related with  $\pi$ - $\pi$  stacking with Tyr332 and the 90% interaction of Ar3 with the protein was probably due to  $\pi$ - $\pi$  stacking with Trp82. With regards to H12, the 78% interaction could be assigned to the H-bond network made with Ser79 and Asp70 through a probable water molecule mediator (Fig. 76) [211].

Figure 76 shows that the benzyl group of Ar3 flipped into the bottom of the gorge to maximize its hydrophobic  $\pi$ - $\pi$  stacking interaction with Trp82.

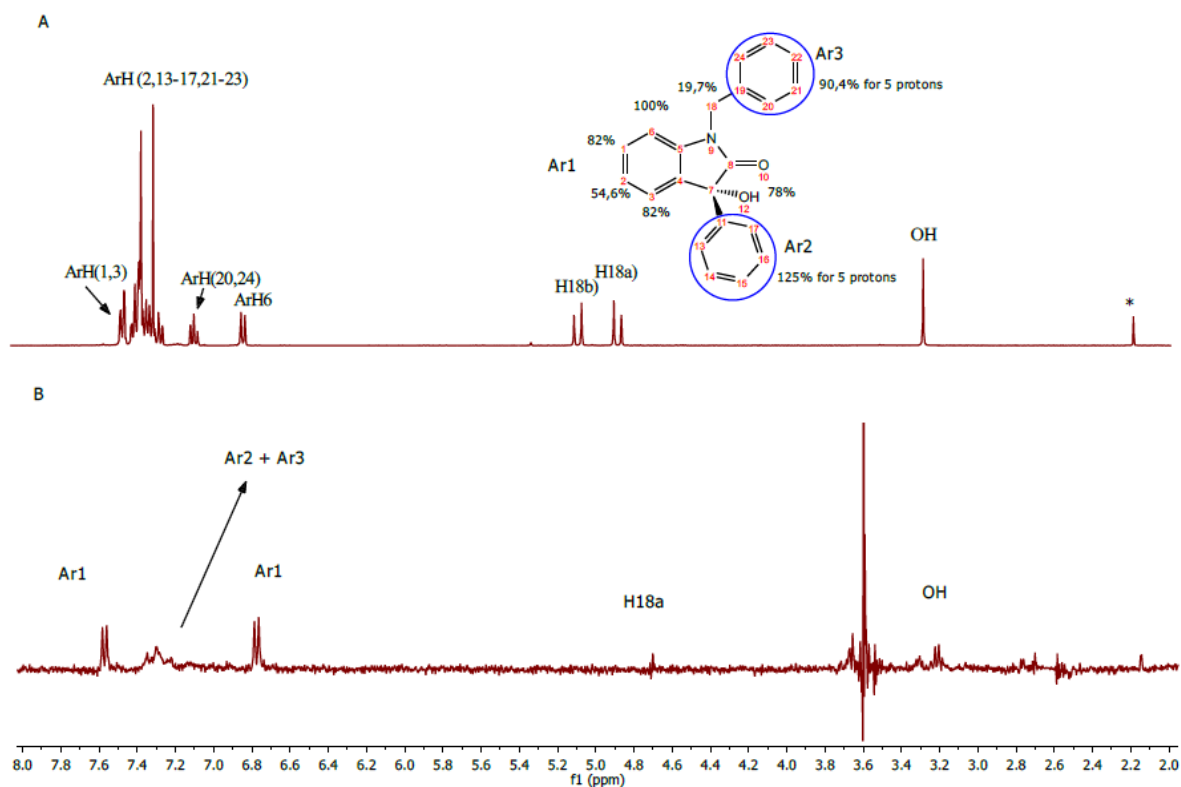


**Figure 75** - STD-NMR of 1-benzyl-3-hydroxy-3-phenylindolin-2-one (17) with BuChE: (A) reference  $^1\text{H}$  spectrum of 17 with BuChE and (B) STD spectrum of the solution of 17 (5 mM) with BuChE (5  $\mu\text{M}$ ) (3s of saturation time). The relative degree of saturation of the individual hydrogens are mapped into the structure and normalized to that of hydrogen H6.

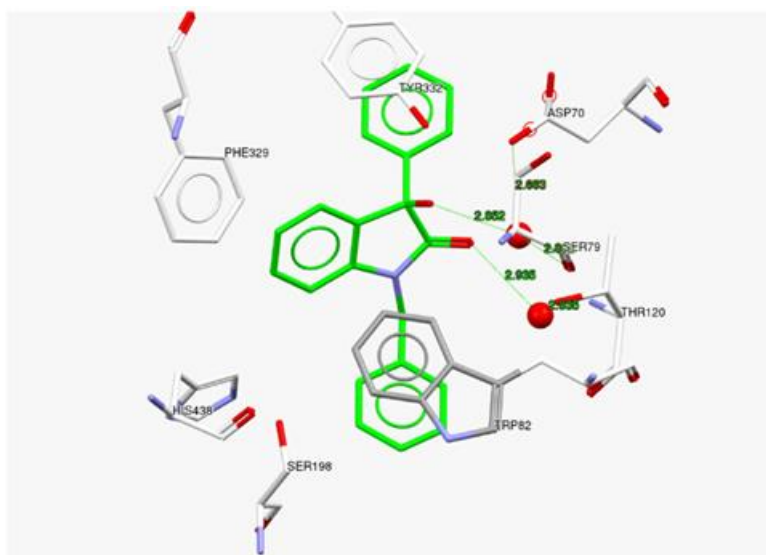


**Figure 76** - Binding mode for compound 17 interaction with hBuChE. Hydrogen bonds are shown as green dotted lines, formed between compound 17 (green color) with the residues in the active site (grey color). Water molecules in the active site are represented as red spheres. Adapted from [211].



Figures 77 and 78 show a molecular docking study of the two enantiomers of compound **17** (**17a** and **17b**) with *h*BuChE. Compound **17a** establishes an H-bond with His 438. The phenyl ring of Ar2 presents a  $\pi$ - $\pi$  stacking with Trp82 and Ar1 shows a  $\pi$ - $\pi$  stacking interaction with Tyr332 (compound **17b**).

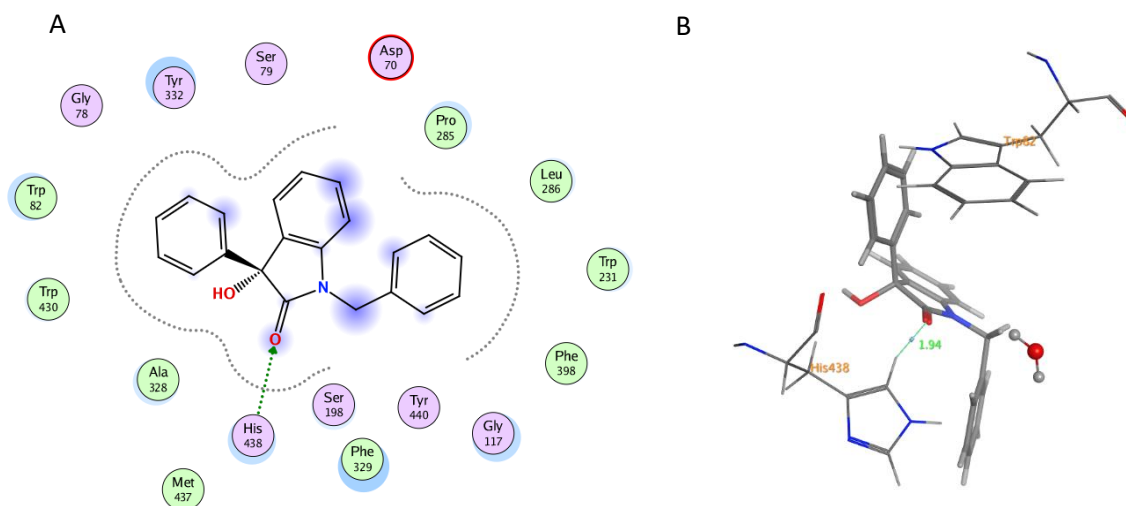


**Figure 77** - (A) Interaction diagram of compound **17a** with *h*BuChE (PDB file 4TPK); (B) Binding mode for compound **17a** with *h*BuChE (PDB file 4TPK).

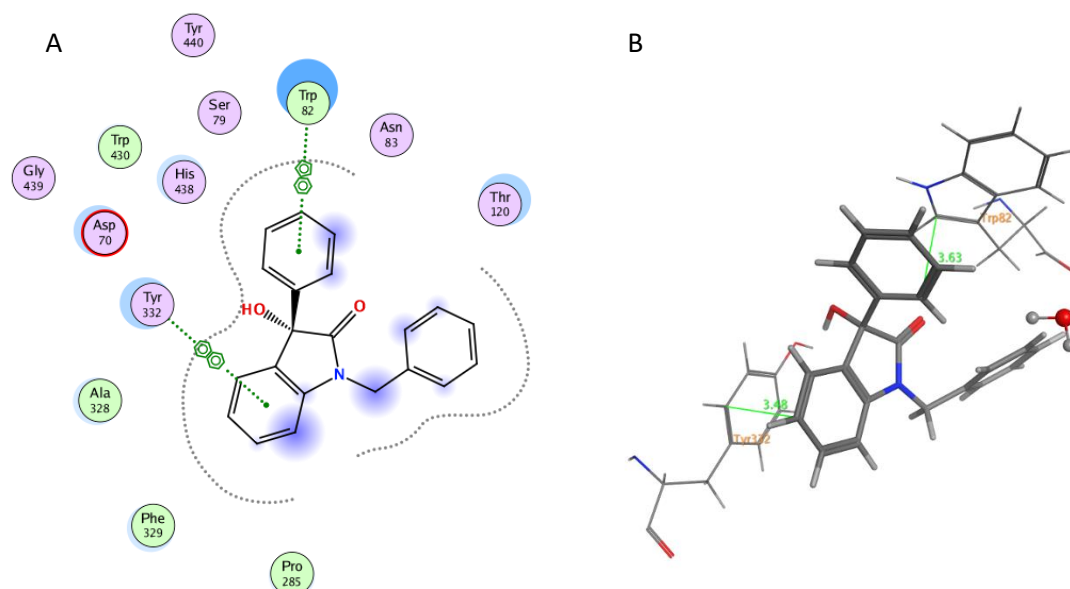


**Figure 78** - (A) Interaction diagram of compound **17b** with *h*BuChE (PDB file 4TPK); (B) Binding mode for compound **17b** with *h*BuChE (PDB file 4TPK).

The STD-NMR interaction of compound **17** (racemate) with AChE wasn't studied due to the poor  $IC_{50}$  results (when compared to BuChE). None the less, a previous molecular docking study using *hAChE* showed key interactions between compound **17** and some *hAChE* active site residues (Fig. 79). This study predicted the presence of a H-bond between the hydroxyl group of compound **17** and the NH group of Trp86, including another H-bond between the carbonyl oxygen of compound **17** and the OH group of Tyr341. There were also indications of the likelihood of  $\pi$ - $\pi$  interactions between the aromatic rings (Ar2 and Ar3) of compound **17** and the Trp86 and Tyr341 residues. In the case of Phe297 (of the acyl binding pocket) there was a distinct edge-to face interaction with the benzyl phenyl group [211].

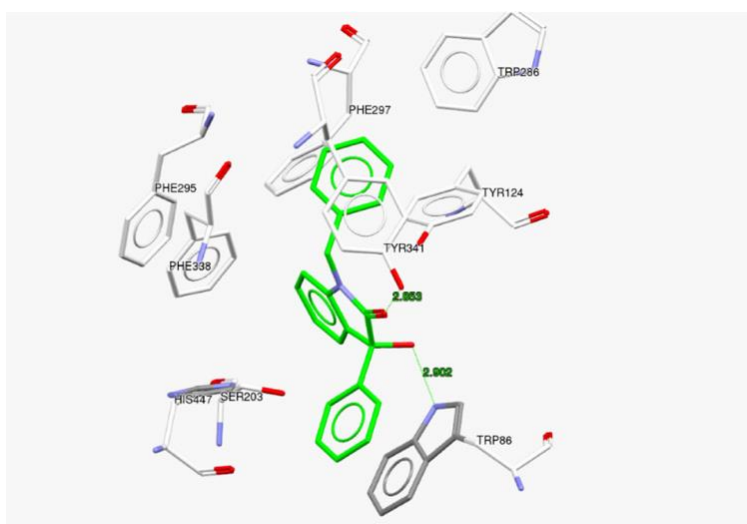


**Figure 79** - Binding mode for compound **17** interaction with *hAChE*. Hydrogen bonds are shown as green dotted lines, formed between compound **17** (green color) with the residues in the active site (grey color). Adapted from [211].

Figures 80 and 81 show a molecular docking study of the two enantiomers of compound **17** (**17a** and **17b**) with *hAChE*. Ar2 and the hydroxyl group of **17a** forms a H-bond with Asp 74. As for **17b**, the most significant interaction is a  $\pi$ - $\pi$  stacking effect between the phenyl ring of Ar1 and Tyr337. The hydroxyl group of **17b** also forms a H-bond with Asp 74.

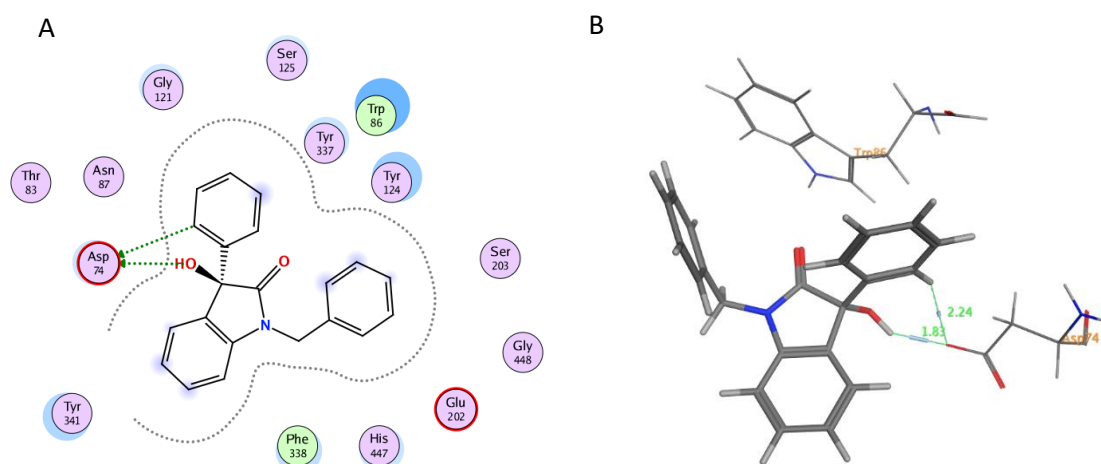


**Figure 80** - (A) Interaction diagram of compound **17a** with *hAChE* (PDB file 4EY7); (B) Binding mode for compound **17a** interaction with *hAChE* (PDB file 4EY7).

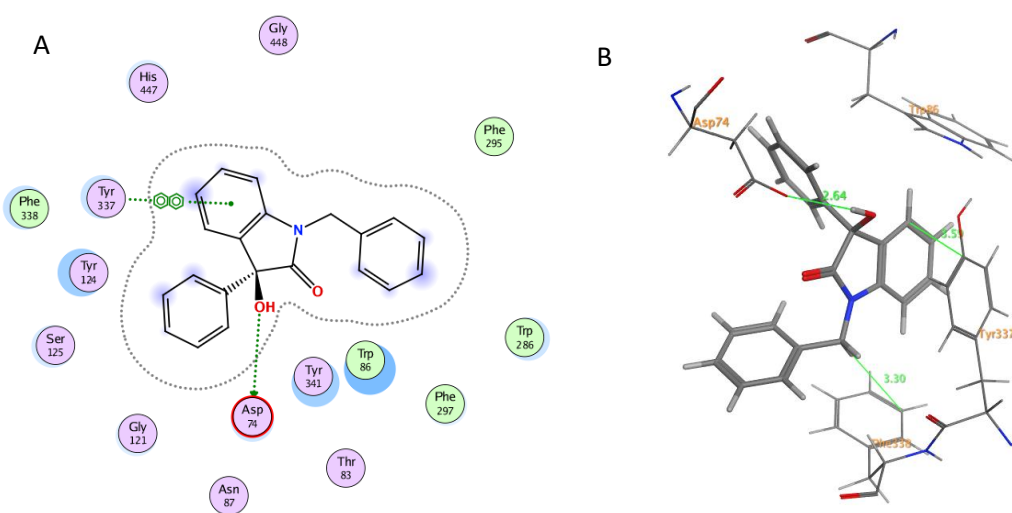


**Figure 81** – (A) Interaction diagram of compound **17b** with *hAChE* (PDB file 4EY7); (B) Binding mode for compound **17b** interaction with *hAChE* (PDB file 4EY7).

It is interesting to observe how compound **17** flipped at the N of Ar1 forcing it to position itself towards the surface peripheral site as it binds with AChE (Fig. 79), whilst it is forced down to the bottom of the gorge in the case of BuChE (Fig. 76). The benzyl group (Ar3) of compound **17** flipped into the bottom of the gorge to maximize its  $\pi$ - $\pi$  stacking interaction with Trp82 of BuChE [211]. The difference in the binding mode of compound **17** with BuChE and AChE could explain the  $IC_{50}$  values obtained with these enzymes (7.41  $\mu$ M for BuChE and 237.18  $\mu$ M for AChE).

#### 4.3.1.7. STD-NMR study of the AChE-4-((3-hydroxy-2-oxo-3-phenylindolin-1-yl)methyl)piperidin-1-ium chloride (48a) interaction and of 4-((3-hydroxy-2-oxo-3-phenylindolin-1-yl)methyl)piperidin-1-ium chloride (48a) with BuChE

Although the  $IC_{50}$  results were only significant for BuChE (18.26  $\mu$ M), the interaction with AChE was also studied (Fig. 82 and S<sub>8</sub>). Donepezil was used to validate this study (see 4.3.1.1).

H19 presented a 100% attenuation and the piperidine ring a 65% STD-attenuation, probably due to CH- $\pi$  interaction with Trp 86. The phenyl ring showed a 47%-59% attenuation, probably due to  $\pi$ - $\pi$  stacking with Tyr 341. According to this study (Fig. 83), we presume that the  $NH_2$  group forms a H-bond interaction with Glu 202, and the ethyl substituent presents an CH- $\pi$  interaction with Phe 338.

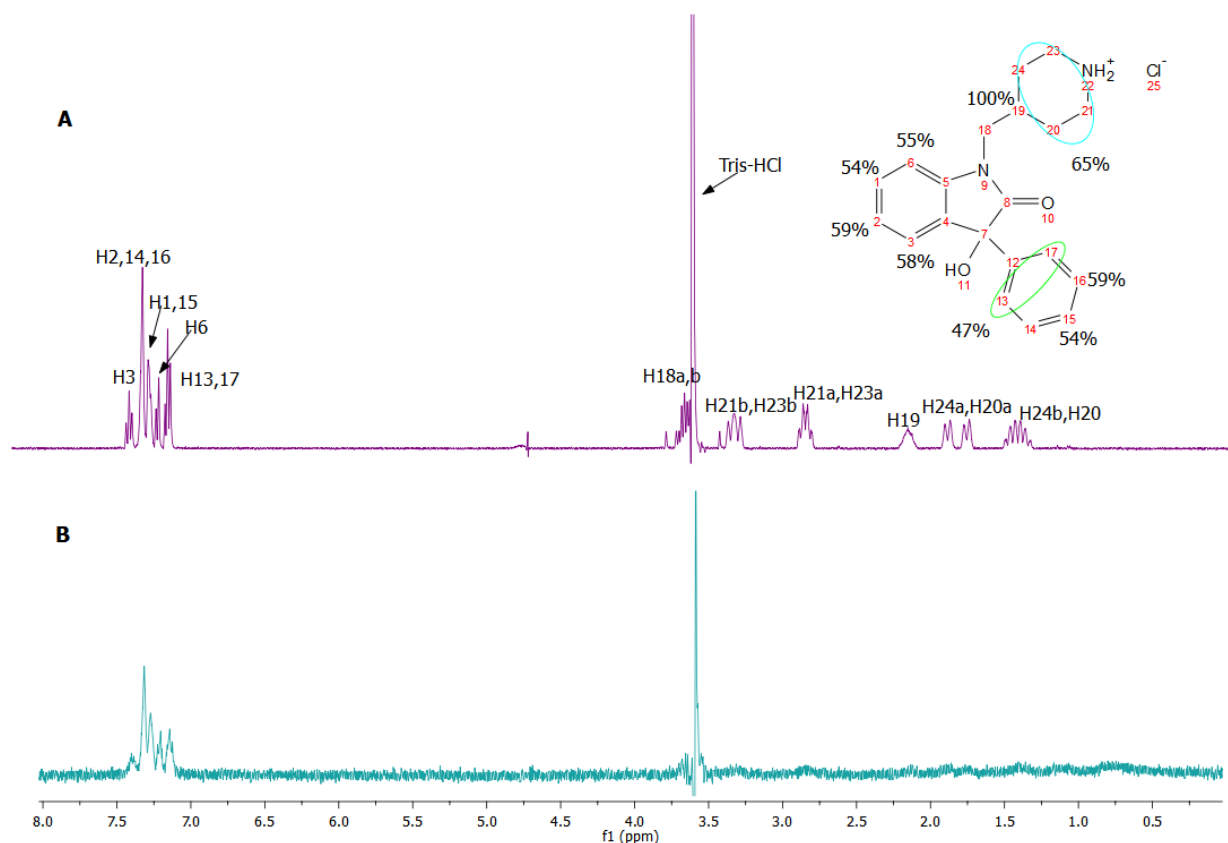


**Figure 82** - STD-NMR of **48a** with eeAChE, performed at 400 MHz, 15°C, and 3 s saturation time. (A) reference spectrum, (B) STD spectrum of compound 48a (0.8 mM) with AChE enzyme (4 $\mu$ M). Binding epitope of 48a from STD NMR experiment. The numerical values designate the fraction of saturation as a percentage, between the ligand protons and the protein active site, normalized to the maximum ligand STD signal (H19; 100%).

Although this was not observed in the STD-NMR experiment (Fig. 82), docking studies (Figs. 83(A)-83(B)) revealed that there is likely to be an CH- $\pi$  interaction between the 3-OH and Phe 338. None the less, we believe that these interactions are not sufficient to make compound **48a** a good inhibitor for AChE which was found to be the case ( $IC_{50}$  of 500.21  $\mu$ M).

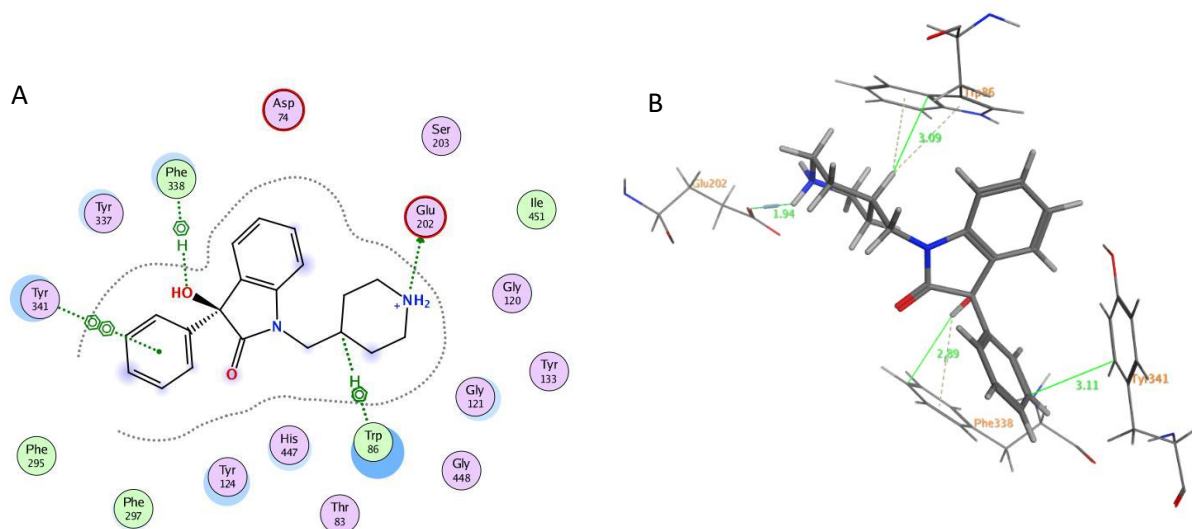


**Figure 83** – (A) Interaction diagram of compound **48a** with *h*AChE; (B) Binding mode for compound **48a** interaction with *h*AChE.

Very different results were obtained, upon conducting a similar study with BuChE. The phenyl group protons presented an STD-attenuation of 74%-100%, probably due to  $\pi$ - $\pi$  stacking with Tyr 332 and the benzyl group protons showed a 79%-100% STD-attenuation attributed to  $\pi$ - $\pi$  stacking with Trp 82 (Figs. 84-85 and S<sub>9</sub>). These interactions would appear to be more stabilizing than those calculated in the case of AChE, suggesting a better level of inhibition of this molecule with this enzyme, which was found to be the case ( $IC_{50}$  of 18.26  $\mu$ M).

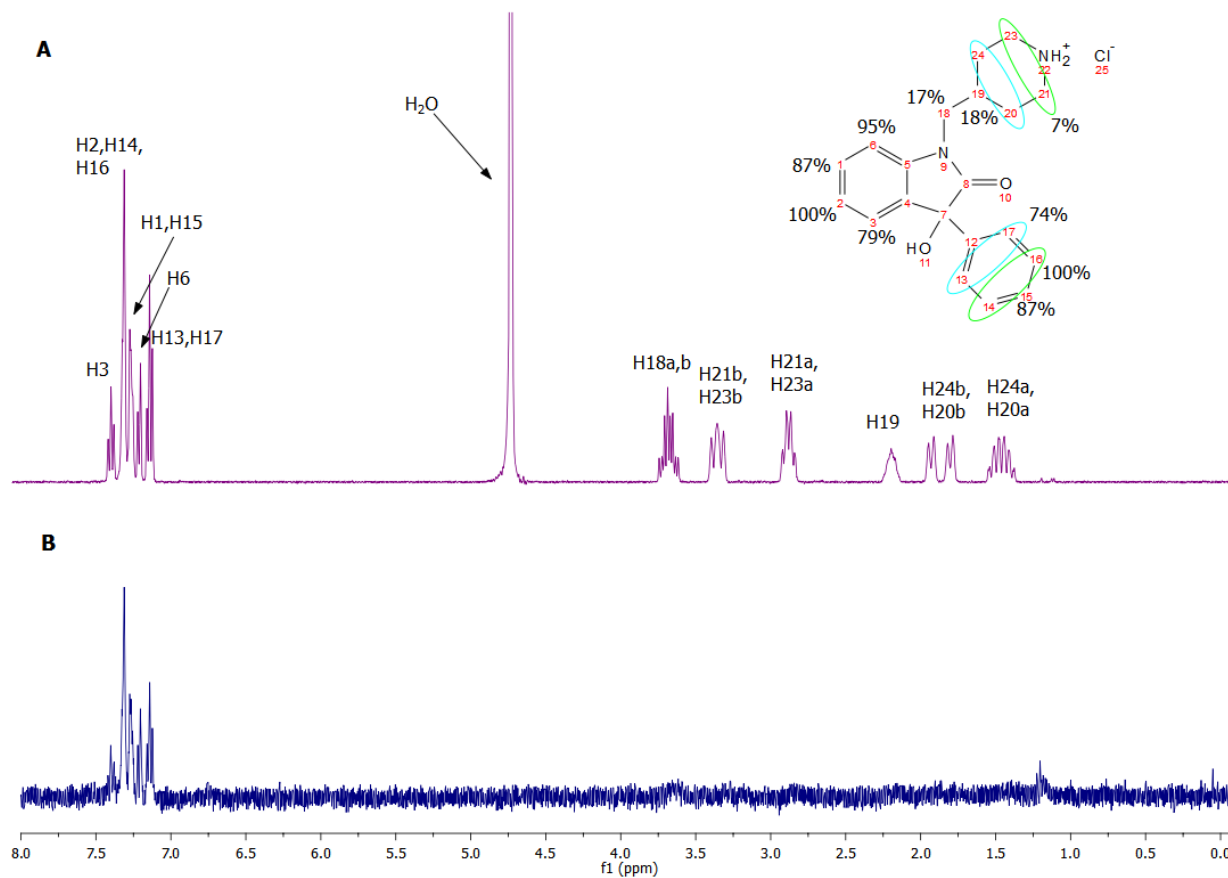


**Figure 84** - STD-NMR of **48a** with BuChE, performed at 400 MHz, 15°C, and 3 s saturation time. (A) reference spectrum, (B) STD spectrum of compound **48a** (0.8 mM) with BuChE enzyme (4μM). Binding epitope of **48a** from STD NMR experiment. The numerical values designate the fraction of saturation as a percentage, between the ligand protons and the protein active site, normalized to the maximum ligand STD signal (H2, H14, H16; 100%).

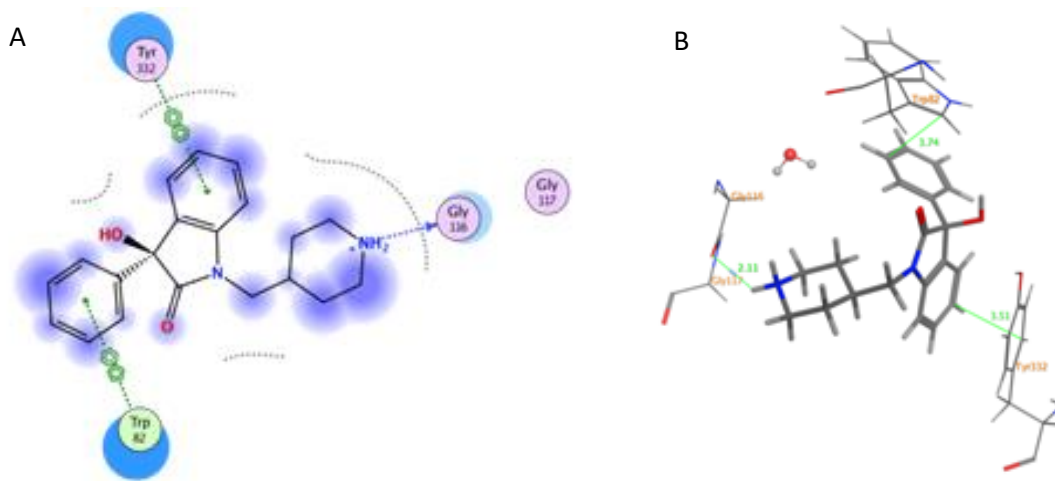


**Figure 85** - (A) Interaction diagram of compound **48a** with hBuChE; (B) Binding mode for compound **48a** interaction with hBuChE.

---

### 4.3. Conclusions

All three sections of the donepezil molecule are required for good interaction with the AChE active-site, but the crucial information obtained from the STD-NMR experiment implies that both the dimethoxyindanone benzene and the *N*-benzyl group show the closest interactions with the enzyme. The indanone cyclopentanone and the piperidine units, also show significant interactions. This would imply that for the design of potential donepezil analogues, these three pharmacophore units should be preserved, and contain suitable functionality to bind with the key *h*AChE residues indicated in the preceding discussion, but at the same time allowing one to alter both sterically and electronically these units to improve the enzyme binding affinity of the analogues.

Rasagiline binds irreversibly to the MAO-B cofactor FAD. The results obtained by the STD-NMR study showed no covalent bonding between rasagiline and FAD, probably due to experiment conditions (pH and temperature). An in depth study of this interaction is of key importance, not only for developing new and better MAO-B inhibitors, but also for understanding the poor inhibition results obtained for our compounds.

The studies of **48a** with both *ee*AChE and *eq*BuChE were in agreement with the IC<sub>50</sub> for the *in vitro* testing. These results were encouraging and further tests were made for this compound, namely toxicological and pharmacological.





## *Chapter 5*

# *Pharmacological and toxicological evaluation of selected target molecules for neurodegenerative diseases*

---

*“All substances are poisons; there is none that is not a poison.*

*The right dose differentiates a poison and a remedy.”*

Paracelsus (1493-1541)

The studies made in this chapter originated the following publication:

1. Bacalhau, P., Fernandes, L., Martins, M. R., Candeias, F., Carreiro, E. P., Totobenazara, J., Guedes, R. C., Caldeira, A. T., Burke, A. J. *In Silico*, NMR and Pharmacological Evaluation of an Oxindole Cholinesterase Inhibitor. *Biochem. Pharmacol.* (submitted)

## 5.1 Introduction

Cholinergic inhibitors are a main group of target drugs for AD and several have been investigated clinically in AD patients, like Tacrine, Galantamine and Heptylphysostigmine. Tacrine showed several side effects as well as liver toxicity, so the development of new cholinergic inhibitors that are tolerable and present low toxicity is paramount [266].

In the development of new drugs, besides their potency, distribution and efficacy, their toxicity is also a very crucial issue, an issue that can prevent the commercialization of any potent pharmaceutical. Acute toxicology is determined using two important parameters; the median lethal dose<sup>5</sup> (LD<sub>50</sub>) and the median lethal concentration<sup>6</sup> (LC<sub>50</sub>) [267].

Ideally, if toxicity testing is intended to provide information on the safety of a compound in humans, the animal model chosen for testing should ideally have similar physiology to humans, and in the way it handles the drug substance pharmacodynamically. Substantial differences in *Absorption, Distribution, Metabolism or Elimination* (ADME) between animal models and humans will reduce the predictive value of the test result. From a practical point of view, often the pharmacokinetics are unknown in humans or in many animal models. The most commonly used animal models are rodent species, like mice and rats, and often toxicity testing is conducted in one or both species. Most toxicity and teratology studies conducted in mice are designed to provide information on potential human toxicity [268]. The *Food and Drug Administration* (FDA) provides human equivalent dose interspecies conversion factors for converting most animal model *No Observed Adverse Effect Levels* (NOAELs) to the human equivalent. The conversion factor for the mouse is 12.1, meaning an observed NOAEL in a mouse of 12.1 mg kg<sup>-1</sup>day<sup>-1</sup> would be converted to 1 mg kg<sup>-1</sup>day<sup>-1</sup> for conservative human administration 1 [268].

Different pharmacological models, mainly those using rodents, were created to select substances that could act as AChE inhibitors [269-273]. However, the cost of the acquisition and maintenance of animals *in vivo*, the need for an adequate physical structure, including care in handling and minimizing animal suffering, justifies the demand for alternative more accessible and low cost methods that have a higher number of individuals, and be able to achieve results in less time than with conventional trials [274].

---

<sup>5</sup> The DL<sub>50</sub> is the estimated dose that, when the toxicant is administered directly to experimental test animals, results in the death of 50% of the population so exposed under the defined conditions of the test.

<sup>6</sup> The LC<sub>50</sub> is the estimated concentration, in the environment to which animals are exposed, that kill 50% of the population so exposed under the defined conditions of the test.

The brine shrimp *Artemia salina* Leach, an anostracan crustacean, is to date an important model for the routine use of this species in aquatic toxicology. Indeed, the use of cysts as “starting” biological material solves one of the major biological, technological and financial bottlenecks in routine ecotoxicology, namely the need for culturing or maintenance of livestock of test organisms in a healthy state and in sufficient numbers [275]. Presently, *Artemia salina* L. is used as a bioassay species for a variety of objectives: investigation of source of toxicity in chemical mixtures and environmental samples, acute screening of chemicals, detection of toxins and in pharmaceuticals, and studies of models of toxic action of substances [276, 277].

The brine shrimp model appears as a screening alternative that allows a great number of samples to be tested at low-cost, in a simple and quick way. Moreover, there are studies that indicate the existence of a good correlation between the two assays, suggesting that the brine shrimp bioassay is a useful alternative model [275, 278].

This chapter presents the acute toxicity study of selected target like drugs using two different biological models for two different applications, the citotoxicity in *A. salina* L. (LC<sub>50</sub>) and the lethal dose in *Swiss* mice (LD<sub>50</sub>). Studies *in vivo* and *ex vivo* for IC<sub>50</sub> determination of selected inhibitors are also presented in this chapter.

## 5.2 Materials and Methods

### 5.2.1 Samples

Compounds used in the *A. salina* assay: donepezil hydrochloride, compound **48a**, rasagiline mesylate, pargyline hydrochloride, and potassium dichromate sample solutions were prepared in a saline solution. Compound **21** was prepared in a mixture of 50% DMSO in saline solution.

Compound **48a**, used in the animal acute toxicity assay, was prepared in distilled water.

Compounds used in the *in vivo* animal assay: donepezil hydrochloride and compound **48a**, were prepared in distilled water.

Compounds used in the *ex vivo* animal assay: donepezil hydrochloride, galantamine bromide, rivastigmine tartrate, rasagiline mesylate, pargyline hydrochloride, compound **48a**, compound **17b**, compound **18**, compound **21** and compound **48b**, were prepared in phosphate buffer.

## 5.2.2 Citotoxicity in *Artemia salina* L.

The toxicity of standard and sample solutions was evaluated using the *A. salina* L. lethality bioassay in order to determine the median lethal concentration (LC<sub>50</sub>) [267]. The procedure was performed according to the Artokit M protocol (MicroBioTests, Inc.) [279]. In a multiwell test plate, 100 µL of each solution was added to 900 µL of a saline medium. In each well were added 10 *A. salina* L. nauplii, previously rehydrated and hatched from cysts, that were placed in a saline medium in absence of light during 48 h. Assays were repeated nine times for each concentration. Plates were observed after 24h of incubation, at 25 °C, using a Research Stereomicroscope System (Olympus SZX9) and dead nauplii counted. LC<sub>50</sub> was determined using GraphPad Prism 5™ software. Potassium dichromate was used as a positive control (3.125 µg mL<sup>-1</sup> to 150 µg mL<sup>-1</sup>). A negative control was prepared with a saline medium without DMSO and another negative control was prepared with 50% DMSO.

We used the following criteria to make our final conclusions on the toxicity of these compounds [278]:

- LC<sub>50</sub> values superior to 1000 µg mL<sup>-1</sup> indicated that the compounds were non-toxic;
- LC<sub>50</sub> values between 500 and 1000 µg mL<sup>-1</sup> indicated that the compounds had low toxicity;
- LC<sub>50</sub> values inferior to 500 µg mL<sup>-1</sup> indicated that the compounds were toxic.

## 5.2.3 Acute toxicity in animal model

### 5.2.3.1 Animals

The acute toxicity study was carried out using female *Swiss* albino mice (*Mus musculus*), with 8 weeks old, weighting 23 ± 1 g. They were housed in a controlled environment (12 h light/dark cycles, 23 ± 1 °C) with food and water *ad libitum*. Food was withheld 16 h before the experiments. Procedures were conducted in accordance with the National Institutes of Health Guide for Care and Use of Laboratory Animals Guidelines and European Community Guidelines. All procedures involving animals were supervised by a research coordinator accredited by *Federation of European Laboratory Animal Science Association* (FELASA) n° 020/08.

### 5.2.3.2 Acute intraperitoneal toxicity evaluation

Acute toxicity of compound 48a was evaluated in *swiss* albino mice and the LD<sub>50</sub> was determined according to the OECD *Up-and-Down* standard procedure [280, 281].

The animals were divided into two groups of 3 mice each. The compound administration was by intraperitoneal (i.p.) injection in the upper left quadrant of the animal's abdomen. The animals were kept in observation for 15 days, during which they were housed in a controlled environment (12 h light/dark cycles, 23 ± 1 °C) with food and water *ad libitum*.

### 5.2.4 *Ex vivo* pharmacological evaluation

#### 5.2.4.1 Animals

The IC<sub>50</sub> study was carried out using male *Swiss* albino mice (*Mus musculus*), with 8 weeks old, weighting 23 ± 1 g. They were housed in a controlled environment (12 h light/dark cycles, 23 ± 1 °C) with food and water *ad libitum*. Food was withheld 16 h before the experiments.

Procedures were conducted in accordance with the National Institutes of Health Guide for Care and Use of Laboratory Animals Guidelines and European Community Guidelines. All procedures involving animals were supervised by a research coordinator accredited by FELASA n° 020/08 (Federation of European Laboratory Animal Science Association).

#### 5.2.4.2 Spectrophotometric measurement of cholinesterase and monoamine oxidase activity

Animals were sacrificed by decapitation, and brains and livers were dissected out, washed in ice-cold potassium phosphate buffer (0.2 M, pH 7.6), and homogenized. The brain homogenate was prepared in potassium phosphate buffer 0.1 M, pH 7.6 (1:10, w/v), and then centrifuged at 10000 g and 4 °C for 10 min. The liver homogenate was prepared in potassium phosphate buffer 0.1 M, pH 7.6 (1:10, w/v), and then centrifuged at 1000 g and 4 °C for 15 min.

Donepezil hydrochloride, galantamine bromide, rivastigmine tartrate, compounds **48a** and **48b** were prepared in potassium phosphate buffer (0.2 M, pH 7.6), and were tested against AChE activity in the brain.

Donepezil hydrochloride, galantamine bromide, rivastigmine tartrate, compounds **48a** and **48b** were prepared in potassium phosphate buffer (0.2 M, pH 7.6), compounds **17**, **20** and **21** were prepared in 5% DMSO, and all the compounds were tested against AChE and BuChE activity in the liver.

AChE and BuChE activity was determined following a modified Ellman's method [210], and the IC<sub>50</sub> values were calculated.

Rasagiline mesylate, pargyline hydrochloride and compound **48a** were prepared in potassium phosphate buffer (0.2 M, pH 7.6), compounds **17**, **18** and **21** were prepared in 5% DMSO, and all the compounds were tested against MAO-B activity in the liver.

MAO-B activity was determined following the method described in literature [282, 283], and the IC<sub>50</sub> values were calculated.

Total protein quantification followed the Lowry method [284].

## 5.2.5 *In vivo* pharmacological evaluation

### 5.2.5.1 Animals

The pharmacological evaluation was carried out using male Swiss albino mice (*Mus musculus*), with 8 weeks old, weighting  $28 \pm 2$  g. They were housed in a controlled environment (12 h light/dark cycles,  $23 \pm 1$  °C) with food and water *ad libitum*. Food was withheld 16 h before the experiments. Procedures were conducted in accordance with the National Institutes of Health Guide for Care and Use of Laboratory Animals Guidelines and European Community Guidelines. All procedures involving animals were supervised by a research coordinator accredited by FELASA n° 020/08 (Federation of European Laboratory Animal Science Association).

### 5.2.5.2 Spectrophotometric measurement of cholinesterase activity

The animals were divided into four groups of six animals. The compounds administration was by intraperitoneal (i.p.) injection in the upper left quadrant of the animal's abdomen. Group I was administered with the vehicle (distilled water), group II was administered with 3 mg kg<sup>-1</sup> of donepezil hydrochloride, group III was administered with 3 mg kg<sup>-1</sup> of compound **48a** and group IV was administered with 6 mg kg<sup>-1</sup> of compound **48a**.

Animals were sacrificed by decapitation, 1 h after i.p. injection, and brains and livers were dissected out, washed in ice-cold potassium phosphate buffer (0.2 M, pH 7.6), and homogenized. The brain homogenate was prepared in potassium phosphate buffer 0.1 M, pH 7.6 (1:10, w/v), and then centrifuged at 10000 g and 4 °C for 10 min. The liver homogenate was prepared in potassium phosphate buffer 0.1 M, pH 7.6 (1:10, w/v), and then centrifuged at 1000 g and 4 °C for 15 min. AChE and BuChE activities were determined following a modified Ellman's method [210], and the IC<sub>50</sub> values were calculated.

Total protein quantification followed the Lowry method [284] with some modifications.

### 5.2.6 Statistic analysis

All data was expressed as mean  $\pm$  standard deviation of triplicate measurements. Statistical analysis of data was performed using one-way ANOVA. A probability value of  $p < 0.05$  was considered statistically significant. Multiple comparisons of means were analyzed using the b-Tukey test. Analyses were performed using SPSS<sup>®</sup> 22 Windows, IBM. The dose-response curve and the LC<sub>50</sub> values, as well as the IC<sub>50</sub> for all the samples were determined with the software GraphPad Prism 5<sup>™</sup>.

## 5.3 Results and Discussion

### 5.3.1 Citotoxicity in *Artemia salina* L. of cholinesterase and monoamine oxidase inhibitors

The toxicity of AChE and BuChE inhibitors (donepezil hydrochloride and compound **48a**), as well as the toxicity of MAO-B inhibitors (rasagiline mesylate, pargyline hydrochloride and compound **21**), was evaluated in the bioassay with *A. salina* (Fig. 86).



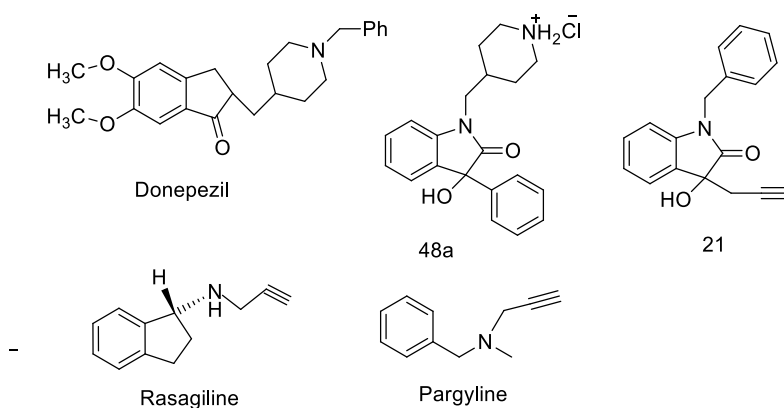


**Figure 86** - Compounds tested for their toxicity with *A. salina*.

Potassium dichromate ( $K_2Cr_2O_7$ ) was used as a positive control and a concentration of  $100 \mu\text{g mL}^{-1}$  caused 100% mortality. The dose-response curve in Figure 87 showed an  $LC_{50}$  value of  $15.04 \mu\text{g mL}^{-1}$ , and the compound was considered very toxic [278], as was expected.

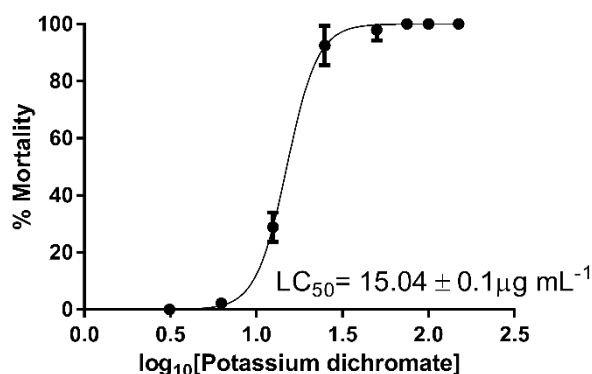


**Figure 87** - Dose-response relation in *A. salina*, in the presence of potassium dichromate.

There was no mortality in the negative control, with and without DMSO and the assay was considered valid for the rest of the samples.

Compound **48a** showed 5% mortality for a concentration of  $1000 \mu\text{g mL}^{-1}$  and it was considered non toxic. The commercial standard, donepezil, used as an AChE inhibitor in AD presented 26% mortality for a concentration of  $1000 \mu\text{g mL}^{-1}$  and was also considered non toxic [278].

Figure 88 (A) shows the dose-response curve for commercial standard rasagiline, used as MAO-B inhibitor in PD. The concentration of  $250 \mu\text{g mL}^{-1}$  yielded a 99% mortality and the compound was considered of high toxicity ( $LC_{50} = 93.33 \mu\text{g mL}^{-1}$ ), although not as high as potassium dichromate. On the other hand, Figure 88 (B) shows the commercial MAO-B inhibitor pargyline,

that wasn't used in PD treatment, and was considered moderately toxic ( $LC_{50} = 387.26 \mu\text{g mL}^{-1}$ ), with 75% mortality for a concentration of  $500 \mu\text{g mL}^{-1}$ . Figure 88 (C) shows compound **21**, one of the synthesized compounds for this research, with a toxic effect ( $LC_{50} = 43.45 \mu\text{g mL}^{-1}$ ) on *A. salina* higher than both commercial standards [278].

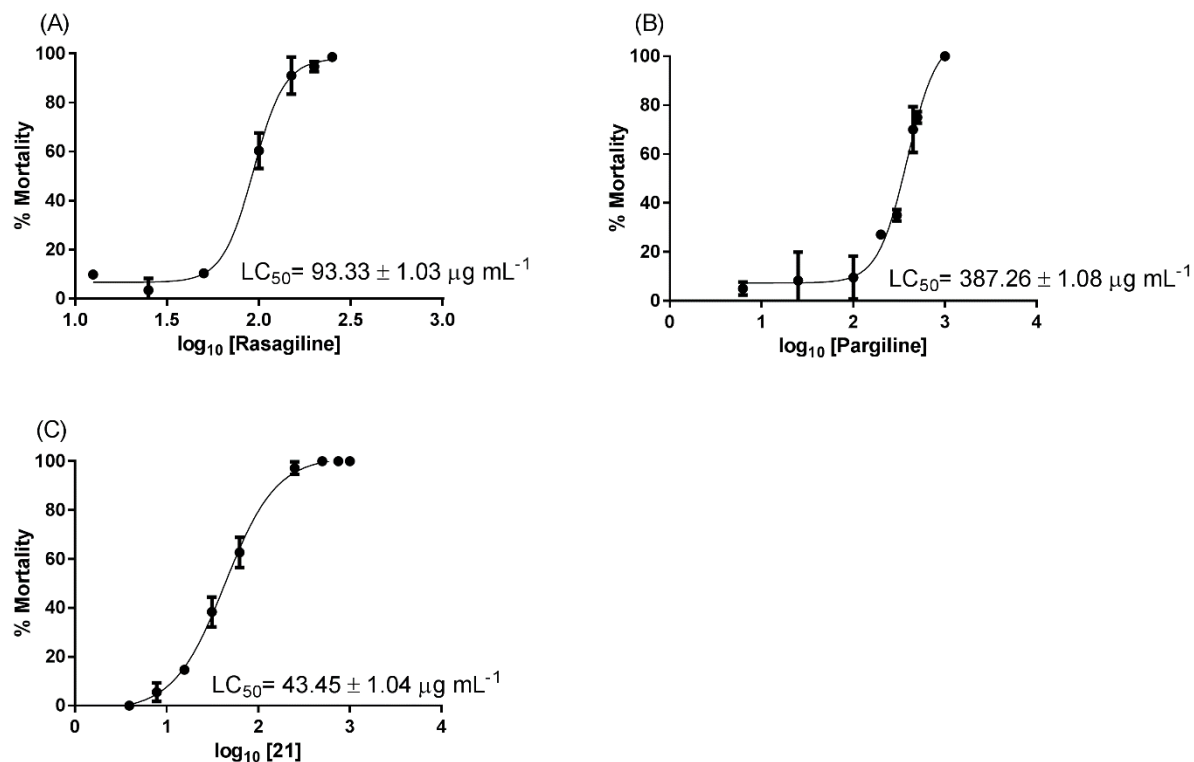


**Figure 88** - Dose-response relation in *A. salina*, in the presence of (A) rasagiline mesylate, (B) pargiline hydrochloride and (C) compound **21**.

### 5.3.2 Acute intraperitoneal toxicity evaluation of cholinesterase inhibitors

Acute toxicity of compound **48a** was evaluated in *swiss* albino mice and the  $LD_{50}$  was determined according to Up and Down procedure [280, 281]. The estimated  $LD_{50}$  was of  $100 \text{ mg kg}^{-1}$ .

Donepezil presented a  $LD_{50}$  of  $45.2 \text{ mg kg}^{-1}$  for oral administration and of  $3.7 \text{ mg kg}^{-1}$  for intravenous administration, according to the literature [285]. When comparing these results with the one for compound **48a**, it is possible to see that the  $LD_{50}$  is twice the value of that for donepezil oral uptake, and is 27 times higher than donepezil for intravenous administration.

### 5.3.3 *Ex vivo* pharmacological evaluation

The biological activity of a drug is linked to its ability to bind to a specific recognition site on target protein. In the *in vitro* assays the activity of the purified enzyme is measured in the presence of an inhibitor. The next step in the characterization of drug effects is the *ex vivo* experiments, which means that the inhibitor is administered by different routes (i.e. orally, intravenous, intraperitoneal) to a living animal or to a human and that the evaluation of drug effects is performed *in vitro* via tissue samples or fluid aliquots (cerebrospinal fluid or blood) of the organism under study [286].

The activity of AChE in the brain was measured in the presence of the three commercial drugs, donepezil hydrochloride, galantamine bromide and rivastigmine tartrate (Fig. 89) as well as compound **48a**, which presented 28% inhibition for the highest concentration tested. Donepezil was the compound with the lower  $IC_{50}$ , followed by rivastigmine and galantamine. The same drugs tested in the brain were also tested in the liver (Fig. 90), along with compounds **17**, **20** and **21**. Contrary to the results obtained for the brain, rivastigmine presented the lowest  $IC_{50}$  for both cholinesterases in the liver, followed by donepezil and galantamine, which is in agreement with the literature [287, 288]. Rivastigmine showed selectivity for AChE, galantamine for BuChE and donepezil showed no selectivity, inhibiting both enzymes with similar  $IC_{50}$ .

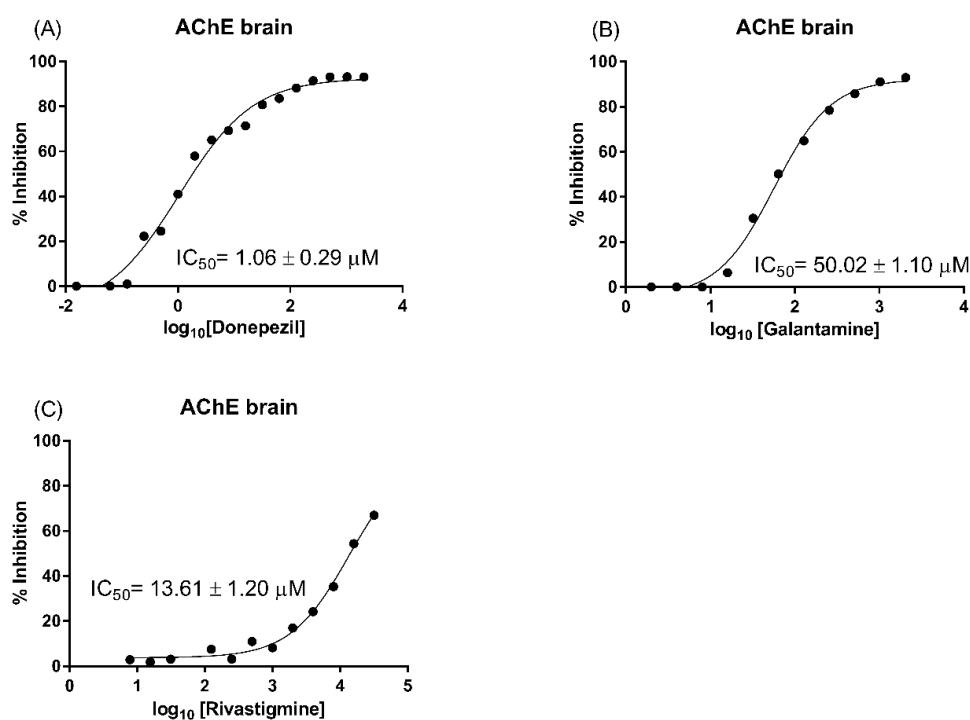


**Figure 89** - Dose-response relation of AChE in the brain of Swiss mice in the presence of (A) donepezil, (B) galantamine and (C) rivastigmine.

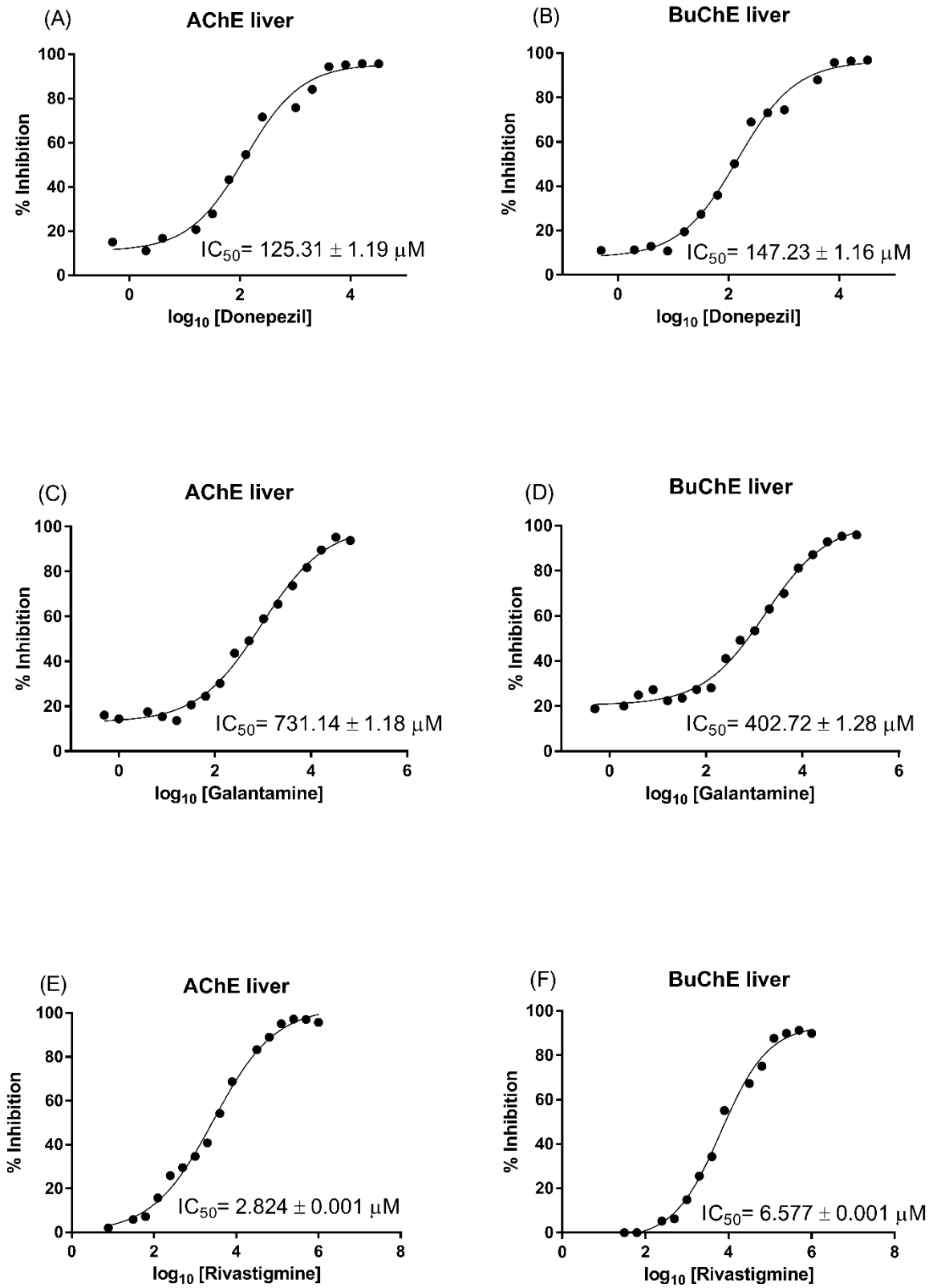
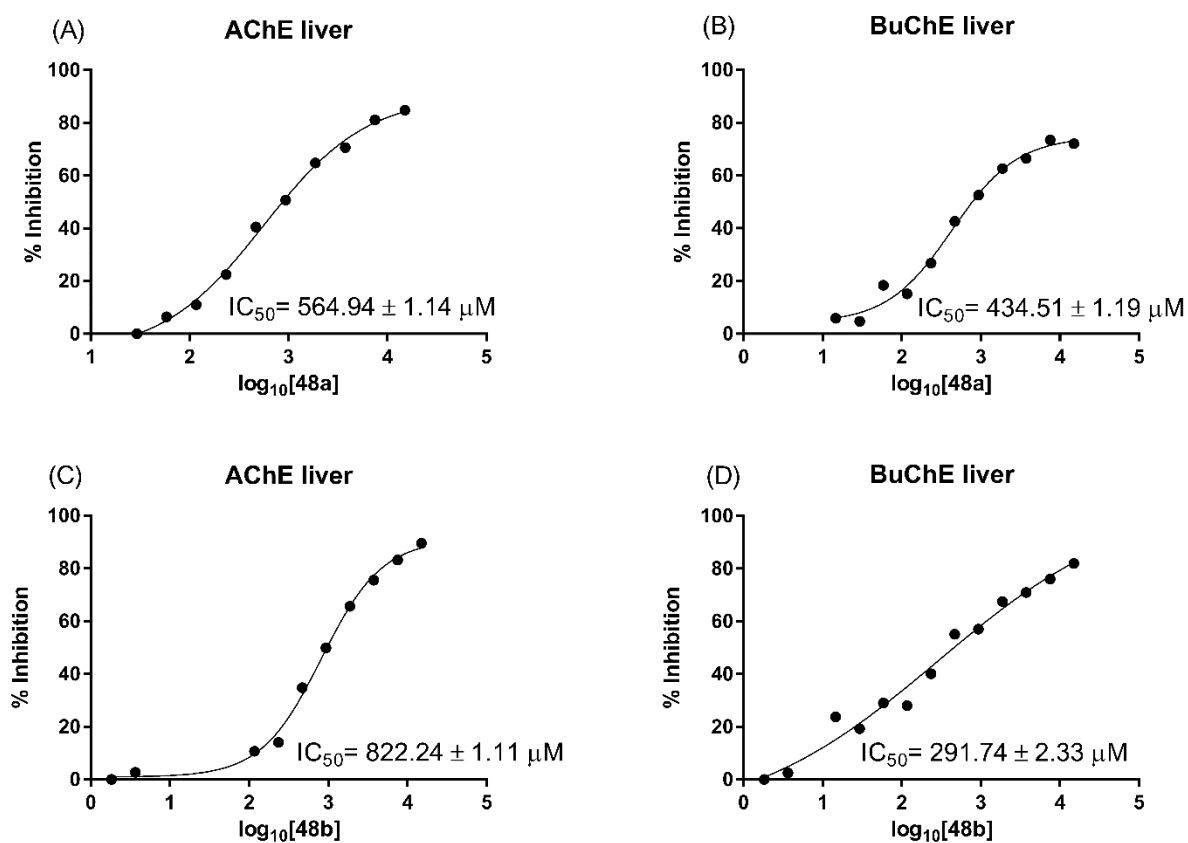


Figure 90 - Dose-response relation of AChE and BuChE in the liver of *swiss* mice, in the presence of (A-B) donepezil, (C-D) galantamine and (E-F) rivastigmine.

The two compounds, **48a** and **48b**, were also tested for AChE and BuChE (Fig. 91). They were both better inhibitors of BuChE, and compound **48b** showed the lowest  $IC_{50}$ . Regarding AChE, it was compound **48a** that presented the best inhibition result. By comparing these results with those of the commercial standards, compound **48a** showed better  $IC_{50}$  results for AChE than galantamine and the same  $IC_{50}$  for BuChE. As for compound **48b**, the  $IC_{50}$  for AChE was a bit higher than that of galantamine, but for BuChE the  $IC_{50}$  value was lower than the one presented by galantamine. The other 3 synthesized compounds didn't inhibit AChE or BuChE.



**Figure 91** - Dose-response relation of AChE and BuChE in the liver of *swiss* mice, in the presence of (A-B) compound **48a**, (C-D) compound **48b**.

Rasagiline mesylate and pargyline hydrochloride were used as standards in MAO-B activity evaluation in the liver. Figure 92 shows the dose-response curves of the tested compounds. Through analysis of the respective  $IC_{50}$  values it is possible to conclude that rasagiline was a potent inhibitor of MAO-B, with an  $IC_{50}$  value of 1.82 nM, which is similar to the  $IC_{50}$  value for human brain (1.4 nM) [197]. Pargyline had a higher  $IC_{50}$  (731.14 nM) than Rasagiline, but Fišar *et al.*

presented a study with a very different  $IC_{50}$  for pargyline (only 8.20 nM), but this value was obtained from a radiochemical assay with pig brain MAO-B [289].

Both standards had  $IC_{50}$  results lower than any of the tested compounds, that showed values ranging from 20.56 to 1558.55  $\mu$ M. This lead to the conclusion that none of the tested compounds was a suitable inhibitor of MAO-B.

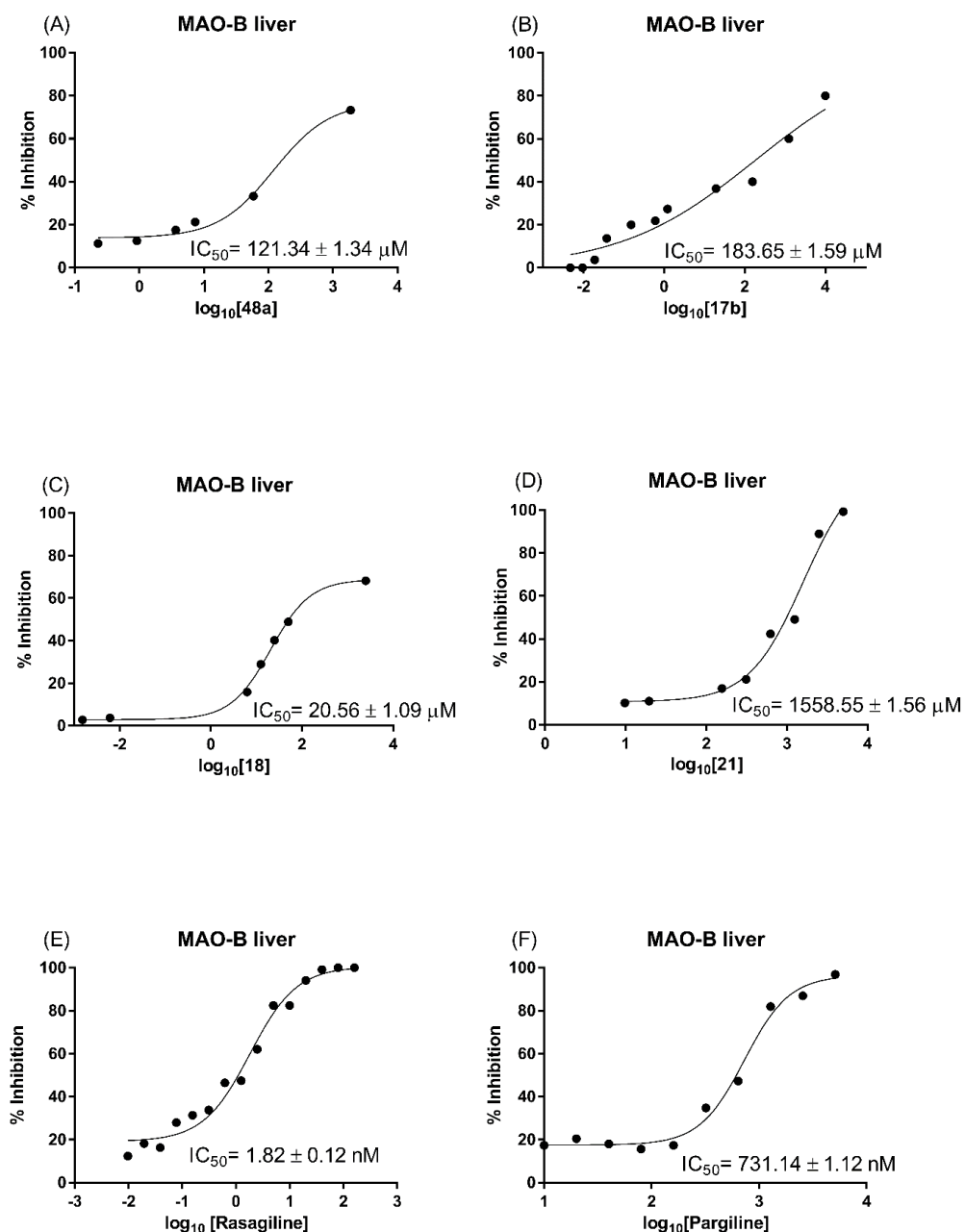


**Figure 92** - Dose-response relation of MAO –B in the liver of *swiss* mice, in the presence of (A) compound **48a**, (B) compound **17**, (C) compound **18**, (D) compound **21**, (E) rasagiline and (F) pargiline.

### 5.3.4 *In vivo* pharmacological evaluation

Both donepezil hydrochloride and compound **48a** decreased AChE activity in the brain, with values significantly different from the control ( $p < 0.05$ ) (Fig. 93 and Table A3). Interestingly, compound **48a** presented higher AChE inhibition than donepezil, although the results were not significantly different ( $p > 0.05$ ). These results suggest that compound **48a** (oxindole based) could have similar brain uptake than donepezil (piperidine based) [287]. The two concentrations of compound **48a** tested decreased AChE activity in the brain by the same percentage, showing no benefits in the administration of a dose higher than  $3 \text{ mg kg}^{-1}$ . With regards to BuChE activity in the brain, no useful results were obtained since it was not possible to quantify this enzyme activity in the brain of a healthy mouse model [290, 291].

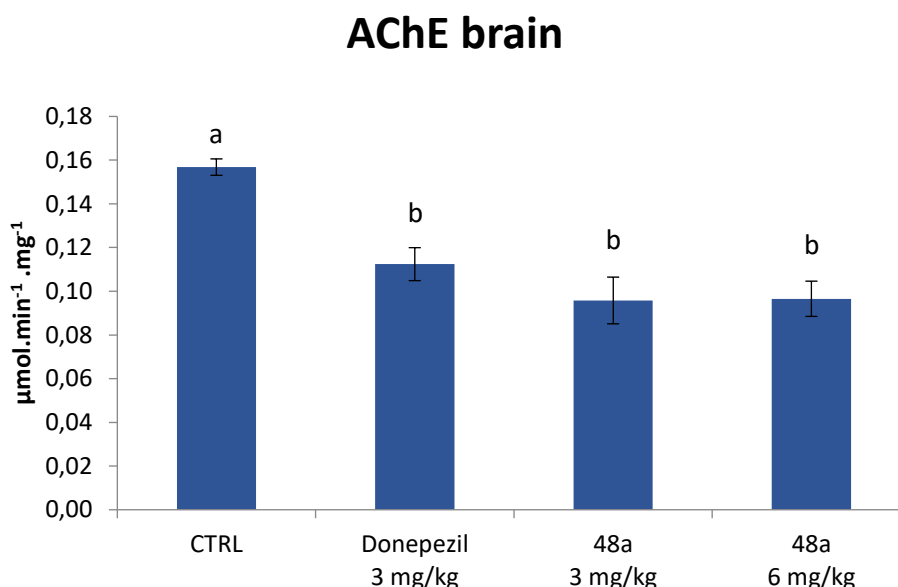


**Figure 93** - *In vivo* AChE activity in the brain of *swiss* mice, in the presence of donepezil and compound **48a**. Different letters represent values significantly different ( $p < 0.05$ ).

Besides the brain, it was possible to determine both AChE and BuChE activity in the liver (Fig. 94 and Table A3). Donepezil and compound **48a** didn't present values significantly different, suggesting no relevant inhibition of both cholinesterases in the liver. On the other hand, the  $3 \text{ mg kg}^{-1}$  of donepezil and compound **48a** presented the same level of inhibition for liver BuChE.

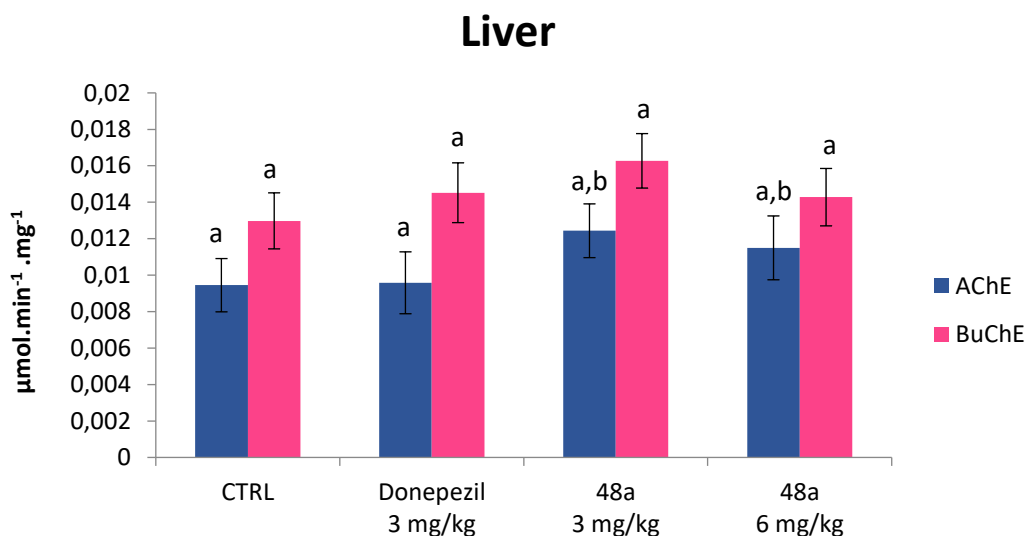


**Figure 94** - *In vivo* AChE and BuChE activity in the liver of *swiss* mice, in the presence of donepezil and compound 48a. Different letters represent values significantly different ( $p < 0.05$ ) to each enzymatic activity.

## 5.4. Conclusions

The results of this study showed that compound **21** presented significant toxicity for *Artemia salina*, with an  $LC_{50}$  of  $43.45 \mu\text{g mL}^{-1}$  and was only tested *ex-vivo* for AChE, BuChE and MAO-B. This compound showed no inhibition for any of the enzymes tested.

On the other hand, compound **48a** showed low toxicity against *Artemia salina* ( $LC_{50} > 1000 \mu\text{g mL}^{-1}$ ) and demonstrated to be less toxic than donepezil, with a  $LD_{50}$  near  $100 \text{ mg kg}^{-1}$ . This compound visibly decreased AChE activity in the brain, having similar results to donepezil, and in the *ex-vivo* assay presented a dual inhibition for the cholinesterases with an  $IC_{50}$  similar to galantamine. In the context of developing new therapeutic drugs for AD, these are encouraging results.







## ***Chapter 6***

### ***Final Considerations and Future Perspectives***

---

*"In my opinion nothing occurs contrary to nature,*

*Except the impossible, and that never occurs."*

Galileu Galilei (1564-1642)



---

The present thesis has its main focus on the study of target drugs in neurodegenerative diseases, involving the screening of commercial drugs used in AD and PD treatment (Chapter 2) and different families of synthesized compounds with biological activity (Chapter 3), their protein-ligand and molecular interactions (Chapter 4) and toxicological and pharmacological studies (Chapter 5).

Two different screening spectroscopic methods were used, namely molecular absorption spectroscopy and fluorescence, to determine the enzymes' kinetic parameters. Molecular absorption spectroscopy was used for AChE, BuChE and MAO-B studies. MAO-B was also studied by fluorescence spectroscopy. Both *ee*AChE and *eq*BuChE presented selectivity for ATCI, but only *eq*BuChE presented selectivity for BTCl. *h*MAO-B belongs to a different enzyme family, presenting selectivity for benzylamine.

In chapter 2, the following active ingredients of prescribed drugs for AD, which included: donepezil, rivastigmine and galantamine, were screened. Molecular absorption spectroscopy was used to compare the different assay conditions for the IC<sub>50</sub> determination of donepezil, rivastigmine and galantamine. It was found that IC<sub>50</sub> can suffer slight to major variation, depending on the assay conditions. According to these studies, the best conditions found were: no pre-incubation at 25 °C with a wavelength of 405 nm and Tris-HCl 0.05 M, pH 8 buffer. Molecular absorption spectroscopy and fluorescence spectroscopy were used to determine the IC<sub>50</sub> values for rasagiline (the active ingredient of a commercial drug used in PD treatment) and pargyline. On comparing the results of the two techniques it was observed that fluorescence spectroscopy was much more accurate than the molecular absorption spectroscopy. Due to its greater sensitivity, less quantity of enzyme was required.

In chapter 3, a wide range of structurally diverse small molecules were screened *in vitro* to test their cholinesterase and monoamine oxidase inhibition potential as MTDLs. Unfortunately, none of the compounds was able to successfully inhibit both cholinesterase and monoamine oxidase. In fact, there were two compounds that presented very good results as dual cholinesterase inhibitors, one was an oxindole derivative (compound **25**) and the other a chromanone derivative (compound **62**). Nonetheless, compound **60**, a diether ester derivative, proved to efficiently inhibit *ee*AChE, and compounds **45** (oxindole derivative) and **74** (rivastigmine analogue) showed good inhibition for *eq*BuChE.

In chapter 4, molecular modelling and STD-NMR studies were carried out to understand how the compounds (ligands) interacted with the enzymes. This was very useful as it allowed us to understand the key structural attributes that allow for good interactions of the ligands with the enzyme active site, and as a corollary it allowed us to understand why these ligands were not suitable for *h*MAO-B inhibition.

All three parts of the donepezil molecule are required for good interaction with the *ee*AChE active-site, but this was substantiated by conducting key STD-NMR experiments, which showed that both the dimethoxyindanone benzene and the *N*-benzyl group had the closest interactions with the enzyme. The indanone cyclopentanone and the piperidine units, also showed significant interactions. This would imply that for the design of potential donepezil analogues, these three pharmacophore units should be preserved, and contain suitable functionality to bind with the key *h*AChE residues, but at the same time allowing one to alter both sterically and electronically these units in order to improve the enzyme binding affinity of the analogues.

Rasagiline binds irreversibly to *h*MAO-B cofactor FAD.

The results on chapter 5 showed that compound **21** presented significant toxicity for *Artemia salina*, with an LC<sub>50</sub> of 43.45 µg mL<sup>-1</sup> and was only tested *ex-vivo* for AChE, BuChE and MAO-B. This compound showed no inhibition for any of the enzymes tested.

On the other hand, 4-((3-hydroxy-2-oxo-3-phenylindolin-1-yl)methyl)piperidin-1-ium chloride (compound **48a**) showed low toxicity against *Artemia salina*, with an LC<sub>50</sub> > 1000 µg mL<sup>-1</sup> and showed to be less toxic than donepezil, with a LD<sub>50</sub> near 100 mg kg<sup>-1</sup>. This compound visibly decreased AChE activity in the brain of *Swiss* mice, with results similar to donepezil, and in the *ex-vivo* assay presented a dual inhibition to both cholinesterases with an IC<sub>50</sub> similar to galantamine, although it didn't inhibit MAO-B.

These are very promising results in the quest for finding new therapeutic drugs for AD. The next step would be to conduct pharmacokinetic and histological studies with 4-[(3-hydroxy-2-oxo-3-phenylindolin-1-yl)methyl]piperidin-1-ium chloride (compound **48a**) in order to better understand its absorption, distribution, as well as its metabolism and elimination.

Studies of compound **48a** (as well as others) with β-secretase might also be undertaken, since this enzyme is involved in the production of β-amiloid oligomers and fibrils, responsible for neuron degeneration in AD.

Future studies involving the design of new MTDLs would be of interest, especially with the challenge of adding neuroprotective properties to progress to a disease modifying drug.







## *References*

---



1. Pina, J.A.E., *Anatomia humana da relação*. 3 ed. 2000: Lidel. 594.
2. [www.what-when-how.com/Function of the nervous system](http://www.what-when-how.com/Function_of_the_nervous_system). 2016.
3. [www.what-when-how.com/Cells of the nervous system](http://www.what-when-how.com/Cells_of_the_nervous_system). 2016.
4. [www.what-when-how.com/Histology of the Nervous System \(The Neuron\)](http://www.what-when-how.com/Histology_of_the_Nervous_System_(The_Neuron)). 2016.
5. Blennow, K., de Leon, M. J., Zetterberg, H., *Alzheimer's disease*. Lancet seminars, 2006. **368** (9533 ): p. 387–403.
6. [www.what-when-how.com/Neurotransmitters](http://www.what-when-how.com/Neurotransmitters). 2016.
7. VanPutte, C., Regan, J., Russo, A., *Seeley's Essentials of Anatomy & Physiology, Ninth Edition*. 2016, New York: McGraw-Hill.
8. [www.what-when-how.com/Synaptic Transmission](http://www.what-when-how.com/Synaptic_Transmission). 2016.
9. Stufflebeam, R. *Introduction to neurons, synapses, action potentials and neurotransmission*. 2016.
10. Seeley, R., VanPutte, C., Regan, J., Russo, A., *Seeley's Anatomy & Physiology, Tenth Edition*. 2014, New York: McGraw-Hill. 1272.
11. [www.what-when-how.com/Overview of the Central Nervous System \(Gross Anatomy of the Brain\)](http://www.what-when-how.com/Overview_of_the_Central_Nervous_System_(Gross_Anatomy_of_the_Brain)). 2016.
12. Carlson, N.R., *Physiology of Behavior, eleventh ed*. 2013, United States of America: Pearson Education, Inc. 771.
13. [http://ec.europa.eu/health/major\\_chronic\\_diseases/diseases/brain\\_neurological/index\\_en.htm](http://ec.europa.eu/health/major_chronic_diseases/diseases/brain_neurological/index_en.htm)
14. Bertram, L., Tanzi, R. E. , *The genetic epidemiology of neurodegenerative disease*. J. Clin. Invest., 2005. **115**(6): p. 1449-1457.
15. Logroscino, G., Tortelli, R. , *Epidemiology of neurodegenerative diseases*, in *Imaging in Neurodegenerative Disorders*, L. Saba, Editor. 2015, Oxford University Press
16. Mills, J.D., Janitz, M., *Transcriptome profiling in neurodegenerative disorders*, in *Imaging in Neurodegenerative Disorders*, L. Saba, Editor. 2015, Oxford University Press
17. Hippus, H., Neundörfer, G., *The discovery of Alzheimer's disease*. Dialogues in Clin. Neurosci., 2003. **5**(1): p. 101-108.
18. Organization, W.H., *Dementia: a public health priority*. 2012.
19. Price, D., *New perspectives on Alzheimer's disease*. Annu. Rev. Neurosci., 1986. **9**: p. 489-512.
20. Williams, B.R., Nazarians, A., Gill, M. A., *A review of rivastigmine: A reversible cholinesterase inhibitor*. Clin. Ther., 2003. **25**(6): p. 1634-1653.

21. Citron, M., *Alzheimer's disease: strategies for disease modification*. Nat. Rev. Drug Disc., 2010. **9**: p. 387-398.
22. Costa, P.T.J., Williams. T- F-, Sommerfield, M., *Clinical practice guideline no. 19: Recognition and initial assessment of Alzheimer's disease and related dementias.*, A.H.C.P.R. US Department of health and human services, Editor. 1996, AHCP publication 97-0702.
23. Francis, P.T., Palmer, A. M., Snape, M., Wilcock, G. K., *The cholinergic hypothesis of Alzheimer's disease: A review of progress*. J Neurol. Neurosurg. Psychiatr., 1999. **66**: p. 137-147.
24. Cummings, J.L., Cole, G., *Alzheimer disease*. JAMA, 2002. **287**: p. 2335-2338.
25. Brookmeyer, R., Corrada, M. M., Curriero, F. C., Kawas, C., *Survival following a diagnosis of Alzheimer's disease*. Arch. Neurol., 2002. **59**: p. 1764-1767.
26. <http://www.brightfocus.org/alzheimers/about/understanding/brain-with-alzheimers.html>.
27. Brimblecombe, R.W., *Drug Actions on Cholinergic Systems*. 1974: University Park Press.
28. Waser, P.G., *Cholinergic Mechanisms*. 1975: Raven.
29. Goldberg, A.M., Hanin, I., *Biology of Cholinergic Function*. 1976: Raven.
30. Zhou, Y., Wang, S., Zhang, Y. , *Catalytic reaction mechanism of acetylcholinesterase determined by Born-Oppenheimer Ab initio QM/MM molecular dynamics simulations*. J. Phys. Chem. B, 2010. **114**(26): p. 8817–8825.
31. Adams, H.R., *Veterinary pharmacology and therapeutics*. 8 ed. 2001: Iowa State University Press. 1201.
32. Voet, D., Voet, J., *Biochemistry*. 2nd Edition ed. 1995, U.S.A.: Wiley.
33. Birdsall, N.J., Hulme, E. C., Stockton, J. M., *Muscarinic receptor subclasses: allosteric interactions*. Cold Spring Harbor Symp Quant Biol, 1983. **48**(1): p. 53-56.
34. Chassaing, C., Dureng, G., Baissat, J., Duchene-Marullaz, P., *Pharmacological evidence for cardiac muscarinic receptor subtypes*. Life Sci, 1984. **35**(17): p. 1739-1745.
35. Ramsay, R.R., Majekova, M., Medina, M., Valoti, M., *Key targets for multi-target ligands designed to combat neurodegeneration*. Frontiers in Neuroscience, 2016. **10**(375).
36. Polinsky, R., *Clinical pharmacology of Rivastigmine: A new-generation acetylcholinesterase inhibitor for the treatment of Alzheimer's disease*. Clinical Therapeutics, 1998. **20**(4): p. 634-647.

- 
37. Greig, N.H., Lahiri, D. K., Sambamurti, K., *Butyrylcholinesterase: an important new target in Alzheimer's disease therapy*. Int. Psychogeriatr., 2002. **14**: p. 77-91.
  38. Jbilo, O., L'Hermite, Y., Talesa, V., Toutant, J.-P., Chatonnet, A., *Acetylcholinesterase and butyrylcholinesterase expression in adult rabbit tissues and during development*. Eur. J. Biochem., 1994. **225**: p. 115-124.
  39. Nicolet, Y., Lockridge, O., Masson, P., Fontecilla-Camps, J. C., Nachon, F., *Crystal structure of human butyrylcholinesterase and of its complexes with substrate and products*. J. Biol. Chem., 2003. **278**(42): p. 41141-41147.
  40. Harel, M., Quinn, D. M., Nair, H. K., Silman, I., Sussman, J. L., *The X-ray structure of a transition state analog complex reveals the molecular origins of the catalytic power and substrate specificity of acetylcholinesterase*. J. Am. Chem. Soc., 1996. **118**: p. 2340-2346.
  41. Bourne, Y., Taylor, P., Marchot, P., *Catalytic power and substrate specificity of acetylcholinesterase*. Cell, 1995. **83**: p. 503-512.
  42. Sussman, J.L., Harel, M., Frolov, F., Oefner, C., Goldman, A., Toker, L., Silman, I., *Atomic structure of acetylcholinesterase from *Torpedo californica*: a prototypic acetylcholine-binding protein*. Science, 1991. **253**: p. 872-879.
  43. Quinn, D.M., *Acetylcholinesterase: Enzyme structure, reaction dynamics, and virtual transition states*. Chem. Rev., 1987. **87**: p. 955-979.
  44. Kua, J., Zhang, Y. K., Eslamin, A. C., Butler, J. R., McCammon, J. A., *Studying the roles of W86, E202, and Y337 in binding of acetylcholine to acetylcholinesterase using a combined molecular dynamics and multiple docking approach*. Protein Sci., 2003. **12**: p. 2675-2684.
  45. Quinn, D.M., Feaster, S. R., Nair, H. K., Baker, N. A., Radic, Z., Taylor, P., *Delineation and decomposition of energies involved in quaternary ammonium binding in the active site of acetylcholinesterase*. J. Am. Chem. Soc., 2000. **122**: p. 2975-2980.
  46. Macdonald, I.R., Martin, E., Rosenberry, T. L., Darvesh, S., *Probing the Peripheral Site of Human Butyrylcholinesterase*. Biochemistry, 2012. **51**(36): p. 7046-7053.
  47. Ishida, T., Kato, S., *Theoretical perspectives on the reaction mechanism of serine proteases: the reaction free energy profiles of the acylation process*. J. Am. Chem. Soc., 2003. **125**(39): p. 12035-12048.
  48. Hedstrom, L., *Serine protease mechanism and specificity*. Chem. Rev., 2002. **102**(12): p. 4501-4523.

- 
49. Chatonnet, A., Lockridge, O., *Comparison of butyrylcholinesterase and acetylcholinesterase*. *Biochem. J.*, 1989. **260**(3): p. 625-634.
  50. Mack, A., Robitzki, A., *The key role of butyrylcholinesterase during neurogenesis and neural disorders: An antisense-5'-butyrylcholinesterase-DNA study*. *Prog. Neurobiol.*, 2000. **60**: p. 607-628.
  51. Lockridge, O., Masson, P., *Pesticides and susceptible populations: people with butyrylcholinesterase genetic variants may be at risk*. *Neurotoxicology*, 2000. **21**(1-2): p. 113-126.
  52. Allon, N., Raveh, L., Gilat, E., Cohen, E., Grunwald, J., Ashani, Y., *Prophylaxis against soman inhalation toxicity in guinea pigs by pretreatment alone with human serum butyrylcholinesterase*. *Toxicol. Sci.*, 1998. **43**(2): p. 121-128.
  53. Broomfield, C.A., Maxwell, D. M., Solana, R. P., Castro, C. A., Finger, A. V., Lenz, D. E., *Protection by butyrylcholinesterase against organophosphorus poisoning in nonhuman primates*. *J. Pharmacol. Exp. Ther.*, 1991. **259**(2): p. 633-638.
  54. Raveh, L., Grunwald, J., Marcus, D., Papier, Y., Cohen, E., Ashani, Y., *Human butyrylcholinesterase as a general prophylactic antidote for nerve agent toxicity. In vitro and in vivo quantitative characterization*. *Biochem. Pharmacol.*, 1993. **45**(12): p. 2465-2474.
  55. Field, M.J., Wymore, T. W., *Multiscale modeling of nerve agent hydrolysis mechanisms: a tale of two Nobel Prizes*. *Phys. Scr.*, 2014. **89**(108004).
  56. Tougu, V., *Acetylcholinesterase: mechanisms of catalysis and inhibition*. *Curr. Med. Chem. - CNS Agents*, 2001. **1**: p. 155-170.
  57. Watson, N.V., Breedlove, S. M. , *The Minds Machine: Foundations of Brain and Behavior, second ed.* 2015: Sinauer Associates.
  58. Bartus, R.T., *On neurodegenerative diseases, models and treatment strategies: Lessons learned and lessons forgotten a generation following the cholinergic hypothesis*. *Ex. Neurol.*, 2000. **163**: p. 495-529.
  59. Terry, A.V., Baccafuso, J. J. , *The cholinergic hypothesis of age and Alzheimer's disease-related cognitive deficits: recent challenges and their implications for novel drug development*. *J. Pharm. Exp. Ther.*, 2003. **36**(3): p. 281-287.
  60. Francis, P.T., Palmer, A. M., Snape, M., Wilcock, G. K., *The cholinergic hypothesis of Alzheimer's disease: a review of progress*. *J. Neurol. Neurosurg. Psychiatry*, 1999. **66**: p. 137-147.
  61. Cummings, J.L., *Alzheimer's disease*. *N. Engl. J. Med.*, 2004. **351**: p. 56-67.

- 
62. Schaeffer, E.L., Figueiro, M., Gattaz, W. F., *Insights into Alzheimer disease pathogenesis from studies in transgenic animal models*. Clinics, 2011. **66**: p. 45-54.
63. Reiman, E.M., *Attack on amyloid- $\beta$  protein*. Nature, 2016. **537**(7618): p. 36-37.
64. Squitti, R., Rossini, P. M., Cassetta, E., Moffa, F., Pasqualetti, P., Cortesi, M., Colloca, A., Rossi, L., Finazzi-Agro, A. , *D-penicillamine reduces serum oxidative stress in Alzheimer's disease patients*. Eur. J. Clin. Invest., 2002. **32**(1): p. 51–59.
65. Champion, D., Dumanchin, C. Hannequin, D., Dubois, B., Belliard, S., Puel, M., Thomas-Anterion, C., Michon, A., Martin, C., Charbonnier, F., Raux, G., Camuzat, A., Penet, C., Mesnage, V., Martinez, M., Clerget-Darpoux, F., Brice, A., Frebourg, T., *Early-onset autosomal dominant Alzheimer disease: prevalence, genetic heterogeneity, and mutation spectrum*. Am. J. Hum. Genet., 1999. **65**: p. 664-670.
66. Strittmatter, W.J., Roses, A. D., *Apolipoprotein E and Alzheimer's disease*. Annu. Rev. Neurosci., 1996. **19**: p. 53-77.
67. Hutton, M., Perez-Tur, J., Hardy, J., *Genetics of Alzheimer's disease*. Biochem., 1998. **33**: p. 117-131.
68. Steiner, H., Haass, C. , *Intramembrane proteolysis by presenilins*. Nat. Rev. Mol. Cell. Biol., 2000. **1**: p. 217-224.
69. Holcomb, L., Gordon, M. N., McGowan, E., Yu, X., Benkovic, S., Jantzen, P., Wright, K., Saad, I., Mueller, R., Morgan, D., Sanders, S., Zehr, C., O'Campo, K., Hardy, J., Prada, C.-M., Eckman, C., Younkin, S., Hsiao, K., Duff, K., *Accelerated Alzheimer type phenotype in transgenic mice carrying both mutant amyloid precursor protein and presenilin 1 transgenes*. Nat. Med., 1998. **4**: p. 97-100.
70. Cole, S.L., Vassar, R., *The Alzheimer's disease  $\beta$ -secretase enzyme, BACE1*. Mol. Neurodegener., 2007. **2**(1): p. 22.
71. Nussbaum, R.L., Ellis, C. E., *Alzheimer's disease and Parkinson's disease*. N. Engl. J. Med., 2003. **348**(14): p. 1356-1364.
72. Kumar, A., Singh, A., Ekavali, *A review on Alzheimer's disease pathophysiology and its management: an update*. Pharmacol. Rep., 2015. **67**: p. 195-203.
73. Rashid, U., Ansari, F. L., *Challenges in designing therapeutic agents for treating Alzheimer's disease - from serendipity to rationality*, in *Drug design and discovery in Alzheimer's disease*, M.I.C. Atta-ur-Rahman, Editor. 2015, Elsevier. p. 40-141.
74. Christen, Y., *Oxidative stress and Alzheimer disease*. Am. J. Clin. Nutr., 2000. **71**(suppl): p. 621S–629S.

- 
75. Perry, G., Cash, A. D., Smith, M. A., *Alzheimer Disease and Oxidative Stress*. J. Biomed. Biotechnol., 2002. **2**(3): p. 120-123.
  76. Yasuda, T., Nakata, Y., Mochizuki, H.,  *$\alpha$ -synuclein and neuronal cell death*. Mol. Neurobiol., 2013. **47**: p. 466-483.
  77. Bellucci, A., Navarria, L., Zaltieri, M., Missale, C., Spanoa, P., *Alpha-synuclein synaptic pathology and its implications in the development of novel therapeutic approaches to cure Parkinson's disease*. Brain Research., 2012. **1432**: p. 95-113.
  78. Obeso, J., Rodriguez-Oroz, M., Goetz, C., Marin, C., Kordower, J., Rodriguez, M., Hirsch, E., Farrer, M., Schapira, A., Halliday, G., *Missing pieces in the Parkinson's disease puzzle* Nature Medicine, 2010. **16**(6): p. 653-661.
  79. Dauer, W., Przedborski, S., *Parkinson's disease: Mechanisms and models*. Neuron., 2003. **39**: p. 889-909.
  80. Corti, O., Lesage, S., Brice, A., *What genetics tells us about the causes and mechanisms of Parkinson's disease*. Physiol. Rev., 2011. **91**: p. 1161–1218.
  81. Šumec, R., Filip, P., Sheardová, K., Bareš, M., *Psychological benefits of nonpharmacological methods aimed for improving balance in Parkinson's disease: A systematic review*. Behav Neurol., 2015: p. 620-674.
  82. Zigmond, M.J., Smeyne, R. J., *Exercise: is it a neuroprotective and if so, how does it work?* Parkinsonism Relat Disord., 2014. **20**( Suppl 1): p. S123–127.
  83. Hokfelt, T., in *Frontiers in Catecholamine Research*, S.S. E. Usdin, Editor. 1973, Pergamon: Elmsford, NY. p. 439.
  84. Vulliet, P.R., Langan, T. A., Weiner, N., *Tyrosine hydroxylase: a substrate of cyclic AMP-dependent protein kinase*. Proc Natl Acad Sci USA, 1980. **77**(1): p. 92-96.
  85. Aghajanian, G.K., Bunney, B. S., in *Frontiers in Catecholamine Research*, S.S. E. Usdin, Editor. 1973, Pergamon: Elmsford, NY. p. 643.
  86. Bartholini, G., Stadler, H., Lloyd, K. G., in *Frontiers in Catecholamine Research*, S.S. E. Usdin, Editor. 1973, Pergamon: Elmsford, NY. p. 471.
  87. Shore, P.A., *Transport and storage of biogenic amines*. Ann Rev Pharm, 1972. **12**: p. 209-226.
  88. Iverson, L.L., in *Frontiers in Catecholamine Research*, S.S. E. Usdin, Editor. 1973, Pergamon: Elmsford, NY. p. 403.
  89. Binda, C., Mattevi, A., Edmondson, D. E., *Structural properties of human monoamine oxidases A and B*. International Review of Neurobiology, 2011. **100**: p. 1-11.



- 
90. Edmondson, D.E., Binda, C., Mattevi, A., *Structural insights into the mechanism of amine oxidation by monoamine oxidases A and B*. Archives of Biochemistry and Biophysics, 2007. **464**(2): p. 269-276.
91. Binda, C., Newton-Vinson, P., Hubalek, F., Edmondson, D. E., Mattevi, A. , *Structure of human monoamine oxidase B, a drug target for the treatment of neurological disorders. .* Nat. Struct. Biol., 2002. **9**: p. 22-26.
92. Gaweska, H., Fitzpatrick, P. F., *Structures and mechanism of the monoamine oxidase family*. Biomol. Concepts 2011. **2**(5): p. 365-377.
93. Geha, R.M., Chen, K., Wouters, J., Ooms, F., Shih, J. C. , *Analysis of conserved active site residues in monoamine oxidase A and B and their three-dimensional molecular modeling. .* J. Biol. Chem., 2002. **277**: p. 17209-17216.
94. Binda, C., Li, M., Hubalek, F., Restelli, N., Edmondson, D. E., Mattevi, A., *Insights into the mode of inhibition of human mitochondrial monoamine oxidase B from high-resolution crystal structures*. Proc. Natl Acad. Sci. USA, 2003. **100**: p. 9750-9755.
95. Son, S.-Y., Ma, J., Kondou, Y., Yoshimura, M., Yamashita, E., Tsukihara, T. , *Structure of human monoamine oxidase A at 2.2-Å resolution: The control of opening the entry for substrates/inhibitors. .* Proc. Nat. Acad. Sci. USA., 2008. **105**: p. 5739-5744.
96. Edmondson, D.E., Binda, C., Mattevi, A., *The FAD Binding Sites of Human Monoamine Oxidases A and B*. NeuroToxicology, 2004. **25**(1–2): p. 63-72.
97. Binda, C., et al., *Crystal structure of human monoamine oxidase B, a drug target enzyme monotonically inserted into the mitochondrial outer membrane*. FEBS Letters, 2004. **564**(3): p. 225-228.
98. Abad, E., Zenn, R. K., Kästnerand, J., *Reaction mechanism of monoamine oxidase from QM/MM calculations*. J. Phys. Chem. B, 2013. **117**(46): p. 14238–14246.
99. Silverman R. B., H., S. J., Catus, W. B., *A mechanism for mitochondrial monoamine oxidase catalyzed amine oxidation*. J. Am. Chem. Soc., 1980. **102**: p. 7126–7128.
100. Edmondson, D.E., *Aminium cation radical mechanism proposed for monoamine oxidase B catalysis: are there alternatives?* Xenobiotica, 1995. **25**: p. 735-753.
101. Kim, J.M., Bogdan, M. A., Mariano, P. S., *Mechanistic analysis of the 3-methylflavin-promoted oxidative deamination of benzylamine. A potential model for monoamine oxidase catalysis*. J.Am.Chem.Soc., 1993. **115**: p. 10591–10595.
102. Fitzpatrick, P.F., *Oxidation of amines by flavoproteins*. Arch. Biochem. Biophys., 2010. **493**: p. 13–25.

- 
103. Lashuel, H.A., Overk, C. R., Oueslati, A., Masliah, E., *The many faces of  $\alpha$ -synuclein: from structure and toxicity to therapeutic target*. Nature Review Neuroscience, 2013. **14**: p. 38-48.
104. Ueda, K., Masliah, E., Xia, Y., Iwai, A., Yoshimoto, M., Saitoh, T. *Novel amyloid component (NAC) differentiates Alzheimer's disease from normal aging plaques*. in Soc. Neurosci. Abstr. 1993.
105. Lee, V., Trojanowski, J., *Mechanisms of Parkinson's disease linked to pathological  $\alpha$ -synuclein: new targets for drug discovery*. Neuron, 2006. **52**: p. 33-38.
106. Mao, X.e.a., *Pathological  $\alpha$ -synuclein transmission initiated by binding lymphocyte-activation gene 3*. Science, 2016. **353**(6307).
107. Abounit, S., Bousset, L., Loria, F., Zhu, S., de Chaumont, F., Pieri, L., Olivo-Marin, J.-C., Melki, R., Zurzolo, C., *Tunneling nanotubes spread fibrillar  $\alpha$ -synuclein by intercellular trafficking of lysosomes*. EMBO J., 2016. **35**: p. 2120–2138.
108. Winner, B., Jappelli, R., Maji, S. K., Desplats, P.A., Boyer, L., Aigner, S., Hetzer, C., Loher, T., Vilar, M., Campioni, S., Tzitzilonis, C., Soragni, A., Jessberger, S., Mira, H., Consiglio, A., Pham, E., Masliah, E., Gage, F. H., Riek, R., *In vivo demonstration that  $\alpha$ -synuclein oligomers are toxic*. Proc. Natl Acad. Sci. USA, 2011. **108**(10): p. 4194-4199.
109. Hsu, L.J., Sagara, Y., Arroyo, A., Rockenstein, E., Sisk, A., Mallory, M., Wong, J., Takenouchi, T., Hashimoto, M., Masliah, E.,  *$\alpha$ -Synuclein Promotes Mitochondrial Deficit and Oxidative Stress*. The American Journal of Pathology, 2000. **157**(2): p. 401-410.
110. Hashimoto, M., Kawahara, K., Bar-On, P., Rockenstein, E., Crews, L., Masliah, E., *The role of  $\alpha$ -synuclein assembly and metabolism in the pathogenesis of Lewy body disease*. Journal of Molecular Neuroscience, 2004. **24**(3): p. 343-352.
111. Cooper, A.A., Gitler, A. D., Cashikar, A., Haynes, C. M., Hill, K. J., Bhullar, B., Liu, K., Xu, K., Strathearn, K. E., Liu, F., Cao, S., Caldwell, K. A., Caldwell, G. A., Marsischky, G., Kolodner, R. D., LaBaer, J., Rochet, J.-C., Bonini, N. M., Lindquist, S.,  *$\alpha$ -Synuclein Blocks ER-Golgi Traffic and Rab1 Rescues Neuron Loss in Parkinson's Models*. Science (New York, N.Y.), 2006. **313**(5785): p. 324-328.
112. Scott, D.A., Tabarean, I., Tang, Y., Cartier, A., Masliah, E., Roy, S., *A pathologic cascade leading to synaptic dysfunction in  $\alpha$ -synuclein-induced neurodegeneration*. The Journal of neuroscience : the official journal of the Society for Neuroscience, 2010. **30**(24): p. 8083-8095.

- 
113. Danzer, K.M., Haasen, D., Karow, A. R., Moussaud, S., Habeck, M., Giese, A., Kretschmar, H., Hengerer, B., Kostka, M. and *Different Species of  $\alpha$ -Synuclein Oligomers Induce Calcium Influx and Seeding*. Journal of Neuroscience, 2007. **27**(34): p. 9220-9232.
  114. Bellucci, A., Zaltieri, M., Navarra, L., Grigoletto, J., Missale, C., Spanoa, P., *From  $\alpha$ -synuclein to synaptic dysfunctions: New insights into the pathophysiology of Parkinson's disease*. Brain Research, 2012. **1476**: p. 183-202.
  115. Youdim, M.B.H., Lavie, L. , *Selective MAO-A and B inhibitors, radical scavengers and nitric oxide synthase inhibitors in Parkinson's disease*. Life Sciences, 1994. **55**(25-26): p. 2077-2082.
  116. Sies, H., Cadenas, E. , *Oxidative stress: damage to intact cells and organs*. Philos Trans R Soc Lond B Biol Sci., 1985. **311**: p. 617–631.
  117. Chinta, S.J., Andersen, J. K., *Redox imbalance in Parkinson's disease*. Biochimica et Biophysica Acta, 2008. **1780**: p. 1362–1367.
  118. Scherman, D., Desnos, C., Darchen, F., Pollak, P., Javoy-Agid, F., Agid, Y. , *Striatal dopamine deficiency in Parkinson's disease: role of aging*. Ann Neurol. , 1989. **26**: p. 551–557.
  119. Jenner, P., Olanow, C. W. , *Oxidative stress and the pathogenesis of Parkinson's disease*. Neurology. , 1996. **47**: p. S161–S170.
  120. Jenner, P., *Presymptomatic detection of Parkinson's disease*. J Neural Transm Suppl. , 1993. **40**: p. 23–36.
  121. Braak, H., Braak, E. , *Pathoanatomy of Parkinson's disease*. J Neurol. , 2000. **247**(Suppl 2): p. II 3–10.
  122. Paxinou, E., Chen, Q., Weisse, M., Giasson, B. I., Norris, E. H., Rueter, S. M., et al. , *Induction of alpha-synuclein aggregation by intracellular nitrative insult*. J Neurosci. , 2001. **21**: p. 8053–8061.
  123. Ischiropoulos, H., Beckman, J. S. , *Oxidative stress and nitration in neurodegeneration: cause, effect, or association?* . J Clin Invest., 2003. **11**: p. 163–169.
  124. Uversky, V.N., Li, J., Fink, A. L. , *Metal-triggered structural transformations, aggregation, and fibrillation of human  $\alpha$ -synuclein*. J Biol Chem., 2001. **23**: p. 44284–44296.
  125. Hashimoto, M., Hsu, L. J., Xia, Y., Takeda, A., Sisk, A., Sundsmo, M., Masliah, E. , *Oxidative stress induces amyloid-like aggregate formation of NACP/ $\alpha$ -synuclein in vitro*. Neuroreport., 1999. **10**: p. 717–721.

126. Thomas, M.P., Chartrand, K., Reynolds, A., Vitvitsky, V., Banerjee, R., Gendelman, H. E. , *Ion channel blockade attenuates aggregated alpha synuclein induction of microglial reactive oxygen species: relevance for the pathogenesis of Parkinson's disease*. J Neurochem., 2007. **100**: p. 503–519.
127. Salomone, S., Caraci, F., Leggio, G. M., Fedotova, J., Drago, F., *New pharmacological strategies for treatment of Alzheimer's disease: focus on disease modifying drugs*. Br. J. Clin. Pharmacol., 2011. **73**(4): p. 504–517.
128. INFARMED. <https://www.infarmed.pt/prontuario/index.php>. 2016 [cited 2016].
129. Kosasa, T., Kuriya, Y., Matsui, K., Yamanishi, Y., *Effect of donepezil hydrochloride (E2020) on basal concentration of extracellular acetylcholine in the hippocampus of rats*. Eur. J. Pharmacol., 1999. **380**: p. 101-107.
130. Anand, R., Gharabawi, G. , *Clinical development of Exelon™ (ENA 713): The ADENA programme*. J Drug Dev Clin Pract, 1996. **8**: p. 9-14.
131. Anand, R., Gharabawi, G., Enz, A. , *Efficacy and safety results of the early phase studies with Exelon (ENA-713) in Alzheimer's disease: an overview*. J. Drug Dev. Clin. Pract., 1996. **8**: p. 109-116.
132. Lilienfeld, S., *Galantamine-a novel cholinergic drug with a unique dual mode of action for the treatment of patients with Alzheimer's disease*. CNS Drug Review, 2002. **8**(2): p. 159-176.
133. Reisberg, B., Doody, R., Stöffler, A., Schmitt, F., Ferris, S., Möbius, H. J., *Memantine in moderate-to-severe Alzheimer's disease*. N. Engl. J. Med., 2003. **348**(14): p. 1333-1341.
134. Scarpini, E., Schelterns, P., Feldman, H., *Treatment of Alzheimer's disease; current status and new perspectives*. Lancet neurol., 2003. **2**(9): p. 539-547.
135. Spencer, C., Noble, S., *Rivastigmine: A Review of its Use in Alzheimer's Disease*. Drugs Aging, 1998. **13**(5): p. 391–411.
136. Sramek, J.J., Frackiewicz, E. J., Cutler, N. R. , *Review of the acetylcholinesterase inhibitor galanthamine*. Expert Opin. Invest. Drugs, 2000. **9**: p. 2393-2402.
137. Zhou, J., Fu, Y., Tang, X. C. , *Huperzine A and donepezil protect rat pheochromocytoma cells against oxygen–glucose deprivation*. Neurosci. Lett., 2001. **306**(1–2): p. 53–56.
138. Geldenhuys, W.J., Darvesh, A. S. , *Pharmacotherapy of Alzheimer's disease: current and future trends*. Expert Rev. Neurother., 2015. **15**(1): p. 3-5.
139. Leon, R., Garcia, A. G., Marco-Contelles, J., *Recent advances in the multitarget-directed ligands approach for the treatment of Alzheimer's disease*. Med. Res. Rev., 2013. **33**(1): p. 139–189.

- 
140. Selkoe, D.J., Hardy, J. , *The amyloid hypothesis of Alzheimer's disease at 25 years*. EMBO Mol. Med., 2016. **8**(6): p. 595-608
  141. Hardy, J., *The amyloid hypothesis for Alzheimer's disease: a critical reappraisal*. J. Neurochem., 2009. **110**(4): p. 1129–1134.
  142. Sevigny, J.e.a., *The antibody aducanumab reduces A $\beta$  plaques in Alzheimer's disease*. Nature 2016. **537**(7618): p. 50-56.
  143. Nunomura, A., Perry, G., Aliev, G., Hirai, K., Takeda, A., Balraj, E. K., Jones, P. K., Ghanbari, H., Wataya, T., Shimohama, S., Chiba, S., Atwood, C. S., Petersen, R. B., Smith, M. A., *Oxidative damage is the earliest event in Alzheimer disease*. J. Neuropathol. Exp. Neurol., 2001. **60**(8): p. 759 767.
  144. Reiter, R., *Oxidative damage in the central nervous system: protection by melatonin*. Prog. Neurobiol., 1998. **56**(3): p. 359-384.
  145. Dysken, M.W., Sano, M., Asthana, S., Vertrees, J. E., Pallaki, M., Llorente, M., Love, S., Schellenberg, G. D., McCarten, J. R., Malphurs, J., Prieto, S., Chen, P., Guarino, P. D., et al., *Effect of vitamin E and memantine on functional decline in Alzheimer disease*. JAMA, 2014. **311**(1): p. 33-44.
  146. Bush, A.J., *Drug development based on the metals hypothesis of Alzheimer's disease*. J. Alzheimers Dis., 2008. **15**(2): p. 223-240.
  147. Bush, A.I., Tanzi, R. E., *Therapeutics for Alzheimer's disease based on the metal hypothesis*. Neurotherapeutics., 2008. **5**(3): p. 421-432.
  148. Huang, X.D., Moir, R. D., Tanzi, R. E., Bush, A. I., Rogers, J. T. , *Redox-active metals, oxidative stress, and Alzheimer's disease pathology*. Ann. N. Y. Acad. Sci., 2004. **1012**: p. 153–163.
  149. Crapper McLachlan, D.R., Dalton, A. J., Kruck, T. P., Bell, M. Y., Smith, W. L., Kalow, W., Andrews, D. F., *Intramuscular desferrioxamine in patients with Alzheimer's disease*. Lancet., 1991. **337**(8753): p. 1304-1308.
  150. Ritchie, C.W., Bush, A. I., Mackinnon, A., Macfarlane, S., Mastwyk, M., MacGregor, L., Kiers, L., Cherny, R., Li, Q., Tammer, A., Carrington, D., Mavros, C., Volitakis, I., Xilinas, M., Ames, D., Davis, S., Beyreuther, K., Tanzi, R. E., Masters, C. L., *Metal-protein attenuation with iodochlorhydroxyquin (clioquinol) targeting A $\beta$  amyloid deposition and toxicity in Alzheimer disease*. Arch. Neurol., 2003. **60**(12): p. 1685-1691.
  151. Lannfelt, L., Blennow, K., Zetterberg, H., Batsman, S., Ames, D., Harrison, J., Masters, C. L., Targum, S., Bush, A. I., Murdoch, R., Wilson, J., Ritchie, C. W., *Safety, efficacy, and biomarker findings of PBT2 in targeting A $\beta$  as a modifying therapy for Alzheimer's*

- disease: a phase IIa, double-blind, randomised, placebo-controlled trial. *Lancet Neurol.* , 2008. **7**(9): p. 779–786.
152. Cavalli, A., Bolognesi, M. L., Minarini, A., Rosini, M., Tumiatti, V., Recanatini, M., Melchiorre, C. J., *Multi-target-directed ligands to combat neurodegenerative diseases*. *J. Med. Chem.*, 2008. **51**(3): p. 347–372.
153. Bajda, M., Guzior, N., Ignasik, M., Malawska, B. , *Multi-target-directed ligands in Alzheimer's disease treatment*. *Curr. Med. Chem.*, 2011. **18**(32): p. 4949 - 4975.
154. Li , Y., Peng , P., Tang , L., Hu, Y., Hu, Y., Sheng, R., *Design, synthesis and evaluation of rivastigmine and curcumin hybrids as site-activated multitarget-directed ligands for Alzheimer's disease therapy*. *Bioorg. Med. Chem.*, 2014. **22**: p. 4717–4725.
155. Cavalli, A., Bolognesi, M. L., Capsoni, S., Andrisano, V., Bartolini, M., Margotti, E., Cattaneo, A., Recanatini, M., Melchiorre, C. , *A small molecule targeting the multifactorial nature of Alzheimer's disease*. *Angew. Chem., Int. Ed.*, 2007. **46**(20): p. 3689–3692.
156. Marco-Contelles, J., León, R., de los Ríos, C., Guglietta, A., Terencio, J., López, M. G., García, A. G., Villarroya, M., *Novel multipotent tacrine–dihydropyridine hybrids with improved acetylcholinesterase inhibitory and neuroprotective activities as potential drugs for the treatment of Alzheimer's disease*. *J. Med. Chem.* , 2006. **49**(26): p. 7607-7610.
157. Gal, S., Zheng, H., Fridkin, M., Youdim, M. B., *Novel multifunctional neuroprotective iron chelator-monoamine oxidase inhibitor drugs for neurodegenerative diseases. In vivo selective brain monoamine oxidase inhibition and prevention of MPTP-induced striatal dopamine depletion*. *J. Neurochem.*, 2005. **95**: p. 79-88.
158. Youdim, M.B.H., *The path from anti Parkinson drug selegiline and rasagiline to multifunctional neuroprotective anti Alzheimer drugs ladostigil and M30*. *Curr. Alzheimer Res.* , 2006. **3**(5): p. 541 - 550.
159. Weinreb, O., Amit, T., Bar-Am, O., Youdim, M. B., *Ladostigil: a novel multimodal neuroprotective drug with cholinesterase and brain-selective monoamine oxidase inhibitory activities for Alzheimer's disease treatment*. *Curr Drug Targets*, 2012. **13**(4): p. 483-494.
160. Tetrad, J.W., Langston, J. W., *The effect of deprenyl (selegiline) on the natural history of Parkinson's disease*. *Science*, 1989. **245**(4917): p. 519-522.
161. Group., P.S., *Effect of deprenyl on the progression of disability in early Parkinson's disease*. *N. Engl. J. Med.*, 1989. **321**: p. 1364-1371.

- 
162. Hart, R.G., Pearce, L. A., Ravina, B. M., Yal thro, T. C., Marler, J. R., *Neuroprotection trials in Parkinson's disease: systematic review*. *Mov. Disord.*, 2009. **24**(5): p. 647-654.
163. Albin, R.L., Frey, K. A. , *Initial agonist treatment of Parkinson disease: a critique*. *Neurology*, 2003. **60**(3): p. 390-394.
164. Spillantini, M.G., Schmidt, M. L., Lee, V. M., Trojanowski, J. Q., Jakes, R., Goedert, M., *Alpha-synuclein in Lewy bodies*. *Nature*, 1997. **388**(6645): p. 839-840.
165. Mandel, S., Grünblatt, E., Riederer, P., Gerlach, M., Levites, Y., Youdim, M. B. H. , *Neuroprotective Strategies in Parkinson's Disease, An Update on Progress*. *CNS Drugs*, 2003. **17**(10): p. 729-762.
166. Ingkaninan, K., de Best, C., Irth, H., van der Heijden, R., Hofte, A., Karabatak, B., Tjaden, U., van der Greef, J., Verpoorte, R. , *High-performance liquid chromatography with on-line coupled UV, mass spectrometric and biochemical detection for identification of acetylcholinesterase inhibitors from natural products*. *J. Chromatogr. A*, 2000. **872**(1-2): p. 61-73.
167. Ingkaninan, K., Temkitthawon, P., Chuenchom, K., Yuyaem, T., Thongnoi, W. , *Screening for acetylcholinesterase inhibitory activity in plants used in Thai traditional rejuvenating and neurotonic remedies*. *J. Ethnopharmacol.*, 2003. **89**(2-3): p. 261-264.
168. Carmona, G.N., Jufer, R. A., Goldberg, S. R., Gorelick, D. A., Greig, N. H., Yu, Q.-S., Cone, E. J., Schindler, C. W. , *Butyrylcholinesterase accelerates cocaine metabolism: In vitro and in vivo effects in nonhuman primates and humans*. *Drug Metab. Dispos.*, 2000. **28**(3): p. 367-371.
169. Cokugras, A., *Butyrylcholinesterase: Structure and physiological importance*. *Turkish J. Biochem.*, 2003. **28**(2): p. 54-61.
170. Kuhl, D., Koeppe, R., Snyder, S., Minoshima, S., Frey, K., Kilbourn, M., *In vivo butyrylcholinesterase Activity is not Increased in Alzheimer's Disease Synapses*. *Annals of Neurology*, 2006. **59**: p. 13-20.
171. Zhao, T., Ding, K., Zhang, L., Cheng, X., Wang, C., Wang, Z., *Acetylcholinesterase and Butyrylcholinesterase Inhibitory Activities of B-Carboline and Quinoline Alkaloids Derivatives from the Plants of Genus Peganum*. *Journal of Chemistry*, 2013: p. 1-6.
172. Van Marum, R., *Current and future therapy in Alzheimer's disease*. *Fundamentals on Clinical Pharmacology*, 2008. **22**(3): p. 265-274.
173. Johnston, J.P., *Some observations upon a new inhibitor of monoamine oxidase in brain tissue*. *Biochemical Pharmacology*, 1968. **17**(7): p. 1285-1297.

- 
174. Youdim, M.B.H., Finberg, J. P. M., Tipton, K. F., *Amine Oxidases*, in *Handbook of Experimental Pharmacology*, N. Weiner, Trendelenburg, U., Editor. 1988, Springer-Verlag: Berlin. p. 119-192.
175. Wolters, E.C. and H. Braak, *Parkinson's disease: premotor clinico-pathological correlations*, in *Parkinson's Disease and Related Disorders*, P. Riederer, et al., Editors. 2006, Springer Vienna: Vienna. p. 309-319.
176. O'Carroll, A.-M., Fowler, C. J., Phillips, J. P., Tobbia, I., Tipton, K. F., *The deamination of dopamine by human brain monoamine oxidase*. *Naunyn-Schmiedeberg's Archives of Pharmacology*, 1983. **322**(3): p. 198-202.
177. Ingkaninan, K., Temkitthawon, P., Chuenchom, K., Yuyaem, T., Thongnoi, W. , *Screening for acetylcholinesterase inhibitory activity in plants used in Thai traditional rejuvenating and neurotonic remedies*. *Journal of Ethnopharmacology*, 2003(89): p. 261-264.
178. Ellman, G., Courtney, K., Andres, V., Featherstone, R., *A new and rapid colorimetric determination of acetylcholinesterase activity*. *Biochemical Pharmacology*, 1961. **7**: p. 88-95.
179. Holt, A.e.a., *A continuous spectrophotometric assay for monoamine oxidase and related enzymes in tissue homogenates*. *Anal. Biochem.*, 1997. **244**: p. 384-392.
180. Zhou, M., Panchuk-Voloshina, N., *A one-step fluorometric method for the continuous measurement of monoamine oxidase activity*. *Anal. Biochem.*, 1997. **253**: p. 169-174.
181. Atkins, P.W., *Physical Chemistry*. 5th ed. 1978: Oxford University Press.
182. Di Giovanni, S., Borloz, A., Urbain, A., Marston, A., Hostettmann, K., Carrupt, P.A., Reist, M., *In vitro screening assays to identify natural or synthetic acetylcholinesterase inhibitors: Thin layer chromatography versus microplate methods*. *Eur. J. Pharmacol. Sci.*, 2008. **33**: p. 109-119.
183. Copeland, R.A., *Enzymes: A practical introduction to structure, mechanism and data analysis*. 2nd Edition ed. 2000, NY: Wiley-VCH.
184. Dowd, J.E., Riggs, D. S., *A comparison of estimates of Michaelis-Menten kinetic constants from various linear transformations*. *J. Biol. Chem.*, 1965. **240**(2): p. 863-869.
185. Grieg, N., Utsuki, T., Ingram, D., Wang, Y., Pepeu, G., Scali, C., Yu, Q., Mamczarz, J., Holloway, H., Giordano, T., Chen, D., Furukawa, K., Sambamurti, K., Brossi, A., Lahiri, D., *Selective butyrylcholinesterase inhibition elevates brain acetylcholine, augments learning and lowers Alzheimer b-amyloid peptide in rodent*. *Proceedings of the National Academy of Sciences of the United States of America*, 2005. **102**(47): p. 17213-17218.



- 
186. Silver, A., *The biology of cholinesterases*. 1974, Amsterdam: Elsevier.
187. Enz, A., Boddeke, H., Gray, J., Spiegel, R., *Pharmacologic and clinicopharmacologic properties of SDZ ENA 713, a centrally selective acetylcholinesterase inhibitor*. Ann New York Acad Sci., 1991. **640**: p. 272-275.
188. Järvinen, P., Vuorela, P., Hatakka, A., Fallarero, A., *Potency determinations of acetylcholinesterase inhibitors using Ellman's reaction-based assay in screening: Effect of assay variants*. Anal. Biochem., 2011. **408**: p. 166-168.
189. Tasso, B., Catto, M., Nicolotti, O., Novelli, F., Tonelli, M., Giangreco, I., Pisani, L., Sparatore, A., Boido, V., Carotti, A., Sparatore, F., *Quinolizidinyl derivatives of bi- and tricyclic systems as potent inhibitors of acetyl- and butyrylcholinesterase with potential in Alzheimer's disease*. Eur. J. Med. Chem., 2011. **46**(6): p. 2170-2184.
190. Guillou, C., Mary, A., Renko, D.Z., Gras, E., Thal, C., *Potent acetylcholinesterase inhibitors: design, synthesis and structure-activity relationships of alkylene linked bis-galanthamine and galanthamine-galanthaminium salts*. Bioorg. Med. Chem. Lett., 2000. **10**(7): p. 637-639.
191. Liston, D.R., Nielsen, J.A., Villalobos, A., Chapin, D., Jones, S.B., Hubbard, S.T., Shalaby, I.A., Ramirez, A., Nason, D., White, W.F., *Pharmacology of selective acetylcholinesterase inhibitors: implications for use in Alzheimer's disease*. Eur. J. Pharmacol., 2004. **486**: p. 9-17.
192. Camps, P., Formosa, X., Galdeano, C., Gómez, T., Muñoz-Torrero, D., Scarpellini, M., Viayna, E., Badia, A., Clos, M. V., Camins, A., Pallàs, M., Bartolini, M., Mancini, F., Andrisano, V., Estelrich, J., Lizondo, Mònica, Bidon-Chanal, A., Luque, F. J., *Novel donepezil-based inhibitors of acetyl- and butyrylcholinesterase and acetylcholinesterase-induced  $\beta$ -amyloid aggregation*. J. Med. Chem., 2008. **51**(12): p. 3588-3598.
193. Esteban, G., Allan, J., Samadi, A., Mattevi, A., Unzeta, M., Marco-Contelles, J., Binda, C., Ramsay, R. R., *Kinetic and structural analysis of the irreversible inhibition of human monoamine oxidases by ASS234, a multi-target compound designed for use in Alzheimer's disease*. Biochimica et Biophysica Acta (BBA) - Proteins and Proteomics, 2014. **1844**(6): p. 1104-1110.
194. Martinez, A., Fernandez, E., Castro, A., Conde, S., Rodriguez-Franco, I., Baños, J.E., Badia, A., *N-Benzylpiperidine derivatives of 1,2,4-thiadiazolidinone as new acetylcholinesterase inhibitors*. Eur. J. Med. Chem., 2000. **35**: p. 913-922.

- 
195. Youdim, M.B.H., Bakhle, Y. S., *Monoamine oxidase: isoforms and inhibitors in Parkinson's disease and depressive illness*. Br. J. Pharmacol., 2006. **147**(S1): p. S287–S296.
196. Finberg, J.P.M., Youdim, M.B.H., Riederer, P., Tipton, K.F., *MAO - The Mother of all Amine Oxidases*. 2013: Springer Vienna.
197. Fowler, C.J., Wiberg, Å., Orelund, L., Winblad, B., *Titration of human brain type-B monoamine oxidase*. Neurochem. Res., 1980. **5**(7): p. 697-708.
198. Usdin, E., *Function and Regulation of Monoamine Enzymes: Basic and Clinical Aspects*. 2015: Palgrave Macmillan UK. 961.
199. Youdim, M.B.H., Gross, A., Finberg, J. P. M., *Rasagiline [N-propargyl-1R(+)-aminoindan], a selective and potent inhibitor of mitochondrial monoamine oxidase B*. Br. J. Pharmacol., 2001. **132**(2): p. 500-506.
200. Veitch, N.C., *Horseradish peroxidase: a modern view of a classic enzyme*. Phytochemistry, 2004. **65**(3): p. 249-259.
201. Zhou, M., Diwu, Z., Panchuk-Voloshina, N., Haugland, R. P., *A Stable Nonfluorescent Derivative of Resorufin for the Fluorometric Determination of Trace Hydrogen Peroxide: Applications in Detecting the Activity of Phagocyte NADPH Oxidase and Other Oxidases*. Anal. Biochem., 1997. **253**: p. 162-168.
202. Gorris, H.H., Walt, D. R., *Mechanistic Aspects of Horseradish Peroxidase Elucidated through Single-Molecule Studies*. J. Am. Chem. Soc., 2009. **131**(17): p. 6277-6282.
203. Krainer, F.W., Glieder, A. , *An updated view on horseradish peroxidases: recombinant production and biotechnological applications*. Appl Microbiol Biotechnol, 2015. **99**: p. 1611-1625.
204. Price, D., *New perspectives on Alzheimer's disease*. Ann. Rev. Neurosci., 1986. **9**: p. 489-512.
205. Wermuth, C.G., *The Practice of medicinal chemistry*. 3rd Ed. ed. 2011: Elsevier. 982.
206. Ariëns, E.J., *Stereoselectivity of bioactive agents: general aspects.*, in *Stereochemistry and biological activity of drugs.*, E.J. Ariëns, Soudjin, W., Timmermans, P. B. M. W. M., Editor. 1983, Blackwell Scientific Publications: Oxford. p. 11-32.
207. Mislow, K., *Molecular Chirality*, in *Topics in Stereochemistry*. 2007, John Wiley & Sons, Inc. p. 1-82.
208. Gal, J., *Chiral drugs from a historical point of view*, in *Chirality in drug research*, E. Francotte, Lindner, W., Editor. 2006, Wiley-VCH. p. 3-26.

- 
209. Burger, A., *Introduction: History and economics of medicinal chemistry*, in *Burger's Medicinal Chemistry, Part I*, M.E. Wolff, Editor. 1980, John Wiley & Sons: New York. p. 7-22.
210. Bacalhau, P., San Juan, A., Marques, C. S., Peixoto, D., Goth, A., Guarda, C., Silva, M., Arantes, S., Caldeira, A. T., Martins, R., Burke, A. J., *New cholinesterase inhibitors for Alzheimer's disease: Structure Activity Studies (SARs) and molecular docking of isoquinolone and azepanone derivatives*. *Bioorg. Chem.*, 2016. **67**: p. 1-8.
211. Totobenazara, J., Bacalhau, P., San Juan, A., Marques, C. S., Fernandes, L., Goth, A., Caldeira, A. T., Martins, R., Burke, A. J., *Design, synthesis and bioassays of 3-substituted-3-hydroxyoxindoles for cholinesterase inhibition*. *Chemistry Select*, 2016. **1**: p. 3580 – 3588.
212. Viana, H., *PhD dissertation*. 2016, University of Evora.
213. Glushkov, V.A., Shklyae, Y. V., *Synthesis of 1(2H)-Isoquinolones*. *Chem. Heterocycl. Compd.*, 2001. **37**(6): p. 663-687.
214. Krane, B.D., Shamma, M., *The isoquinolone alkaloids*. *J. Nat. Prod.*, 1982. **45**: p. 377-384.
215. Shamma, M., Moniot, J. L., *A new benzylisoquinoline alkaloid: N-methylpalaudinium chloride*. *J. Pharm. Sci.*, 1972. **61**(2): p. 295-296.
216. Shamma, M., Moniot, J. L., *Isoquinoline Alkaloids Research, 1972-1977*. 1978, New York: Plenum Press.
217. Gabriel, S., Colman, J., *Ueber die Einwirkung von Natriumalkylaten auf Phtalylglycinester und dessen Homologe*. *Ber. Deut. Chem. Ges.*, 1900. **33**: p. 980.
218. Sulkovski, T.S., Wille, M. A., *US Patent No. 3452027*. *Chem. Abstr.*, 1969. **71**: p. 112830.
219. Travers, D.N., Shammatt, M. A., Shah, K., *Recompression of tablets formed from direct compression bases [proceedings]*. *J. Pharm. Pharmacol.*, 1978. **30**(Suppl.): p. 20P.
220. Hasegava, M.S., Matsumoto, K., Suzuki, Y., Takahasi, I., *US Pat. 5441962*. *Chem. Abstr.*, 1994. **121**: p. 912.
221. Senda, O., Ohtani, O., Katho, E., Miyake, H., Fujiwara, K., *Ger. Offen 3031574*. *Chem. Abstr.*, 1981. **95**: p. 132692.
222. Jossang, A., Jossang, P., Hadi, H. A., Sevenet, T., Bodo, B., *Horsfiline, an oxindole alkaloid from Horsfieldia superba*. *J. Org. Chem.*, 1991. **56**(23): p. 6527–6530.

- 
223. Zhang, H.P., Kamano, Y., Ichihara, Y., Kizu, H., Komiyama, K., Itokawa, H., Pettit, G.R., *Isolation and structure of convolutamydines B-D from marine bryozoan Amathia convoluta*. Tetrahedron, 1995. **51**: p. 5523-5528.
224. Khuzhaev, V.U., Zhalolov, I., Turguniv, K.K., Tashkhodzhaev, B., Levkovich, M.G., Arpova, S.F., Shashkov, A.S., *Alkaloids from Arundo donax. XVII. structure of the dimeric indole alkaloid arundaphine*. Chem. Nat. Compd., 2004. **40**: p. 269-272.
225. Ochi, M., Kawasaki, K., Kataoka, H., Uchio, Y., Nishi, H., *AG-041R, a gastrin/CCK-B antagonist, stimulates chondrocyte proliferation and metabolism in vitro*. Biochem. Biophys. Res. Commun., 2001. **283**(5): p. 1118-1123.
226. Eshba, N.H., Salama, H. M., *5-(2-Oxo-3-Indolinylidene)thiazolidine-2,4-Dione-1,3-Di-Mannich Base Derivatives: Synthesis and Evaluation for Antileukemic Activity*. Pharmazie, 1985. **40**: p. 320-322.
227. Motzer, R.J., Michaelson, M. D., Redman, B. G., Hudes, G. R., Wilding, G., Figlin, R. A., Ginsberg, M. S., Kim, S. T., Baum, C. M., DePrimo, S. E., Li, J. Z., Bello, C. L., Theuer, C. P., George, D. J., Rini, B. I., *Activity of SU11248, a multitargeted inhibitor of vascular endothelial growth factor receptor and platelet-derived growth factor receptor, in patients with metastatic renal cell carcinoma*. J. Clin. Oncol. , 2006. **24**(1): p. 16-24.
228. Akrami, H., Mirjalili, B. F., Khoobi, M., Nadri, H., Moradi, A., Sakhteman, A., Emami, S., Foroumadi, A., Shafiee, A., *Indolinone-based acetylcholinesterase inhibitors: synthesis, biological activity and molecular modeling*. Eur. J. Med. Chem., 2014. **84**: p. 375-381.
229. Driggers, E.M., Hale, S. P., Lee, J., Terrett, N. K., *The exploration of macrocycles for drug discovery--an underexploited structural class*. Nat. Rev. Drug Discov. , 2008. **7**(7): p. 608 - 624.
230. Wang, L., Wang, Y., Tian, Y., Shang, J., Sun, X., Chen, H., Wang, H., Tan, W., *Design, synthesis, biological evaluation, and molecular modeling studies of chalcone-rivastigmine hybrids as cholinesterase inhibitors*. Bioorg. Med. Chem., 2017. **25**(1): p. 360-371.
231. Mustazza, C., Borioni, A., Giudice, M. R., Gatta, F., Ferretti, R., Meneguz, A., Volpe, M. T., Lorenzini, P., *Synthesis and cholinesterase activity of phenylcarbamates related to Rivastigmine, a therapeutic agent for Alzheimer's disease*. European Journal of Medicinal Chemistry, 2002. **37**(2): p. 91-109.

- 
232. Viegas, A., Manso, J., Nobrega, F. L., Cabrita, E. J., *Saturation-Transfer Difference (STD) NMR: A simple and fast method for ligand screening and characterization of protein binding*. J. Chem. Educ., 2011. **88**(7): p. 990–994.
233. Angulo, J., Nieto, P. M., *STD-NMR: Application to transient interactions between biomolecules-a quantitative approach*. Eur. Biophys. J., 2011. **40**(12): p. 1357-1369.
234. Mayer, M., Meyer, B., *Characterization of ligand binding by saturation transfer difference NMR spectroscopy*. Angew. Chem. Int. Ed, 1999. **38**(12): p. 1784-1788.
235. Berger, S., Braun, S., *200 and More NMR Experiments - A Practical Course*. 2014.
236. Meyer, B., Peters, T., *NMR spectroscopy techniques for screening and identifying ligand binding to protein receptors*. Angew. Chem. Int. Ed., 2003. **42**(8): p. 864–890.
237. Cokugras, A., *Butyrylcholinesterase: Structure and Physiological Importance*. Turkish Journal of Biochemistry, 2003. **28**: p. 54-61.
238. Carmona, G., *Butyrylcholinesterase accelerates cocaine metabolism: in vitro and in vivo effects in nonhuman primates and humans*. Drug Metabolism and Disposition, 1999. **28**: p. 367-371.
239. Cousin X., H.T., Liévin P., Toutant J. P., Chatonnet A. , *A cholinesterase genes server (ESTHER): a database of cholinesterase-related sequences for multiple alignments, phylogenetic relationships, mutations and structural data retrieval*. Nucleic Acids Res., 1996. **24**: p. 132–136.
240. Simon, S., Massoulié, J., *Cloning and Expression of Acetylcholinesterase from Electrophorus: Splicing pattern of the 3' exons in vivo and in transfected mammalian cells*. JBC, 1997. **272**: p. 33045-33055.
241. Bar-On, P., Millard, C. B., Harel, M., Dvir, H., Enz, A., Sussman, J. L., Silman, I. , *Kinetic and Structural Studies on the Interaction of Cholinesterases with the Anti-Alzheimer Drug Rivastigmine*. Biochemistry, 2002. **41**: p. 3555-3564.
242. Brus , B.K., U.; Turk , S.; Pišlar , A.; Coquelle , N.; Kos , J.; Stojan , J.; Colletier , J.-P.; Gobec , S., *Discovery, biological evaluation, and crystal structure of a novel nanomolar selective butyrylcholinesterase inhibitor*. J. Med. Chem., 2014. **57**: p. 8167–8179.
243. Kryger, G., Silman, I., Sussman, J. L., *Structure of acetylcholinesterase complexed with E2020 (Aricept): implications for the design of new anti-Alzheimer drugs*. Structure, 1999. **7**: p. 297–307.
244. Daranas, A.H., Khatib, S. K., Lysek, R., Vogel, P., Gavín, J. A. , *Determining the Role of the Aromatic Ring of N-Arylmethyl ent-conduramine F-1 in their Interactions with  $\alpha$ -*

- Glucosidases by Saturation Transfer Difference NMR Spectroscopy Experiments.* Chemistry Open, 2012. **1**(1): p. 13-16.
245. Harel, M., Schalk, I., Ehret-Sabatier, L., Bouet, F., Goeldner, M., Hirth, C., and P.H. Axelsen, Silman, I., and Sussman, J. L. , *Quaternary ligand binding to aromatic residues in the active-site gorge of acetylcholinesterase.* Proc. Natl Acad. Sci. USA, 1993. **90**: p. 9031-9035.
246. Harel, M., Silman, I., *Conversion of acetylcholinesterase to butyrylcholinesterase: modeling and mutagenesis.* Proc. Natl Acad. Sci. USA, 1992. **89**: p. 10827-10831.
247. Inoue, A., Kawai, T., Wakita, M., Imura, Y., Sugimoto, H., Kawakami, Y., *The simulated binding of (+/-)-2,3-dihydro-5,6-dimethoxy-2-[(1-(phenylmethyl)-4-piperidinyl)methyl]-1H-inden-1-one hydrochloride (E2020) and related inhibitors to free and acylated acetylcholinesterases and corresponding structure-activity analyses.* J. Med. Chem., 1996. **39**: p. 4460-4470.
248. Dougherty, D., *Cation- $\pi$  interactions in chemistry and biology: A new view of benzene, Phe, Tyr, and Trp.* Science, 1996. **271**: p. 163-168.
249. M. Nishio, M.H., Y. Umezawa, Y., *The CH/P interaction: Evidence, nature and consequences.* 1998, New York.
250. Cardozo, M.G., Imura, Y., Sugimoto, H., Yamanishi, Y., Hopfinger, A. J., *QSAR analyses of the substituted indanone and benzylpiperidine rings of a series of indanone-benzylpiperidine inhibitors of acetylcholinesterase.* J. Med. Chem., 1992. **35**: p. 584-589.
251. Greenblatt, H.M., Guillou, C., Guenard, D., Argaman, A., Botti, S., Badet, B., Thal, C., Silman, I., Sussman, J.L. , *The complex of a bivalent derivative of galanthamine with torpedo acetylcholinesterase displays drastic deformation of the active-site gorge: implications for structure-based drug design.* J Am Chem Soc. , 2004. **126**(47): p. 15405-15411.
252. Greenblatt, H.M., Kryger, G., Lewis, T., Silman, I., Sussman, J. L., *Structure of acetylcholinesterase complexed with (-)-galanthamine at 2.3 Å resolution.* FEBS Letters, 1999. **463**(3): p. 321-326.
253. Bartolucci, C., Perola, E., Pilger, C., Fels, G., Lamba, D., *Three-dimensional structure of a complex of galanthamine (Nivalin®) with acetylcholinesterase from Torpedo californica: Implications for the design of new anti-Alzheimer drugs.* Proteins: Struct., Funct., Bioinf., 2001. **42**(2): p. 182-191.

- 
254. Cheung, J., Rudolph, M. J., Burshteyn, F., Cassidy, M. S., Gary, E. N., Love, J., Franklin, M. C., Height, J. J., *Structures of human acetylcholinesterase in complex with pharmacologically important ligands*. *J. Med. Chem.*, 2012. **55**(22): p. 10282–10286.
255. Bacalhau, P., San Juan, A., Goth, A., Caldeira, A. T., Martins, R., Burke, A. J., *Insights into (S)-rivastigmine inhibition of butyrylcholinesterase (BuChE): Molecular docking and saturation transfer difference NMR (STD-NMR)*. *Bioorg. Chem.*, 2016. **67**: p. 105-109.
256. Finberg, J.P.M., Lamensdorf, I., Commissiong, J. W., youdim, M. B. H., *Pharmacology and neuroprotective properties of rasagiline*. *J. Neural. Transm.*, 1996. **48**: p. 95-101.
257. Youdim, M.B., Wadia, A., Tatton, W., Weinstock, M., *Parkinson drug rasagiline and its cholinesterase inhibitor derivatives exert neuroprotection unrelated to MAO inhibition in cell culture and in vivo*. *Ann. N. Y. Acad. Sci.*, 2001. **939**: p. 450-458.
258. Binda, C., Hubalek, F., Li, M., Herzig, Y., Sterling, J., Edmondson, D. E., Mattevi, A., *Crystal structures of monoamine oxidase B in complex with four inhibitors of the N-propargylaminoindan class*. *J. Med. Chem.*, 2004. **47**: p. 1767-1774.
259. Youdim, M.B.H., Edmondson, D., Tipton, K. F., *The therapeutic potential of monoamine oxidase inhibitors*. *Nature Rev. Neuroscience*, 2006. **7**: p. 295-309.
260. Viegas, A., Manso, J., Nóbrega, F., Cabrita, E., *J. Chem. Educ.*, 2011. **88**: p. 990-994.
261. Angulo, J., Nieto, P. M., *Eur. Biophys. J.*, 2011. **40**: p. 1357-1369.
262. Meyer, B., Peters, T. and *Angew. Chem. Int. Ed.*, 2003. **42**: p. 864 - 890.
263. Daranas, A., Khatib, S., Lysek, R., Vogel, P., Gavin, J., *Chemistry Open*, 2012. **1**: p. 13-16.
264. San Juan, A.B., P.; Marques; C. S.; Peixoto, D.; Goth, A.; Martins, M. R.; Caldeira, A. T.; Burke, A. J., *Identification of privileged scaffolds as cholinesterase inhibitor (ChEI) towards in silico functional group optimization based on a unique structure between the peripheral sites of AChE and BuChE*. *Bioorg. Med. Chem.*, (submitted).
265. Mayer, M., Meyer, B. and *Angew. Chem. Int. Ed.*, 1999. **38**: p. 1784-1788.
266. Smith, C.P., Bores, G. M., Petko, W., Li, M., Selk, D. E., Rush, D. K., Camacho, F., Winslow, J. T., Fishkin, R., Cunningham, D. M., Brooks, K. M., Roehr, J., Hartman, H. B., Davis, L., Vargas, H., *Pharmacological activity and safety profile of P10358, a novel, orally active acetylcholinesterase inhibitor for Alzheimer's disease*. *JPET*, 1997. **280**(2): p. 710-720.
267. Hodgson, E., Levi, P. E., *A Textbook of Modern Toxicology*. 2nd ed. 1997: Appleton & Lange. 496.

- 
268. Gohlke, H., Klebe, G. and *Angew. Chem., Int. Ed. Engl.*, 2002. **41**: p. 2644- 2676.
269. Oboh, G., Ademiluyi, A.O., Akinyemi, A.J., *Inhibition of acetylcholinesterase activities and some pro-oxidant induced lipid peroxidation in rat brain by two varieties of ginger (Zingiber officinale)*. *Exp. Toxicol. Pathol.*, 2012. **64**: p. 315–319.
270. Mejri, N., Said, N. M., Guizani, S., Essouissi, I., Saidi, M. , *Preliminary studies of acetylcholinesterase activity in the rat brain using N-phenylferrocenecarboxamide labelled by the technetium-99*. *Nucl. Med. Biol.*, 2013. **40**: p. 561–566.
271. Ozarowski, M.M., P. L.; Bogacz, A.; Gryszczynska, A.; Kujawska, M.; Jodynys-Liebert, J.; Piasecka, A.; Napieczynska, H.; Szulc, M.; Kujawski, R.; et al., *Rosmarinus officinalis L. leaf extract improves memory impairment and affects acetylcholinesterase and butyrylcholinesterase activities in rat brain*. *Fitoterapia*, 2013. **91**: p. 261–271.
272. Singh, M.K., M.; Kukreja, H.; Chugh, R.; Silakari, O.; Singh, D., *Acetylcholinesterase inhibitors as Alzheimer therapy: From nerve toxins to neuroprotection*. *Eur. J. Med. Chem.*, 2013. **70**: p. 165–188.
273. Yang, W.N.H., H.; Hu, X.D.; Feng, G.F.; Qian, Y.H. , *The effects of perindopril on cognitive impairment induced by D-galactose and aluminum trichloride via inhibition of acetylcholinesterase activity and oxidative stress*. *Pharmacol. Biochem. Behav.* , 2013. **114–115**: p. 31–36.
274. Silva, C.B., Pott, A., Elifio-Esposito, S., Dalarmi, L., Nascimento, K. F., Burci, L. M., Oliveira, M., Dias, J. F. G., Zanin, S. M. W., Miguel, O. G., Miguel, M. D., *Effect of Donepezil, Tacrine, Galantamine and Rivastigmine on Acetylcholinesterase Inhibition in Dugesia tigrina*. *Molecules*, 2016. **21**(53): p. 1-11.
275. Parra, A.L., Yhebra, R. S., Sardiñas, I. Guerra, Buela, L. I., *Comparative study of the assay of Artemia salina L. and the estimate of the medium lethal dose (LD<sub>50</sub> value) in mice, to determine oral acute toxicity of plant extracts*. *Phytomedicine*, 2001. **8**(5): p. 395-400.
276. Persoone, G., Wells, P., *Artemia in aquatic toxicology: a review*. Morphology, Genetics, Strain Characterization, Toxicology. Vol. 1. 1987, Wetteren (Belgium) Universa Press.
277. Meyer, B.N., Ferrigni, N. R., Putnam, L. E., Jacobsen, L. B., Nichols, D. E., McLaughlin, J. L., *Brine Shrimp: A convenient genral bioassay for active plant constituents*. *J. Med. Plants*, 1982. **45**: p. 31-34.
278. Déciga-Campos, M., Rivero-Cruz, I., Arriaga-Alba, M., Castañeda-Corral, G., Angeles-López, G., Navarrete, A., Mata, R., *Acute toxicity and mutagenic activity of Mexican plants used in tradicional medicine*. *J. Ethnopharmacol.*, 2007(110): p. 334-342.



- 
279. <http://www.microbiotests.be/SOPs/Artokit%20M%20SOP%20-%20A5.pdf>.
280. Malone, M.H., Robichaud, R. C., *A Hippocratic screen for pure or crude drug materials*. Lloydia, 1962. **25**(4): p. 320-332.
281. *OECD Guideline for testing of chemicals: Acute oral toxicity - Up-and-down procedure. Environmental Health and Safety Monograph Series on Testing and Assessments n° 425*. 2001.
282. Holt, A., Sharman, D. F., Baker, G. B., Palcic, M. M., *A continuous spectrophotometric assay for monoamine oxidase and related enzymes in tissue homogenates*. Anal. Biochem., 1997(244): p. 384-392.
283. Mishra, N., Sasmal, D., *Modulation of brain amines and dopaminergic behavior by a novel, reversible and selective MAO-B inhibitor*. Brain Research, 2012(1470): p. 45-51.
284. Lowry, O.H., Rosebrough, N. J., Farr, A. L., Randall, R. J. , *Protein measurement with the folin phenol reagent*. J. Biol. Chem., 1951(193): p. 265-275.
285. Pfizer Global Environment, H., and Safety Operations. [http://www.pfizer.com/sites/default/files/products/material\\_safety\\_data/Donepezil\\_HCl\\_FCT\\_05-Oct-2015.pdf](http://www.pfizer.com/sites/default/files/products/material_safety_data/Donepezil_HCl_FCT_05-Oct-2015.pdf). 2015 [cited 2017].
286. Wermuth, C.G., *The Practice of Medicinal Chemistry*. 3rd Ed. ed. 2011: Elsevier.
287. Geerts, H.G., P.; Grantham, C.; Bode, W.; Anciaux, K.; Sachak, S., *Brain levels and acetylcholinesterase inhibition with galantamine and donepezil in rats, mice, and rabbits*. Brain Research, 2005. **1033**: p. 186-193.
288. Williams, B., Nazarians, A., Gill, M., *A Review of Rivastigmine: A Reversible Cholinesterase Inhibitor*. Clinical Therapeutics, 2003. **25**(6): p. 1634-1653.
289. Fišar, Z., Hroudová, J., Raboch, J., *Inhibition of monoamine oxidase activity by antidepressants and mood stabilizers*. Neuroendocrinol Lett, 2010. **31**(5): p. 645-656.
290. Cutler, N.R.P., R. J.; Sramek, J. J.; et al., *Dose-dependent CSF acetylcholinesterase inhibition by SDZ ENA 713 in Alzheimer's disease*. . Acta Neurol. Scand., 1998. **97**: p. 244-250.
291. Ballard, C.G., *Advances in the treatment of Alzheimer's disease: Benefits of dual cholinesterase inhibition*. Eur. Neurol., 2002. **47**: p. 64-70.



## *Appendix*

---



## Appendix 1. Enzymatic Monitorization

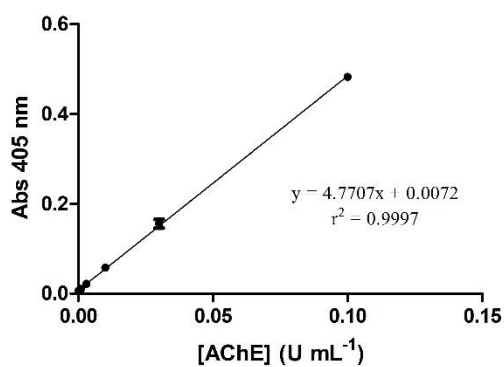


Figure S<sub>1</sub> - AChE calibration curve.

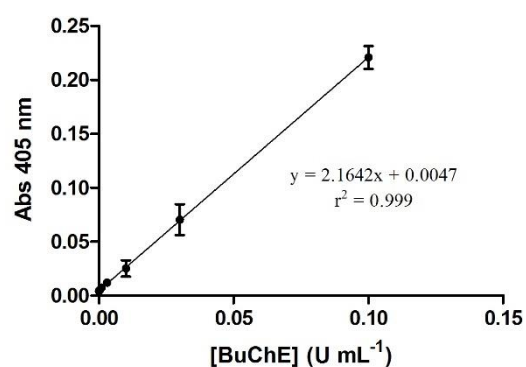


Figure S<sub>2</sub> - BuChE calibration curve.

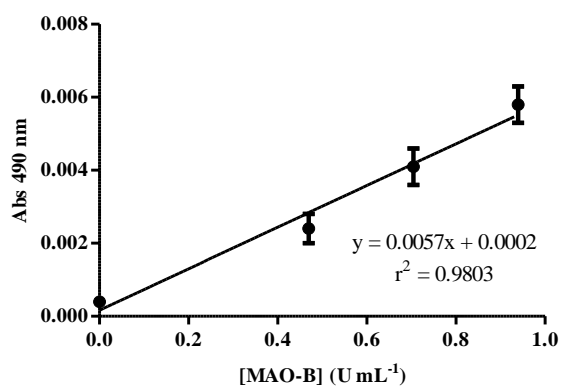


Figure S<sub>3</sub> - MAO-B calibration curve.

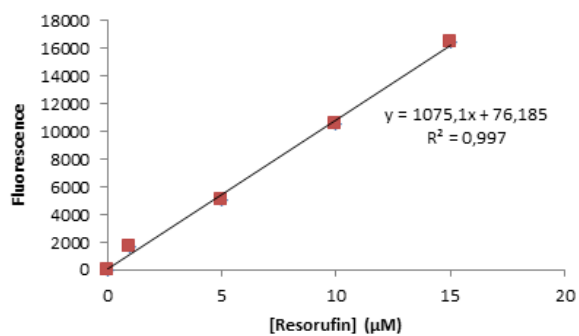


Figure S<sub>4</sub> - Resorufin calibration curve.



## Appendix 2. STD-NMR sobreposition spectra

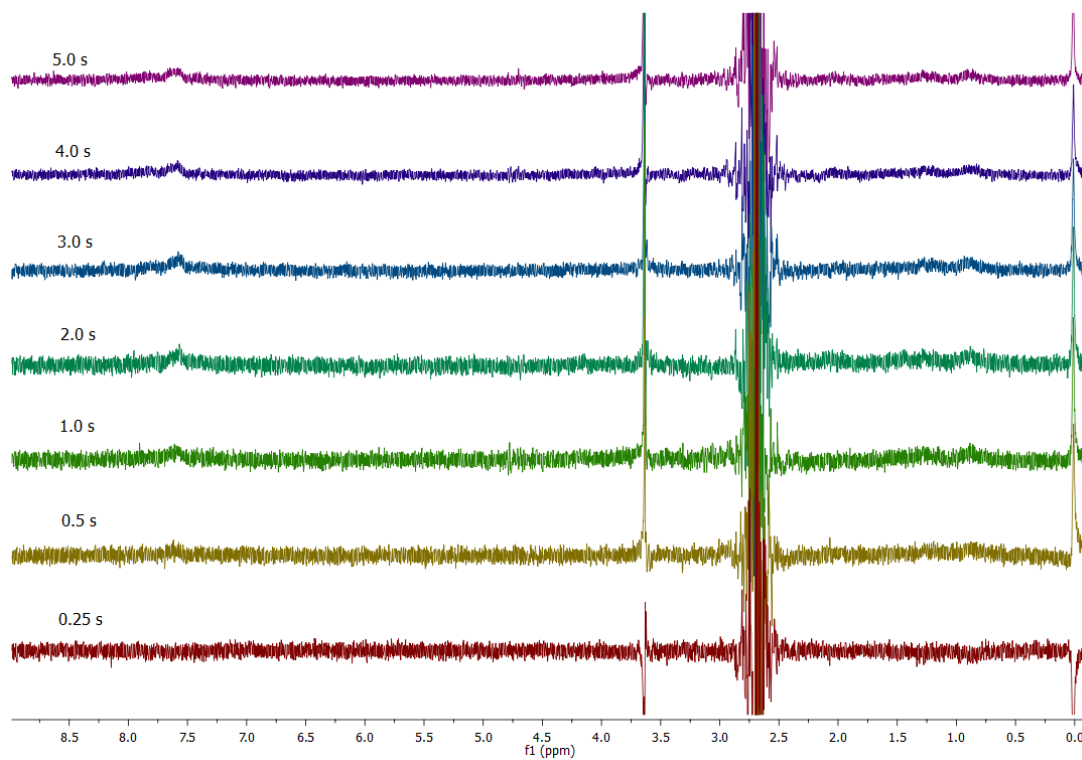


Figure S<sub>5</sub> – STD-NMR sobreposition spectrum of compound 6 with AChE at different relaxation time.

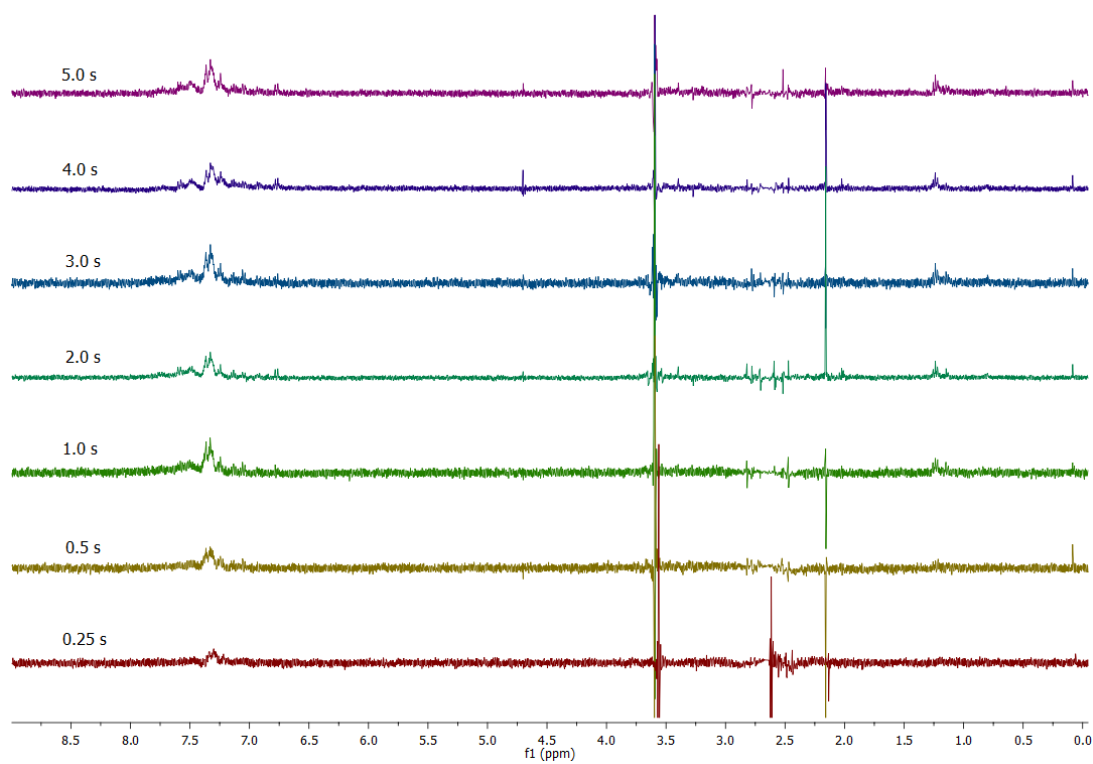
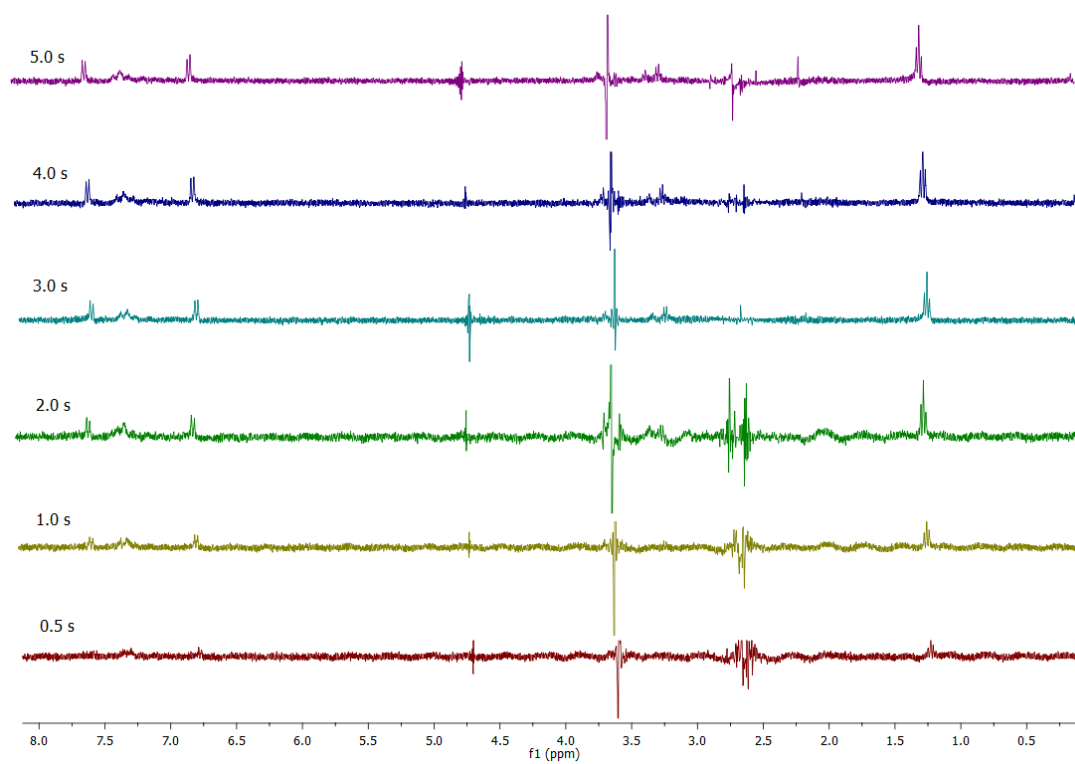
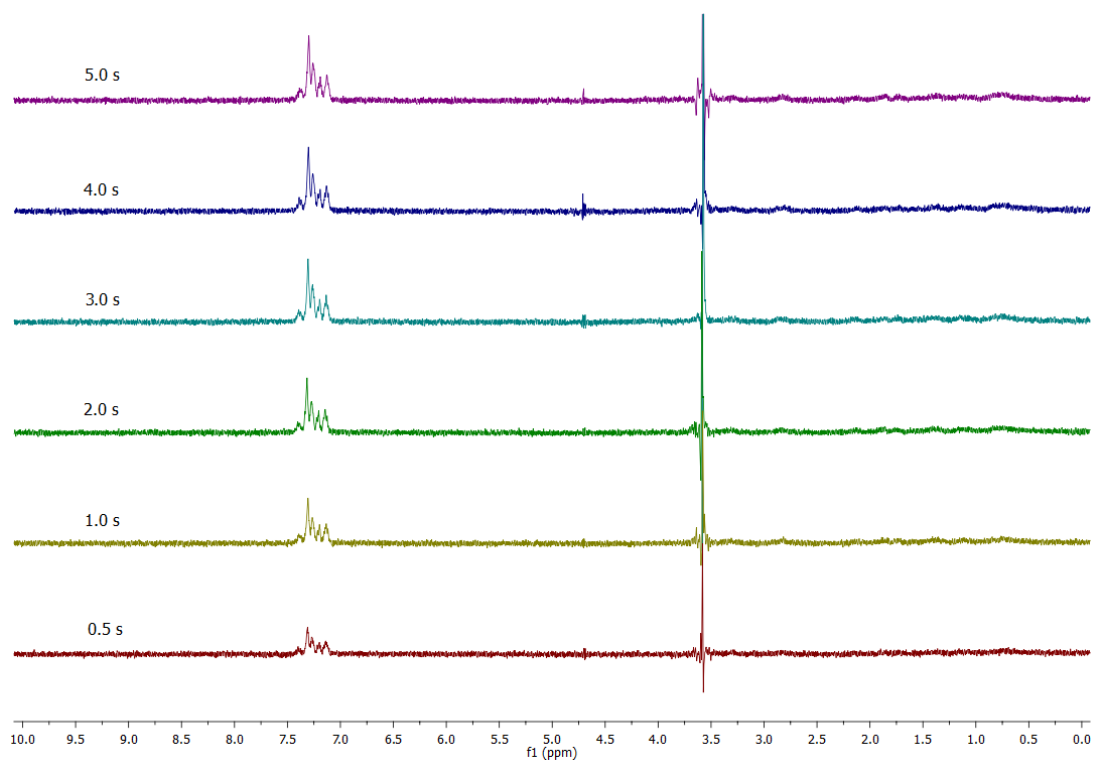


Figure S<sub>6</sub> – STD-NMR sobreposition spectrum of compound 6 with BuChE at different relaxation time.



**Figure S7** – STD-NMR sobreposition spectrum of compound 17 with BuChE at different relaxation time.



**Figure S8** – STD-NMR sobreposition spectrum of compound 48a with AChE at different relaxation time.



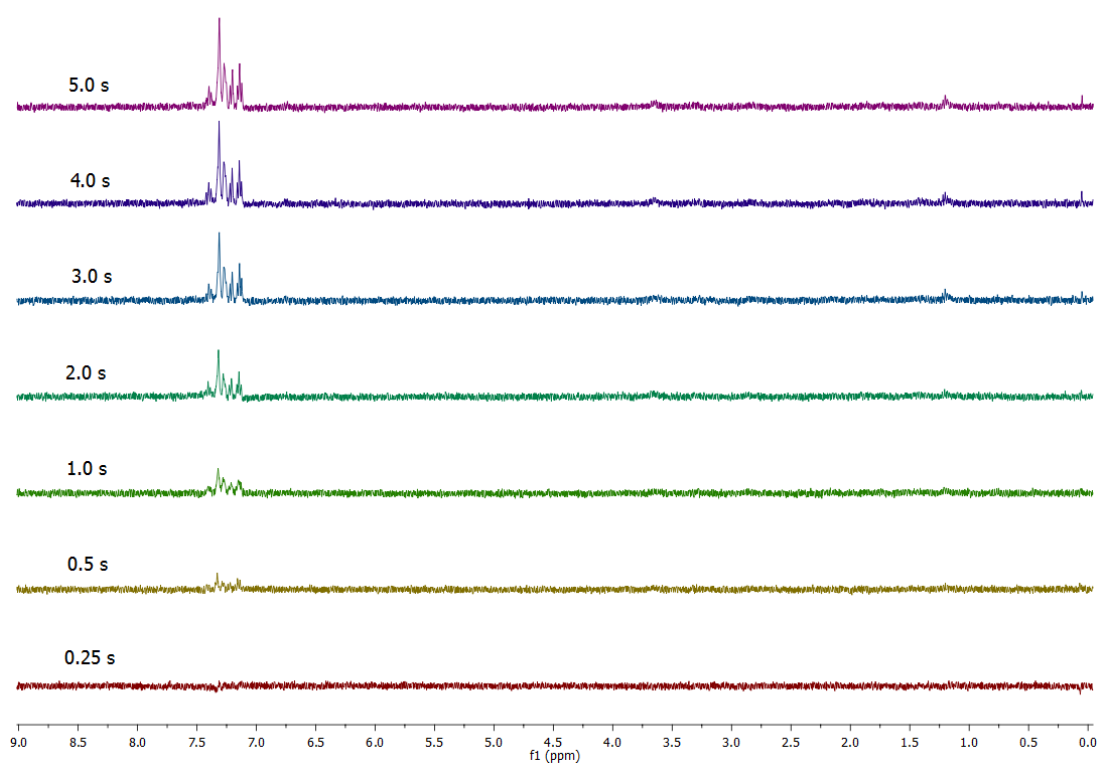


**Figure S9** - STD-NMR sobseposition spectrum of compound 48a with BuChE at different relaxation time.



### Appendix 3. Statistical Analysis

**Table A 1** - Analysis of variance (ANOVA) of enzymatic activity of isoquinolinone, azepanone, indolinone, and diether ester derivatives.

		Sum of Squares	df	Mean Square	F	Sig.
AChE_Isoquinolinone and Azepanone derivatives	Between groups	8205392.510	13	631184.039	223.150	0.000
	Within groups	79198.427	28	2828.515		
	Total	8284590.936	41			
BuChE_Isoquinolinone and Azepanone derivatives	Between groups	2413383.856	10	241338.386	1855.865	0.000
	Within groups	2860.900	22	130.041		
	Total	2416244.756	32			
AChE_Indolinone derivatives	Between groups	11949392.899	38	314457.708	30.135	0.000
	Within groups	813929.731	78	10434.996		
	Total	12763322.631	116			
BuChE_Indolinone derivatives	Between groups	10076855.387	40	251921.385	321.955	0.000
	Within groups	64162.875	82	782.474		
	Total	10141018.262	122			
AChE_Diether ester (no pre-incubation)	Between groups	78964.801	4	19741.200	245.266	0.000
	Within groups	804.889	10	80.489		
	Total	79769.690	14			
AChE_Diether ester (pre-incubation)	Between groups	15134.177	4	3783.544	177.157	0.000
	Within groups	213.570	10	21.357		
	Total	15347.747	14			
BuChE_Diether ester (no pre-incubation)	Between groups	3329630.083	4	832407.521	103.168	0.000
	Within groups	80684.614	10	8068.461		
	Total	3410314.696	14			
BuChE_Diether ester (pre-incubation)	Between groups	719114.929	4	179778.732	1183.661	0.000
	Within groups	1518.836	10	151.884		
	Total	720633.765	14			

**Table A 2** - Analysis of variance (ANOVA) of enzymatic activity of chromanone and chromanol derivatives and rivastigmine analogues.

		Sum of Squares	df	Mean Square	F	Sig.
AChE_Chromanone and Chromanol derivatives	Between groups	934813.149	6	155802.191	1358.983	0.000
	Within groups	1605.047	14	114.646		
	Total	936418.195	20			
BuChE_Chromanone and Chromanol derivatives	Between groups	5056197.131	6	842699.522	9657.277	0.000
	Within groups	1221.648	14	87.261		
	Total	5057418.779	20			
AChE_Rivastigmine analogues	Between groups	1357075.325	2	678537.662	158.511	0.000
	Within groups	25684.210	6	4280.702		
	Total	1382759.535	8			
BuChE_Rivastigmine analogues	Between groups	3091014.826	7	441573.547	978.504	0.000
	Within groups	7220.384	16	451.274		
	Total	3098235.210	23			

**Table A 3** - Analysis of variance (ANOVA) of enzymatic activity for the brain and liver of *Swiss* mice in the presence of compound **48a** and donepezil.

		Sum of Squares	df	Mean Square	F	Sig.
AChE_brain	Between Groups	0.006	3	0.002	6.634	0.005
	Within Groups	0.004	15	0.0003		
	Total	0.010	18			
AChE_liver	Between Groups	0.00003	3	0.00001	3.926	0.030
	Within Groups	0.00004	15	0.000003		
	Total	0.00007	18			
BuChE_liver	Between Groups	0.000008	3	0.000003	0.518	0.676
	Within Groups	0.00008	15	0.000005		
	Total	0.00009	18			

---

## Appendix 4. Publications

This thesis originated the following publications (available on the digital version and online):

6. Bacalhau, P., San Juan, A., Marques, C., Peixoto, D., Burke, A.J., Caldeira, A., Martins, M.R. *The role of cholinesterases in Alzheimer's disease: screening of target compounds*. *Neurodegener Dis.* **15(suppl 1)**, 741 (2015).
7. Bacalhau, P., San Juan, A., Marques, C., Peixoto, D., Goth, A., Guarda, C., Silva, M., Arantes, S., Caldeira, A. T., Martins, M. R., Burke, A. J. New cholinesterase inhibitors for Alzheimer's disease: Structure Activity Studies (SARs) and molecular docking of isoquinolone and azepanone derivatives. *Bioorg. Chem.* **67**, 1–8 (2016).
8. Bacalhau, P., San Juan, A., Goth, A., Caldeira, A. T., Martins, M. R., Burke, A. J. Insights into (S)-rivastigmine inhibition of butyrylcholinesterase (BuChE): Molecular docking and saturation transfer difference NMR (STD-NMR). *Bioorg. Chem.* **67**, 105–109 (2016).
9. Viana, H., Carreiro, E. P., Goth, A., Bacalhau, P., Caldeira, A. T., Martins, M. R. and Burke, A. J., ChemInform Abstract: Sequential Alcohol Oxidation/putative Homo Claisen—Tishchenko-Type Reaction to Give Esters: A Key Process in Accessing Novel Biologically Active Lactone Macrocycles. *ChemInform*, **47** (47) (2016).
10. Viana, H., Carreiro, E., Goth, A., Bacalhau, P., Caldeira, A.T., Martins, M. R., Burke, A. J. Sequential Alcohol Oxidation/putative Homo Claisen-Tishchenko-Type Reaction to give esters: A Key process in accessing novel biologically active lactone macrocycles. *RSC Adv.* **6**, 63214-63223 (2016).
11. Totobenazara, J., Bacalhau, P., San Juan, A., Marques, C. S., Fernandes, L., Goth, A., Caldeira, A. T., Martins, R., Burke, A. J., Design, Synthesis and Bioassays of 3-Substituted-3-Hydroxyoxindoles for Cholinesterase Inhibition. *Chemistry Select*, **1**, 3580 – 3588 (2016).
12. Bacalhau, P., Fernandes, L., Martins, M. R., Candeias, F., Carreiro, E. P., Totobenazara, J., Guedes, R. C., Caldeira, A. T., Burke, A. J. *In Silico*, NMR and Pharmacological Evaluation of an Oxindole Cholinesterase Inhibitor. *Biochem. Pharmacol.* (submitted)



UNIVERSIDADE DE ÉVORA